DEVELOPMENT AND APPLICATIONS OF A MODIFIABLE AEROSOL PLATFORM

DEVELOPMENT AND APPLICATIONS OF A MODIFIABLE AEROSOL PLATFORM

By MATHURA THIRUGNANASAMPANTHAR, B.SC.

A Thesis Submitted to the School of Graduate Studies in Partial Fulfilment of the Requirements for the Degree of Doctor of Philosophy

DOCTOR OF PHILOSOPHY (2024)

Chemical Engineering, McMaster University

1280 Main St W, Hamilton, Ontario L8S 4L7

TITLE: Development and Applications of a Modifiable Aerosol Platform

AUTHOR: Mathura Thirugnanasampanthar
B.Sc. (McMaster University, Canada)

SUPERVISOR: Dr. Zeinab Hosseinidoust

NUMBER OF PAGES: xxv, 184

LAY ABSTRACT

Many respiratory infections are spread through the air by pathogen-containing droplets released from the airways of infected individuals as they breathe, talk, cough, sneeze, or laugh. Facemasks are an easy-to-adopt infection control strategy to guard against airborne infectious agents. An aerosol platform was built at McMaster University amidst the coronavirus pandemic to perform facemask material filtration tests using information from the American Society for Materials and Testing standard F2101-19. However, we soon identified ambiguous aspects of the standard that can potentially prevent the reliable operation of the test platform and the gathering of reproducible test results. The first objective was to modify the test setup and develop precise procedures to address ambiguities of the standard. Modifications of the platform and detailed procedures ensured more accurate and consistent testing of facemask materials. Next, we used the platform to study how long pathogens stay viable within aerosol droplets. Droplets containing the bacteriophage Phi6, a surrogate for the severe acute respiratory syndrome coronavirus 2 (SARS-CoV-2), were used to study how droplet size, mucus composition, and environmental conditions (like temperature and humidity) affect pathogen survival. Lastly, we adapted our aerosol platform to investigate the inhaled delivery of antibacterial agents to target lung infections. Using cultures of human airway epithelial cells and *Pseudomonas aeruginosa* biofilms, we tested the antibacterial efficacy of aerosolized antibiotics and bacteriophages (viruses that kill bacteria). In summary, this thesis work has developed an aerosol platform for conducting reliable material filtration efficiency tests, probing virus stability within airborne droplets, and modelling inhaled drug delivery to the lungs.

ABSTRACT

Pathogen-containing droplets expelled into the air as infected individuals speak, cough, sneeze, or laugh may infect proximal secondary hosts. Facemasks are an effective, low-cost method to help prevent airborne transmission mediated by pathogen-laden droplets in the environment. To understand the testing of facemask materials to protect against airborne pathogens, we followed the American Society for Testing and Materials (ASTM) standard F2101-12 and built an in-house test platform. However, the standard lacks clear guidelines. To address this, we built an aerosol platform at McMaster University to generate and test droplets containing viable bacteria, allowing us to assess the filtration performance of different facemask materials. We created optimized procedures to ensure the generation and sampling of infectious aerosols are consistent and reliable. The operation, maintenance, and sterilization of the platform were also detailed.

Airborne disease transmission is a complex phenomenon influenced by multiple factors. Conditions such as muco-obstructive airway disorders can increase the viscosity and solute content of airway lining fluid. Therefore, individual variability in airway mucus composition and initial droplet size may influence transmission dynamics. Thirdly, environmental conditions such as temperature and humidity can change the aerosol microenvironment and alter encapsulated pathogen viability. Evidence suggests infectious aerosols originate from the breakup of the airway lining fluid, and the site of origin within the airways can affect the size of pathogen-laden droplets. Using the bacteriophage Phi6 as a stand-in for the SARS-CoV-2 virus, we examined how droplet size, mucus composition, pathogen load, and environmental conditions (temperature and humidity) affect pathogen survival. Our findings may provide insight into the dynamics of airborne transmission and can help improve strategies to reduce the spread of respiratory infections.

Lastly, we adapted the platform to conduct in vitro lung exposure studies of deposition, safety, and efficacy of bactericidal agents. The human airway epithelial cell line, Calu-3, cultured in an air-liquid interface system, was used to recapitulate the physiological characteristics of the respiratory mucosa. *Pseudomonas aeruginosa* biofilms cultured for 24 hours were placed within the impactor and exposed to aerosolized bactericidal agents. Preliminary results show that our cell-integrated exposure platform can assess in vitro safety, efficacy, and dosage of inhaled therapeutics. This setup can potentially help gather pre-clinical data to support in vivo studies of treatments for respiratory diseases. This platform has significant potential for expanding aerosol research at McMaster University to evaluate the effectiveness of personal protective equipment, study how infectious aerosols spread, and explore inhaled delivery of therapeutic agents to the lungs. These findings contribute to our understanding of airborne transmission and may inform strategies to reduce the spread of infections.

ACKNOWLEDGEMENTS

I want to thank my supervisor, Dr. Zeinab Hosseinidoust, and my wonderful project advisor, Prof. Myrna Dolovich, for their patience, support, and guidance over the last four years and for trusting me with the aerosol project. I also want to thank Prof. Carlos Filipe for being part of my supervisory committee! Your smile always put me at ease, and your insightful comments and thought-provoking questions made me view my work in a new light. A special thank you goes to Rod Rhem and Paul Gatt. I could not have gone far without these wonderful folks who taught me about wing-nuts, O-rings, and Allen wrenches! Next, my special lab mates! These amazing folks picked me up when I was down, made me laugh, and kept me humble: Fereshteh Bayat, Mellissa Gomez, Ekaterina Kvitka, Lei Tian, and Kyle Jackson! I must also extend my gratitude to Dhanyashri Maddibonia, who believed in my abilities and welcomed a (very nervous) volunteer into the Hosseinidoust (then Biohybrids) lab family. I must also thank my ever-pessimistic and long-suffering parents! Thank you for keeping me motivated, amused, well-fed (mostly), clothed, and housed for 28 years despite my failing to pursue medicine! I must also thank my wonderful cousin, Vishkan, who supported and believed me regardless of whether I was at my best or worst! Last but not least, I want to thank my wonderful partner. I am so grateful to have you in my life and by my side. You have made me the happiest I have ever been, and I am so excited to share the next adventure with you!

This thesis is dedicated to Prof. Myrna B. Dolovich.

TABLE OF CONTENTS

LIST OF FIGURES

Chapter 2

Chapter 3

Figure 3. Downstream components of the aerosol platform. *The figure depicts* ***(a)*** *a fully-assembled six-stage viable cascade impactor,* ***(b)*** *a glass Petri dish containing 27 mL of trypticase soy agar and balance on metal platforms on the second impactor stage,* ***(c)*** *a 60-cm-high glass aerosol mixing chamber positioned over the inlet of the six-stage cascade impactor,* ***(d)*** *a condenser tube,* ***(e)*** *a TSI airflow meter used to monitor airflow through the aerosol platform,* ***(f)*** *a downstream vacuum pressure gauge, and (g) a GAST vacuum pump.*

Figure 4. Components of the inflow and outflow lines. *Bacterial feed delivery to the atomizer at 170 µL/min is controlled using the syringe pump. Compressed airflow delivery to the atomizer at 1.5 L/min is filtered through a HEPA capsule filter and is controlled using a pressure gauge and monitored using an upstream airflow meter. The humidified air to the 60-cm-high glass aerosol mixing chamber at 26.8 L/min is room air that is passed through a water-to-gas humidifier and filtered through a HEPA capsule filter before entering the system. The outflow line shows the rate of airflow suctioned from the system at 28.3 L/min.*

Figure 5. Bacterial feed line. *The figure depicts the syringe pump containing a 5 mL syringe connected via a luer-lok adapter to the silicone tubing that will connect to the feed inlet valve on the single-jet Blaustein atomizer.*

Figure 6. Bacterial feed, compressed air, and humidified air lines. *The figure depicts the placement of the Blaustein atomizer single-jet module within the notch machined into the top plate of the 60-cm-high glass aerosol mixing chamber, secured by wingnuts. Also shown are the feed line, compressed airline, and humidified airline.*

Figure 7. Agar plate loading. *The figure depicts the placement of a glass Petri dish on metal platforms protruding from the second stage of the impactor.*

Figure 8. Facemask placement*. The figure depicts the placement of facemask material secured between the inlet cone and the first stage of the impactor.*

Figure 9. Placement of 60-cm-high glass aerosol mixing chamber on assembled impactor*. The figure depicts the position of the 60-cm-high glass aerosol mixing chamber, secured by black Velcro strap to the stand, over the inlet of the 6-stage viable cascade impactor. Also shown is the polyurethane airflow line that connects to the vacuum pump.*

Figure 10. Trial 1 - Positive control run plates. *Positive control runs performed in the absence of test material* ***(a)*** *before and* ***(b)*** *after the facemask material challenge runs were conducted.*

Figure 11. Stage distribution of viable bacteria-laden droplets from positive control runs from three independent trials. *Viable bacterial droplets collected below each impactor stage before* ***(white)*** *and after* ***(red)*** *positive-hole correction in the absence of test materials. Positive control run data from three independent trials are represented (n=3).*

Figure 12. Total counts and mean size of viable bacteria-laden droplets from positive control runs from three independent trials. (a) *Total counts and* ***(b)*** *mean size of viable bacteria-laden droplets collected cross all impactor stages before* ***(white)*** *and after* ***(red)*** *positive-hole correction*

in the absence of test materials. Positive control run data from three independent trials are represented (n=3).

Figure 13. Bacterial filtration efficiencies of test materials from three independent trials. *Bacterial filtration efficiency calculated using viable droplet-laden droplet counts before* ***(white)*** *and after* ***(red)*** *positive-hole correction for three test materials: single-ply bandana, 3-ply mask, and N95 face filtering respirator (FFR). Data from three independent trials are represented (n=3).*

Figure 14. Trial 1 – Bandana and 3-ply mask plates. *(a) Bandana and (b) 3-ply facemask material challenge plates.*

Figure 15. Trial 1 – Negative control and N95 challenge run plates. *(a) Negative control and (b) N95 face filtering respirator (FFR) material challenge plates.*

Chapter 4

Figure 1. The illustration depicts the in-house experimental setup for bacterial filtration efficiency (BFE) testing of facemask materials per American Society for Testing and Materials standard F2101-19. *Schematic of the BFE test workflow comprised of three main components:* ***(left)*** *the aerosol generation module,* ***(centre)*** *a 60-cm-high glass aerosol mixing chamber, and* ***(right)*** *the aerosol collection module, all housed within a custom-built biological safety cabinet. Blaustein single-jet module, operated in atomizer mode, was used to generate polydisperse bacterial aerosol droplets. Glass Petri dishes prepared with 27 mL of semi-solid bacterial culture media were inserted into the impactor to collect size-fractioned droplets through impaction.*

Figure 2. Effect of peptone water concentration on the mean size, total count, and stage distribution of viable bacteria-laden droplets. *The impact of varying peptone water concentration on* ***(a)*** *mean size,* ***(b)*** *total count, and* ***(c)*** *stage distribution of viable bacteria-laden droplets is shown (n=5). All other operating variables for aerosol generation were kept constant according to* ***Table S3*** *as peptone water concentration was varied, while the remaining parameters were adjusted as specified in* ***Table 1****. Regions shaded in grey indicate ASTM standard F2101-19 specified range for* ***(a)*** *mean size and* ***(b)*** *total count of viable bacteria-laden droplets. Asterisks indicate statistically significant differences, defined as *p-value<0.05, ** p-value <0.01, *** p-value <0.001, **** p-value <0.0001.*

Figure 3. Effect of relative humidity on the mean size, total count, and stage distribution of viable bacteria-laden droplets. *The impact of varying the relative humidity on* ***(a)*** *mean size,* ***(b)*** *total count, and* ***(c)*** *stage distribution of collected viable bacteria-laden droplets is shown (n=5). All other operating variables for aerosol generation were kept constant according to* ***Table S7*** *as the relative humidity was varied, while the remaining parameters were adjusted as specified in* ***Table 1****. Regions shaded in grey indicate ASTM standard F2101-19 specified range for* ***(a)*** *mean size and* ***(b)*** *total count of viable bacteria-laden droplets. Asterisks indicate statistically significant differences, defined as *p-value<0.05, ** p-value <0.01, *** p-value <0.001, **** p-value <0.0001.*

Figure 4. Effect of bacterial concentration on the mean size, total counts, and stage distribution of viable bacteria-laden droplets. *The impact of varying bacterial concentration on* ***(a)*** *mean size,* ***(b)*** *total count, and* ***(c)*** *stage distribution of viable bacteria-laden droplets is shown (n=5). All other operating variables for aerosol generation were kept constant according to* ***Table S11*** *as bacterial concentration was varied. The remaining parameters were adjusted as specified in* ***Table 1****. Regions shaded in grey indicate ASTM standard F2101-19 specified range for* ***(a)*** *mean size and* ***(b)*** *total count of viable bacteria-laden droplets. Asterisks indicate statistically significant differences, defined as *p-value<0.05, ** p-value <0.01, *** p-value <0.001, **** p-value <0.0001.*

Figure 5. Effect of atomizer airflow rate on mean size, total counts, and stage distribution of viable bacteria-laden droplets. *The impact of varying atomizer airflow rates on* ***(a)*** *mean size,* ***(b)*** *total counts, and* ***(c)*** *stage distribution of viable bacteria-laden droplets is shown (n=5). All other operating variables for aerosol generation were kept constant according to* ***Table S15*** *as the atomizer airflow rate was varied. The remaining parameters were adjusted as specified in* ***Table 1****. Regions shaded in grey indicate ASTM standard F2101-19 specified range for* ***(a)*** *mean size and* ***(b)*** *total count of viable bacteria-laden droplets. Asterisks indicate statistically significant differences, defined as *p-value<0.05, ** p-value <0.01, *** p-value <0.001, **** p-value <0.0001.*

Figure 6. Effect of atomizer feed flow rates on mean size, total counts, and stage distribution of viable bacteria-laden droplets. *The impact of varying atomizer feed flow rate on* ***(a)*** *mean size,* ***(b)*** *total count, and* ***(c)*** *stage distribution of viable bacteria-laden droplets is shown (n=5). All other operating variables for aerosol generation were kept constant according to* ***Table S19*** *as the atomizer feed flow rate was varied. The remaining parameters were adjusted as specified in* ***Table 1****. Regions shaded in grey indicate ASTM standard F2101-19 specified range for* ***(a)*** *mean size and* ***(b)*** *total count of viable bacteria-laden droplets. Asterisks indicate statistically significant differences, defined as *p-value<0.05, ** p-value <0.01, *** p-value <0.001, **** p-value <0.0001.*

Figure 7. Dependence of bacterial filtration efficiency and breathability on test material. (a) *Scanning electron microscope images of 1-ply bandana, 3-ply mask (filter layer), and N95 face filtering respirator (filter layer).* ***(b)*** *Bacteria-laden droplets collected below impactor stages in the presence and absence of test materials are shown (n=3). Dotted lines are added to guide the eye and have no scientific significance.* ***(c)*** *Bacterial filtration efficiency, and* ***(d)*** *pressure differential of test materials (n=3). Significance was defined as *p<0.05, **p<0.01, ***p<0.001, ****p<0.0001. These operating values generate bacterial challenge consisting of 1700 to 3000 viable bacteria-laden droplets with a mean size of 2.7 to 3.3 μm: ≥80% relative humidity, 1.5% w/v peptone water concentration, 1×10^5 CFU/mL bacterial concentration, 1.5 L/min and 170 μL/min atomizer airflow and feed flow rates.*

Figure S1*. Scan of single aerosol run collection plate.*

Figure S2*. Stage distribution of the nominal doses of fluorescein-containing droplets.*

Figure S3*. Stage distribution of viable bacteria-laden aerosol droplets (n=25).*

Figure S4. *The illustration depicts potential mechanisms impacting viable bacteria-laden droplet size and count.*

Chapter 5

Figure 1. Schematic of the aerosol platform and the experimental workflow. *(**a**) The platform contains three main components: the Blaustein single-jet atomizer, a 60-cm-high aerosol mixing chamber, and a 6-stage viable cascade impactor. Phi6 concentrations 1×10^5 and 5×10^5 plaque-forming units per millilitre (PFU/mL) were selected to reflect sputum RNA concentrations reported in infectious SARS-CoV-2 patients. Virus suspensions in peptone water reflect solute concentrations in the airway lining fluid in healthy (1.5% w/v) and disease (3.0% and 6.0% w/v) states. Low (15±5%) and intermediate (50±5%) relative humidity at 24±1.6°C reflects seasonal fluctuations in indoor environments. (**b**) The schematic depicts the viable virus-laden droplet detection method. The deposition of Phi6 on soft agar containing the host bacteria Pseudomonas syringae results in plaque formation owing to lytic phage activity. (**c**) Scanned image of six collection plates with plaques at the site of impaction of infective Phi6 aerosol droplets. Plaque counts were converted to coincidence-corrected whole number values and used to calculate total droplet counts and the size range of viral aerosols. Schematics created with Biorender.*

Figure 2. Effect of solute content on viable virus-laden droplet counts, collected under low and intermediate relative humidity conditions and varying virus concentrations, below the first (initial size range of ≥18.65 to ≥20.28 µm), second (initial size range of 12.52 to ≥18.65 µm), and third (initial size range of 8.79 to 13.62 µm) impactor stages. *Phi6 bacteriophage suspensions with concentrations of (**a,c,e**) 1×10^5 PFU/mL and (**b,d,f**) 5×10^5 PFU/mL were prepared in 1.5% (**coral**), 3% (**yellow**), and 6% (**turquoise**) w/v peptone water solutions and aerosolized into 15±5% (**circles**) and 50±5% (**inverted triangles**) relative humidity conditions at 24±1.6°C. Graphs present coincidence-corrected viable droplet counts collected below the (**a,b**) first, (**c,d**) second, (**e,f**) third impactor stages. Significance was determined using one-way ANOVA followed by Tukey's multiple comparisons test * - $p<0.05$, ** - $p<0.01$, *** - $p<0.001$.*

Figure 3. Effect of solute content on viable virus-laden droplet counts, collected under low and intermediate relative humidity conditions and varying virus concentrations, below the fourth (initial size range of 5.59 to 9.56 µm), fifth (initial size range of 2.93 to 6.09 µm) and sixth (initial size range of 1.73 to 3.19 µm) impactor stages. *Phi6 bacteriophage suspensions with concentrations of (**a,c,e**) 1×10^5 PFU/mL and (**b,d,f**) 5×10^5 PFU/mL were prepared in 1.5% (**coral**), 3% (**yellow**), and 6% (**turquoise**) w/v peptone water solutions and aerosolized into 15±5% (**circles**) and 50±5% (**inverted triangles**) relative humidity conditions at 24±1.6°C. Graphs present coincidence-corrected viable droplet counts collected below the (**a,b**) fourth, (**c,d**) fifth, and (**e,f**) sixth impactor stage. Significance was determined using one-way ANOVA followed by Tukey's multiple comparisons test * - $p<0.05$, ** - $p<0.01$, **** - $p<0.0001$.*

Figure S1. Initial droplet size calculation for an impactor airflow rate of 28.3 LPM. *The initial size of droplets, collected below each impactor stage under the standard impactor airflow rate of 28.3 LPM, will vary depending on the solute content (1.5, 3, and 6% w/v) and equilibration conditions (15±5% or 50±5% relative humidity at 24±1.6°C) within the 60-cm-high aerosol mixing*

chamber. The dotted lines indicate the initial size of 18.05 µm for droplets generated from 1.5% w/v peptone water solution and equilibrated at 15±5% RH (top) and initial size of 9.53 µm for droplets generated from 6% w/v peptone water solution and equilibrated at 50±5% RH (bottom) collected below the second stage of the impactor with a 4.7 µm cut-off value under an impactor airflow rate of 28.3 LPM.

Figure S2. Effect of varied impactor airflow rates on initial and equilibrated droplet sizes. *The graph illustrates similar initial size ranges of droplets generated from three different peptone water solutions (1.5, 3, and 6% w/v) and equilibrated under two different environmental conditions (15±5% or 50±5% relative humidity at 24±1.6°C) within the 60-cm-high aerosol mixing chamber and collected under varied impactor airflow rates.*

Figure S3. Effect of varied peptone water concentration, relative humidity conditions, and impactor airflow rates on the nominal dose of fluorescein-laden droplets collected below impactor stages. *Solutions containing 1 mg/mL sodium fluorescein, prepared in 1.5% (**coral**), 3% (**yellow**), and 6% (**turquoise**) w/v peptone water solutions, were atomized into 15±5% (**circles**) and 50±5% (**inverted triangles**) relative humidity conditions at 24±1.6°C. The graph presents the percentage nominal dose average from three trials conducted for the six conditions (n=3). Spectrophotometric measurements of fluorescein wash samples were performed under excitation and emission wavelengths of 490±5 and 515±5 nm, respectively. Doses recovered below each impactor stage across the six conditions, analysed using two-way ANOVA followed by Tukey's multiple comparisons, were found to be non-significant, ns - p>0.05.*

Figure S4. Effect of virus concentration, solute content, and relative humidity on viable droplet counts with initial size range of 1.73 to ≥20.28 µm. *Phi6 bacteriophage suspensions with concentrations of 1×10^5 PFU/mL (**a,b**) and 5×10^5 PFU/mL (**c,d**) were prepared in 1.5% (**salmon**), 3% (**grey**), and 6% (**turquoise**) w/v peptone water solutions and aerosolized into 15±5% (**circles**) and 50±5% (**triangles**) relative humidity conditions at 24±1.6°C. Graphs present coincidence-corrected viable droplet counts collected below all impactor stages. Significance determined using ordinary one-way ANOVA followed by Tukey's multiple comparisons test defined as * - p<0.05, ** - p<0.01, **** - p<0.0001.*

Figure S5. Initial size range influences solute-, relative humidity-, and virus concentration-dependent changes in viable virus-laden droplet counts. (a,c) *Intensity maps and (**b,d**) 3D plots present viable virus-laden droplet counts with initial size range of 1.73 to ≥20.28 µm generated from Phi6 suspensions with concentrations of (**a,b**) 1×10^5 PFU/mL and (**c,d**) 5×10^5 PFU/mL prepared in 1.5%, 3%, and 6% w/v peptone water solutions and aerosolized into 15±5% and 50±5% relative humidity conditions at 24±1.6°C.*

Chapter 6

Figure 1. The illustration depicts the platform configuration for exposing P. aeruginosa biofilms and Calu-3 airway epithelial cell cultures to airflow or aerosolized phage droplets. (a) *Aerosol exposure platform; **(b)** Calu-3 cells under 10x Magnification; **(c)** SEM image of Pa bacterial cells; **(d)** TEM image of Pseudomonas phage vB_Pae-TbilisiM32; **(e)** 6-stage viable cascade impactor simulates deposition pattern within the human respiratory tract.*

Figure 2. Effect of airflow and phage exposure on (a) Calu-3 barrier integrity and (b) P. aeruginosa metabolic activity. (a) *FITC-dextran permeability across Calu-3 cells exposed to airflow and phage did not significantly differ from unexposed cells, indicating cell barrier integrity was uncompromised by airflow or phage exposure.* ***(b)*** *The absorbance of 490 nm wavelength of light reflects the metabolic activity of viable P. aeruginosa cells; absorbance values of P. aeruginosa cells exposed to phage were significantly lower than unexposed or airflow-exposed cells, indicating phage-mediated killing of bacterial cells has occurred. Phage = exposure to phage aerosol droplets, Airflow = airflow exposure within the platform, and Control = unexposed samples. Results from 3-4 replicate trials are shown, with each data point representing an individual transwell insert (n=5-10). One-way ANOVA followed by Tukey's post-hoc test was used to analyse data sets (****p<0.0001).*

Figure 3. Effect of airflow and phage exposure on the viability of (a) Calu-3 and (b) P. aeruginosa cells. (a) *DAPI- and NucGreen-stained Calu-3 cells.* ***(b)*** *Syto9- and propidium iodide-stained bacterial cells.* ***(a)*** *Fluorescent images show airflow and phage exposure did not reduce the viability of Calu-3 cells as the number of live cells stained in blue and dead cells stained in green are comparable to the unexposed condition.* ***(b)*** *Live P. aeruginosa cells were stained green by Syto9, and fluorescent images show similar densities of live cells in airflow-exposed and unexposed conditions but significantly fewer live cells in the phage-exposed condition, indicative of phage-mediated lysis of bacterial cells. (+) Phage = phage exposure, (-) Phage = airflow exposure, (-) Control = unexposed.*

Figure 4. Platform configuration for exposing P. aeruginosa biofilms to size-fractioned droplets of aerosolized phage suspension and antibiotic solution. (a) *The aerosol exposure platform consists of a 10-cm-high aerosol mixing chamber and a 6-stage viable cascade impactor, which separates droplets according to aerodynamic cut-off size.* ***(b)*** *TEM image of anti-Pseudomonas phage virions.* ***(c)*** *SEM image of ciprofloxacin flakes.* ***(d-f)*** *Transwell inserts lined with foil or containing biofilm cultures were placed below alternate stages of the impactor and exposed to droplets generated from the aerosolization of phage suspension (7×10^8 PFU/mL) or ciprofloxacin solution (7.5 mg/mL).*

Figure 5. Dose distribution profiles and antibacterial efficacy of aerosol droplets. (a) *Dose distribution profiles of phage- and ciprofloxacin-free carrier solutions containing 10 mg/mL of fluorescein were determined using the spectrofluorimetric method ($\lambda_{ex}/\lambda_{em}$ 490±5/515±5 nm).* ***(b)*** *Dose distribution profiles of phage and ciprofloxacin were determined using the plaque assay and spectrofluorimetric method, respectively ($\lambda_{ex}/\lambda_{em}$ 270±5/445±5 nm). Viability of planktonic biofilm bacteria quantified 24 hours after exposure to size-fractioned droplets of* ***(c)*** *phage and phage-free carrier or* ***(d)*** *ciprofloxacin and ciprofloxacin-free carrier. Viability of sessile biofilm bacteria quantified 24 hours after exposure to size-fractioned droplets of* ***(e)*** *phage and phage-free carrier or* ***(f)*** *ciprofloxacin and ciprofloxacin-free carrier. Metabolic activity was measured using the XTT assay (λ_{abs} 490 nm), where high absorbance corresponds to high metabolic activity of viable cells. Multiple unpaired t-tests: ns indicates insignificant, *– p<0.05, **– p≤0.01, and ***– p≤0.001. Each symbol represents a technical replicate data point. Stages 1-6 cut-off values: ≥7, 4.7, 3.3, 2.1, 1.1, 0.65 μm.*

LIST OF TABLES

Chapter 3

Chapter 4

LIST OF ABBREVIATIONS

COVID-19	coronavirus disease 2019
SARS-COV-2	severe acute respiratory syndrome coronavirus 2
PPE	personal protective equipment
ASTM	American Society for Testing and Materials
BFE	bacterial filtration efficiency
CDC	Centers for Disease Control and Prevention
HCW	health care worker
NIOSH	National Institute for Occupational Safety and Health
ALF	airway lining fluid
COPD	chronic obstructive pulmonary disease
CF	cystic fibrosis
CELEBS	controlled electrodynamic levitation and extraction of bioaerosol onto a substrate
DPI	dry powder inhaler
MDI	metered dose inhaler
AMR	antimicrobial resistance
MDR	multi-drug resistance
ALI	air-liquid interface
LPM	liters per minute
VCI	viable cascade impactor
BSC	biosafety cabinet
CFU	colony-forming units
PFU	plaque-forming units
PBS	phosphate buffered saline
TSB	tryptic soy broth
TSA	tryptic soy agar
TSAY	tryptic soy agar with yeast extract
TSAY+	tryptic soy agar with yeast extract and magnesium sulphate
MPS	mean particle size
FFR	face filtering respirator
DP	differential pressure
ALF	airway lining fluid
RH	relative humidity
TEM	transmission electron microscopy
SEM	scanning electron microscopy
FBS	fetal bovine serum
FITC	fluorescein isothiocyanate
HCL	hydrochloric acid
DPBS	Dulbecco’s phosphate buffered saline

DECLARATION OF ACADEMIC ACHIEVEMENT

This Ph.D. dissertation is organized in the style of a sandwich thesis based on in press, submitted and prepared works.

IN-PRESS, PEER-REVIEWED WORKS

1. Jarad, N. A., Prasad, A., Rahmani, S., Bayat, F., **Thirugnanasampanthar, M.**, Hosseinidoust, Z., Soleymani, L., & Didar, T. F. (2024). Smart fabrics with integrated pathogen detection, repellency, and antimicrobial properties for healthcare applications. Advanced Functional Materials.
2. Bayat, F., Hilal, A., **Thirugnanasampanthar, M.**, Filipe, C. D. M., Didar, T. F., & Hosseinidoust, Z. (2024). Portable, high throughput platform technology for rapid target identification in personalized phage therapy. Nature Communications. 55: 5626.
3. Tian, L., Jackson, K., Leon, H., Khan, S., **Thirugnanasampanthar, M.**, Mellissa, G., Bayat, F., Didar, T. F., & Hosseinidoust, Z. (2024). High-Throughput Fabrication of Functional Virus-Built Microgels for Killing Antibiotic-Resistant Bacteria. Nature Protocols. 19: 1591-1622.
4. **Thirugnanasampanthar, M.**, Gomez, M., Dolovich, M. B., & Hosseinidoust, Z. (2023). Anti-biofilm activity of aerosolized phage vs. ciprofloxacin using an *in vitro* lung deposition platform. Drug Delivery to the Lungs Conference. 34: 324-327.
5. **Thirugnanasampanthar, M.**, Feng, M., Bayat, F., Rhem, R. G., Dolovich, M. B., & Hosseinidoust, Z. (2022). An *in vitro* exposure platform for investigating bacterial and epithelial cell responses to aerosolized phage challenge. Drug Delivery to the Lungs Conference. 33: 352-355.
6. **Thirugnanasampanthar, M.**, Rhem, R. G., Dolovich, M. B., & Hosseinidoust, Z. (2021). Investigating the effects of fluid composition on bacterial aerosol production. Drug Delivery to the Lungs Conference. 32: 25-28.

MANUSCRIPTS UNDER REVIEW

1. **Thirugnanasampanthar, M.**, Kvitka, E., Gomez, M., Rhem, R. G., Dolovich, M. B., & Hosseinidoust, Z. Protocol for bacterial filtration efficiency evaluations of facemask materials using viable bacteria-laden aerosol droplets. Star Protocols.
2. **Thirugnanasampanthar, M.**, Tian, L., Libera, D. D., Rhem, R. G., Gomez, M., Jackson, K., Fox-Robichaud, A. E., Dolovich, M. B., & Hosseinidoust, Z. (2024). Unravelling the impact of operational parameters and environmental conditions on the quality of viable bacterial aerosols. PNAS Nexus.
3. **Thirugnanasampanthar, M.**, Gomez, M., Kvitka, E., Jackson, K., Rhem, R. G., M. B., & Hosseinidoust, Z. An impactor-based aerosol platform for probing indoor, short-range transmission dynamics: a Phi6 bacteriophage study. Environmental Science and Technology.
4. **Thirugnanasampanthar, M.**, Feng, M., Gomez, M., Bayat, F., Rhem, R. G., Dolovich, M. B., & Hosseinidoust, Z. An in vitro exposure platform for investigating bacterial and epithelial cell responses to aerosolized phage challenge. ACS Omega.

PRESENTATIONS

1. **Thirugnanasampanthar, M.**, Gomez, M., Dolovich, M. B., & Hosseinidoust, Z. (2024). Aerosol platform for investigating therapeutic phage and antibiotic delivery to the lungs. St. Joseph's Hospital, Firestone Institute for Respiratory Health, Regional Respirology Research Rounds (Oral Presentation).
2. **Thirugnanasampanthar, M.**, Gomez, M., Dolovich, M. B., & Hosseinidoust, Z. (2023). Anti-biofilm activity of aerosolized phage vs. ciprofloxacin using an in vitro deposition platform. Drug Delivery to the Lungs Conference (Poster Presentation).
3. **Thirugnanasampanthar, M.**, Gomez, M., Dolovich, M. B., & Hosseinidoust, Z. (2023). Anti-biofilm activity of aerosolized phage vs. ciprofloxacin using an in vitro deposition platform. Centre of Excellence in Protective Equipment and Materials, Annual Symposium (Oral Presentation).
4. **Thirugnanasampanthar, M.**, Gomez, M., Dolovich, M. B., & Hosseinidoust, Z. (2023). An *in-vitro* lung deposition platform for assessing nebulized phage efficacy against chronic bacterial infections. The McMaster Engineering Technology Research and Innovation Conference (Oral Presentation).
5. **Thirugnanasampanthar, M.**, Feng, M., Rhem, R. G., Dolovich, M. B., & Hosseinidoust, Z. (2022). An *in vitro* exposure platform for investigating bacterial and epithelial cell responses to aerosolized phage challenge. Drug Delivery to the Lungs, International Conference (Poster Presentation).
6. **Thirugnanasampanthar, M.** (2022). Use of Infectious Aerosols for Evaluating Material Filtration Efficiency. Centre of Excellence in Protective Equipment and Materials, First Annual Symposium (Oral Presentation).
7. **Thirugnanasampanthar, M.**, Rhem, R. G., Dolovich, M. B., & Hosseinidoust, Z. (2021). Investigating the Effects of Fluid Composition on Bacterial Aerosol Production. Drug Delivery to the Lungs, International Conference (Oral Presentation).
8. Dolovich, M.B., **Thirugnanasampanthar, M**. (2021). Regulatory Guidance and Standards Required for the detection, prevention of transmission, and development and approval of inhaled vaccines and treatments for SARS -CoV-2 infections. International Society for Aerosols in Medicine, International Conference (Oral Presentation).

Chapter 1. Thesis objectives and outline

1.1. THESIS OBJECTIVES

This thesis explored three objectives using the aerosol platform.

Objective 1 – Bacterial filtration efficiency evaluations of facemask materials using an in-house aerosol platform designed according to ASTM F2101-19.
The onset of the coronavirus pandemic led to the widespread use of facemasks to protect against airborne transmission of severe acute respiratory syndrome coronavirus 2 (SARS-CoV-2). Pathogen-containing droplets expelled into the air by infected individuals can infect proximal secondary hosts. The first objective was to explore the vague aspects of standardized procedures used to conduct filtration efficiency testing of facemask materials (American Society for Materials and Testing standard, ASTM F2101-19). The ASTM F2101-19 standard is used in North America to evaluate the filtration efficiencies of facemask materials using a challenge of viable bacterial aerosol droplets. However, vague and unspecified aspects of the standard necessitate a trial-and-error approach to arriving at optimized parameters, leading to lost time. We constructed the aerosol platform according to specifications in the ASTM standard F2101-19 to perform bacterial filtration efficiency (BFE) testing of materials. ***Chapter 3*** *explains the detailed protocol for operating the in-house ASTM F2101-19 setup for testing facemask BFE.* ***Chapter 4*** *discusses five unspecified parameters in the ASTM standard F2101-19 and how varying parameter input values impact viable bacterial aerosol size and counts.*

Objective 2 – In vitro model to assess viable aerosol droplet counts over short timescales in indoor environments, using Phi6 bacteriophage as a surrogate for SARS-CoV-2.
The second objective was to develop an in vitro model to assess viable droplet count changes over short timescales, a complex phenomenon influenced by multiple factors. One variable is the identity of the encapsulated pathogen; the bacteriophage Phi6 is an accepted surrogate for SARS-CoV-2 surrogate. Evidence suggests infectious aerosols originate from the breakup of the airway mucus. The second variable explored was the matrix composition that encapsulates the pathogen. Thirdly, environmental conditions (temperature and humidity) can influence the aerosol microenvironment to alter encapsulated pathogen viability within aerosol droplets. ***Chapter 5*** *investigates the roles of initial droplet size range, suspension matrix, ambient relative humidity, and pathogen load on the number of viable droplets following a short timescale of exposure to indoor conditions.*

Objective 3 – Modelling inhaled delivery of bactericidal agents to study safety, efficacy, and dose deposition profiles of antibiotics and bacteriophages against P. aeruginosa using modified versions of the aerosol platform.
The third objective was to explore the application of the aerosol platform (described in Chapter 3) to investigate the delivery of inhaled therapeutics to the lungs. The human airway epithelial cell line, Calu-3, cultured in an air-liquid interface system to mimic the physiological characteristics of the respiratory mucosa, was placed within the impactor and exposed to aerosol droplets to evaluate cellular responses to phage exposure. Transwells containing *P. aeruginosa* biofilms were placed within the viable cascade impactor and exposed to aerosolized phage and antibiotic droplets. Assays performed 24 hours later were used to determine the effect of phage and antibiotic

exposure on *P. aeruginosa* cells. Preliminary results from this cell-integrated aerosol exposure platform suggest the developed platform may provide *in vitro* safety, efficacy, and dose deposition profiles of inhaled therapeutics. ***Chapter 6*** *presents research related to the third objective.*

1.2. THESIS OUTLINE

This thesis contains seven chapters: this introduction, a review of relevant literature, detailed protocols and procedures for operating the aerosol platform, three research chapters, and the concluding chapter.

Chapter 2 - Literature review
Chapter 2 reviews background literature relevant to understanding the experimental approach and research conducted in this thesis.

Chapter 3 - Protocol for bacterial filtration efficiency evaluations of facemask materials using viable bacteria-laden aerosol droplets
Chapter 3 discusses the operational details of the aerosol platform, serving as the experimental and methodological foundation for research in chapters 4, 5, and 6. *Submitted to Star Protocols.*

Chapter 4 - Unravelling the impact of operational parameters and environmental conditions on the quality of viable bacterial aerosols
Chapter 4 focuses on how changes in the operating parameters of the aerosol platform affect the size, quantity, and distribution of viable aerosol droplets containing the bacterial pathogen *Staphylococcus aureus*. *Under revision, PNAS Nexus.*

Chapter 5. An impactor-based aerosol platform for probing indoor, short-range transmission dynamics: a Phi6 bacteriophage study
Chapter 5 explores the use of the aerosol platform to understand the mechanism of airborne virus spread in indoor environments during winter and summer in temperate zones by analyzing the viability of the SARS-CoV-2 surrogate bacteriophage Phi6 within six aerosol droplet size ranges. *Submitted to Environmental Science and Technology.*

Chapter 6 - An in vitro exposure platform for investigating bacterial and epithelial cell responses to aerosolized phage challenge
Chapter 6 discusses the adaptation of the aerosol platform to examine the dose distribution profile, safety, and efficacy of inhaled phage delivery to the lungs for treating *P. aeruginosa* infections. *Chapter combines two 4-page conference abstracts submitted to the Drug Delivery to the Lungs Conference. Submitted to ACS Omega.*

Chapter 7 - Conclusions and future directions
Chapter 7 summarizes the thesis contributions and discusses future research on airborne pathogen transmission mechanisms and inhaled delivery of therapeutic aerosols to the lungs.

Chapter 2. Literature review

2.1. INTRODUCTION

Evidence for airborne spread of severe acute respiratory syndrome coronavirus 2 (SARS-CoV-2) rapidly accumulated during the 2019 pandemic.[1–3] Understanding airborne transmission requires understanding of aerosols.[4] An aerosol is a collection of liquid droplets, solid particles, or liquid droplets and solid particles suspended in a gaseous medium such as air for some time to allow measurement or observation.[5] Infectious aerosol describes a collection of liquid droplets, solid particles, or liquid droplets and solid particles containing viable pathogens (bacteria, viruses, and fungi).[6] Some studies refer to aerosols less than 5 μm as particles and aerosols greater than 5 μm as droplets.[6] Other studies refer to aerosols in the liquid state as droplets and aerosols in the dry state as particles.[7] ***In this thesis, aerosol droplets refer to aerosols generated from a liquid solution or suspension, regardless of initial size, transformed size, or state (dry).***

This review discusses the generation of viable bacteria- and virus-containing aerosol droplets, the factors that affect the transformation of these droplets, and the importance of aerodynamic size in determining airborne residence time and deposition efficiency upon inhalation. It will also cover standardized test methods for evaluating the filtration efficiencies of facemask materials. Additionally, the review will discuss the factors that influence the viability of pathogens encapsulated within aerosol droplets, focusing on the relationship between the physiochemical transformation of aerosol droplets and the rate of pathogen viability loss to further understanding of aerosol transmission dynamics. Finally, the review will delve into therapeutic aerosol generation, delivery, and targeted deposition for treating lower airway infections caused by *Pseudomonas aeruginosa*.

2.2. RESPIRATORY AEROSOL GENERATION, AIRBORNE RESIDENCE TIME, AND DEPOSITION EFFICIENCY

Expiratory human activities such as breathing, speaking, sneezing, coughing, laughing, or singing can generate respiratory aerosol droplets (**Figure 1**).[5,7–9] The bronchiole-fluid-film-burst model describes the generation of droplets ≤1 μm from deep within the airways during respiration.[5,10] During exhalation, the bronchioles contact and fluid films form where the walls of the bronchioles contact.[5] During inhalation, collapsed bronchioles expand, and the films rupture to create fine aerosol droplets.[5] Forceful expiratory activities such as coughing create turbulent, high-velocity airflows and cause shear-stress-induced breakup of the airway lining at the air-liquid interface, giving rise to droplets in the 1 to 20 μm range.[5,10] Activities such as speaking, laughing, and singing generate ≥20 μm droplets from the vibration of vocal cords and the movements of the mouth, lips and tongue.[7,10] The size distribution, quantity, and composition of respiratory aerosol droplets can vary depending on the site of origin within the respiratory tract.[8] The size distribution and composition of respiratory droplets at the point of origin within the airways will change when droplets are expelled into the environment, continuing to evolve with time and exposure conditions.[5] The rate of these changes will have consequences for the airborne residence period of the droplets, the site of deposition if inhaled, and the viability of encapsulated pathogens.[11]

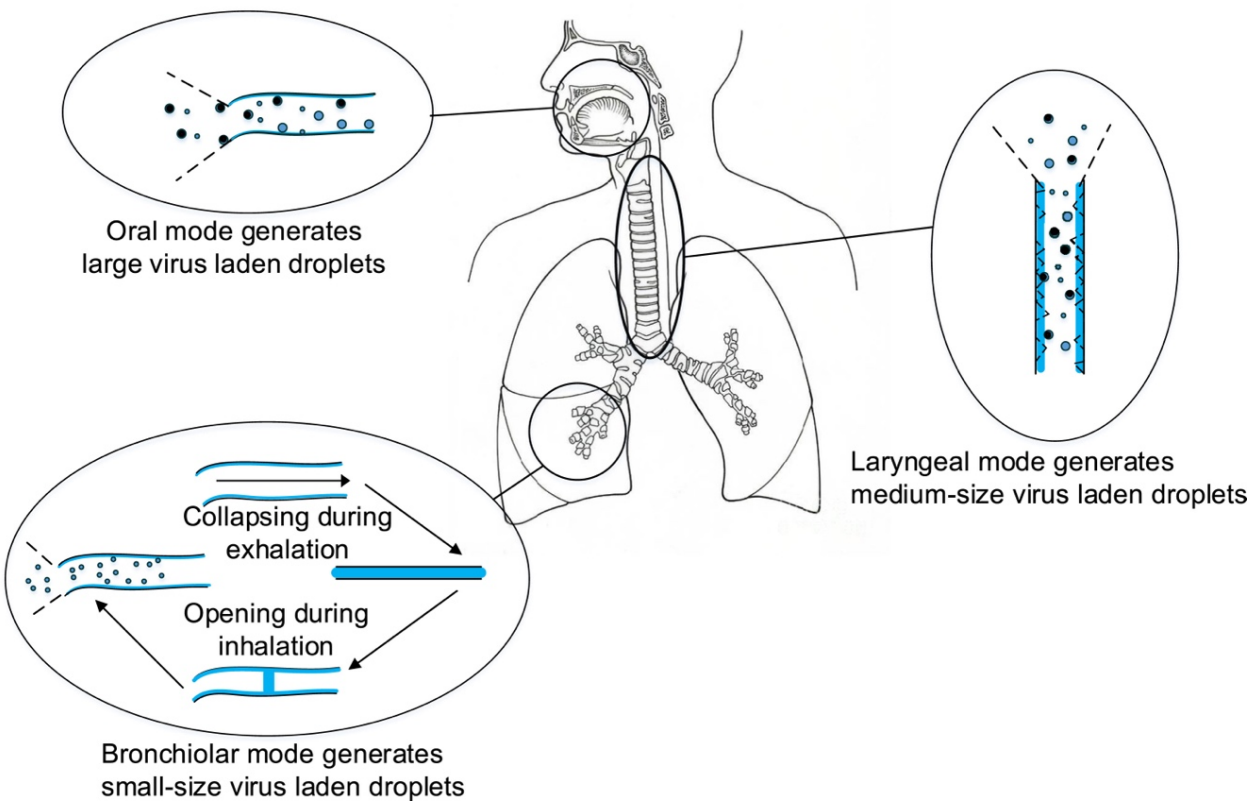

Figure 1. Respiratory droplet site of origin within airways dictates initial droplet size distribution. Adapted from Niazi et al.[9]

The size distributions of infectious aerosols determines the airborne residence time, airway deposition efficiency, and airborne transmission potential (**Figure 2**).[4,12,13] SARS-CoV-2 entry factors are found on mucosal surfaces lining the upper respiratory tract, including the nasal epithelial.[14] For infectious aerosols to reach the airways of a potential host, they must remain suspended in the air.[15] Aerosol droplet size is inversely related to residence time in the air; larger droplets experience faster settling, decreasing the risk of inhalation.[15,16] Settling velocities of 119, 746, and 2985 µm/sec were calculated for 1, 5, and 10 µm droplets, respectively.[15] A 10 µm particle falling from a height of 1 meter will reach the ground in approximately 5 minutes. A 5 µm droplet will reach the ground in 22 minutes, while a 1-µm-sized droplet will remain airborne for over 9 hours before settling from a height of 1 meter in still air.[15]

In addition to airborne residence time, the aerodynamic size also influences the deposition efficiency within the airways. Total deposition is the fraction of inhaled aerosol retained within the airways. Mechanisms that govern the deposition of aerosols in the micron range are inertial impaction and gravitational sedimentation, while submicron-sized aerosols deposit by diffusion. Total deposition calculated for 1, 3, and 5 µm-sized droplets was 21%, 71%, and 90%.[17] In agreement with theoretical predictions, experimental data shows peak deposition efficiencies of 25%, 68%, and 83% for the 1, 3 and 5 µm sized droplets.[18] Based on airborne residence time and deposition efficiency, infectious droplets <5 µm in size are most likely to mediate airborne transmission.[4]

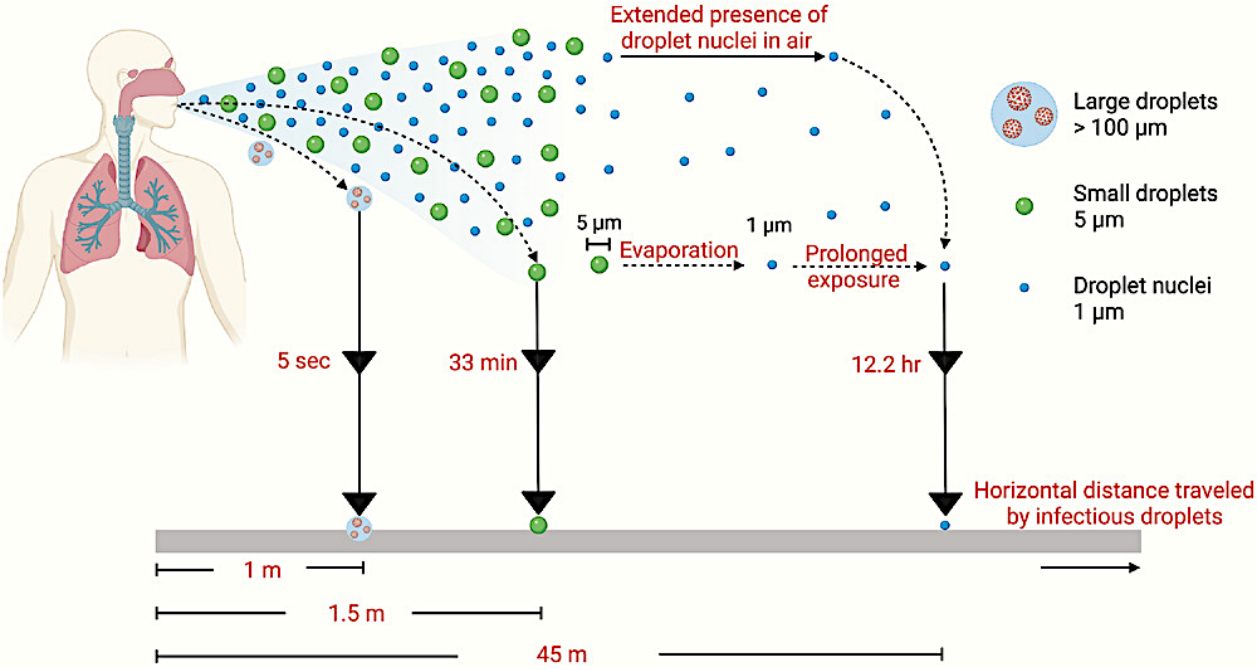

Figure 2. Droplet size dictates the distance travelled by respiratory droplets from a source. Adapted from Joseph et al.[13]

2.3. EVALUATING FILTRATION PERFORMANCE OF FACEMASKS MATERIALS AGAINST VIABLE BACTERIAL DROPLETS

Aerosolized transmission of respiratory infections, such as SARS-CoV-2 and *Mycobacterium tuberculosis*, occurs when infectious aerosols are generated and expelled into the environment, remain suspended or transported some distance from the source, and are subsequently inhaled by a susceptible individual.[6] A cost-efficient and easy-to-adopt strategy for controlling airborne transmission is the use of face masks.[20,21] Facemasks and respirators, as source control devices, ***protect others*** by limiting the emission of infectious droplets from the wearer; as respiratory protection devices, facemasks and respirators ***protect the wearer*** from infectious droplets in the environment.[19]

The Centers for Disease Control and Prevention (CDC) recommended the use of N95 or higher-performing respirators for health care workers (HCWs) when encountering or entering the vicinity of individuals with confirmed or suspected cases of COVID-19.[22] Title 42 of the *Code of Federal Regulations* (CFR) part 84, published in June of 1995 by the National Institute for Occupational Safety and Health (NIOSH), outlines a rigorous testing protocol for the certification of N-, P-, and R-series of air-purifying particulate respirators.[23] Each of the three classes of respirators exhibits different levels of resistance to oil: N-series respirators are not resistant to oil, R-series respirators are resistant to oil, and P-series respirators are oil-proof.[23] The test agent used to challenge N-series respirators is sodium chloride aerosols.[23] R- and P-series respirators certification involves dioctyl phthalate aerosol challenge.[23] While NIOSH-approved respirators are considered the gold standard for filtration performance, a limited number of testing facilities and a lengthy testing procedure means N95 respirators make up a small fraction of the masks readily available to the public.[24] Severe shortages of N95 respirators experienced throughout the

COVID-19 pandemic put the lives of HCWs and patients at risk.[22] The lack of N95 respirators and the influx of novel mask materials can generate confusion and increase the risk of transmission when poorly performing masks are selected.[24]

The American Society for Testing and Materials (ASTM) standard F2101-19 outlines requirements for performing bacterial filtration efficiency (BFE) testing of medical face mask materials using the level two bacterial pathogen *Staphylococcus aureus*.[25] The ASTM F2101-19 test procedure differs from NIOSH protocols for certifying N95 respirators in several ways.[26] Charged droplets can exhibit significantly reduced material penetration relative to uncharged aerosols.[27] Thus, N95 respirators are challenged with uncharged sodium chloride droplets delivered at a flow rate of 85 LPM. Charge neutralization is not a requirement in the ASTM procedure but requires bacterial aerosol delivery at a volumetric airflow rate of 28.3 LPM.[26] Secondly, laser photometers are used to size and count sodium chloride droplets, whereas bacterial droplets are sized using a six-stage viable cascade impactor and detected on agar plates.[26] Thirdly, the NIOSH challenge period can take 90 to 100 minutes to deposit 200 mg of aerosolized sodium chloride droplets onto the respirator; the ASTM specifies a two-minute aerosol challenge delivering between 1700 and 3000 viable bacterial droplets to assess the filtration performance of materials.[26] Fourthly, the entire respirator with an area of 150 cm^2 is challenged during NIOSH testing while the area of the material subjected to the bacterial aerosol challenge can vary.[26] Lastly, the filtration performance of N95 respirators is assessed based on the penetration of 0.1 to 0.3 µm-sized uncharged sodium chloride droplets. The ASTM standard assesses filtration performance using 1700 to 3000 viable bacterial droplets with a mean aerodynamic size of 3.0±0.3 µm.[26] Test conditions for certificating NIOSH respirators simulate 'worst case' scenarios, using the most penetrating particle size (0.1 to 0.3 um) to obtain a relatively conservative filtration efficiency value.[23,26]

Chapters 3 and 4 will discuss using ASTM standard F2101-19 test setup for BFE testing of facemask materials using a viable bacterial aerosol challenge. The in-house aerosol platform comprises a Blaustein atomizer single-jet module, a 60-cm-high glass aerosol mixing chamber, and a six-stage viable cascade impactor (**Figure 1**). **Chapter 3** provides in-depth operational details for each platform component. **Chapter 4** discusses shortcomings of the ASTM standard F2101-19 that can prolong the time to achieve test conditions required for conducting facemask filtration evaluations and provides optimized test values for reproducibly generating bacterial aerosol challenge within the specified size and count range. The review by Groth et al. provides comparisons of atomizers, impactors, and pathogen-containing droplet collection techniques for studying viable aerosol droplets.[28]

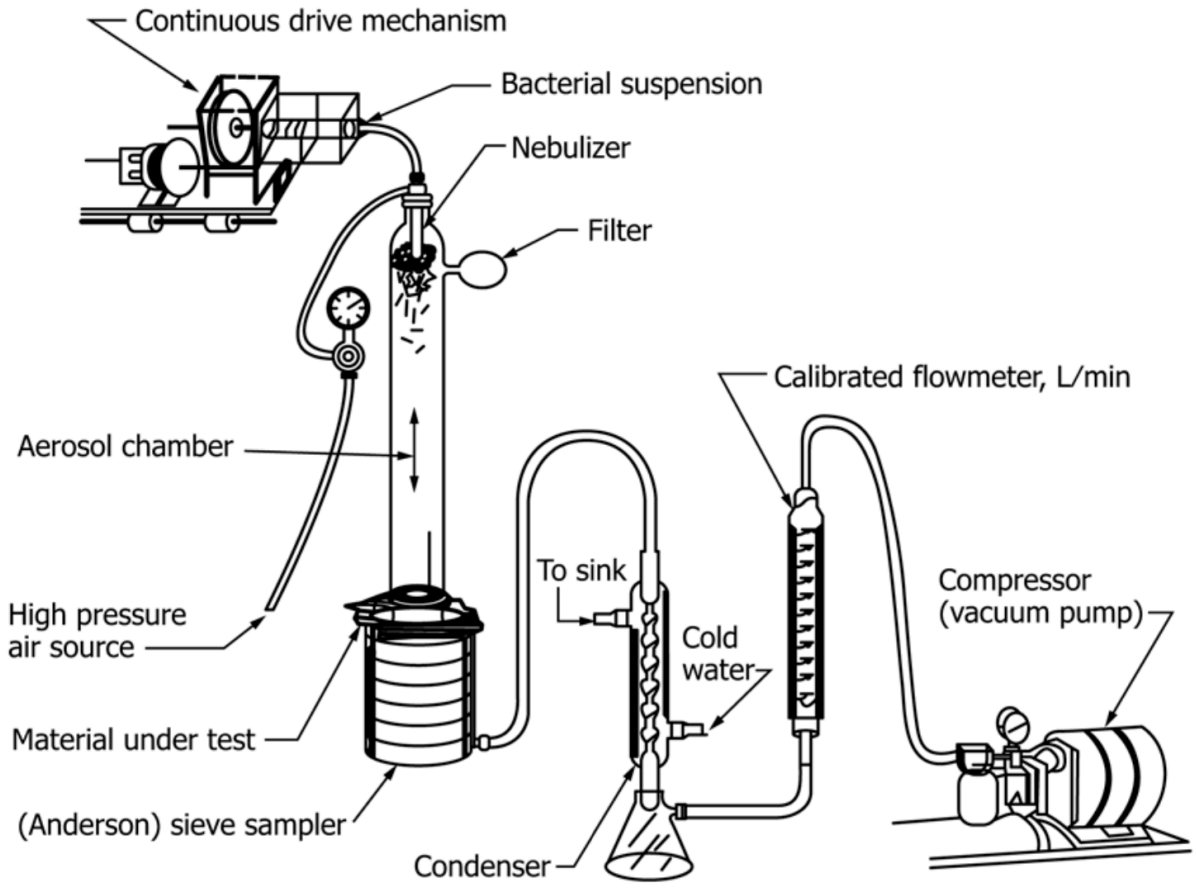

Figure 3. Bacterial filtration efficiency test platform for medical facemask material evaluations. Adapted from ASTM standard F2101-19.[25]

2.4. RELEVANCE OF VIRUS VIABILITY WITHIN AEROSOL DROPLETS FOR AIRBORNE TRANSMISSION OF INFECTION

Droplet size range, composition, and pathogen load are biological factors (related to the pathogen and host) influencing the persistence of infectious agents within aerosol droplets expelled from the airways (**Figure 4**).[29–34] The human respiratory tract has a relative humidity of 99.5% and a temperature of 37ºC.[35] Relative humidity describes the amount of water vapour present in the air compared to the maximum amount air can hold at a given temperature.[29] The amount of water vapour needed to saturate the air increases with temperature.[29] The humidity and temperature of the external environment relative to the airways will drive biophysiochemical transformations of droplets transported out of the airways.[9,36,37]

Droplet size range and composition may vary depending on the site and mechanism of origin from the airways.[38] Individual heterogeneity in saliva and airway lining fluid (ALF) composition can influence virus persistence within expelled respiratory aerosol droplets.[39–42] The solids concentration of the ALF, described as the dry weight percentage per unit volume, is made up of a mixture of salts, lipids, globular proteins, mucin biopolymers, and cellular debris.[43,44] Analysis of sputum samples collected from three cohorts of individuals revealed an elevation in solids concentration with increasing airway disease severity.[45] Solids concentration was 1-2%, 1.5-6%,

and 5-9% w/v for healthy, chronic obstructive pulmonary disease (COPD) and cystic fibrosis (CF) samples, respectively.[45] Additionally, the quantity of aerosol droplets produced by SARS-CoV-2 patients was higher than healthy subjects.[40,46] Onset and progression of infection may alter the rheological and viscoelastic properties of the ALF to change expelled droplet counts.[47] Furthermore, pathogen load within expelled droplets may vary depending on the site of origin within the airways and the progression of the infection.[48–51] Clinical evidence indicates the ALF can function as a reservoir for SARS-CoV-2 and a source of infectious aerosols.[48,50–52] Sputum samples collected from SARS-CoV-2 patients show a peak viral load of 10^4 to 10^7 copies/mL approximately 5 to 6 days after symptom onset.[50] These results reveal pathogen concentration and exhaled droplet counts can change with the onset and progression of SARS-CoV-2 infection. In summary, biophysiochemical changes in droplets transported out of the airways depend on initial droplet size range, composition, pathogen load, and environmental conditions.

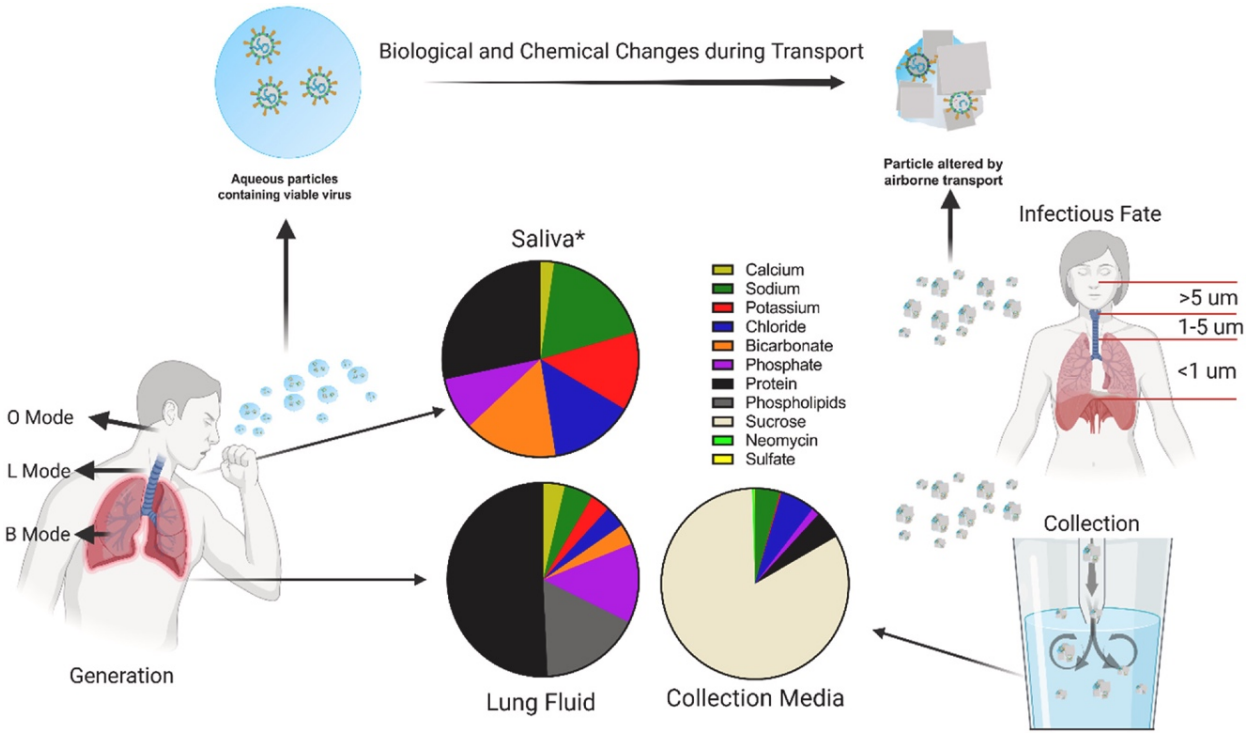

Figure 4. Factors influencing biological, physical, and chemical transformation of pathogen-containing droplets. Adapted from Santarpia et al.[34]

2.5. INSTRUMENTS FOR LABORATORY STUDIES OF PATHOGEN-LADEN AEROSOL DROPLETS

Biological aerosols or bioaerosols contain materials derived from or containing living organisms (e.g. cells, bacteria, fungi, viruses, spores, and pollen).[53] Low concentrations, instability of enclosed pathogens, transport by air currents, and biophysiochemical transformation of aerosols over time can complicate the field study of bioaerosols.[54] Instruments and platforms for conducting laboratory studies of aerosols under controlled conditions are valuable for investigating aerosol dynamics. Goldberg drums are instruments that age aerosols to study pathogen viability change over time (**Figure 5**).[55] The Goldberg drum rotates to keep aerosol droplets suspended for

prolonged periods (minutes, hours, or days) under specific relative humidity conditions.[54–56] A nebulizer generates polydisperse aerosol droplets that fill the chamber.[54] The time required to fill the chamber with aerosols can mask changes occurring over short timescales.[55,57] At the endpoint, aged droplets are extracted through the sampling port onto a filter membrane for analysis.[54,55] The advantage of the Goldberg drum is the ability to assess viability changes over long timescales.[54] However, the extraction procedure prevents the sizing of droplets at the endpoint and the matching of the physical transformation of the droplet to pathogen viability.[54,57] Moreover, larger droplets may deposit on the walls of the chamber with time, and the droplets that remain suspended for extraction and analysis at the endpoint may be biased towards smaller aerodynamic size ranges and may exclude data from larger droplets ranges due to sedimentation.[54]

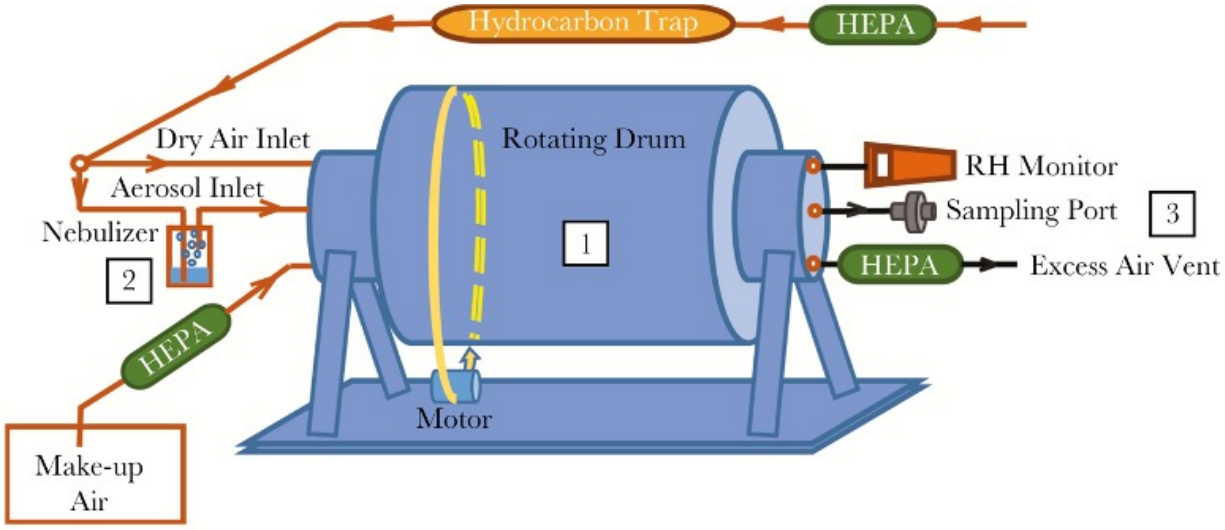

Figure 5. Rotating Goldberg drum. Adapted from Kormuth et al.[55]

Controlled electrodynamic levitation and extraction of bioaerosols onto a substrate or CELEBS is a technique for studying the biophysiochemical transformation of pathogen-laden droplets (**Figure 6**).[58] The advantage of the CELEBS platform is the ability to generate and study pathogen viability within monodisperse droplets over timescales ranging from seconds to hours.[57] An electrical field levitates monodisperse droplets while airflow around the droplets maintains specific humidity and temperature conditions.[57] The viability of pathogens within the droplet is assessed by depositing droplets onto a substrate of susceptible cell cultures.[57] While extremely powerful, limitations of the CELEBS platform include the ability to generate and analyze 50 µm-sized droplets and the need for complex and expensive instrumentation to conduct these trials that is not easily reproducible in other laboratories. **Chapter 5** discusses the use of the aerosol platform to investigate viability changes within aerosol droplets with initial size ranges of ≥18.65 to ≥20.28, 12.52 to ≥20.28, 8.79 to 13.62, 5.59 to 9.56, 2.93 to 6.09, and 1.73 to 3.19 µm using the SARS-CoV-2 surrogate bacteriophage Phi6. The droplets are equilibrated for 3 to 20 seconds as they traverse the 60-cm-high glass mixing chamber before collection on agar substrates. The work investigates the influence of initial droplet size, composition, and pathogen load on viability following short timescales of exposure.

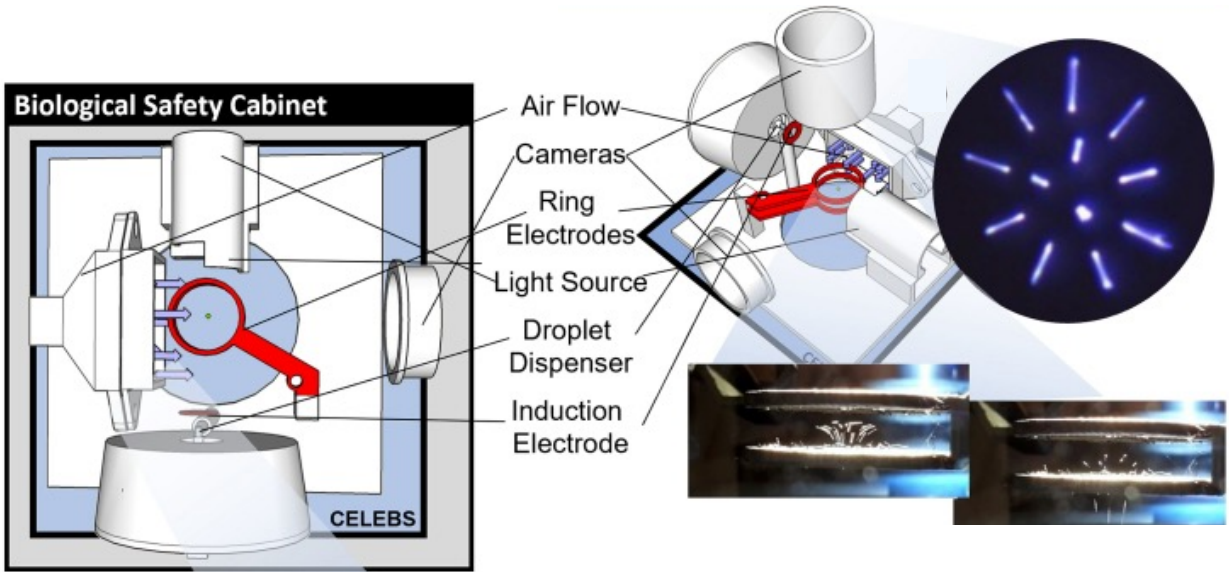

Figure 6. Controlled electrodynamic levitation and extraction of bioaerosols onto a substrate or CELEBS technique. Adapted from Oswin et al.[58]

2.6. INHALED DELIVERY OF BACTERICIDAL AGENTS TO THE LUNGS

Inhaled drug delivery is a non-invasive administration route that achieves high local drug concentrations, reduces systemic exposure, circumvents diluting effects of first-pass metabolism, and can be self-administered in the absence of healthcare professionals.[59] Four different types of devices are currently available to deliver therapeutics to the lungs: dry powder inhalers (DPI), metered-dose inhalers (MDI), and nebulizers (jet, mesh, and ultrasonic).[60] Liquid and powder formulations for inhalation can be delivered by nebulizers and DPIs, respectively. DPIs rely on inspiration to draw the medication into the lungs.[61,62] Consequently, DPIs cannot be administered to very young children, those with breathing difficulties, or individuals who are critically ill or on ventilators. In contrast, nebulizers use compressed air, vibrations, or sound waves to generate aerosols; tidal breathing alone is sufficient to deliver nebulized aerosol droplets to the lungs.[63] Nebulizers are also easier to use than DPIs without specialized techniques, manual dexterity, or actuation-inhalation coordination for successful operation.[64] Furthermore, nebulizers are more reliable than DPI for generating a consistent size distribution of aerosols as it is not dependent on patient technique.

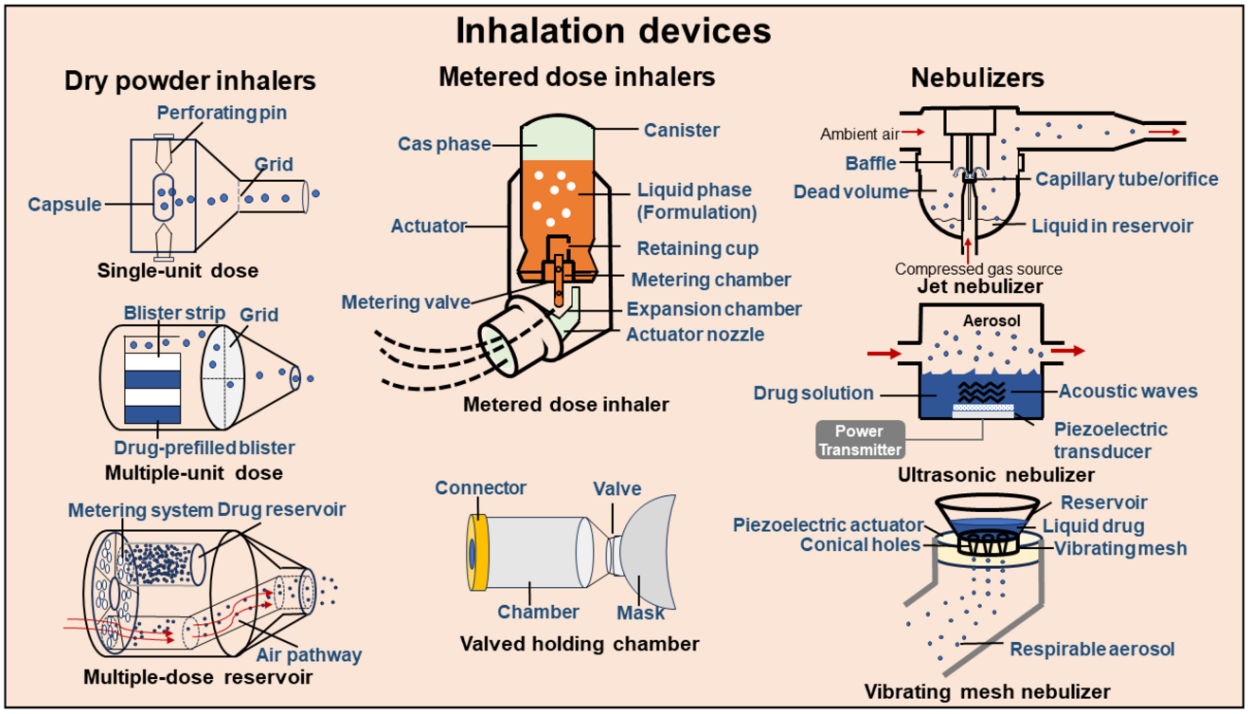

Figure 7. Inhalation devices for drug delivery to the lungs. Adapted from Peng et al.[65]

P. aeruginosa is an extracellular, gram-negative bacterial pathogen that readily forms robust biofilms, resulting in low penetrance of antimicrobial agents and evasion from host immune defences.[66,67] Inhaled antibiotics for long-term control of chronic *P. aeruginosa* infections can give rise to multi-drug resistant (MDR) strains.[68] Emergence of MDR *P. aeruginosa* strains can lead to a rapid decline in lung function, need for lung transplantation, and early mortality in CF patients.[69] Antibiotic-resistant *P. aeruginosa* strains isolated from CF patients are frequently sensitive to phage infection.[70–72] Bacteriophages are viruses that infect bacteria with high strain specificity.[73] Phage therapy uses these natural predators to combat MDR bacteria.[74,75] The sharp rise in antimicrobial resistance, paralleled with increased recognition of the role of the human microbiome in health, has reignited interest in inhaled administration of phage therapy for *P. aeruginosa* lung infections (**Figure 8**).[76–79]

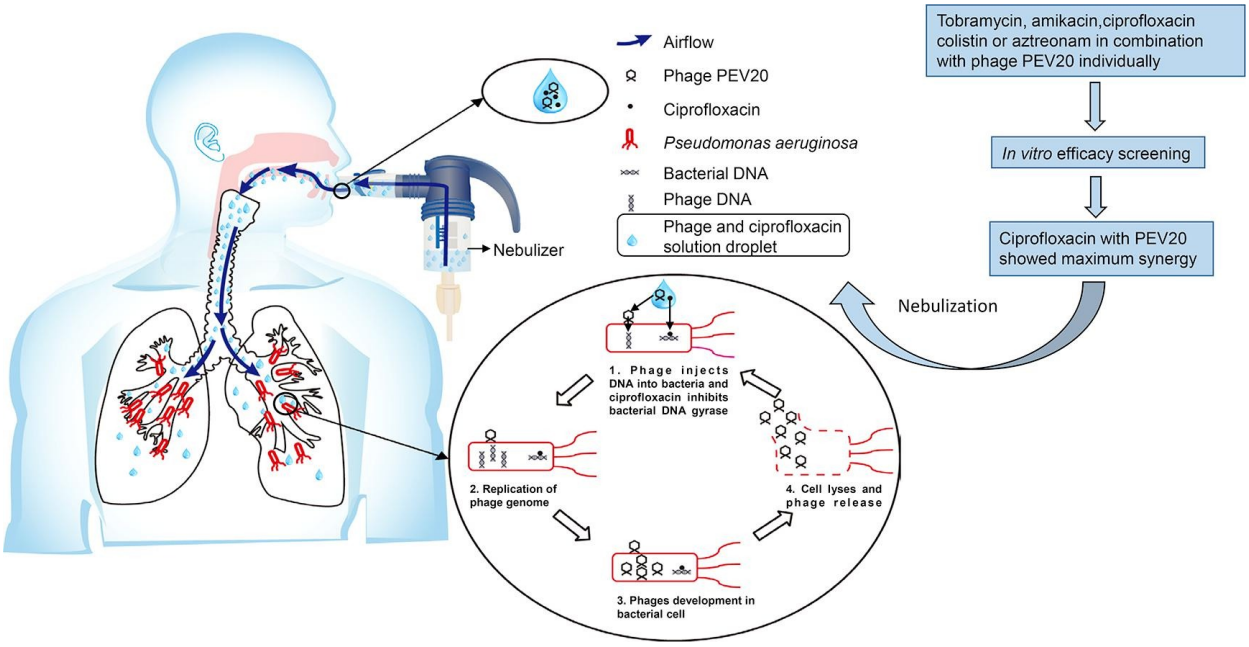

Figure 8. Nebulized delivery of phage and antibiotic droplets to target *P. aeruginosa* lung infections. Adapted from Lin et al.[79]

Although phages were discovered independently in 1915 and 1917, before the discovery of antibiotics, interest in phage therapy declined for most of the 20th century.[80] Phages possess several beneficial properties which are absent in antibiotics. One of the most important properties is selective toxicity towards host bacterial strains. Unlike antibiotics, phages spare 'bystander' organisms and are less disruptive to the microbiome.[81] Secondly, phages self-propagate in the presence of host bacteria, which allows a few viable virions to quickly multiply at the site of infection and lyse suspectable bacteria in the vicinity.[82] Obligate lytic phages are usually selected for therapeutic applications because they induce the lysis of host bacterial cells quickly after infection.[83] Conversely, phages which follow a lysogenic life cycle are unsuitable for therapeutic applications as they can remain stably integrated within the host bacteria after infection until a trigger causes the phage to enter the lytic cycle involving phage genome replication, host cell lysis, and progeny virion release.[84]

In vitro platforms are needed to gather pre-clinical information to establish the safety, dosage, and efficacy of promising antibacterial agents such as bacteriophages for inhaled delivery. Cooney et al. demonstrated a modification of the six-stage viable cascade impactor platform to model airway deposition of bactericidal droplets with Calu-3 airway epithelial cells (**Figure 9**).[85] **Chapter 6** discusses adapting the aerosol platform as an *in vitro* lung exposure system to assess antibacterial efficacy of aerosol droplets containing lytic anti-Pseudomonas bacteriophage and antibiotic ciprofloxacin against 24-hour biofilm cultures of *P. aeruginosa.* Assays on air-liquid interface (ALI) cultures of Calu-3 airway epithelial cells exposed to aerosolized droplets containing anti-Pseudomonas bacteriophage assessed the *in vitro* safety profile.

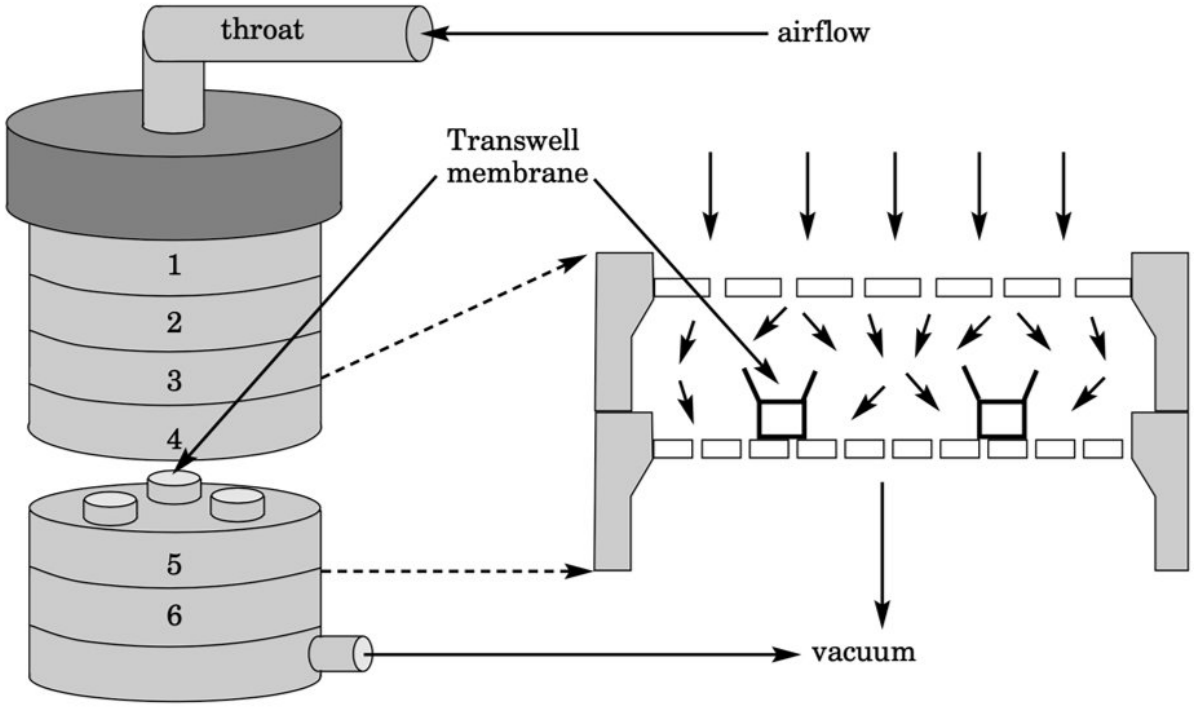

Figure 9. ***In vitro*** **lung exposure platform.** Transwell-cultures integrated into viable six-stage cascade impactor was used to model inhaled therapeutics delivery to the lungs. Adapted from Cooney et al.[85]

2.7. REFERENCES

1. Wang, C. C. *et al.* Airborne transmission of respiratory viruses. *Science* vol. 373 Preprint at https://doi.org/10.1126/science.abd9149 (2021).
2. Prather, K. A. *et al.* Airborne transmission of SARS-CoV-2. *Science* vol. 370 303–304 Preprint at https://doi.org/10.1126/science.abf0521 (2020).
3. Morawska, L. *et al.* How can airborne transmission of COVID-19 indoors be minimised? *Environ Int* **142**, 105832 (2020).
4. Fennelly, K. P. Particle sizes of infectious aerosols: implications for infection control. *The Lancet Respiratory Medicine* vol. 8 Preprint at https://doi.org/10.1016/S2213-2600(20)30323-4 (2020).
5. Morawska, L., Buonanno, G., Mikszewski, A. & Stabile, L. The physics of respiratory particle generation, fate in the air, and inhalation. *Nature Reviews Physics* **4**, 723–734 (2022).
6. Jones, R. M. & Brosseau, L. M. Aerosol transmission of infectious disease. *J Occup Environ Med* **57**, (2015).
7. Pöhlker, M. L. *et al.* Respiratory aerosols and droplets in the transmission of infectious diseases. *Rev Mod Phys* **95**, 045001 (2023).
8. Morawska, L. Droplet fate in indoor environments, or can we prevent the spread of infection? *Indoor Air* **16**, 335–347 (2006).
9. Niazi, S., Groth, R., Spann, K. & Johnson, G. R. The role of respiratory droplet physicochemistry in limiting and promoting the airborne transmission of human coronaviruses: A critical review. *Environmental Pollution* **276**, 115767 (2021).
10. Dhand, R. & Li, J. Coughs and Sneezes: Their Role in Transmission of Respiratory Viral Infections, including SARS-CoV-2. *American Journal of Respiratory and Critical Care Medicine* vol. 202 Preprint at https://doi.org/10.1164/rccm.202004-1263PP (2020).
11. Fernandez, M. O., Thomas, R. J., Oswin, H., Haddrell, A. E. & Reid, J. P. Transformative Approach To Investigate the Microphysical Factors Influencing Airborne Transmission of Pathogens. *Appl Environ Microbiol* **86**, (2020).
12. Gralton, J., Tovey, E., McLaws, M. L. & Rawlinson, W. D. The role of particle size in aerosolised pathogen transmission: A review. *Journal of Infection* vol. 62 Preprint at https://doi.org/10.1016/j.jinf.2010.11.010 (2011).
13. Joseph, J. *et al.* Role of bioaerosol in virus transmission and material-based countermeasures. *Exploration* **2**, 20210038 (2022).
14. Sungnak, W. *et al.* SARS-CoV-2 entry factors are highly expressed in nasal epithelial cells together with innate immune genes. *Nat Med* **26**, (2020).
15. Scheuch, G. Breathing Is Enough: For the Spread of Influenza Virus and SARS-CoV-2 by Breathing only. *J Aerosol Med Pulm Drug Deliv* **33**, (2020).
16. Wells, W. F. On air-borne infection: Study II. Droplets and droplet nuclei. *Am J Epidemiol* **20**, 611–618 (1934).
17. Yu, C. P., Nicolaides, C. P. & Soong, T. T. Effect of random airway sizes on aerosol deposition. *Am Ind Hyg Assoc J* **40**, (1979).
18. Kim, C. S. & Hu, S. C. Total respiratory tract deposition of fine micrometer-sized particles in healthy adults: Empirical equations for sex and breathing pattern. *J Appl Physiol* **101**, (2006).

19. Lai, J. *et al.* Relative efficacy of masks and respirators as source control for viral aerosol shedding from people infected with SARS-CoV-2: a controlled human exhaled breath aerosol experimental study. *EBioMedicine* **104**, (2024).
20. Leung, N. H. L. *et al.* Respiratory virus shedding in exhaled breath and efficacy of face masks. *Nat Med* **26**, 676–680 (2020).
21. Tellier, R., Li, Y., Cowling, B. J. & Tang, J. W. Recognition of aerosol transmission of infectious agents: A commentary. *BMC Infectious Diseases* vol. 19 Preprint at https://doi.org/10.1186/s12879-019-3707-y (2019).
22. De Perio, M. A. *et al.* Strategies for Optimizing the Supply of N95 Filtering Facepiece Respirators during the Coronavirus Disease 2019 (COVID-19) Pandemic. *Disaster Med Public Health Prep* **14**, (2020).
23. Qian, Y., Willeke, K., Grinshpun, S. A., Donnelly, J. & Coffey, C. C. Performance of N95 respirators: Filtration efficiency for airborne microbial and inert particles. *Am Ind Hyg Assoc J* **59**, (1998).
24. Konda, A. *et al.* Aerosol Filtration Efficiency of Common Fabrics Used in Respiratory Cloth Masks. *ACS Nano* **14**, (2020).
25. ASTM F2101. Standard Test Method for Evaluating the Bacterial Filtration Efficiency (BFE) of Medical Face Mask Materials , Using a Biological Aerosol of Staphylococcus aureus. *American Society for Testing and Materials* **i**, (2019).
26. Rengasamy, S., Shaffer, R., Williams, B. & Smit, S. A comparison of facemask and respirator filtration test methods. *J Occup Environ Hyg* **14**, (2017).
27. Walsh, D. C. & Stenhouse, J. I. T. The effect of particle size, charge, and composition on the loading characteristics of an electrically active fibrous filter material. *J Aerosol Sci* **28**, (1997).
28. Groth, R. *et al.* Toward Standardized Aerovirology: A Critical Review of Existing Results and Methodologies. *Environ Sci Technol* **58**, 3608 (2024).
29. Tang, J. W. The effect of environmental parameters on the survival of airborne infectious agents. *Journal of the Royal Society Interface* vol. 6 Preprint at https://doi.org/10.1098/rsif.2009.0227.focus (2009).
30. Huynh, E. *et al.* Evidence for a semisolid phase state of aerosols and droplets relevant to the airborne and surface survival of pathogens. *Proc Natl Acad Sci U S A* **119**, (2022).
31. French, A. J. *et al.* Environmental Stability of Enveloped Viruses Is Impacted by Initial Volume and Evaporation Kinetics of Droplets. *mBio* **14**, (2023).
32. Bangiyev, R., Chudaev, M., Schaffner, D. W. & Goldman, E. Higher Concentrations of Bacterial Enveloped Virus Phi6 Can Protect the Virus from Environmental Decay. *Appl Environ Microbiol* **87**, e0137121 (2021).
33. Dabisch, P. *et al.* The influence of temperature, humidity, and simulated sunlight on the infectivity of SARS-CoV-2 in aerosols. *Aerosol Science and Technology* **55**, (2021).
34. Santarpia, J. L., Reid, J. P., Wu, C. Y., Lednicky, J. A. & Oswin, H. P. The aerobiological pathway of natural respiratory viral aerosols. *TrAC Trends in Analytical Chemistry* **172**, 117557 (2024).
35. Labiris, N. R. & Dolovich, M. B. Pulmonary drug delivery. Part I: Physiological factors affecting therapeutic effectiveness of aerosolized medications. *British Journal of Clinical Pharmacology* vol. 56 588–599 Preprint at https://doi.org/10.1046/j.1365-2125.2003.01892.x (2003).

36. Niazi, S., Groth, R., Spann, K. & Johnson, G. R. The role of respiratory droplet physicochemistry in limiting and promoting the airborne transmission of human coronaviruses: A critical review. *Environmental Pollution* vol. 276 Preprint at https://doi.org/10.1016/j.envpol.2020.115767 (2021).
37. Groth, R., Cravigan, L. T., Niazi, S., Ristovski, Z. & Johnson, G. R. In situ measurements of human cough aerosol hygroscopicity. *J R Soc Interface* **18**, (2021).
38. Bourouiba, L. Fluid Dynamics of Respiratory Infectious Diseases. *Annu Rev Biomed Eng* **23**, 547–577 (2021).
39. Edwards, D. A. *et al.* Inhaling to mitigate exhaled bioaerosols. *Proc Natl Acad Sci U S A* **101**, (2004).
40. Edwards, D., Salzman, J., Devlin, T. & Langer, R. Nasal Calcium-Rich Salts for Cleaning Airborne Particles from the Airways of Essential Workers, Students, and a Family in Quarantine. *Mol Front J* **04**, 36–45 (2020).
41. Edwards, D. A. *et al.* Exhaled aerosol increases with COVID-19 infection, age, and obesity. *Proc Natl Acad Sci U S A* **118**, (2021).
42. Haddrell, A. *et al.* Differences in airborne stability of SARS-CoV-2 variants of concern is impacted by alkalinity of surrogates of respiratory aerosol. *J R Soc Interface* **20**, (2023).
43. Fahy, J. V. & Dickey, B. F. Airway Mucus Function and Dysfunction. *New England Journal of Medicine* **363**, (2010).
44. Song, D., Cahn, D. & Duncan, G. A. Mucin biopolymers and their barrier function at airway surfaces. *Langmuir* **36**, (2020).
45. Hill, D. B. *et al.* A biophysical basis for mucus solids concentration as a candidate biomarker for airways disease. *PLoS One* **9**, (2014).
46. Gutmann, D. *et al. Aerosol Measurement Identifies SARS-CoV 2 PCR Positive Adults Compared with Healthy Controls*. *medRxiv* (2022).
47. Bourouiba, L. The Fluid Dynamics of Disease Transmission. *Annu Rev Fluid Mech* **53**, 473–508 (2021).
48. Cevik, M. *et al.* SARS-CoV-2, SARS-CoV, and MERS-CoV viral load dynamics, duration of viral shedding, and infectiousness: a systematic review and meta-analysis. *Lancet Microbe* **2**, e13–e22 (2021).
49. Meyerowitz, E. A., Richterman, A., Gandhi, R. T. & Sax, P. E. Transmission of sars-cov-2: A review of viral, host, and environmental factors. *Annals of Internal Medicine* vol. 174 69–79 Preprint at https://doi.org/10.7326/M20-5008 (2021).
50. Pan, Y., Zhang, D., Yang, P., Poon, L. L. M. & Wang, Q. Viral load of SARS-CoV-2 in clinical samples. *The Lancet Infectious Diseases* vol. 20 Preprint at https://doi.org/10.1016/S1473-3099(20)30113-4 (2020).
51. He, X. *et al.* Temporal dynamics in viral shedding and transmissibility of COVID-19. *Nat Med* **26**, 672–675 (2020).
52. Zou, L. *et al.* SARS-CoV-2 Viral Load in Upper Respiratory Specimens of Infected Patients. *New England Journal of Medicine* **382**, (2020).
53. Huang, Z. *et al.* Bioaerosols in the atmosphere: A comprehensive review on detection methods, concentration and influencing factors. *Science of The Total Environment* **912**, 168818 (2024).
54. Santarpia, J. L., Ratnesar-Shumate, S. & Haddrell, A. Laboratory study of bioaerosols: Traditional test systems, modern approaches, and environmental control. *Aerosol Science and Technology* **54**, 585–600 (2020).

55. Kormuth, K. A. *et al.* Influenza Virus Infectivity Is Retained in Aerosols and Droplets Independent of Relative Humidity. *J Infect Dis* **218**, 739–747 (2018).
56. Löndahl, J. & Alsved, M. Abrupt decreases in infectivity of SARS-CoV-2 in aerosols. *Proc Natl Acad Sci U S A* **119**, e2208742119 (2022).
57. Oswin, H. P. *et al. The Dynamics of SARS-CoV-2 Infectivity with Changes in Aerosol Microenvironment*. https://doi.org/10.1101/2022.01.08.22268944 doi:10.1101/2022.01.08.22268944.
58. Oswin, H. P. *et al.* Measuring stability of virus in aerosols under varying environmental conditions. *Aerosol Science and Technology* **55**, 1315–1320 (2021).
59. Ruge, C. C., Kirch, J. & Lehr, C. M. Pulmonary drug delivery: From generating aerosols to overcoming biological barriers-therapeutic possibilities and technological challenges. *The Lancet Respiratory Medicine* vol. 1 Preprint at https://doi.org/10.1016/S2213-2600(13)70072-9 (2013).
60. Julia Altube, M. *et al.* Inhaled lipid nanocarriers for pulmonary delivery of glucocorticoids: previous strategies, recent advances and key factors description. *Int J Pharm* 123146 (2023) doi:10.1016/J.IJPHARM.2023.123146.
61. Tiddens, H. A. W. M., Bos, A. C., Mouton, J. W., Devadason, S. & Janssens, H. M. Inhaled antibiotics: Dry or wet? *European Respiratory Journal* vol. 44 Preprint at https://doi.org/10.1183/09031936.00090314 (2014).
62. Ke, W.-R. *et al.* Administration of dry powders during respiratory supports. *Ann Transl Med* **9**, (2021).
63. Bassetti, M., Vena, A., Russo, A. & Peghin, M. Inhaled Liposomal Antimicrobial Delivery in Lung Infections. *Drugs* vol. 80 Preprint at https://doi.org/10.1007/s40265-020-01359-z (2020).
64. Talwar, D. *et al.* The emerging role of nebulization for maintenance treatment of chronic obstructive pulmonary disease at home. *Lung India* vol. 38 Preprint at https://doi.org/10.4103/lungindia.lungindia_68_20 (2021).
65. Peng, S. *et al.* Nano-Formulations for Pulmonary Delivery: Past, Present, and Future Perspectives. *Pharmaceutics 2024, Vol. 16, Page 161* **16**, 161 (2024).
66. Hassett, D. J. *et al.* Pseudomonas aeruginosa biofilm infections in cystic fibrosis: Insights into pathogenic processes and treatment strategies. *Expert Opinion on Therapeutic Targets* vol. 14 Preprint at https://doi.org/10.1517/14728220903454988 (2010).
67. Høiby, N., Bjarnsholt, T., Givskov, M., Molin, S. & Ciofu, O. Antibiotic resistance of bacterial biofilms. *International Journal of Antimicrobial Agents* vol. 35 Preprint at https://doi.org/10.1016/j.ijantimicag.2009.12.011 (2010).
68. Cystic Fibrosis Canada. *CANADIAN CONSENSUS STATEMENT ON AEROSOLIZED ANTIBIOTIC USE IN CYSTIC FIBROSIS*. (2020).
69. Lechtzin, N. *et al.* Outcomes of adults with cystic fibrosis infected with antibiotic-resistant Pseudomonas aeruginosa. *Respiration* **73**, (2006).
70. Chan, B. K. *et al.* Phage selection restores antibiotic sensitivity in MDR Pseudomonas aeruginosa. *Sci Rep* **6**, (2016).
71. Chang, R. Y. K. *et al.* Proof-of-principle study in a murine lung infection model of antipseudomonal activity of phage PEV20 in a dry-powder formulation. *Antimicrob Agents Chemother* **62**, (2018).
72. Alemayehu, D. *et al.* Bacteriophages φMR299-2 and φNH-4 can eliminate Pseudomonas aeruginosa in the murine lung and on cystic fibrosis lung airway cells. *mBio* **3**, (2012).

73. Hyman, P. & Abedon, S. T. Bacteriophage Host Range and Bacterial Resistance. in *Advances in Applied Microbiology* vol. 70 217–248 (Academic Press Inc., 2010).
74. Loh, B. *et al.* Encapsulation and Delivery of Therapeutic Phages. *Appl Environ Microbiol* **87**, (2021).
75. Burrowes, B., Harper, D. R., Anderson, J., McConville, M. & Enright, M. C. Bacteriophage therapy: Potential uses in the control of antibiotic-resistant pathogens. *Expert Review of Anti-Infective Therapy* vol. 9 Preprint at https://doi.org/10.1586/eri.11.90 (2011).
76. Chan, H. K. & Chang, R. Y. K. Inhaled Delivery of Anti-Pseudomonal Phages to Tackle Respiratory Infections Caused by Superbugs. *Journal of Aerosol Medicine and Pulmonary Drug Delivery* vol. 35 Preprint at https://doi.org/10.1089/jamp.2021.0045 (2022).
77. Wang, X. *et al.* Prospects of Inhaled Phage Therapy for Combatting Pulmonary Infections. *Frontiers in Cellular and Infection Microbiology* vol. 11 Preprint at https://doi.org/10.3389/fcimb.2021.758392 (2021).
78. Bodier-Montagutelli, E. *et al.* Inhaled phage therapy for the treatment of acute Pseudomonas aeruginosa lung infections. in (2018). doi:10.1183/13993003.congress-2018.pa2649.
79. Lin, Y. *et al.* Synergy of nebulized phage PEV20 and ciprofloxacin combination against Pseudomonas aeruginosa. *Int J Pharm* **551**, 158–165 (2018).
80. Wittebole, X., De Roock, S. & Opal, S. M. A historical overview of bacteriophage therapy as an alternative to antibiotics for the treatment of bacterial pathogens. *https://doi.org/10.4161/viru.25991* **5**, 226–235 (2013).
81. Chan, B. K., Abedon, S. T. & Loc-Carrillo, C. Phage cocktails and the future of phage therapy. *Future Microbiol* **8**, 769–783 (2013).
82. Choi, V., Rohn, J. L., Stoodley, P., Carugo, D. & Stride, E. Drug delivery strategies for antibiofilm therapy. *Nature Reviews Microbiology 2023* 1–18 (2023) doi:10.1038/s41579-023-00905-2.
83. Adesanya, O., Oduselu, T., Akin-Ajani, O., Adewumi, O. M. & Ademowo, O. G. An exegesis of bacteriophage therapy: An emerging player in the fight against anti-microbial resistance. *AIMS Microbiol* **6**, 204–230 (2020).
84. Kortright, K. E., Chan, B. K., Koff, J. L. & Turner, P. E. Phage Therapy: A Renewed Approach to Combat Antibiotic-Resistant Bacteria. *Cell Host and Microbe* vol. 25 Preprint at https://doi.org/10.1016/j.chom.2019.01.014 (2019).
85. Cooney, D., Kazantseva, M. & Hickey, A. J. Development of a size-dependent aerosol deposition model utilising human airway epithelial cells for evaluating aerosol drug delivery. *ATLA Alternatives to Laboratory Animals* **32**, (2004).

Chapter 3. Protocol for bacterial filtration efficiency evaluations of facemask materials using viable bacteria-laden aerosol droplets

Preface. This chapter discusses the operational details of the aerosol platform, serving as the experimental and methodological foundation for research in chapters 4, 5, and 6. ***The results and conclusions presented in this chapter are valid under specific conditions and assumptions outlined in the study. Therefore, the accuracy and reliability of the findings depend on defined test conditions. These results may not be applicable under all circumstances or in different environments. Users of this information should exercise caution and consider additional factors relevant to their specific context before applying these results to describe and interpret real-world phenomena.***

Contributions. I developed and optimized the experimental procedures, conducted the aerosol trials, and incorporated edits from coauthors. Ekaterina Kvitka photographed the components of the aerosol platform (**Figures 2, 3**), wrote sections of the protocol, designed the graphical abstract, and edited the final manuscript draft. Dr. Mellissa Gomez assisted with the manuscript organization, wrote protocol sections, and edited the final manuscript draft. Dr. Fereshteh Bayat and Kyle Jackson wrote protocol sections and edited the final manuscript draft. Rod G. Rhem constructed the aerosol platform and provided input to troubleshoot issues and optimize operational parameters. Dr. Zeinab Hosseinidoust and Prof. Myrna B. Dolovich were responsible for funding acquisition, methods development, project administration, supervision, weekly meetings, and review and scientific editing of the final manuscript drafts. Paul Gatt, Justin Bernar, John Colenbrander from the Chemical and Mechanical Engineering Machine Shop and Doug Keller were instrumental in helping to design and build the aerosol platform.

Citation. This chapter is under review, STAR PROTOCOLS.
Thirugnanasampanthar, M., Kvitka, E., Gomez, M., Jackson, K., Bayat, F., Rhem, R. G., Dolovich, M. B., & Hosseinidoust, Z. (2024). Protocol for bacterial filtration efficiency evaluations of facemask materials using viable bacteria-laden aerosol droplets.

3.1. SUMMARY

This protocol details step-by-step procedures for determining the bacterial filtration efficiencies of facemask materials according to the ASTM standard F2101-19.[1] Also addressed are methods for the reproducible generation, collection, and enumeration of viable bacteria-laden aerosols containing the bacterial pathogen *Staphylococcus aureus*. The optimized operating parameters generate 1700 to 3000 viable bacteria-laden aerosol droplets between 2.7 to 3.3 µm. For complete details on the use and execution of this protocol, please refer to Thirugnanasampanthar et al.[2]

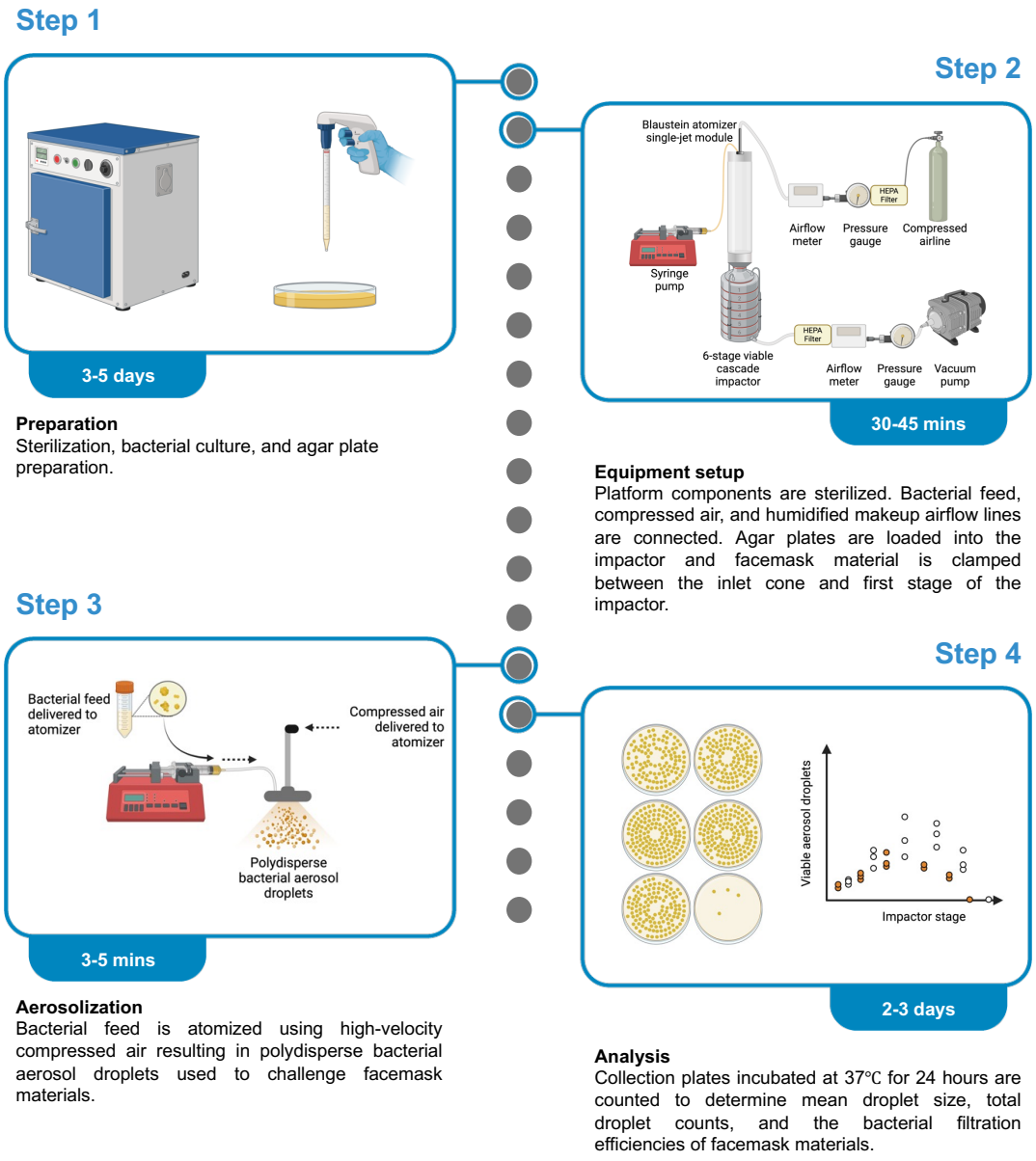

Graphical abstract – Illustration depicts four main steps involved in bacterial filtration efficiency evaluations of facemask materials within the aerosol platform.

3.2. BEFORE YOU BEGIN

The American Society for Testing and Materials (ASTM) standard F2101-19 provides the blueprint for a test platform for generating viable bacteria-laden aerosol droplets and conducting bacterial filtration efficiency evaluations on facemask materials.[1] We constructed and optimized the ASTM standard F2101-19 test setup for filtration efficiency testing of facemask materials. Over a year was spent designing the infrastructure, optimizing test conditions, and verifying test results. Identified limitations and ambiguities of the standard can potentially hinder reproducible data from being generated by independent laboratories. This work aims to guide the setup and validation of bacterial filtration efficiency test platforms based on the ASTM standard F2101-19 to obtain highly reproducible and repeatable test results.

Viable bacteria-laden aerosol generation begins with the bacterial feed suspension preparation in peptone water, a commonly used microbial growth medium.[3] The feed suspension delivery to the Blaustein atomizer single-jet module, at a flow rate of 10.2 mL/h, is controlled using a syringe pump. Compressed air delivery to the atomizer, at an airflow rate of 1.5 litres per minute (LPM), is controlled using a pressure gauge and monitored using an airflow meter. The high-velocity airflow from the atomizer nozzle breaks up the liquid feed, forming polydisperse aerosol droplets. These droplets are propelled downwards into a 60-cm-high glass aerosol mixing chamber and mixed with the makeup air drawn into the chamber.

A downstream vacuum pump draws the aerosol droplets from the glass chamber at a volumetric airflow rate of 28.3 LPM and into the six-stage viable cascade impactor, which separates the droplets based on aerodynamic size. Glass Petri dishes containing 27 mL of agar medium are loaded into the six-stage viable cascade impactor to collect droplets through impaction.[4] The viable bacteria-laden droplets are detected based on the number of colony-forming units (CFU) observed on the agar medium after 18-24 hours of incubation at 37°C. Coincidence correction is applied to raw count values to account for the likelihood of multiple viable bacteria-laden droplets impinging on the same region of the agar medium to produce a single CFU.[5]

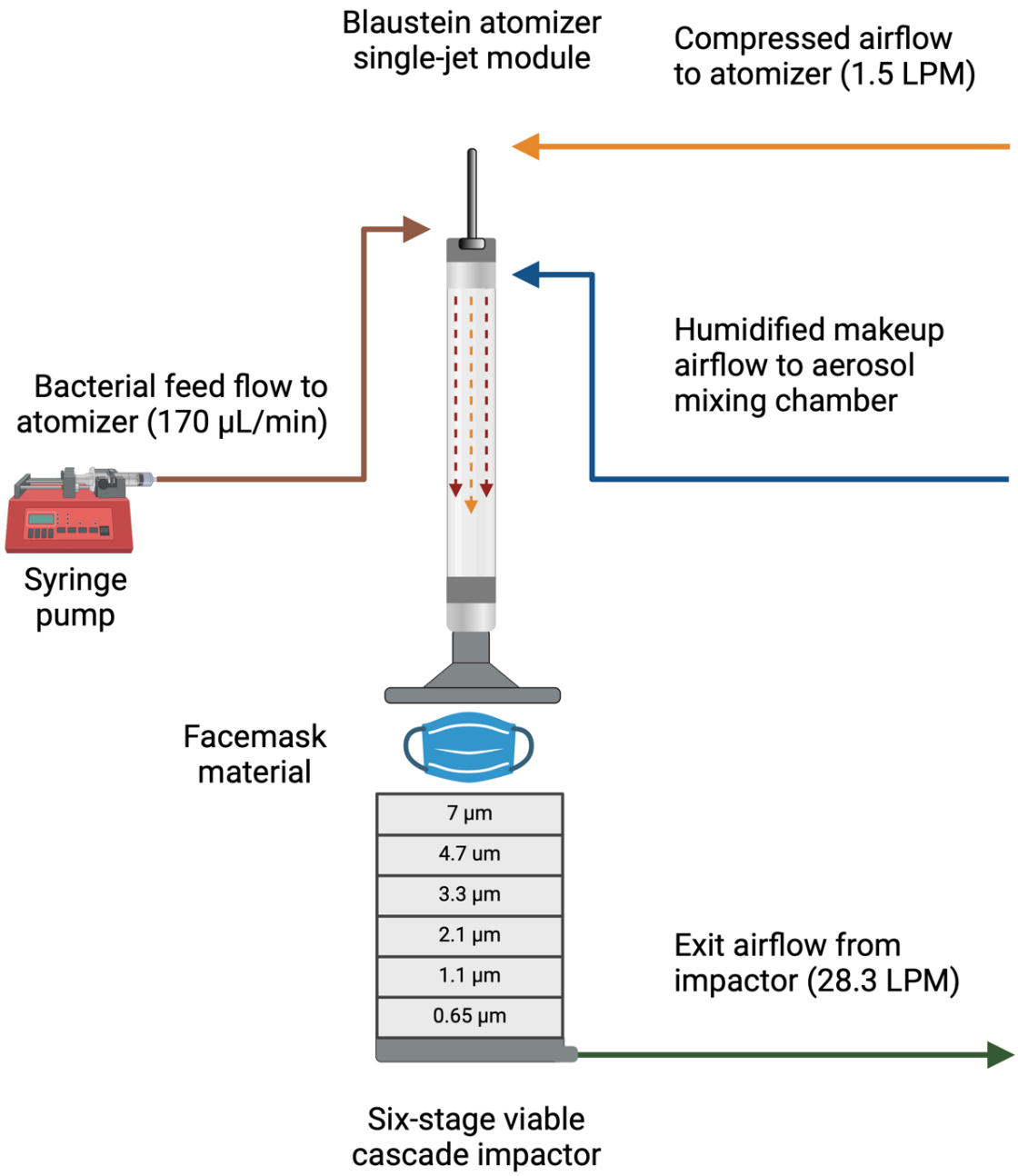

Figure 1. Aerosol platform inflow and outflow lines. Schematic depicts the three inflow lines: bacterial feed delivery to the atomizer at 170 µL/min, compressed airflow delivery to the atomizer at 1.5 L/min, and the humidified makeup air to the 60-cm-high glass aerosol mixing chamber. The outflow line carries the suctioned from the system at 28.3 L/min.

3.3. KEY RESOURCES TABLE

REAGENT or RESOURCE	SOURCE	IDENTIFIER
Antibodies		
Bacterial and virus strains		
Staphylococcus aureus subsp. *aureus* Rosenbach	ATCC	ATCC 6538
Biological samples		
Chemicals, peptides, and recombinant proteins		
Sodium chloride	Fisher Scientific	S271-500
Glycerol	Fisher Scientific	BP229-1
Trypticase soy broth	BD	B211825
Phosphate buffered saline	Fisher Scientific	BP2944-100
Molecular grade agar	Fisher BioReagents	BP1423500
Peptone water	Thermo Scientific	CM0009
Ultrapure water	Millipore Direct-Q	ZRQSVP3WW
Bleach disinfectant tablets	Berkshire	EZBDT101
Ethyl alcohol	Greenfield Global	64-17-5
Critical commercial assays		
Deposited data		
Experimental models: Cell lines		
Experimental models: Organisms/strains		
Oligonucleotides		
Recombinant DNA		
Software and algorithms		
Other		
Syringe pump	Fisherbrand	780100I
Pressure gauge	IMI NORGREN	R72G-2AK-RFG
Upstream flow meter	Omega	FMA-A2317
Blaustein Atomizer Single-Jet Model	CH Technologies	ARGBLM2
10-40 Blaustein expansion plate	CH Technologies	ARGBLM0031
6-stage viable cascade impactor	Tisch Environmental	TE-10-800
Glass petri dishes	PYREX	3160-100
Downstream flow meter	TSI	5300 Series
Vacuum pump	GAST	0823-101Q-G608NEX
Temperature and humidity sensor	SensorPush	HT.w
Water-to-gas humidifier	PermaPure	FC-125-240-5MP
Capsule filter	TSI	1602051
Steam sterilizer	Yamato	SM301
Precision balance	Mettler Toledo	ME203E
Analytical balance	Mettler Toledo	XS105
Forced air oven	VWR	89511-414

Microbiological incubator	Fisherbrand	151030518
Incubator shaker	Fisher Scientific	11-675-209
Refrigerated centrifuge	Eppendorf	5430R
Ultra freezer	Innova	U353
Fridge	Frigidaire	16 CF
1 L Glass media bottle	Fisherbrand	FB8001000
250 mL Glass media bottle	Fisherbrand	FB800250
0.22 µm Sterile syringe filters	Fisher Scientific	13100106
0.45 µm Sterile syringe filters	Fisher Scientific	13100107
15 mL centrifuge tube	VWR	10025-686
50 mL centrifuge tube	VWR	10025-696
Plastic petri dishes	Fisher Scientific	FB0875712
5 mL syringe	BD	309646
10 mL Polystyrene serological pipets	Basix	14955234
25 mL Polystyrene serological pipets	Basix	14955235
50 mL Polystyrene serological	Basix	14955236
0.5 – 10 µl Filtered tip	VWR	76322-132
20 - 200 µl Filtered tip	VWR	76322-150
100 - 1000 µl Filtered tip	VWR	76322-154
0.5 – 10 µl Mechanical pipetter	Sartorius	728020
20 – 200 µl Mechanical pipetter	Sartorius	728060
100 – 1000 µl Mechanical pipetter	Sartorius	728070
1 - 100 mL Pipet controller	Fisher Scientific	14559561
1.7 mL Microcentrifuge tubes	Corning	C3207
Light-duty tissue wipers	VWR	82003-820
8 x 12 Autoclave bags	Fisherbrand	44-561
Autoclave indicator tape	Fisherbrand	15-904
Rainbow tape	Fisherbrand	1590110R
Inoculating loops	VWR	89126870
L-Shaped cell spreaders	Fisherbrand	14-665-231
Weighing dish	Fisherbrand	02-202-101
Aluminum weighing dish	Fisherbrand	08-732-101
1/16’’ x 3/16’’ ID/OD silicone tubing	McMaster-Carr	51135K608
1/8’’ x 1/4’’ ID/OD Firm polyurethane tubing	McMaster-Carr	5648K74
1/4’’ x 3/8’’ ID/OD Firm polyurethane tubing	McMaster-Carr	5648K71
Tube coupling sockets for 1/6’’ barbed tube ID	McMaster-Carr	51525K281
Push-to-connect tube fitting for 3/8’’ OD tube	McMaster-Carr	5779K16
Push-to-connect tube fitting for 1/2’’ X 3/8’’ tube OD	McMaster-Carr	5779K355
Diverting valve for 3/8 tube ID	McMaster-Carr	3037N12

3.4. MATERIALS AND EQUIPMENT SETUP

Tryptic soy broth recipe

Reagent	Final concentration (g/L)	Amount
Tryptic soy broth	N/A	15 g
Total	**-**	**500 mL**

Note: Dissolve in 500 mL of deionized water and autoclave.

Tryptic soy agar recipe

Reagent	Final concentration (g/L)	Amount
Tryptic soy broth	N/A	15 g
Agar	N/A	7.5
Total	**-**	**500 mL**

Note: Dissolve in 500 mL of deionized water and autoclave.

Peptone water recipe

Reagent	Final concentration (g/L)	Amount
Peptone water	N/A	7.5 g
Total	**-**	**500 mL**

Note: Dissolve in 500 mL of ultrapure water and autoclave.

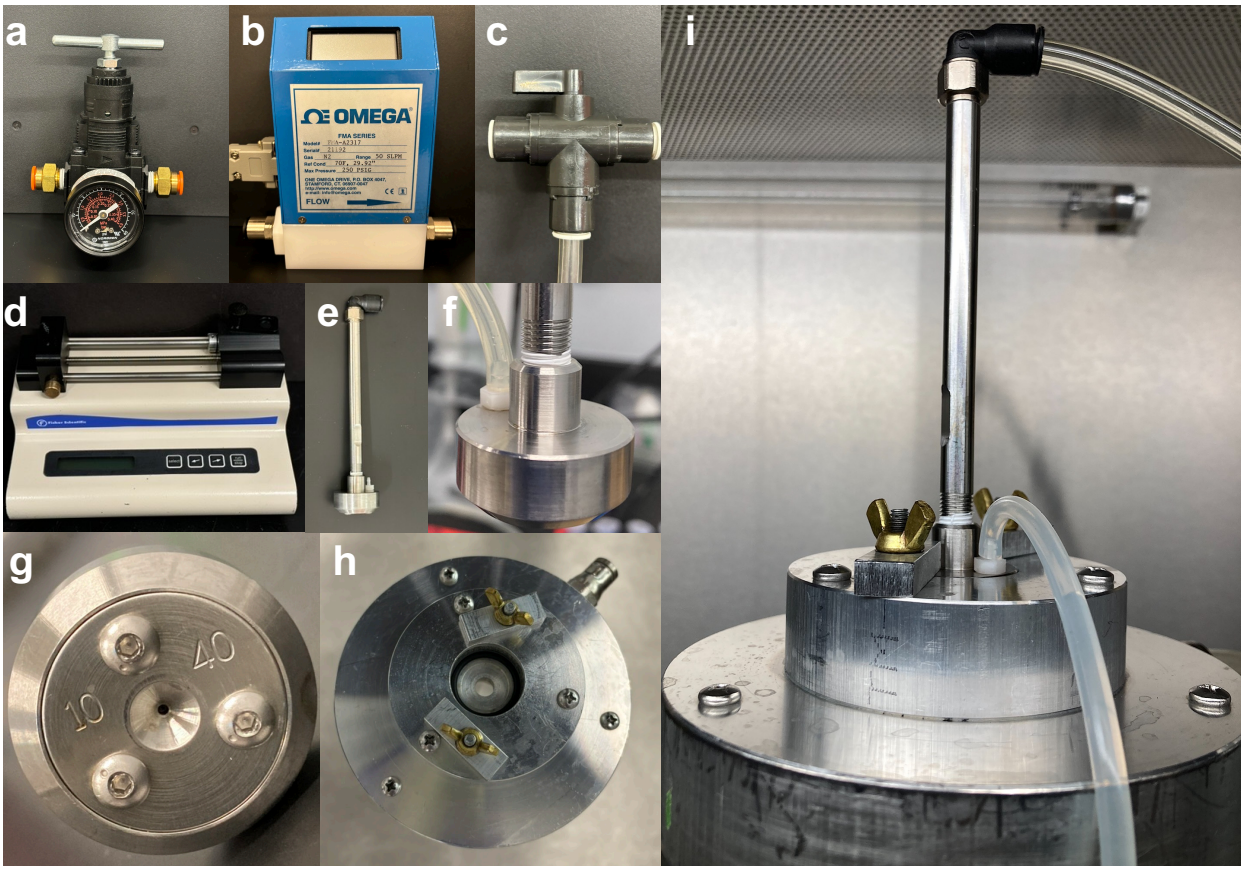

Figure 2. Upstream components of the aerosol platform. The figure depicts **(a)** a pressure gauge controlling the compressed airflow to the atomizer, **(b)** an OMEGA airflow meter used to monitor the atomizer airflow, **(c)** a diverting valve, **(d)** a syringe pump, **(e)** single-jet Blaustein atomizer, **(f)** atomizer nozzle with the feed inlet port attached to the silicone tubing, **(g)** 10-40 expansion plate with a 0.0254 mm diameter jet, **(h)** top-down view of the notch designed into the top-plate of the aerosol chamber that accommodates the single-jet Blaustein atomizer containing a black O-ring, and (i) single-jet atomizer secured into the notch on top of the aerosol mixing chamber secured with wing-nuts.

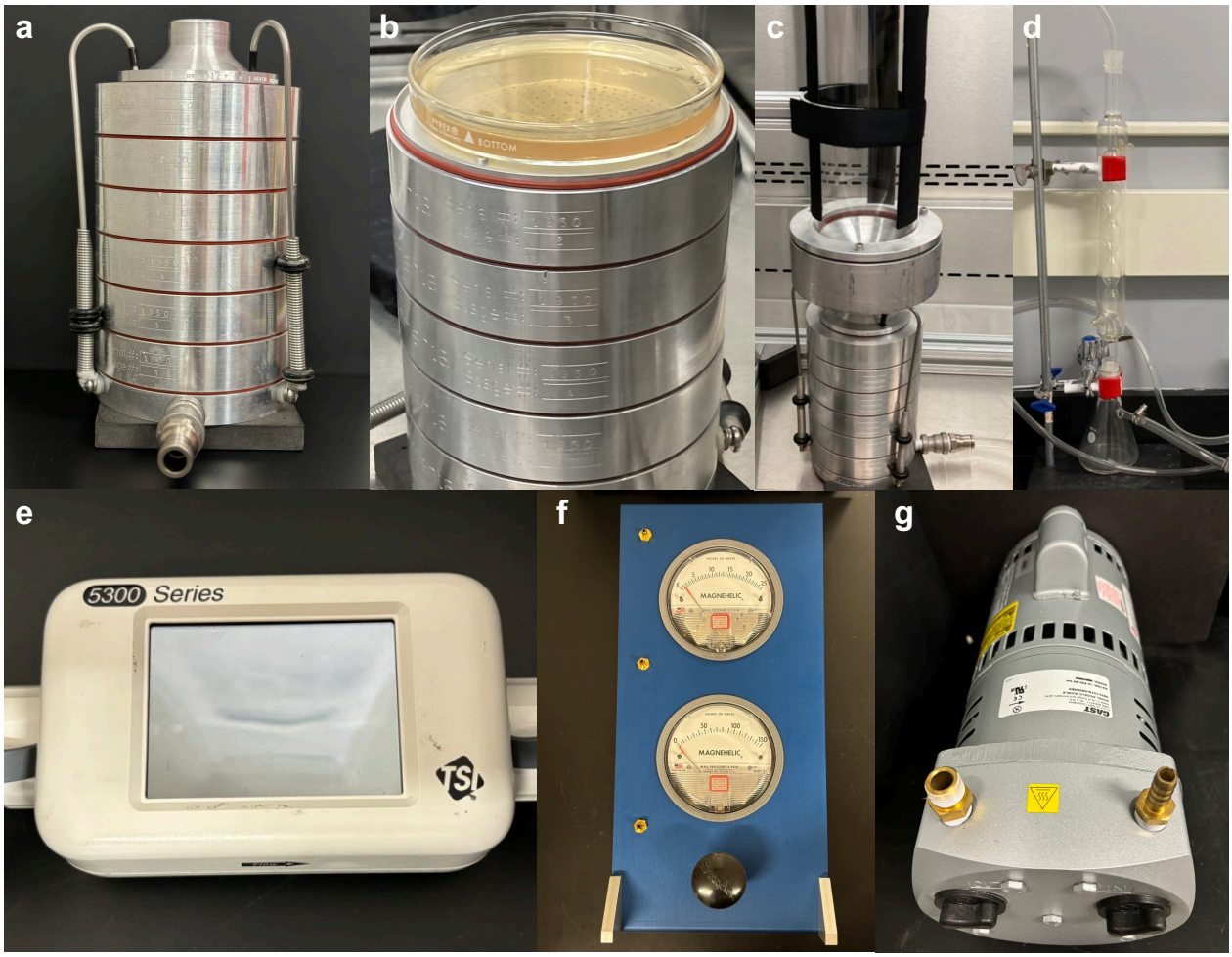

Figure 3. Downstream components of the aerosol platform. The figure depicts **(a)** a fully-assembled six-stage viable cascade impactor, **(b)** a glass Petri dish containing 27 mL of trypticase soy agar and balance on metal platforms on the second impactor stage, **(c)** a 60-cm-high glass aerosol mixing chamber positioned over the inlet of the six-stage cascade impactor, **(d)** a condenser tube, **(e)** a TSI airflow meter used to monitor airflow through the aerosol platform, **(f)** a downstream vacuum pressure gauge, and (g) a GAST vacuum pump.

3.5. STEP-BY-STEP METHOD DETAILS

Sterilization of glass Petri dishes
Timing: 2-3 hours
This section describes the sterilization of glass Petri dishes.

1. Place glass Petri dishes with lids into 8×12-inch autoclave bags in an inverted position (lid down) to prevent moisture accumulation during the autoclave cycle.
2. Seal the autoclave bag with indicator tape to secure the plates.
3. Sterilize the Petri dishes at 121°C and 15 psi of pressure for 20 minutes.
4. After sterilization, dry the Petri dishes in an oven at 60°C for at least 48 hours.

Note: *Ensure the autoclaved plates are sufficiently dry before preparing the TSA agar medium. All items are sterilized using 70% ethanol, prepared with 100% ethanol diluted with deionized water.*

Tryptic soy agar preparation
Timing: 2-3 hours
This section describes the preparation and sterilization of tryptic soy agar medium, 12 hours before pouring the plates.

1. Weigh out 7.5 g of agar and 15 g of trypticase soy broth
2. Add dry ingredients to 500 mL of deionized water in an autoclave-safe 1L glass bottle.
3. Mix the contents, partially close the lid, and place an autoclave indicator tape.
4. Sterilize the media in a steam sterilizer set to 121^{o}C for 20 min.
5. After sterilization, place the media bottles in a water bath (or equivalent) set to 50-60^{o}C to prevent media from solidifying.

Tryptic soy agar plate preparation
Timing: 2-3 hours
This section describes the preparation of Petri dishes with 27 mL of TSA agar medium under sterile conditions.

1. Turn on the biosafety cabinet (BSC) and allow the fan to operate until airflow reaches 100% or until the screen indicator reads “OK”.
2. Remove all items from the cabinet and sanitize the space by spraying with 70% ethanol and wiping dry surfaces with paper towels.
3. Before bringing them into the BSC, spray the items with 70% ethanol: autoclave bags containing sterilized Petri dishes, pipette gun, 25 mL serological pipettes, and sterilized TSA media.
4. Let all the items dry inside the BSC before starting the work.
5. Carefully open the autoclave bag with Petri dishes without touching the inner surfaces of the plate or lid.
6. Arrange the plates in the working area, avoiding corners and edges of the BSC to prevent poured plates from having slanted or uneven surfaces.
7. Pipette 27 mL of media into each plate using sterile serological pipettes; draw up 30 mL of TSA using a 25 mL serological pipette (33 mL capacity) and dispense until 3 mL remains in the pipette to prevent bubbles.
8. Let the poured plates solidify inside the BSC for 20-25 minutes without the lid to prevent condensation.
9. Once the plates are dry, cover them with lids and store them in stacks of 10 packed inside new autoclave bags
10. Stored plates at room temperature for up to 1 month.

Note: *Leaving the plates under the airflow for significantly longer than 25 minutes can result in loss of moisture and reduced volume of the agar layer. Insufficient drying time can cause moisture retention and increase the risk of contamination during storage. Lastly, avoid passing arm over poured plates to minimize risk of contamination.*

Bacterial culture preparation from single colony isolate
Timing: 30 minutes
This section describes the preparation of a bacterial streak plate and an overnight culture from a single colony isolate within a sterile environment (sterilized BSC).

1. Bacterial stocks are stored at -80°C in vials with 25% v/v glycerol.

2. Using a sterile inoculation loop, streak *S. aureus* bacteria from the frozen, 25% v/v glycerol stocks onto 100 mm × 15 mm TSA plates.
3. Incubate the streak plate at 37°C for 16–18 hours in a stationary incubator to allow for bacterial growth.

Note: *We recommend preparing multiple glycerol stocks from an overnight culture of a single colony isolate but only using one working stock (labelled) at a time, to avoid cross contamination and minimize the effects of freeze-thaw. If abnormal growth or contamination occurs, discard the working stock vial and use a new vial.*

Overnight bacterial culture preparation

Timing: 1 day

This section describes overnight culture preparation from a single colony isolate within a sterile environment (sterilized BSC).

1. Aliquot 5 mL of sterile TSB into two sterile culture tubes.
2. Designate one tube for the overnight (ON) bacterial culture and the other as a sterility control for the media.
3. Use an inoculation loop to transfer a single bacterial colony isolate from the streaked plate into the 5 mL aliquot of TSB in the designated culture tube.
4. Place both culture tubes into an incubator set to 37°C with an orbital shaker at 180 rpm to grow the bacteria for 16–18 hours.
5. The next day, confirm the absence of growth in the control tube and transfer the overnight culture from the incubator to the fridge (4°C) for storage.
6. Do not store overnight culture longer than 3-5 days.

Washing and resuspension of the bacterial culture and dilution plating

Timing: 1 hour

This section describes pelleting, resuspension, dilution, and plating of an overnight bacterial culture.

1. Centrifuge the overnight culture at 7000 × g for 5 minutes to pellet the bacterial cells.
2. Carefully decant the supernatant into a sterile container to isolate the bacterial pellet.
3. Add 5 mL of sterile phosphate-buffered saline (PBS) to the bacterial pellet and resuspend the bacteria by vortexing.
4. Label six sterile Eppendorf tubes with the following dilution values: 10^{-1}, 10^{-2}, 10^{-3}, 10^{-4}, 10^{-5}, 10^{-6}.
5. Aliquot 900 µL of sterile PBS into each labelled Eppendorf tube.
6. Transfer 100 µL of the washed bacterial culture into the first Eppendorf tube for a 10^{-1} dilution.
7. Ensure thorough mixing by pipetting up and down and vortexing the tube.
8. Transfer 100 µL from the 10^{-1} dilution tube to the 10^{-2} dilution tube and mix again.
9. Repeat this process for all dilutions (10^{-3}, 10^{-4}, 10^{-5}, 10^{-6}).
10. Plate 100 µL of 10^{-5} dilution in triplicates onto 100×15 mm TSA plates.
11. Uniformly spread the bacterial suspension on agar using a sterile L-shaped spreader.
12. Repeat the procedure for the 10^{-6} dilution.
13. Allow plates to dry in the BSC for 3-5 minutes.
14. Invert the plates and incubate at 37°C for 16–18 h for bacterial growth.

Bacterial feed preparation
Timing: 1 hour

1. Determining the concentration of the washed bacterial culture
    a. Following the incubation period, choose the plates with 30-300 colonies.
    b. Count the colonies on the selected plates to determine the bacterial concentration.
    c. Calculate the average colony count from the three replicate plates.
    d. Use the average colony count to calculate the concentration of the washed overnight culture using the formula: *CFU/mL* (Colony-forming units/milliliter) = $(number\ of\ colonies \times dilution\ factor)$/ *volume plated in mL.*
2. Bacterial feed suspension preparation.
    a. Aliquot 10 mL of 1.5% w/v peptone water solution to a sterile 15 mL falcon tube.
    b. Vortex the bacterial suspension in PBS to ensure thorough mixing.
    c. Add an appropriate volume of the overnight culture (based on the concentration) to the peptone water solution to prepare a 1×10^5 feed suspension.
3. Serial dilution and plating of bacterial feed suspension.
    a. Label sterile Eppendorf tubes with the dilution factor.
        i. 10^{-1}, 10^{-2}, and 10^{-3}.
    b. Add 900 µL of sterile PBS into each labeled tube.
    c. Transfer 100 µL of the feed suspension into the Eppendorf tube labeled 10^{-1}.
    d. Thoroughly mix by pipetting up and down and vortexing the tube.
    e. Transfer 100 µL from the 10^{-1} dilution tube to the 10^{-2} dilution tube and mix again.
    f. Repeat the dilution process until the desired dilution.
    g. Take 100 µL of each dilution and plate in triplicates onto 100×15 mm TSA plates.
    h. Ensure uniform spreading of the bacterial suspension on the agar plates using a sterile L-shaped spreader.
    i. Let the plates dry in the BSC for 3-5 minutes.
    j. Transfer the plates to a static incubator set to 37°C for 16–18 hours for bacterial growth to confirm the concentration of the feed suspension used to generate bacteria-laden aerosol droplets.

Note: *We commend preparing the bacterial feed an hour before the aerosol trials to prevent bacteria from continuing to multiply in the fresh peptone water media at room temperature, resulting in a higher bacterial concentration during aerosolization than the concentration indicated by the dilution plates.*

Connect inflow and outline lines
Timing: 15-25 minutes

This section describes the equipment setup and connections prior to conducting an aerosol run.

1. Flow meters (**Figure 4**).
    a. Connect the upstream (OMEGA) and downstream (TSI) airflow meters to a power outlet.
    b. Make sure that flow meters are initially reading at 0.00 LPM.
2. BSC
    a. Turn on the BSC and wait 10-15 minutes for the sterile air curtain to stabilize.
    b. Sterilize reachable surfaces of the BSC with 70% ethanol spray, followed by wiping down with paper towels.

   c. The surfaces sprayed with 70% ethanol should be completely dry before sterile work can commence.
3. Inflow – Compressed airflow to Blaustein atomizer single-jet module (**Figure 4**).
   a. Compressed air valve
   b. HEPA capsule filter
   c. Upstream pressure gauge
   d. Upstream airflow meter
   e. Atomizer
4. Inflow – Humidified airflow to 60-cm-high glass aerosol mixing chamber (**Figure 4**).
   a. HEPA capsule filter
   b. Perma-pure water-to-air humidifier
   c. Aerosol mixing chamber
5. Outflow – Airflow from 6-stage viable cascade impactor (**Figure 4**)
   a. Impactor outlet
   b. Condenser
   c. HEPA capsule filter
   d. Downstream pressure gauge
   e. Downstream airflow meter
   f. Vacuum pump

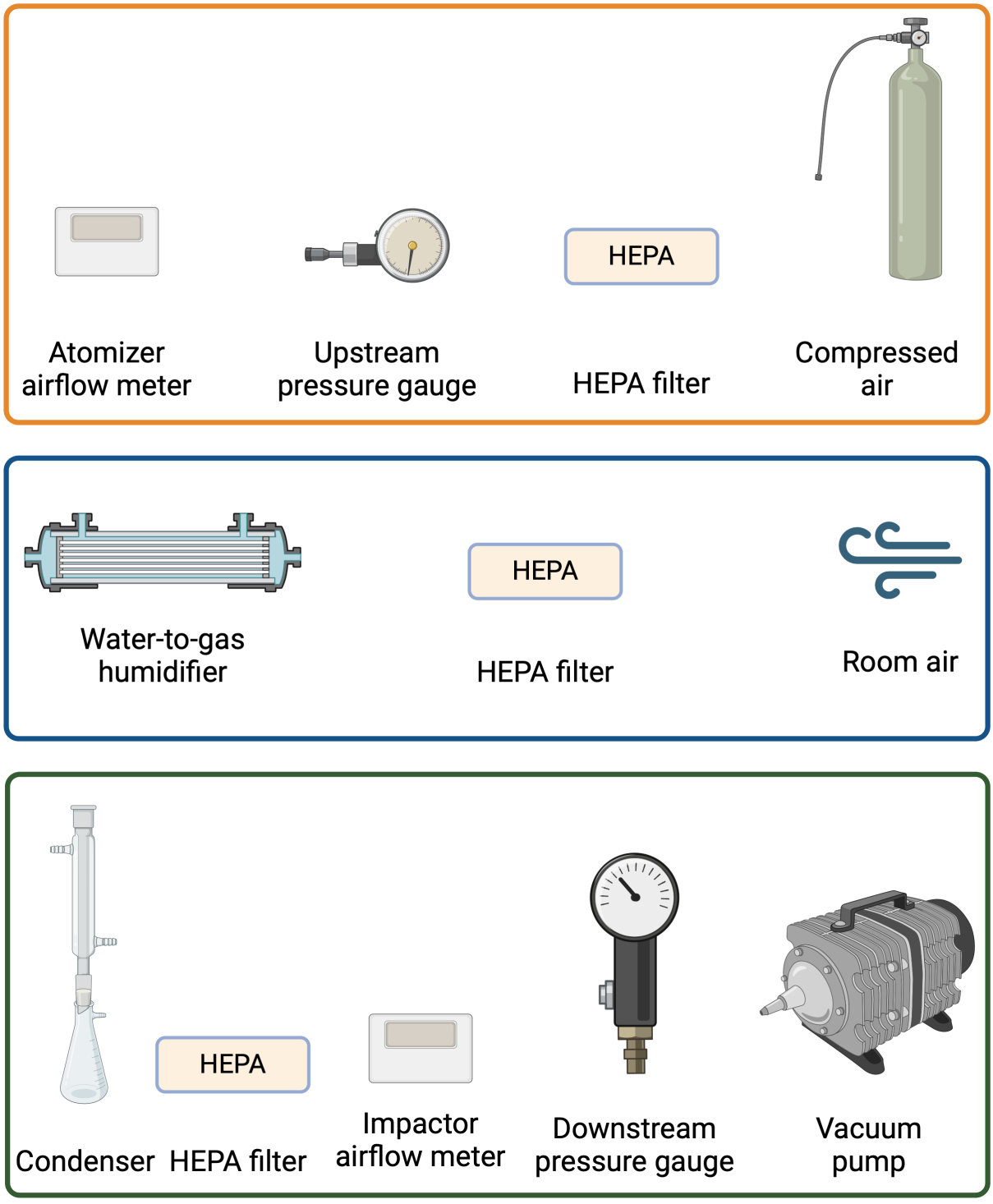

Figure 4. Components of the inflow and outflow lines. Bacterial feed delivery to the atomizer at 170 µL/min is controlled using the syringe pump. Compressed airflow delivery to the atomizer at 1.5 L/min is filtered through a HEPA capsule filter and is controlled using a pressure gauge and monitored using an upstream airflow meter. The humidified air to the 60-cm-high glass aerosol mixing chamber at 26.8 L/min is room air that is passed through a water-to-gas humidifier and

filtered through a HEPA capsule filter before entering the system. The outflow line shows the rate of airflow suctioned from the system at 28.3 L/min.

Equipment sterilization and assembly
Timing: 45 minutes

1. 60-cm-high glass mixing chamber.
    a. Carefully remove the glass chamber from the stand.
    b. Place the chamber in a horizontal position within the BSC.
    c. Sterilize the chamber by spraying the inner surfaces with 70% ethanol.
    d. Rotate the chamber to ensure the ethanol covers all regions.
    e. Return the chamber to a vertical position and secure it on the stand to allow excess ethanol to drain.
    f. Use the compressed air line to dry the inner surfaces of the glass chamber before use.
2. Blaustein atomizer single-jet module operated in atomizer mode (**Figure 4**).
    a. Connect the compressed air line to the atomizer.
    b. Submerge the atomizer in 200 mL of 70% ethanol solution.
    c. Turn on the compressed airflow valve and allow medium-velocity airflow through the submerged atomizer to clean the nozzle.
    d. Maintain airflow through the submerged atomizer for 2-3 minutes; air bubbles will form.
    e. Remove the atomizer from the ethanol bath and allow high-velocity airflow to dry the atomizer nozzle.
    f. Use a Kim wipe to dab the nozzle of the atomizer to ensure it is free of ethanol before proceeding to the aerosolization step.
3. Syringe pump delivers bacterial feed to Blaustein atomizer single-jet module (**Figures 5, 6**).
    a. Connect the syringe pump to a power outlet inside the BSC.
    b. Ensure the 5 mL BD syringe and a flow rate of 10.2 mL/hr are selected.
    c. Carefully attach a length of sterilized silicone tubing to the 5 mL BD syringe using a sterile coupling socket.
    d. Aspirate the desired feed solution into the 5 mL BD syringe and securely affix it to the syringe pump.
    e. Connect the other end of the silicone tubing to the feed inlet port on the atomizer nozzle.
4. 6-Stage viable cascade impactor (**Figures 7-9**)
    a. Sterilize all impactor stages by spraying with 70% ethanol.
    b. Wipe down the stages with paper towels to remove excess ethanol.
    c. Use the compressed air line to dry the stages and ensure the stage perforations are unobstructed.
    d. Examine perforations on the stages by holding them up to the light to ensure the absence of obstructions, especially for the lower stages with finer perforations.
    e. Place prepared glass petri dishes on the raised metal platforms, and place the dry, sterilized stage over the dish.

f. If performing a facemask material challenge, place the material between the inlet cone and first stage of the impactor, noting whether the inner or outer surface of the material is oriented towards the droplets.
g. Secure the assembled impactor with the three spring-loaded clamps.

5. Connect
   a. Bacterial feed line to Blaustein atomizer (**Figure 5**).
      i. Attach silicone tubing to the sterile 5 mL BD syringe using a sterile tube coupling socket.
      ii. Load the syringe with an appropriate volume of the bacterial feed.
      iii. Attach the other end of the silicone tubing to the feed inlet port of the atomizer.
   b. Compressed airline to Blaustein atomizer (**Figure 6**).
      i. Affix the feed tubing from the tubing attached to the atomizer to the top of the 60-cm sterilized chamber.
      ii. Affix the atomizer to the top of the aerosol mixing chamber and secure it with wingnuts to finger tight.
   c. Humidified makeup airline to 60-cm-high glass mixing chamber (**Figure 6**).
      i. Connect the humidified makeup airline to the chamber.
      ii. Internal humidity within the aerosol platform should be ≥80% relative humidity during droplet generation and collection period.
   d. Place the aerosol chamber on the 6-stage viable cascade impactor assembled with the collection plates (**Figures 7-9**).
   e. Securely attach the outlet airline to the impactor (**Figures 8,9**).

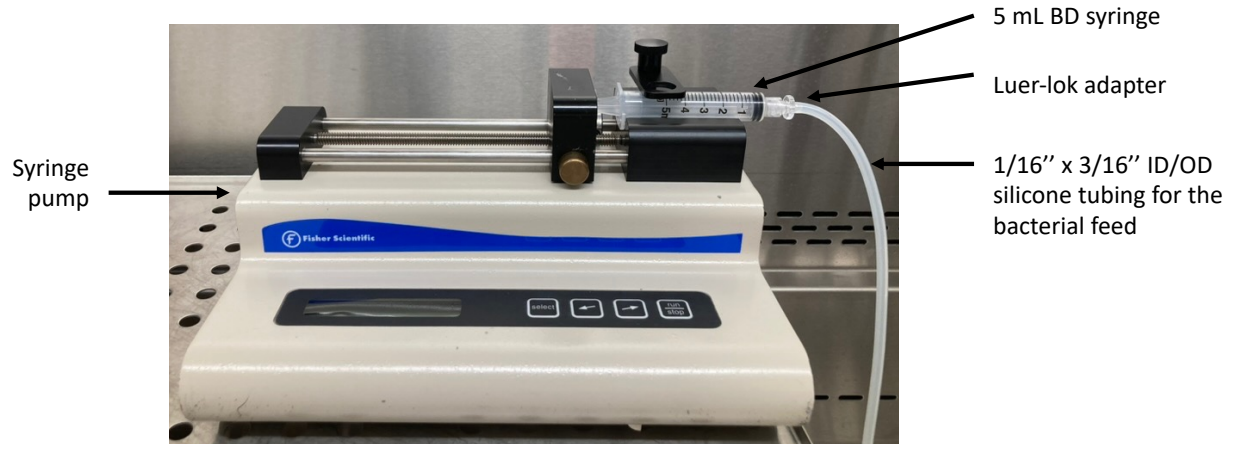

Figure 5. Bacterial feed line. The figure depicts the syringe pump containing a 5 mL syringe connected via a luer-lok adapter to the silicone tubing that will connect to the feed inlet valve on the single-jet Blaustein atomizer.

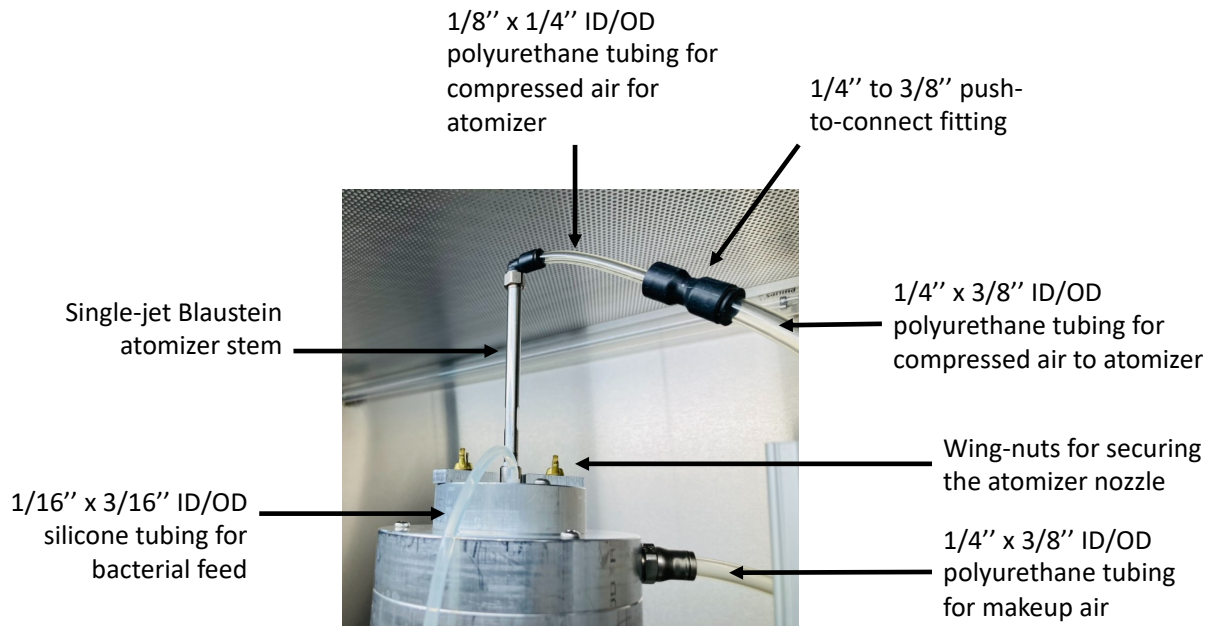

Figure 6. Bacterial feed, compressed air, and humidified air lines. The figure depicts the placement of the Blaustein atomizer single-jet module within the notch machined into the top plate of the 60-cm-high glass aerosol mixing chamber, secured by wingnuts. Also shown are the feed line, compressed airline, and humidified airline.

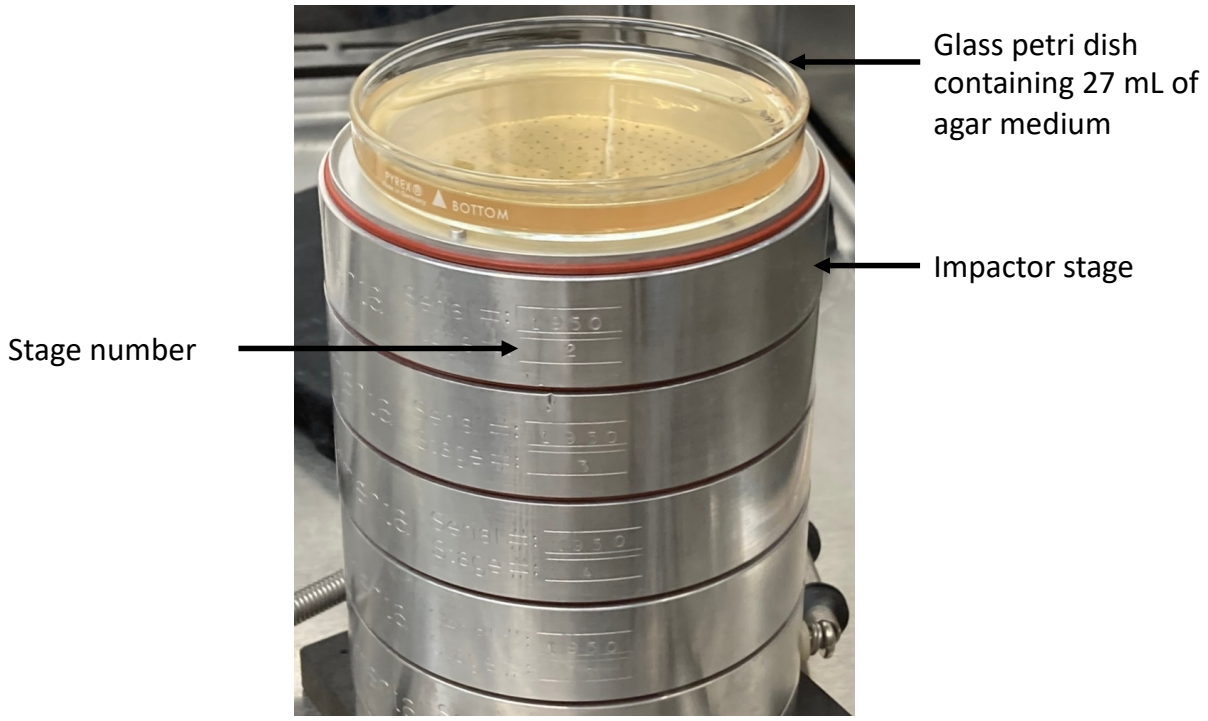

Figure 7. Agar plate loading. The figure depicts the placement of a glass Petri dish on metal platforms protruding from the second stage of the impactor.

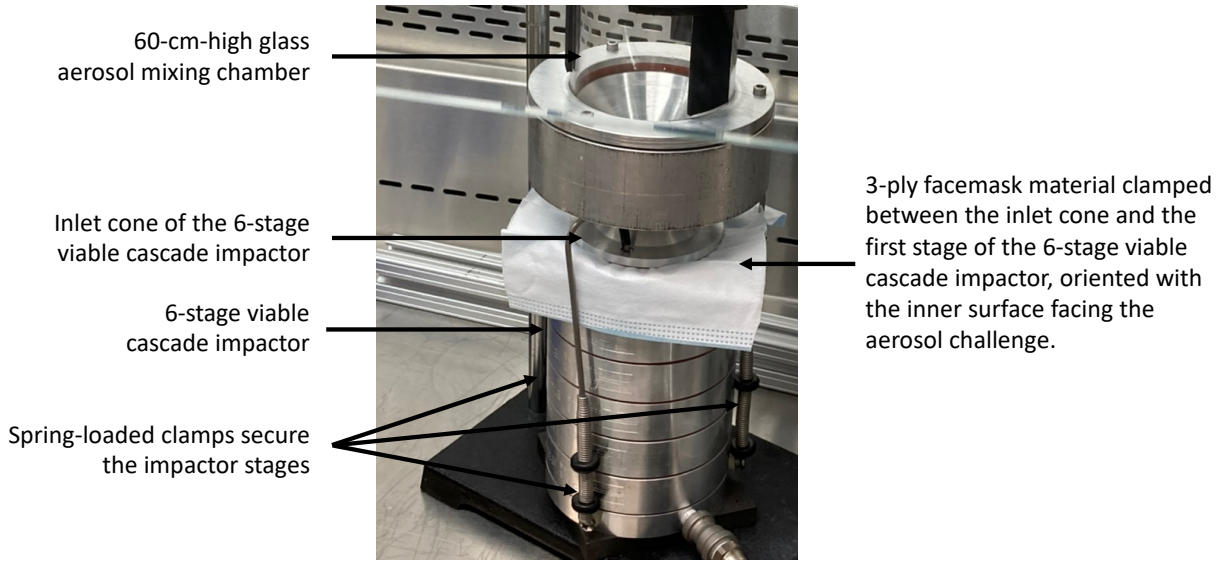

Figure 8. Facemask placement. The figure depicts the placement of facemask material secured between the inlet cone and the first stage of the impactor.

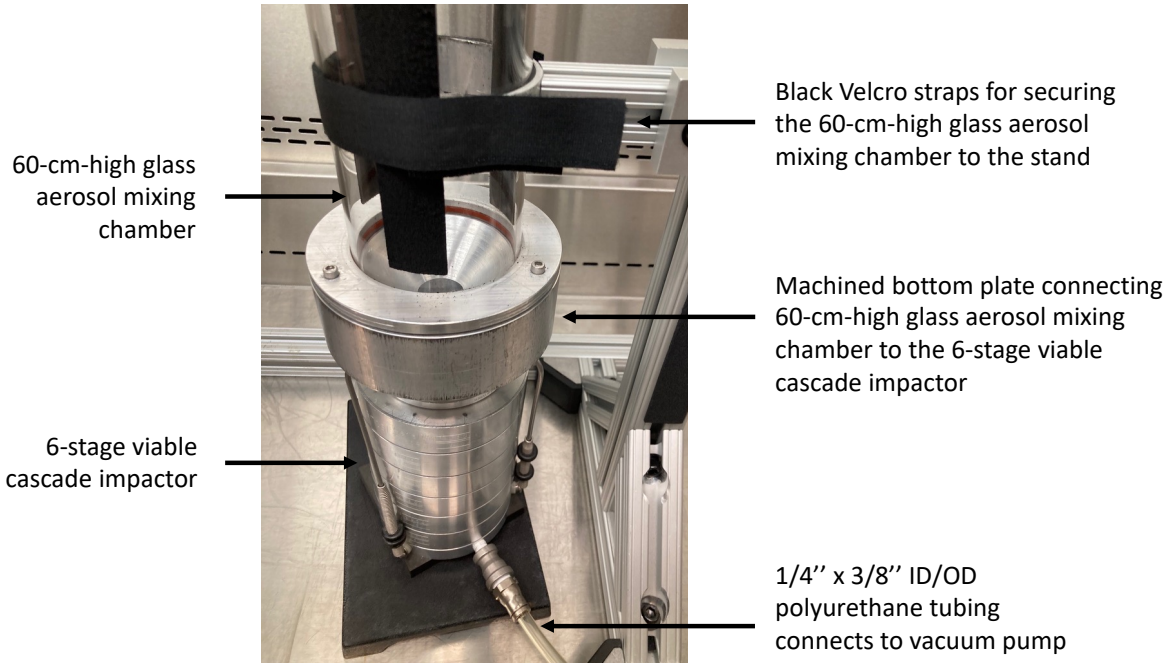

Figure 9. Placement of 60-cm-high glass aerosol mixing chamber on assembled impactor. The figure depicts the position of the 60-cm-high glass aerosol mixing chamber, secured by black Velcro strap to the stand, over the inlet of the 6-stage viable cascade impactor. Also shown is the polyurethane airflow line that connects to the vacuum pump.

Pre-run check
Timing: 3-5 minutes
This section describes the steps needed to conduct a single aerosol exposure run.

1. Confirm one end of the silicone tube connects to the atomizer feed inlet port and the other end of the tube connects via the luer-lok adapter to the 5 mL syringe filled with the required volume of liquid feed for aerosol generation.
2. Syringe pump setting
    a. Verify the syringe pump dispenses the feed at the desired flow rate.
    b. Verify the correct syringe volume and model is selected.
3. Check for the presence of air bubbles within the feed tube.
    a. If present, turn on the syringe pump.
    b. Allow the pump to operate such that there are no air or air bubbles in the feed tube.
    c. Stop the syringe pump.
4. Blaustein atomizer single-jet module
    a. Confirm atomizer nozzle placement on top of the aerosol mixing chamber within the notch.
    b. Ensure the atomizer is secured in place by the wing nuts.
5. Confirm air-tight seal throughout the system.
    a. O-rings must be intact, and seals should be air-tight.
    b. Between the aerosol mixing chamber and the cascade impactor.
    c. Between each stage of the impactor system.
    d. Between the impactor system and the exit port.
6. Turn on the compressed airflow to the atomizer nozzle to test for blockage.
    a. Confirm the diverting valve directs compressed air to the atomizer nozzle at the correct flow rate under the specified upstream pressure.
7. Ambient humidity and temperature within the BSC.
    a. The HT.w SensorPush device placed within the BSC records the ambient humidity and temperature and this information is digitally accessed.

Perform aerosol exposure runs
Timing: ~5 minutes
Aerosol generation and collection within the platform.

1. Turn on the compressed airflow valve and ensure the diverting valve directs the airflow to the atomizer nozzle.
2. Monitor the upstream airflow meter and adjust the pressure gauge to achieve an airflow rate of 1.5 LPM through the atomizer nozzle.
3. Ensure the airflow to the atomizer nozzle remains stable at 1.5 LPM.
4. Plug in the vacuum pump.
5. Monitor the downstream airflow meter and adjust the downstream pressure gauge to achieve an airflow rate of 28.3 LPM through the aerosol platform.
6. Allow the downstream airflow rate to stabilize at 28.3 LPM.
7. Maintain the airflow within the system for at least one minute to allow the internal environment to stabilize.
8. Set a timer for two minutes.
9. Turn on the syringe pump to dispense the feed suspension at 10.2 mL/h.

10. Start the timer as soon as the liquid feed reaches the feed inlet port of the atomizer nozzle; the yellow coloration of the peptone water should be visible as it reaches the feed inlet port.
11. Once the timer indicates one minute has passed, stop dispensing feed from the syringe pump.
12. Maintain the airflow through the atomizer nozzle and the aerosol platform to continue any present aerosol to traverse the system.
13. At the end of 2 minutes, redirect the compressed airflow away from the atomizer using the diverting valve, turn off the vacuum pump, and shut off the compressed airflow valve.

Disassemble and reset apparatus for the next aerosol trials
Timing: 15-20 minutes

1. Glass Petri dishes and facemask material
    a. Carefully detach the aerosol mixing chamber from the impactor.
    b. If a material was challenged during the run, remove the sample clamped between the inlet cone and the first stage of the impactor.
    c. Check the material for any damage that can interfere with the filtration test results before discarding; damage can result in poor filtration efficiency result.
    d. Remove the collection plates from the impactor, cover them with a lid, invert them, and transfer them to the static incubator.
2. Bacterial feed
    a. Withdraw the feed remaining in the tube into the syringe.
    b. Detach the silicone feed tube from the atomizer feed port.
    c. Detach the silicone feed tube from the syringe.
    d. Place the used silicone feed tube into an autoclavable container for sterilization and subsequent reuse.
    e. Carefully detach the syringe from the syringe pump, dispense the remaining feed into a liquid waste container, and dispose of the syringe into a solid waste container inside the BSC.
    f. Attach a sterile 5 mL syringe with a sterile luer-lok adapter to the syringe pump.
    g. Connect a new, sterile silicone feed tube to the syringe via the luer-lok adapter and load the syringe with the next test solution.
3. Six-stage viable cascade impactor
    a. Disassemble the impactor such that all stages are exposed.
    b. Spray all impactor stages with 70% ethanol solution.
    c. Wipe all impactor stages dry using tissue wipes.
    d. Allow impactor stages to air dry within the BSC for approximately 5-10 minutes.
    e. Place fresh collection agar plates below each impactor stage and secure stages using the spring-loaded clamps (**Figure 8**).
    f. Reassemble the impactor with the collection plates.
    g. Re-secure the aerosol mixing chamber on top of the impactor.
4. Blaustein atomizer single-jet module
    a. Fill a small plastic beaker with 50 - 80 mL of 70% ethanol.
    b. Remove the atomizer nozzle from the aerosol mixing chamber and submerge in the ethanol solution to sterilize and remove bacteria.
    c. Turn on the compressed air valve and direct the air to the atomizer nozzle using the diverting valve.

d. Allow the compressed air to flow through the submerged atomizer nozzle for 1-2 minutes.
e. Remove the atomizer from the ethanol solution and use a tissue wipe to dry the nozzle of the atomizer and ensure no ethanol is remaining.
f. Allow air to run through the atomizer for 4-5 minutes to dry the nozzle completely.
g. Ensure the O-ring is present at the base of the notch.
h. Place the atomizer on top of the aerosol mixing chamber and secure it with the wing nuts.
i. The system is now ready for the next aerosol experiment.

Critical*: Wiping and not merely spraying with 70% ethanol and air drying is necessary as mechanical force may help remove any contamination. After sterilization with 70% ethanol, care must be taken to ensure that the ethanol has completely dried prior to starting a new experiment. Any remaining ethanol residue may cause unintended pathogen inactivation during the experiment.*

3.6. EXPECTED OUTCOMES

A single experimental trial comprises a positive control run, three facemask material challenge runs, a second positive control run, and finally, a negative control run. This experimental sequence was performed three times, and the data analysis is discussed. The target outcome is the generation of 1700 to 3000 viable bacteria-laden droplets with mean aerodynamic size between 2.7 to 3.3 µm, as required by the ASTM standard F2101-19.[1]

Counted and corrected values of viable bacteria-laden droplet counts

Counts of viable bacteria-laden droplets reflect colony counts on agar plates containing 27 mL of tryptic soy agar (TSA) medium (**Figure 10**). TSA is a common nutritional medium for culturing bacteria, including *S. aureus*. The impaction of viable bacteria-laden droplets on the agar medium will produce visible colonies when incubated at 37°C for 18-24 h (**Figure 10**). Each stage of the 6-stage viable cascade impactor contains 400 uniform jets (holes); the diameter of these jets decreases from the first to the sixth stage from 1.18 to 0.25 mm (See manual).[6] The maximum number of colonies per plate is 400 because there are only 400 perforations for droplets to travel through. However, multiple viable bacteria-laden droplets travelling through the same jet may only produce a single bacterial colony, leading to an underestimate of the total counts of viable bacteria-laden droplets. Therefore, the ***corrected*** value, based on the the positive-hole correction factor table, accounts for the possible masking effect of multiple viable bacteria-laden droplets impacting the same region of the collection medium.[2] The bacterial colonies on the positive control plates were counted and converted into co-incidence-corrected whole-number values (**Figures 11, 12**). The total counts from the two positive control runs were averaged and used to calculate the bacterial filtration efficiencies of test materials.

The mean size and total counts of viable bacteria-laden droplets

The expected outcome for positive control runs is the collection of 1700 – 3000 viable bacteria-laden droplets, with a mean aerodynamic size range between 2.7 to 3.3 µm after coincidence correction (**Figure 12; Tables 5-7**). The aerodynamic diameter or size of droplets determines the site of collection within the impactor: larger droplets impact collection plates below the upper stages; smaller droplets impact collection plates below the lower stages.[7] Stage cut-off diameter

(d_{50}) describes a 50% collection efficiency for droplets with the specified diameter. Stages collect droplets greater than the d_{50} value with greater than 50% collection efficiency and droplets less than the d_{50} value with lower than 50% collection efficiency. The mean aerodynamic size of viable bacteria-laden droplets, $\overline{D}_{\mathrm{ae}}$ (µm), was calculated according to **Equation 1**, where d_{50} specifies the stage cut-off diameter, i specifies the impactor stage number, N_c is the coincidence-corrected stage droplet count, N_T specifies the coincidence-corrected count total from all six impactor stages.[3,4] The total viable bacteria-laden droplet counts for all six impactor stages, N_T, was calculated according to **Equation 2**; N_c is the coincidence-corrected stage count, and i specifies the impactor stage number.[2]

$$\overline{D}_{\mathrm{ae}} = \frac{\sum_{i=1}^{6} d_{50,i} \times N_{\mathrm{c},i}}{N_{\mathrm{T}}} \qquad \textbf{Equation 1}$$

$$N_T = \sum_{i=1}^{6} N_{\mathrm{c},i} \qquad \textbf{Equation 2}$$

Table 5. Trial 1 – Control run results

d_{50}	Positive A N_R	Positive B N_R	***Positive A*** $\boldsymbol{N_C}$	***Positive B*** $\boldsymbol{N_C}$	Negative N_R	Negative N_C
7	201	175	***279***	***230***	0	0
4.7	171	211	***223***	***300***	0	0
3.3	322	293	***654***	***527***	0	0
2.1	343	315	***779***	***620***	0	0
1.1	292	301	***524***	***559***	0	0
0.65	14	13	***14***	***13***	0	0
MDS	3.22	3.20	***2.98***	***2.97***	-	-
Total	1343	1308	***2473***	***2249***	0	0
N_{AVG}	1326		***2361***		0	

d_{50} = Stage cut-off diameter (µm); N_R = Raw counts; N_C = Coincidence-corrected counts
MDS = Mean droplet size (µm); N_{AVG} = Average counts of two positive control runs

Table 5 – Sample calculations

$$Mean\ droplet\ size, \overline{D}_{\mathrm{ae}} = \frac{\sum_{i=1}^{6} d_{50,i} \times N_{\mathrm{c},i}}{N_{\mathrm{T}}}$$

$$= \frac{[7 \times 279 + 4.7 \times 223 + 3.3 \times 654 + 2.1 \times 779 + 1.1 \times 524 + 0.65 \times 14]}{[279 + 223 + 654 + 779 + 524 + 14]}$$

$$= 2.98\ \mu m$$

$$Total\ droplet\ counts, N_{\mathrm{T}} = \sum_{i=1}^{6} N_{\mathrm{c},i}$$

$$Positive\ control\ A, total\ droplet\ counts,\ N_{\mathrm{T,A}}$$

$$= 279 + 223 + 527 + 620 + 559 + 13$$

$$= 2473$$

$$Positive\ control\ B, total\ droplet\ counts, N_{\mathrm{T,B}}$$

$$= 230 + 300 + 654 + 779 + 524 + 14$$

$$= 2249$$

$$Positive\ controls, total\ droplet\ count\ average,\ N_{\mathrm{AVG}}$$

$$= \frac{2473 + 2249}{2}$$

$$= 2361$$

Table 6. Trial 2 – Control run results

d_{50}	Positive A N_R	Positive B N_R	Positive A N_C	Positive B N_C	Negative N_R	Negative N_C
7	178	170	236	221	0	0
4.7	214	233	306	349	0	0
3.3	296	269	539	447	0	0
2.1	325	309	670	592	0	0
1.1	287	260	506	420	0	0
0.65	9	14	9	14	0	0
MDS	3.23	3.28	3.02	3.12	-	-
Total	1309	1255	2255	2043	0	0
N_{AVG}	1282		2143		0	

d_{50} = Stage cut-off diameter (µm); N_R = Raw counts; N_C = Coincidence-corrected counts
MDS = Mean droplet size (µm); N_{AVG} = Average counts of two positive control runs

Table 7. Trial 3 – Control run results

d_{50}	Positive A N_R	Positive B N_R	Positive A N_C	Positive B N_C	Negative N_R	Negative N_C
7	220	186	319	250	0	0
4.7	245	206	379	289	0	0
3.3	324	289	664	513	0	0
2.1	353	335	857	727	0	0
1.1	343	328	779	686	0	0
0.65	28	27	29	28	0	0
MDS	3.24	3.14	2.93	2.85	-	-
Total	1513	1371	3027	2493	0	0
N_{AVG}	1442		2760		0	

d_{50} = Stage cut-off diameter (µm); N_R = Raw counts; N_C = Coincidence-corrected counts
MDS = Mean droplet size (µm); N_{AVG} = Average counts of two positive control runs

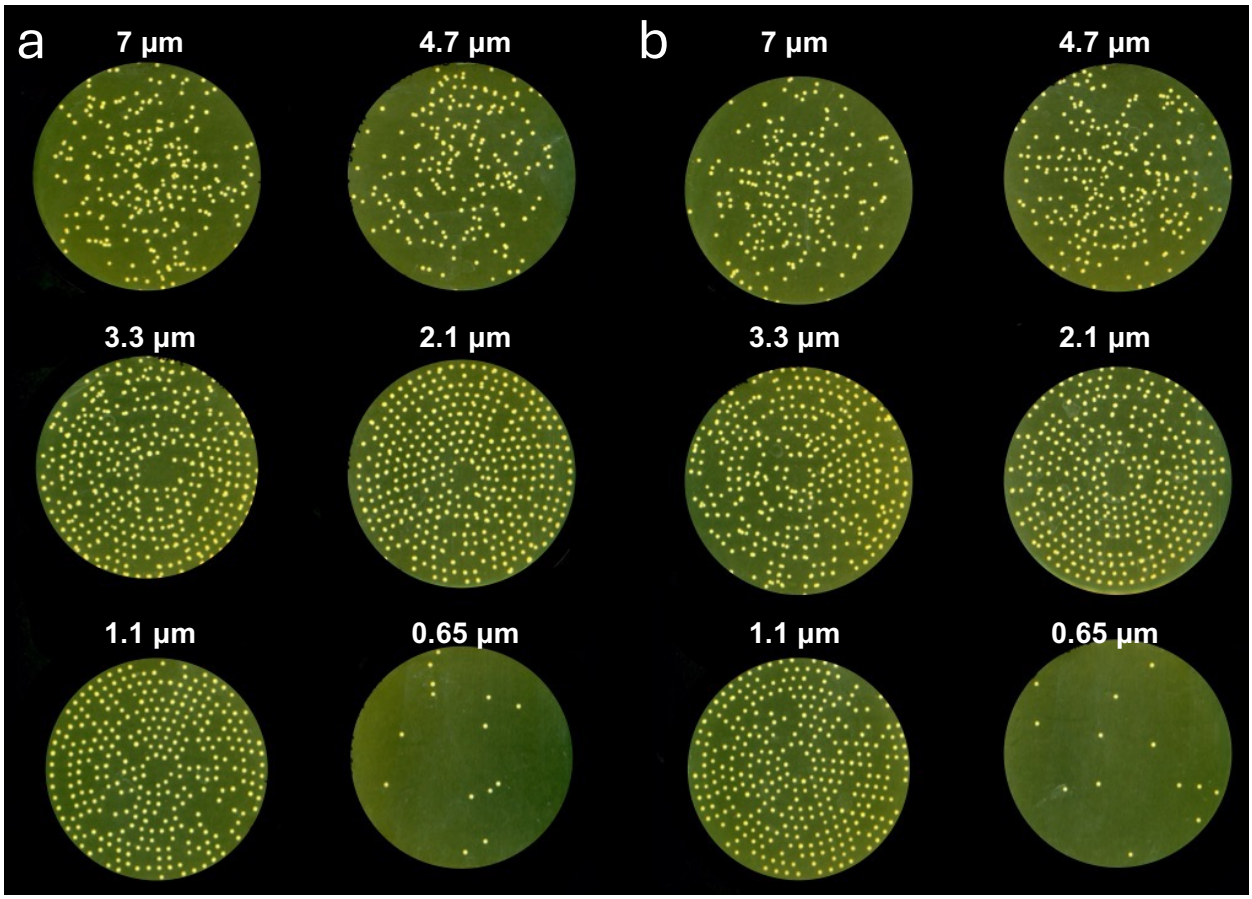

Figure 10. Trial 1 - Positive control run plates. Positive control runs performed in the absence of test material **(a)** before and **(b)** after the facemask material challenge runs were conducted.

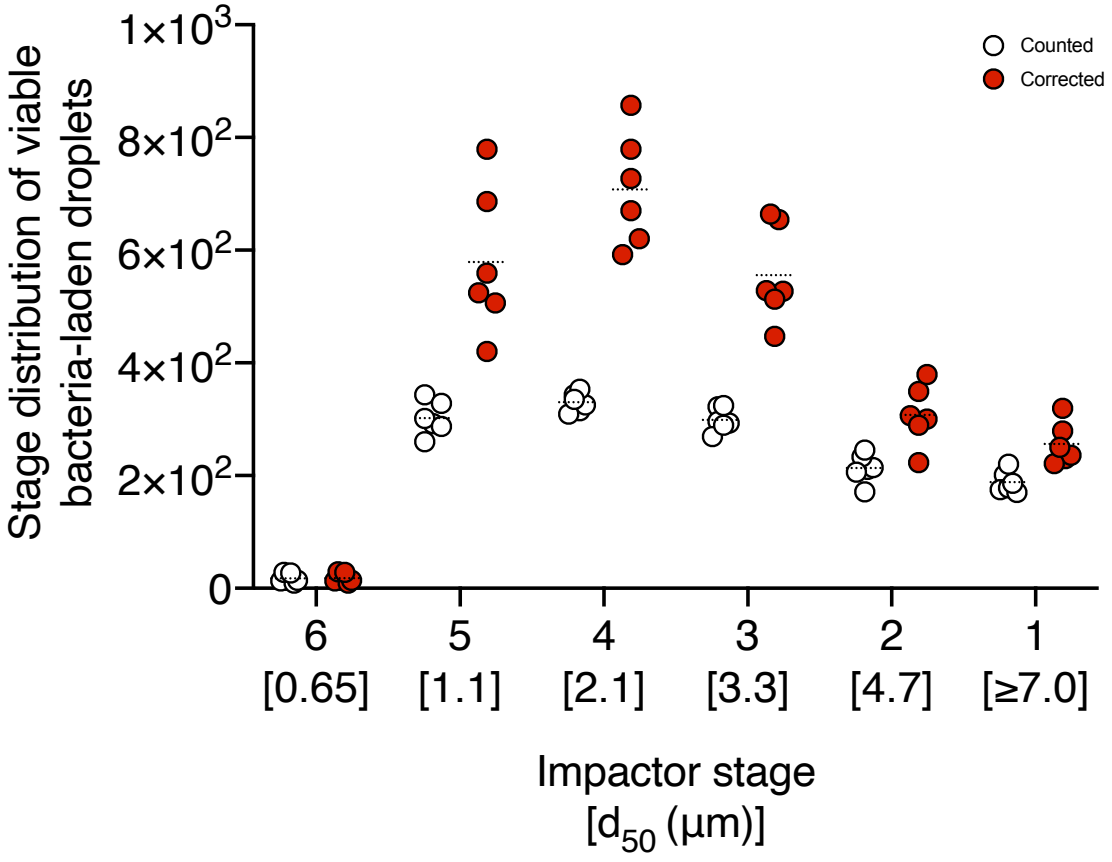

Figure 11. Stage distribution of viable bacteria-laden droplets from positive control runs from three independent trials. Viable bacterial droplets collected below each impactor stage before **(white)** and after **(red)** positive-hole correction in the absence of test materials. Positive control run data from three independent trials are represented (n=3).

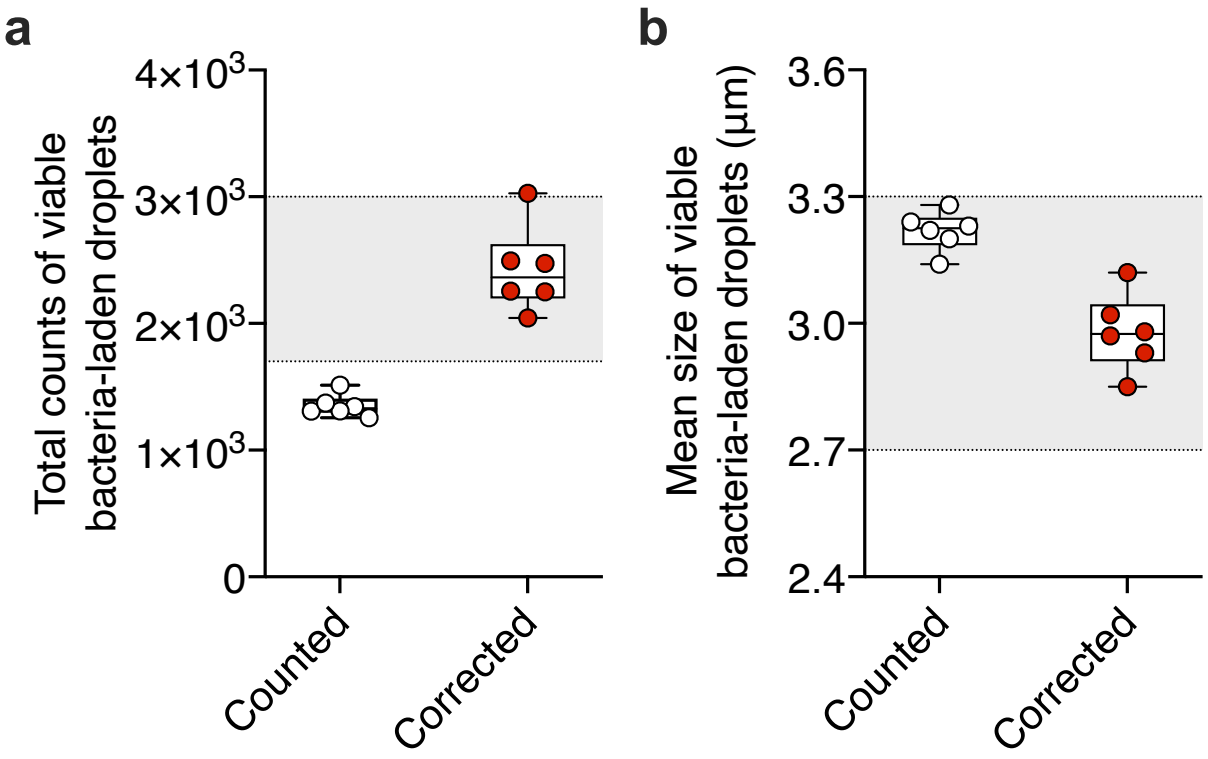

Figure 12. Total counts and mean size of viable bacteria-laden droplets from positive control runs from three independent trials. (a) Total counts and **(b)** mean size of viable bacteria-laden droplets collected cross all impactor stages before **(white)** and after **(red)** positive-hole correction in the absence of test materials. Positive control run data from three independent trials are represented (n=3).

The bacterial filtration efficiencies of facemask materials

Mask filtration efficiency expresses the fraction of viable bacteria-laden droplets captured by the material relative to the number encountered by the material (**Figures 13, Tables 8-10**). BFE values were calculated according to **Equation 3**, where N_{AVG} is the number of viable bacteria-laden droplets encountered by the material (average of the two positive control runs) and N_{M} is the number of droplets penetrating the test material.

$$\mathrm{BFE}\ (\%) = \frac{(N_{AVG} - N_{\mathrm{M}})}{N_{\mathrm{AVG}}} \times 100\% \qquad \textbf{Equation 3}$$

Table 8. Trial 1 – Bacterial filtration efficiency results

d_{50}	N_R Bandana	***N_C Bandana***	N_R 3-Ply	N_C 3-Ply	N_R N95-FFR	N_C N95-FFR
7	177	***234***	0	0	0	0
4.7	198	***273***	0	0	0	0
3.3	289	***513***	0	0	0	0
2.1	326	***675***	0	0	0	0
1.1	309	***592***	1	1	0	0
0.65	21	***22***	0	0	0	0
MDS (µm)		***2.9***		1.1	-	-
N_M		***2309***		1	0	0
BFE (%)		***2.20***		99.96		100

d_{50} = Stage cut-off diameter (µm); N_R = Raw counts; N_C = Coincidence-corrected counts
MDS = Mean droplet size (µm); N_M = Penetrating droplet counts; BFE = Bacterial filtration efficiency

Table 8 – Sample calculation

$$\text{BFE (\%)} = \frac{(N_{AVG} - N_M)}{N_{AVG}} \times 100\% \qquad \textbf{Equation 3}$$

$$Bandana\ bacterial\ filtration\ efficiency\ (\%) = \left[1 - \frac{[Droplets\ in\ the\ presence\ of\ test\ material]}{[Average\ droplets\ in\ the\ absence\ of\ test\ material]}\right] \times 100$$

$$= \left[1 - \frac{[2309]}{2361}\right] \times 100$$

$$= 2.20\%$$

Table 9. Trial 2 – Bacterial filtration efficiency results

d_{50}	N_R Bandana	N_C Bandana	N_R 3-Ply	N_C 3-Ply	N_R N95-FFR	N_C N95-FFR
7	138	169	0	0	0	0
4.7	145	180	0	0	0	0
3.3	227	335	0	0	0	0
2.1	267	440	0	0	0	0
1.1	251	395	3	3	0	0
0.65	17	17	0	0	0	0
MDS (µm)		2.93		1.1	-	-
N_M		1536		3	0	0
BFE (%)		28.52		99.86		100

d_{50} = Stage cut-off diameter (µm); N_R = Raw counts; N_C = Coincidence-corrected counts
MDS = Mean droplet size (µm); N_M = Penetrating droplet counts; BFE = Bacterial filtration efficiency

Table 10. Trial 3 – Bacterial filtration efficiency results

d_{50}	N_R Bandana	N_C Bandana	N_R 3-Ply	N_C 3-Ply	N_R N95-FFR	N_C N95-FFR
7	154	194	0	0	0	0
4.7	205	287	0	0	0	0
3.3	276	469	1	1	0	0
2.1	325	670	2	2	0	0
1.1	323	659	4	4	0	0
0.65	28	29	0	0	0	0
MDS		2.78		1.7	-	-
N_M		2308		7	0	0
BFE (%)		16.38		99.75		100

d_{50} = Stage cut-off diameter (µm); N_R = Raw counts; N_C = Coincidence-corrected counts
MDS = Mean droplet size (µm); N_M = Penetrating droplet counts; BFE = Bacterial filtration efficiency

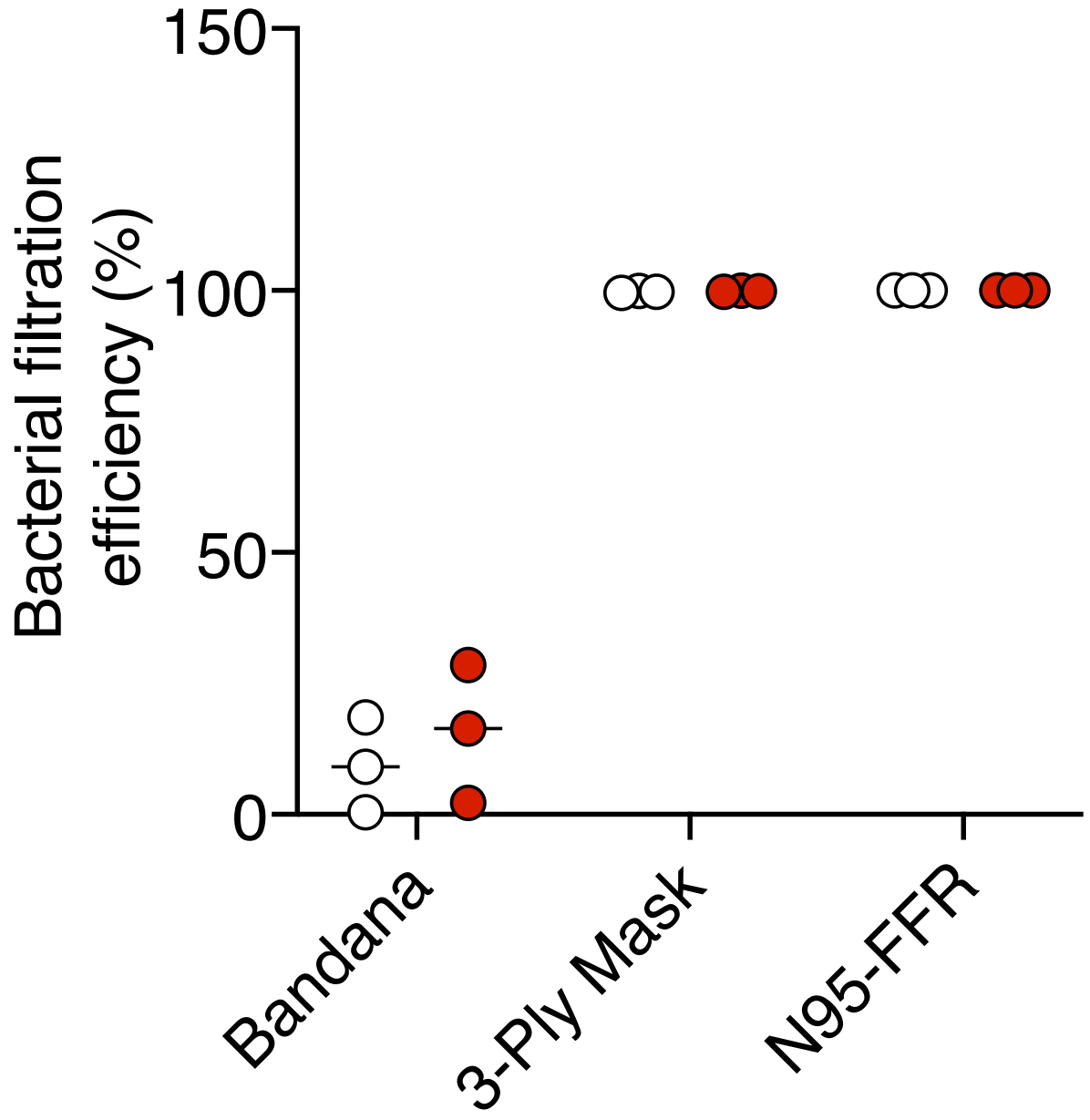

Figure 13. Bacterial filtration efficiencies of test materials from three independent trials. Bacterial filtration efficiency calculated using viable droplet-laden droplet counts before **(white)** and after **(red)** positive-hole correction for three test materials: single-ply bandana, 3-ply mask, and N95 face filtering respirator (FFR). Data from three independent trials are represented (n=3).

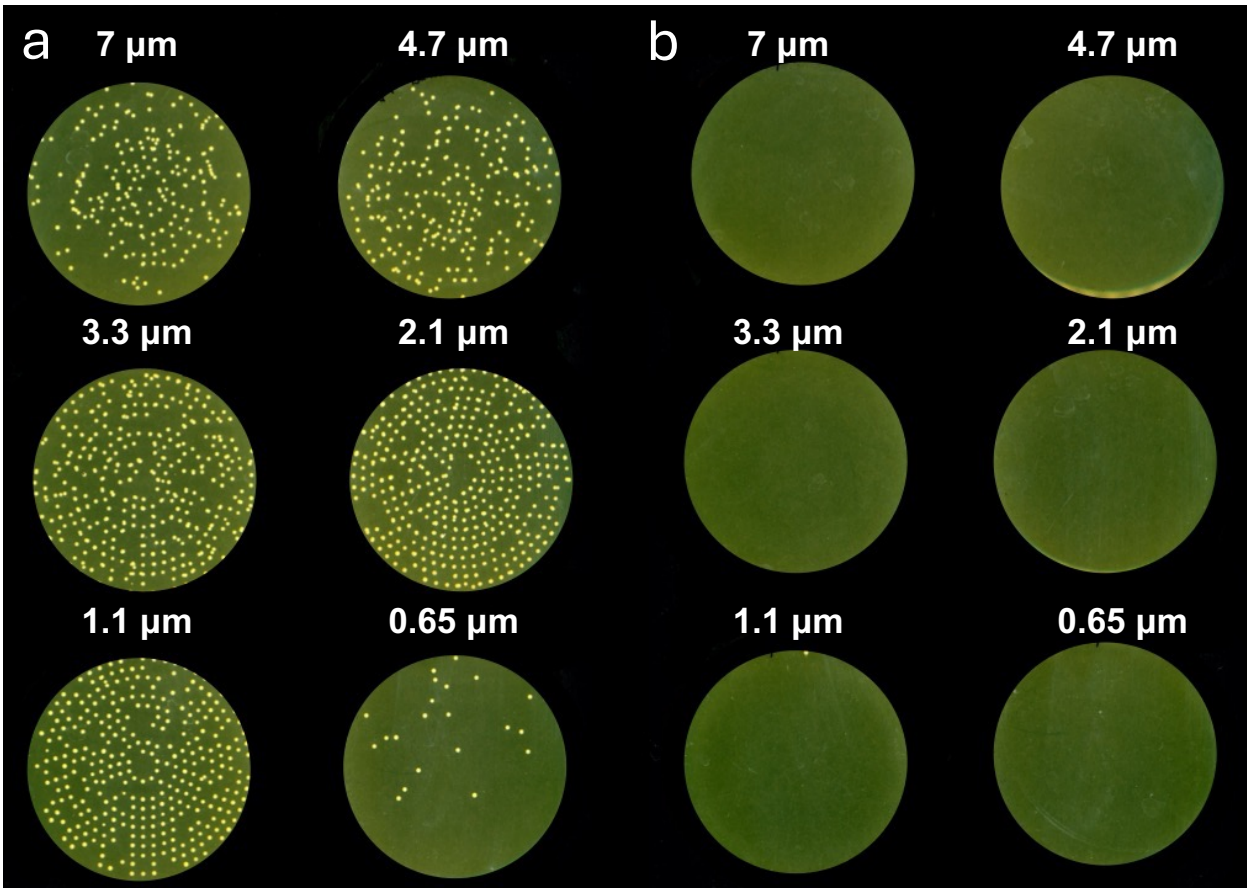

Figure 14. Trial 1 – Bandana and 3-ply mask plates. (a) Bandana and (b) 3-ply facemask material challenge plates.

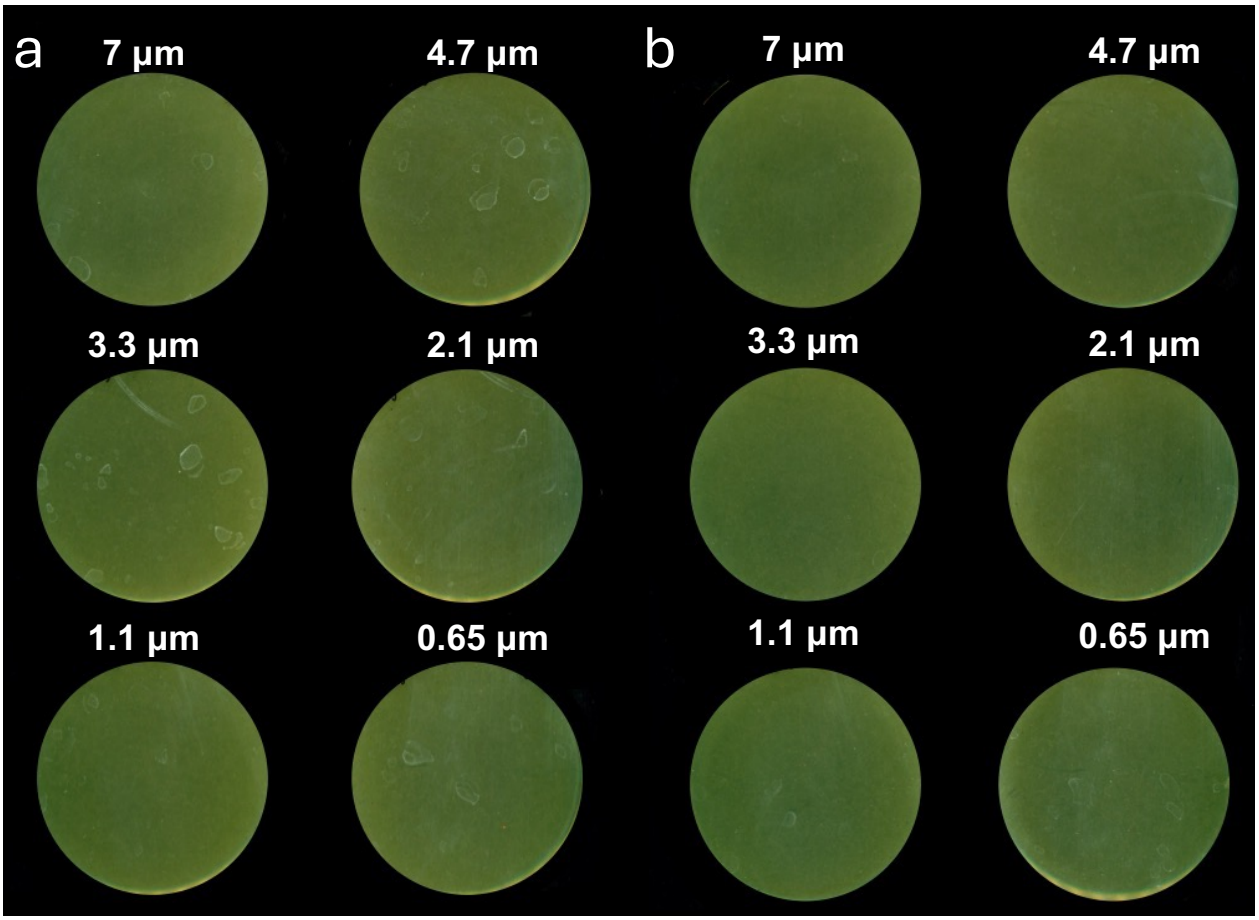

Figure 15. Trial 1 – Negative control and N95 challenge run plates. (a) Negative control and (b) N95 face filtering respirator (FFR) material challenge plates.

3.7. LIMITATIONS

Only a fraction of the viable bacteria-laden droplets generated by the atomizer reach the impactor for collection. Aerosolized droplets can be lost within the 60-cm-high glass aerosol mixing chamber, the inlet cone of the impactor, and on the stages of the impactor.[8] Assuming each viable bacteria-laden droplet collected within the impactor contained a single viable bacterial cell, it indicates approximately 10-15% of the aerosol droplets generated from the atomization of 170 µL of 1×10^5 CFU/mL suspension reach the collection plates. The remaining 85-90% of the droplets may go undetected due to the loss of viability of enclosed bacteria and due to deposition within the system. Additionally, the size and composition of the droplets will change from the point of generation to collection due to inflight evaporation.[9] The colony size does not indicate the number of viable bacterial cells within the droplet that produced the colony-forming unit. We measured the mean size and the total counts of viable bacterial droplets under a temperature range of 24±2ºC and relative humidity of ≥80%. Viable bacteria-laden droplet size and counts are subject to change if experimental conditions are outside the specified range.[9,10,11]

3.8. TROUBLESHOOTING

Problem 1
Less than 1700 colonies after positive hole correction.
Potential solution
Increase liquid feed flow rate, airflow rate, or bacterial concentration.

Problem 2
More than 3000 colonies after positive hole correction.
Potential solution
Decrease liquid feed flow rate, airflow rate, or bacterial concentration.

Problem 3
Colony counts higher on lower stages; mean droplet size is less than 2.7 μm.
Potential solution
Reduce atomizer airflow rate, increase the humidity.

Problem 4
Colony counts higher on upper stages; mean droplet size is greater than 3.3 μm.
Potential solution
Increase atomizer airflow rate, decrease the humidity of makeup airflow.

Problem 5
Fungal contamination on agar plates.
Potential solution
Provide adequate time for plates to dry, ensure sterile handling and proper storage of dried agar plates.

3.9. REFERENCES

1. Standard Test Method for Evaluating the Bacterial Filtration Efficiency (BFE) of Medical Face Mask Materials, Using a Biological Aerosol of Staphylococcus aureus. doi:10.1520/F2101-22.
2. Thirugnanasampanthar, M., Rhem, R. G., Dolovich, M. B. & Hosseinidoust, Z. Investigating the Effects of Fluid Composition on Bacterial Aerosol Production. in *JOURNAL OF AEROSOL MEDICINE AND PULMONARY DRUG DELIVERY* vol. 35 A3–A3 (MARY ANN LIEBERT, INC 140 HUGUENOT STREET, 3RD FL, NEW ROCHELLE, NY 10801 USA, 2022).
3. Margot, H., Zwietering, M. H., Joosten, H., O'Mahony, E. & Stephan, R. Evaluation of different buffered peptone water (BPW) based enrichment broths for detection of Gram-negative foodborne pathogens from various food matrices. *Int. J. Food Microbiol.* **214**, 109–115 (2015).
4. ANDERSEN, A. A. New sampler for the collection, sizing, and enumeration of viable airborne particles. *J. Bacteriol.* **76**, (1958).
5. Macher, J. M. Positive-Hole Correction of Multiple-Jet Impactors for Collecting Viable Microorganisms. *Am. Ind. Hyg. Assoc. J.* **50**, (1989).
6. TE-10-800-Viable-Cascade-Impactor.pdf.
7. Jensen, P. A. & Millie P. Schafer William G. Lindsley, B. F. L., Brett J. Green, Francoise M. Blachere, Stephen B. Martin. Sampling and Characterization of Bioaerosols. *NIOSH Manual of Analytical Methods* 4–7 (2005).
8. Lim, K. S. & Lee, K. W. Collection efficiency and particle loss of virtual impactors with different methods of increasing pressure drop. *J. Aerosol Sci.* **37**, 1188–1197 (2006).
9. Fernandez, M. O., Thomas, R. J., Oswin, H., Haddrell, A. E. & Reid, J. P. Transformative Approach To Investigate the Microphysical Factors Influencing Airborne Transmission of Pathogens. *Appl. Environ. Microbiol.* **86**, (2020).
10. Lin, K. & Marr, L. C. Humidity-Dependent Decay of Viruses, but Not Bacteria, in Aerosols and Droplets Follows Disinfection Kinetics. *Environ. Sci. Technol.* **54**, (2020).
11. Fernandez, M. O. *et al.* Assessing the airborne survival of bacteria in populations of aerosol droplets with a novel technology. *J. R. Soc. Interface* **16**, (2019).

Chapter 4. Unravelling the impact of operational parameters and environmental conditions on the quality of viable bacterial aerosols

Preface. This chapter describes the work conducted to understand how changes in operational parameters impact the size and counts of viable bacterial aerosol droplets. ASTM standard F2101-19 provides the blueprint for a standardized test platform and details the procedures for mask filtration testing using viable bacterial droplets. However, the standard fails to specify operating values for parameters involved in bacterial aerosol generation, namely bacterial concentration, suspension media concentration, relative humidity, and atomizer airflow and feed flow rates. Variable test values and procedures can interfere with the repeatability and reproducibility of results. To address this limitation, we systematically investigated the effect of changing the values for these five operating conditions on resultant bacterial aerosol properties. Values for operating parameters that produced bacterial droplets within ASTM-specified count and size range were defined. Importantly, bacterial filtration efficiencies of N95 respirators and 3-ply masks, evaluated under optimized test conditions, agree with measurements previously reported in the literature. This work can aid the validation and standardization of aerosol platforms based on ASTM standard F2101-19. Moreover, changes in viable bacterial aerosols under changing test conditions provide insight into airborne pathogen transmission dynamics. ***The results and conclusions presented in this chapter are valid under specific conditions and assumptions outlined in the study. Therefore, the accuracy and reliability of the findings depend on defined test conditions. These results may not be applicable under all circumstances or in different environments. Users of this information should exercise caution and consider additional factors relevant to their specific context before applying these results to describe and interpret real-world phenomena.***

Contributions. I conducted the bulk of the experimentation (excluding mask SEM imaging), performed all formal data analysis, troubleshooting, methods development, data visualization, and writing of the original manuscript draft, and incorporated revisions from co-authors. Rod G. Rhem constructed the aerosol platform, tested the performance of the atomizer, assisted with preliminary test trials, and provided significant insight that helped troubleshoot issues and optimize operational parameters. Lei Tian performed SEM imaging of mask materials (**Figure 4a**), assisted with data visualization, and reviewed and edited early manuscript drafts. Dr. Mellissa Gomez edited and revised all manuscript drafts, providing invaluable insights into data handling, analysis, and interpretation that were instrumental in finalizing the manuscript. Kyle Jackson edited and revised late manuscript drafts, providing significant insight into the presentation and discussion of the results. Danielle Della Libera was a thesis student mentee whom I trained on the aerosol platform and helped prepare agar plates that I used in a subset of the aerosol trials. Alison E. Fox-Robichaud reviewed the final manuscript draft. Dr. Zeinab Hosseinidoust and Prof. Myrna B. Dolovich were responsible for funding acquisition, methods development, project administration, supervision, weekly meetings, and review and scientific editing of the final manuscript drafts. Paul Gatt, Justin Bernar, John Colenbrander from the Chemical and Mechanical Engineering Machine Shop and Doug Keller were instrumental in helping to design and build the aerosol platform.

Citation. This chapter is under revision, PNAS Nexus.
Thirugnanasampanthar, M., Tian, L., Rhem, R. G., Libera, D. D., Gomez, M., Jackson, K., Fox-Robichaud, A. E., Dolovich, M. B., & Hosseinidoust, Z. (2024). Unravelling the impact of operational parameters and environmental conditions on the quality of viable bacterial aerosols.

4.1. ABSTRACT

Viable pathogen-laden droplets of consistent quality are essential for reliably assessing the protection offered by facemasks against airborne infections. We identified a significant gap in guidance within standardized tests for evaluating the filtration efficiencies of facemask materials using viable bacteria-laden aerosol droplets. An aerosol platform, built according to the American Society for Testing and Materials (ASTM) standard F2101-19, was used to validate and standardize facemask filtration test procedures. We utilized this platform to investigate the impact of varying five operating parameters, namely suspension media composition, relative humidity, pathogen concentration, and atomizer airflow and feed flow rates, on the aerosol quality of viable bacteria-laden aerosols. We achieved consistent generation of 1700 to 3000 viable bacteria-laden droplets sized between 2.7 to 3.3 µm under the following optimized test conditions: 1.5% w/v peptone water concentration, ≥80% relative humidity at 24±2°C, 1×10^5 CFU/mL bacterial concentration, 1.5 L/min atomizer airflow rate, and 170 µL/min feed flow rate. We also explored the consequence of deviating from these optimized test parameters on viable bacteria-laden aerosol quality. These results highlight the importance of controlling these parameters when studying airborne transmission and control.

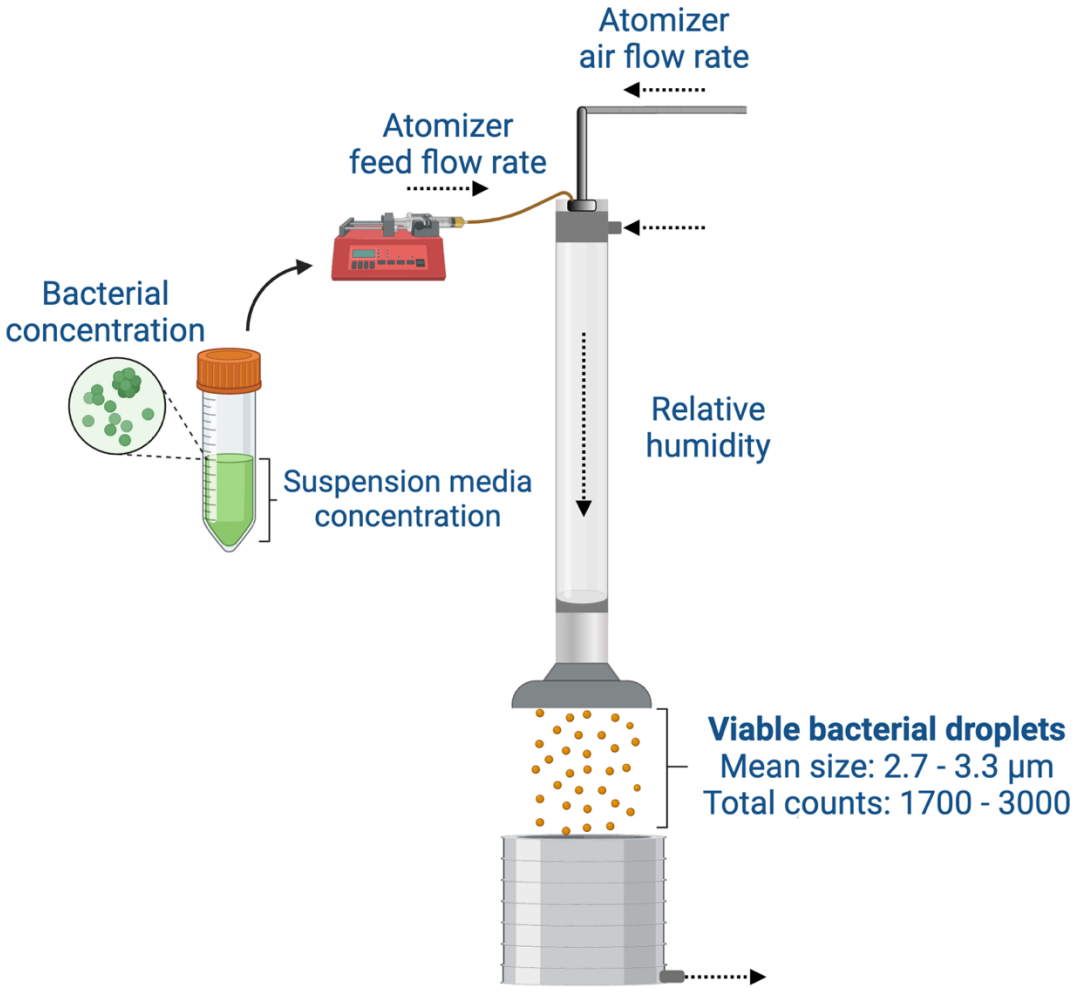

Graphical abstract – The illustration depicts the experimental platform, and the five parameters investigated for their effect on the size and count of viable bacterial droplets.

4.2. SIGNIFICANCE STATEMENT

Our research addresses a less explored aspect of air quality – the lack of reproducibility in standardized testing. We were part of a team that founded the Center of Excellence for Protective Equipment and Materials (CEPEM) at McMaster University in the early days of the COVID-19 pandemic. Working closely with government regulators, government labs, and the industry sector, we realized that protective material, challenged with infectious aerosols according to standardized guidelines, received a different filtration efficiency rating in different labs worldwide and even in the same region. We found this observation alarming and a potential public health concern and thus spent 3+ years investigating the root cause of this lack of reproducibility.

4.3. INTRODUCTION

Facemasks have been widely adopted by essential service workers, including healthcare professionals and the general public, to mitigate the transmission of airborne infections.[1–3] The ability of facemasks to prevent inhalation of harmful particles and droplets can vary significantly depending on the filtration efficiency of the material used.[4,5] Materials with suboptimal filtration efficiency may endanger public health and impede effective disease control measures. Regulatory approval of mask products in many jurisdictions is contingent on the outcome of standardized filtration efficiency tests conducted per established regulatory guidelines, such as the American Society for Testing and Materials (ASTM) and the National Institute for Occupational Safety and Health (NIOSH).[6] Importantly, the manufacturing, sale, and commercialization of high-efficiency mask products cannot proceed without regulatory approval. Therefore, delays in obtaining reliable test results can directly impact the availability of mask products.

The shared experience of the pandemic coronavirus disease 2019 (COVID-19) brought attention to less scrutinized aspects of standard tests used to assess the quality of personal protective equipment, especially facemasks. The ASTM F2100-23 outlines a multitude of tests for evaluating medical facemask materials.[7] More specifically, ASTM F2101-19 provides the guidelines for conducting bacterial filtration efficiency (BFE) testing, which involves challenging mask materials with droplets containing *Staphylococcus aureus*.[8] Due to the lack of a standardized viral aerosol testing method, procedures based on the ASTM F2101-19 standard have been widely adopted to assess the filtration performance of facemasks using viable bacteria-laden aerosols.[9,10] The F2101-19 standard outlines procedures for the generation, collection, and enumeration of these infectious aerosols (**Figure 1**), mandating that test materials be challenged with 1700 to 3000 viable bacteria-laden droplets with mean aerodynamic size of 2.7 to 3.3 μm, delivered over two minutes.[8] However, the F2101-19 standard neglects to specify nearly half of the hardware specifications and operating conditions required to generate bacterial aerosols within the mandated range necessary for conducting filtration tests (**Table 1**). The operating conditions highlighted in **Table 1** can take significant time to optimize. This delay can lead to lost time and capital, inconsistent outcomes between labs, and impede third-party verification of test results.

We developed and optimized an in-house custom aerosol platform per ASTM F2101-19 specifications to address the identified knowledge gap.[8] Utilizing the platform, the variation in the quality of generated bacterial aerosols in response to the manipulation of five key unspecified parameters, highlighted in **Table 1**, was explored. Experimental results were analyzed and interpreted according to established theories in aerosol transport mechanics, elucidating the conditions necessary for generating bacterial aerosols of consistent quality.

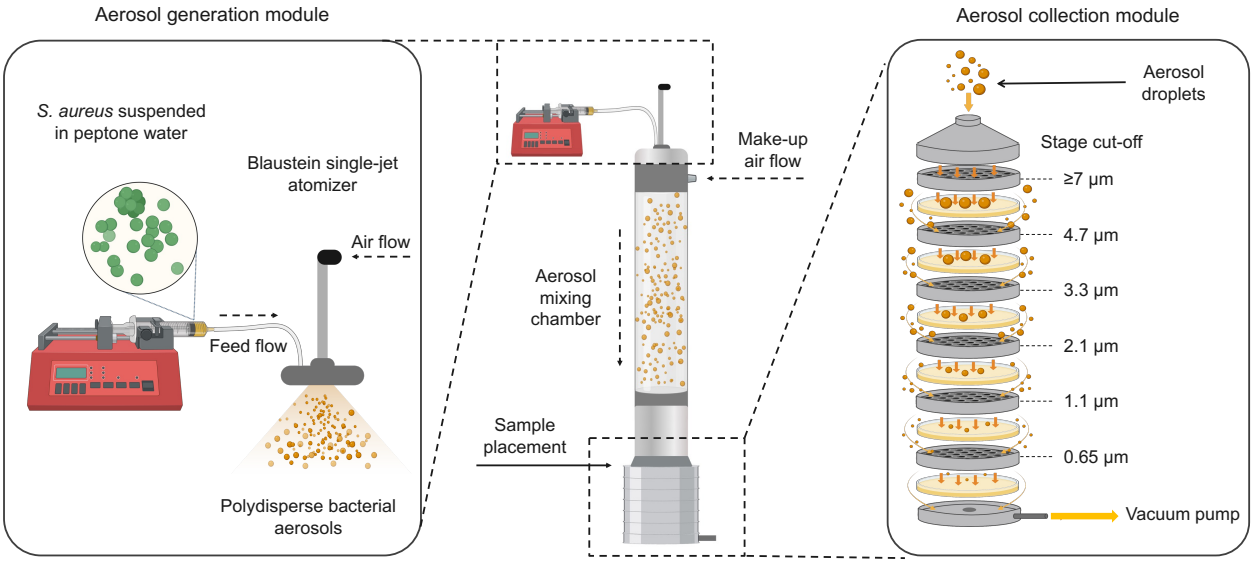

Figure 1. The illustration depicts the in-house experimental setup for bacterial filtration efficiency (BFE) testing of facemask materials per American Society for Testing and Materials standard F2101-19. Schematic of the BFE test workflow comprised of three main components: **(left)** the aerosol generation module, **(centre)** a 60-cm-high glass aerosol mixing chamber, and **(right)** the aerosol collection module, all housed within a custom-built biological safety cabinet. Blaustein single-jet module, operated in atomizer mode, was used to generate polydisperse bacterial aerosol droplets. Glass Petri dishes prepared with 27 mL of semi-solid bacterial culture media were inserted into the impactor to collect size-fractioned droplets through impaction.

Table 1. Operating variables in bacterial aerosol generation, collection, and mask challenge

	Variables	*Values specified in ASTM F2101-19*	*Test values*
Aerosol generation	Peptone water concentration (% w/v)	-	**1.5**, 3.0, 6.0
	Temperature (°C)	-	**24±2**
	Relative humidity (%)	-	0-20, 40-60, **80-100**
	S. aureus concentration (CFU/mL)	~1×10^5	1×10^4, **1×10^5**, 1×10^6
	Atomizer airflow rate (L/min)	-	0.5, **1.5**, 2.5
	Atomizer feed flow rate (µL/min)	-	100, **170**, 240
	Aerosol generation module	-	Blaustein atomizer single-jet module
	Atomizer feed flow duration (min)	1	1
	Atomizer airflow duration (min)‡	2	4
	Aerosol chamber dimensions (cm)¥	8×60	8×60
	Total counts (CFU) †	2350±650	2350±650
	Mean size (µm)	3.0±0.3	3.0±0.3
Aerosol collection	Glass Petri plate dimensions (mm)	15×100	15×100
	Tryptic soy agar volume (mL) †	-	27
	Impactor airflow rate (L/min)	28.3	28.3
	Impactor airflow duration (min) ‡	2	4
	Aerosol collection module	Six-stage viable cascade impactor	Six-stage viable cascade impactor
Aerosol enumeration	Incubation temperature (°C)	37±2	37±2
	Incubation humidity (%)	-	40-60
	Incubation time (h)§	48±4	24±4
Sample preparation	Mask conditioning temperature (°C)	21±5	21±5
	Mask conditioning humidity (%)	85±5	85±5
	Mask conditioning duration (h)	≥4	≥4
	Mask challenge area (cm^2)	-	49
	Airflow velocity through mask (cm/s)	-	9.6

*Shaded region indicates test values for ambiguous or unspecified variables involved in bacterial aerosol generation; bolded values were held constant as values of a single variable was altered.

‡Atomizer and impactor airflow was maintained for two minutes prior to aerosol generation to allow humidity and temperature within the system to stabilize.

¥The glass chamber functions as a baffle for the Blaustein atomizer which enables it to be operated as a nebulizer within the platform.[11]

†Collection medium volume and coincidence-correction table values are based on publications by

J Macher and A. A. Andersen.[12,13]
[§]ATCC 6538 product handling sheet specifies a shorter incubation period of 24 h.[14]

4.4. MATERIALS AND METHODS

4.4.1. Solution preparation

Saline solution was prepared by dissolving 9 g/L of sodium chloride (Fisher Scientific S271-500) in deionized water. Tryptic soy broth (TSB) was prepared by dissolving 30 g/L tryptic soy broth (BD B211825) in deionized water. Tryptic soy agar (TSA) media was prepared by dissolving 30 g/L tryptic soy broth (BD B211825) and 15 g/L agar (Fisher BioReagents BP1423500) in deionized water. Varying concentrations of peptone water solutions were prepared by dissolving 15 g/L, 30 g/L, and 60 g/L of peptone water (Thermo Scientific CM0009) in ultrapure water (MilliporeSigma SYNSVHFUS). Dry reagents were weighed using Precision Balance (Mettler Toledo ME203E). All solutions were sterilized by autoclaving at 121°C for 20 minutes (Yamato Steam Sterilizer SM301).

4.4.2. Bacterial aerosol generation, collection, and detection

As depicted in **Figure 1**, three components comprise the aerosol exposure platform: Blaustein Atomizer Single-Jet Model (CH Technologies ARGBLM2), a 60-cm high and 8-cm wide glass aerosol mixing chamber, and a 6-stage viable cascade impactor (Tisch Environmental TE-10-800). A PushSensor thermometer-hygrometer (HT.w 16794383), placed inside the BSC with the aerosol platform, was used to monitor ambient temperature and humidity fluctuations. Atomization of bacterial suspensions containing *Staphylococcus aureus* (ATCC 6538) generates viable bacteria-laden aerosol droplets. Compressed air, filtered through an inline HEPA capsule filter (TSI 1602051), was delivered to the atomizer at a controlled flow rate (0.5, 1.5, or 2.5 L/min). A volumetric airflow rate of 28.3 L/min was maintained within the system using a downstream vacuum pump (GAST 0823-101Q-G608NEX) and monitored using a downstream flow meter (OMEGA FMA-A2317). Glass petri dishes (Pyrex 3160-100) prepared with 27 mL of TSA are placed beneath each impactor stage to collect aerosols through impaction. The airflow through the system is maintained for two minutes to stabilize the humidity and temperature before aerosol generation. The four-minute experimental runtime consists of two minutes of airflow before aerosol generation, one minute of aerosol generation, and one minute of airflow post-aerosol generation. Airflow continued for an additional minute after the liquid feed flow stopped to allow all generated droplets to reach the impactor. Aerosol collection plates were incubated for 24±4 h at 37°C to allow bacterial colony formation.[14] **Supporting Information Sections S1-S3 (Tables S1, S2; Figures S1, S2)** provide additional details on platform operation, test value selection, and loss quantification.

4.4.3. Determining the mean size and total count of viable bacteria-laden droplets

Bacterial colonies on collection plates were manually counted and converted into co-incidence-corrected whole-number values using a positive-hole correction factor to account for the co-incidence error.[13] The mean aerodynamic diameter of viable bacteria-laden droplets, $\overline{D}_{ae}$ (μm), was calculated according to **Equation 1**, where d_{50} specifies the stage cut-off diameter, i specifies the impactor stage number, N_c is the coincidence-corrected stage droplet counts, N_T specifies the coincidence-corrected count for viable bacteria-laden droplets across all six stages.[15,16] The total counts of viable bacteria-laden droplets for the six stages of the impactor, N_T, was calculated

according to **Equation 2**, where N_c is the coincidence-corrected stage count, and i specifies the impactor stage number.[13] For additional details, including information on loss quantification within the system, please refer to **Supporting Information Sections S1 and S2.**

$$\bar{D}_{ae} = \frac{\sum_{i=1}^{6} d_{50,i} \times N_{c,i}}{N_T} \quad \textbf{Equation 1}$$

$$N_T = \sum_{i=1}^{6} N_{c,i} \quad \textbf{Equation 2}$$

4.4.4. Determining the bacterial filtration efficiency and airflow resistance of test materials

Bacterial filtration efficiency trials adhered to ASTM standard F2101-19 specifications.[8] The total count and mean size of viable bacteria-laden droplets composing the aerosol challenge were determined using two positive control runs conducted before and after test material challenges. The negative control run, performed at the end of the experimental period, was used to verify the sterility of the system. Microbial growth was absent on all negative control plates.

Test materials for bacterial filtration efficiency determination included commercial respirators and masks: Kimberly-Clark, Kimtech™ N95 Pouch Respiratory (NIOSH 53358), 3-Ply Face Masks (Amazon B08R5P19BX), and Levi's 100% cotton bandanas (Amazon B09697R47T). The test material, placed between the inlet cone and the first stage of the impactor, covers an area of 49 cm^2 with the outer surface oriented towards the aerosol challenge to simulate mask protection of the wearer against infectious aerosols.[17] The 49 cm^2 area of the material experienced an airflow velocity of 9.6 cm/s, with droplets delivered at a volume flow rate of 28.3 L/min. The droplets that penetrate the test material, collected within the impactor according to aerodynamic size, are used to calculate the filtration efficiency of the material.

Bacterial filtration efficiency expresses the fraction of viable droplets captured by the material relative to the number of viable droplets encountered by the material. Bacterial filtration efficiency values were calculated according to Error! Reference source not found.**3**, where N_{AVG} is the n umber of viable bacteria-laden droplets encountered by the material (based on the average of two positive control runs), and N_M is the number of droplets penetrating the test material. For additional details, refer to **Supporting Information Sections S1 and S7**.

$$\text{BFE}\ (\%) = \frac{(N_{AVG} - N_M)}{N_{AVG}} \times 100\% \quad \textbf{Equation 3}$$

The differential pressure (DP) test assesses resistance to airflow across the test material. DP tests were performed according to standard specifications, subjecting test materials to 27 cm/s airflow velocity, while the BFE testing subjects the material to 9.6 cm/s airflow velocity.[8,18,19] For additional details regarding DP testing, refer to **Supporting Information Section S2.**

4.4.5. Electron microscopy of test materials

Scanning electron microscopy (SEM) was used to visualize the microstructural features of

mask materials. Samples, coated with a 10 nm layer of gold (Edwards High Vacuum Coater S150B), were imaged (TESCAN VEGA-II LSU) using 10 kV accelerating voltage, 60× magnification, 16.66 mm working distance, and 3.61 mm view field.

4.4.6. Statistical analysis

Group means were analyzed using ordinary one-way ANOVA followed by Tukey's multiple comparisons test in GraphPad PRISM 9. The threshold for significance is p-value<0.05. Group means from five independent aerosol trials were used to evaluate the effect of changing test values on total counts and mean size of viable bacteria-laden droplets.

4.4.7. Data Availability

The data generated in this study is provided in the Source Data file and is available online.

4.5. RESULTS AND DISCUSSION

4.5.1. Effect of peptone water concentration on viable bacteria-laden aerosol properties

To assess the impact of suspension media concentration on aerosol properties, we quantified the mean size (**Figure 2a**), total counts (**Figure 2b**), and stage distribution (**Figure 2c**) of viable bacteria-laden droplets generated from 1.5%, 3%, and 6% w/v peptone water suspensions. Without guidance from the standard and convention in applied microbiology, we selected peptone water concentrations (1.5%, 3% and 6% w/v) to reflect sputum solids concentrations in healthy, moderate, and severe muco-obstructive airway disease states.[20] The solids fraction of human airway mucus is a mixture of mucin, salts, globular proteins, lipids, DNA, and cellular debris.[21,22] The complex composition of mucus is challenging to simulate. However, the prepared peptone water solutions contain similar concentrations of solids (proteins and salts) to reflect that of airway mucus in health and disease states.[20,23] **Table S3** provides the operating values held constant during these trials. **Tables S4-S6** provide stage-specific viable bacteria-laden droplet count data for the three peptone water concentrations.

The mean size of viable bacteria-laden droplets increased from 2.90±0.08 to 3.29±0.04 and 3.64±0.09 μm with increases in peptone water concentration (**Figure 2a**). Total droplet counts increased from 2455±320 to 2662±263 before decreasing to 2083±174 for 1.5%, 3.0%, and 6.0% w/v peptone water concentrations, respectively (**Figure 2b**). **Figure 2c** shows the stage distribution percentage of viable bacteria-laden droplets under varied peptone water concentrations. The collection of viable bacteria-laden droplets generated from 1.5% w/v peptone water solutions is left-skewed, with the highest fraction of droplets collecting below stage four with a 2.1 μm cut-off diameter (**Figure 2c**). Meanwhile, the highest percentage of viable bacteria-laden droplets generated from 3% and 6% w/v peptone water solutions collect below the third impactor stage with a 3.3 μm cut-off diameter (**Figure 2c**). Only bacterial suspensions prepared in 1.5% and 3% w/v peptone water concentrations produced aerosol droplets within the ASTM-specified size and count range, as indicated by the shaded regions in **Figure 2a** and **2b**, respectively. Notably, 3% w/v peptone water concentration resulted in bacteria-laden droplets at the upper limit of the acceptable size range, while 6% w/v peptone water concentration produced droplets greater than the specified size range.

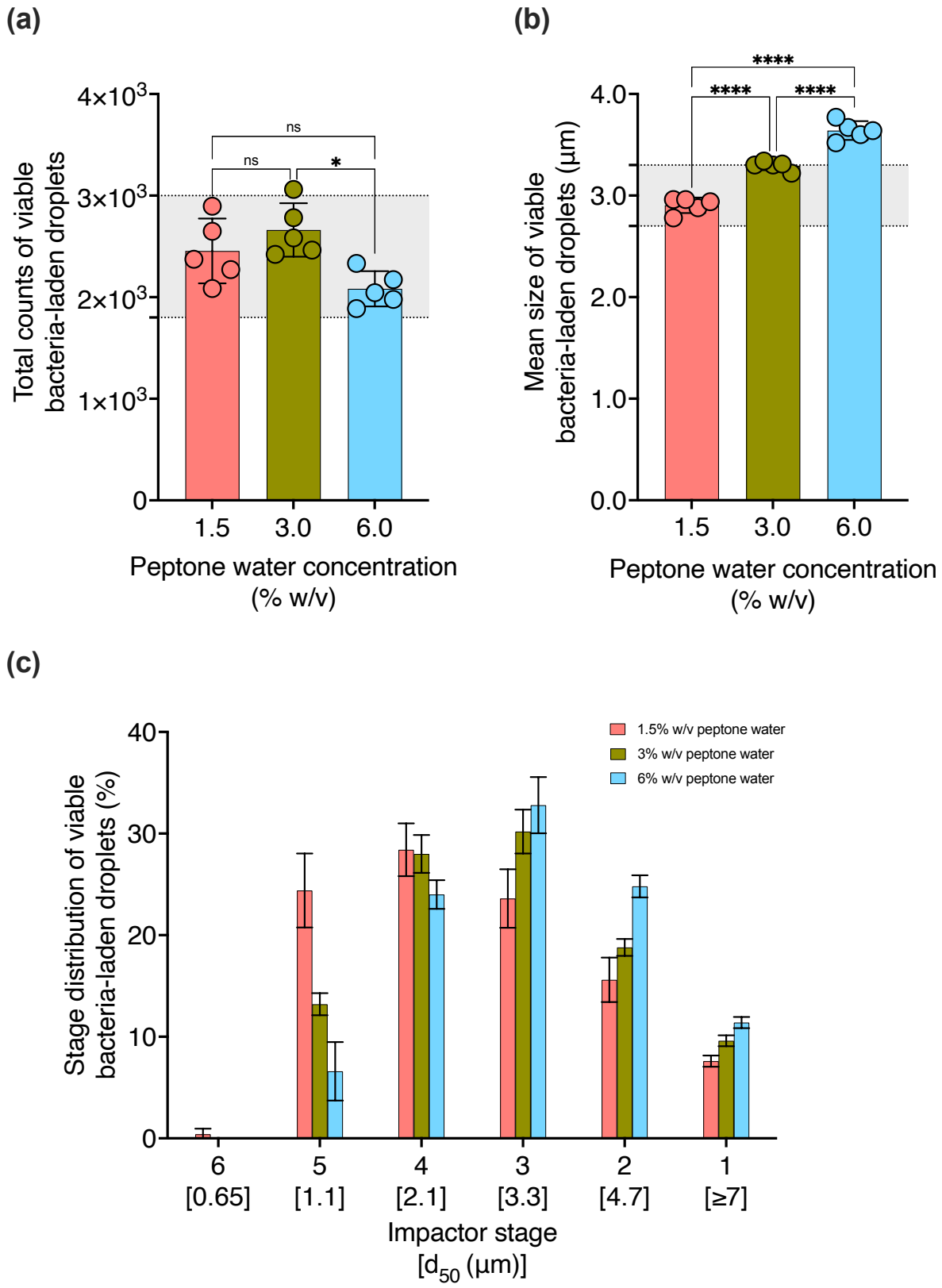
(a)
Total counts of viable bacteria-laden droplets
4×10^3
3×10^3
2×10^3
1×10^3
0
ns
ns
*
1.5
3.0
6.0
Peptone water concentration (% w/v)
(b)
Mean size of viable bacteria-laden droplets (µm)
4.0
3.0
2.0
1.0
0.0
****
****
****
1.5
3.0
6.0
Peptone water concentration (% w/v)
(c)
Stage distribution of viable bacteria-laden droplets (%)
40
30
20
10
0
1.5% w/v peptone water
3% w/v peptone water
6% w/v peptone water
6 [0.65]
5 [1.1]
4 [2.1]
3 [3.3]
2 [4.7]
1 [≥7]
Impactor stage [d50 (µm)]

Figure 2. Effect of peptone water concentration on the mean size, total count, and stage distribution of viable bacteria-laden droplets. The impact of varying peptone water concentration on **(a)** mean size, **(b)** total count, and **(c)** stage distribution of viable bacteria-laden droplets is shown (n=5). All other operating variables for aerosol generation were kept constant according to **Table S3** as peptone water concentration was varied, while the remaining parameters were adjusted as specified in **Table 1**. Regions shaded in grey indicate ASTM standard F2101-19 specified range for **(a)** mean size and **(b)** total count of viable bacteria-laden droplets. Asterisks indicate statistically significant differences, defined as *p-value<0.05, ** p-value <0.01, *** p-value <0.001, **** p-value <0.0001.

4.5.2. Effect of relative humidity on viable bacteria-laden aerosol properties

To examine the impact of RH on aerosol properties, we measured the mean size (**Figure 3a**), total counts (**Figure 3b**), and stage distribution (**Figure 3c**) of viable bacteria-laden droplets under conditions of RH ≤20%, 40-60%, and ≥80%. **Table S7** provides the operating values held constant during these trials. **Tables S8-S10** provide stage-specific viable bacteria-laden droplet count data collected under varied RH conditions. The mean size of viable bacteria-laden droplets increased from 2.67±0.06 to 2.91±0.04 and 2.92±0.08 μm with increasing RH (**Figure 3a**). Total counts of viable bacteria-laden droplets decreased from 4691±842 to 3416±556 and 2658±307 under increasing RH (**Figure 3b**). The highest percentage of viable bacteria-laden droplets exposed to ≤20% RH conditions are collected below the fourth and fifth impactor stages with cut-off diameters of 2.1 and 1.1 μm, respectively (**Figure 3c**). Under high ≥80% RH conditions, the highest percentage of viable bacteria-laden droplets are collected below the third and fourth stages with cut-off diameters of 3.3 and 2.1 μm, respectively (**Figure 3c**).

Only the mean size and total counts of viable bacteria-laden droplets collected under the ≥80% RH condition fell within the ASTM-specified range, as indicated by the shaded regions in **Figure 3a** and **3b**, respectively. This finding highlights a pitfall of the ASTM F2101-19 standard; different geographical locations or weather conditions may alter the quality of the aerosol. The range of RH that produces the required quality of aerosols is not naturally achievable in many parts of the world or all year round. A humidity-controlled chamber or laboratory may be required to produce bacterial aerosols of consistent quality.

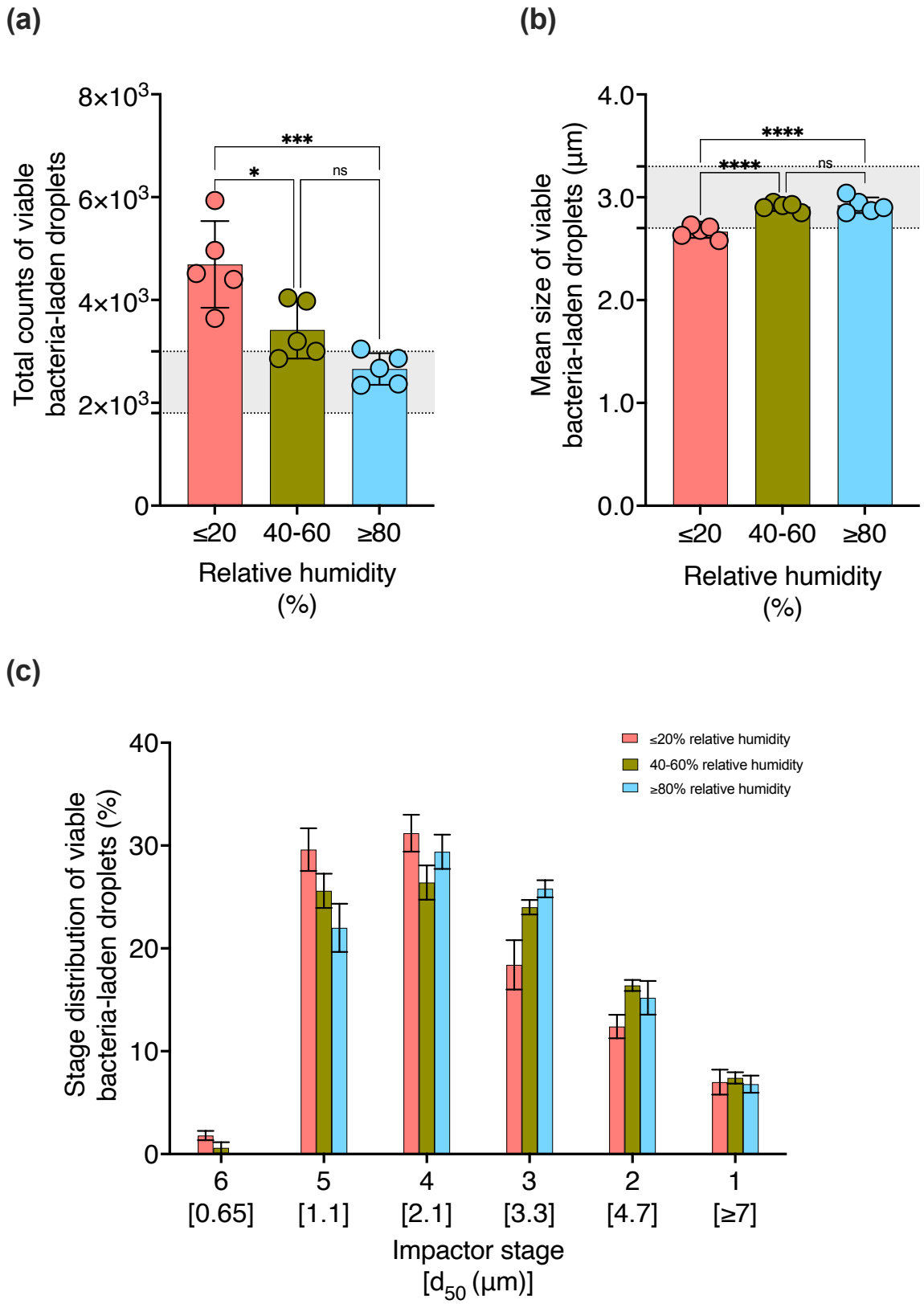
(a)
Total counts of viable bacteria-laden droplets
8×10^3
6×10^3
4×10^3
2×10^3
0
***
*
ns
≤20
40-60
≥80
Relative humidity (%)
(b)
Mean size of viable bacteria-laden droplets (µm)
4.0
3.0
2.0
1.0
0.0
****
****
ns
≤20
40-60
≥80
Relative humidity (%)
(c)
Stage distribution of viable bacteria-laden droplets (%)
40
30
20
10
0
≤20% relative humidity
40-60% relative humidity
≥80% relative humidity
6 [0.65]
5 [1.1]
4 [2.1]
3 [3.3]
2 [4.7]
1 [≥7]
Impactor stage [d50 (µm)]

Figure 3. Effect of relative humidity on the mean size, total count, and stage distribution of viable bacteria-laden droplets. The impact of varying the relative humidity on **(a)** mean size, **(b)** total count, and **(c)** stage distribution of collected viable bacteria-laden droplets is shown (n=5). All other operating variables for aerosol generation were kept constant according to **Table S7** as the relative humidity was varied, while the remaining parameters were adjusted as specified in **Table 1**. Regions shaded in grey indicate ASTM standard F2101-19 specified range for **(a)** mean size and **(b)** total count of viable bacteria-laden droplets. Asterisks indicate statistically significant differences, defined as *p-value<0.05, ** p-value <0.01, *** p-value <0.001, **** p-value <0.0001.

The noticeable increase in the mean size of viable bacteria-laden droplets, observed under increasing peptone water concentration (**Figure 2a**) or increasing RH (**Figure 3a**), can be explained by the factors affecting the equilibrium between the droplet phase and gas phase water activity. The composition of peptone water, the bacterial suspension medium specified by ASTM, is a 2:1 mixture of peptone and sodium chloride, a hygroscopic salt.[8] Increased concentration of hygroscopic solutes decreases droplet phase water activity,[24] promoting moisture absorption and resulting in larger equilibrated droplet sizes (**Figure 2a**). Meanwhile, increased RH within the aerosol mixing chamber reflects a higher gas phase water activity, driving the phase equilibrium towards the swelling of droplets containing hygroscopic solutes (**Figure 3a**). The interplay between solute concentration, hygroscopicity, and humidity contributes to the observed trends in bacteria-laden droplet size (**Figures 2a, 3a**). **Equation 4** describes this interplay, where R_{eq} (μm) is the equilibrium radius of a droplet, R_0 (μm) is the starting radius of the droplet, C_{s} (g/mL) is the peptone water concentration, and RH is the relative humidity.[25] This equation illustrates why the equilibrium radius of the droplet will increase with the increase in solute concentration or RH when the remaining parameter is held constant.

$$R_{\mathrm{eq}} = R_0 \left(\frac{C_{\mathrm{s}}}{1 - \mathrm{RH}} \right)^{\frac{1}{3}} \qquad \textbf{Equation 4}$$

Unlike the trend observed for the mean size, a significant decrease in total counts of viable bacteria-laden droplets occurred with increasing peptone water concentration (**Figure 2b**) or RH (**Figure 3d**). This decline in total counts may result from droplet loss along the walls of the aerosol mixing chamber, primarily due to gravitational sedimentation and inertial impaction. Gravitational sedimentation refers to the settling of droplets (1 to 8 μm) under the force of gravity; inertial impaction refers to the deposition of droplets (>5 μm) due to abrupt changes in the carrier flow velocity.[26] The terminal settling velocity characterizes gravitational sedimentation, signifying the faster settling of larger droplets.[27] Using **Equation 5**, the terminal settling velocity V_{s} (m/s) of droplets can be calculated, where ρ_{d} (kg/m^3) is the droplet density, D_{d} (m) is the droplet diameter, g (m/s^2) is gravitational acceleration, and μ (kg/m•s) is the dynamic viscosity of the carrier medium.[26,27] Specifically, Equation 6 shows droplets with a larger diameter will experience a higher settling velocity.

$$V_{\mathrm{s}} = \frac{\rho_{\mathrm{d}} {D_{\mathrm{d}}}^2}{18\mu} g \qquad \textbf{Equation 5}$$

The Stokes number governs inertial impaction, where a higher value represents an increased likelihood of deposition for larger droplets (inertial impaction at bends) and narrow regions of the chamber (inertial impaction due to flow constriction).[27] The dimensionless Stokes number Stk can be calculated according to **Equation 6**, where ρ_{d} (kg/m^3) is the droplet density, D_{d} (m) is the droplet diameter, u (m/s) is the mean velocity of the carrier medium, μ (kg/m•s) is the dynamic viscosity of the carrier medium, and d (m) is the diameter of the tube.[26,27] **Equation 6** indicates that if all other parameters are kept constant, droplets with a larger diameter will have a higher Stokes number and, thus, a higher likelihood of deposition.[26,27] **Equations 5** and **6** explain why increased wall loss may lead to decreased droplet counts as droplet size increases (**Figures 2,3**).

$$Stk = \frac{\rho_{\mathrm{d}} {D_{\mathrm{d}}}^2 u}{18\mu d} \qquad \textbf{Equation 6}$$

Both deposition mechanisms, namely gravitational sedimentation and inertial impaction, can impact relaxation time, the time required for aerosol droplets to adapt to changes in the velocity of the carrier medium.[28] Droplet relaxation time τ (s), calculated according to **Equation 7**, where D_{ae} (m) is the droplet aerodynamic diameter, ρ_{o} (kg/m^3) is the density of water, C_{C} is the Cunningham slip correction factor, and μ (kg/m•s) is the gas viscosity.[28,29]

$$\tau = \frac{{D_{\mathrm{ae}}}^2 \rho_{\mathrm{o}} C_{\mathrm{c}}}{18\mu} \qquad \textbf{Equation 7}$$

As shown in **Equation 7**, with increases in aerodynamic size, droplet relaxation time also increases, contributing to the loss of larger droplets that require more time to adjust to the changing trajectories of the gaseous carrier medium. The tendency of larger droplets to experience significant deposition within the system explains the decrease in total counts of viable bacteria-laden droplets with increasing peptone water concentration (**Figure 2b**) or RH (**Figure 3b**). The interplay between gravitational sedimentation, inertial impaction, relaxation time, and droplet size underscores the dynamic behaviour of aerosol droplets within the platform and substantiates the observed trends in droplet counts.

4.5.3. Effect of bacterial concentration on viable bacteria-laden aerosol properties

To examine the impact of pathogen concentration on viable aerosol properties, we quantified the mean size (**Figure 4a**), total count (**Figure 4b**), and stage distribution (**Figure 4c**) of viable bacteria-laden droplets generated from feed suspensions with concentrations of 1×10^4, 1×10^5, and 1×10^6 CFU/mL. The standard discusses a 5×10^5 CFU/mL bacterial concentration and diluting as needed to reach the specified size and count range.[8] Based on this guideline, we selected 1×10^5 CFU/mL as a midpoint value and included concentrations one logarithmic order higher and lower, covering a relevant concentration range. **Table S11** provides the operating values held constant during these trials. **Tables S12-S14** provide stage-specific viable bacteria-laden droplet count data using varied bacterial feed suspensions.

The mean size of viable bacteria-laden droplets exhibited an increase from 2.63±0.15 and 3.01±0.07 to 3.60±0.03 µm, corresponding to a logarithmic increase in bacterial concentration (**Figure 4a**). Correspondingly, total counts varied from 277±103 and 2197±435 to 13339±133 for 1×10^4, 1×10^5, and 1×10^6 CFU/mL feed concentrations, respectively (**Figure 4b**). **Figure 4c** shows the stage distribution of viable bacteria-laden droplets generated from three bacterial feed concentrations. A large fraction of viable bacteria-laden droplets generated from 1×10^4 CFU/mL

feed suspensions collect below stages four and five with lower cut-off sizes (**Figure 4c**). Meanwhile, droplets generated from 1×10^5 CFU/mL feed suspensions primarily collect below stages three and four with larger cut-off sizes (**Figure 4c**). A feed concentration of 1×10^5 CFU/mL was the only condition that resulted in droplets within the size and count range specified by ASTM, as indicated by the shaded regions in **Figures 4a** and **4b**, respectively.

We atomized 0.17 mL of 1×10^4, 1×10^5 and 1×10^6 CFU/mL bacterial feed suspensions, resulting in 1700, 17000, and 170000 viable bacterial cells in the volume of atomized feed, respectively. We collected 277±103 viable bacteria-laden droplets from the atomization of 0.17 mL of 1×10^4 CFU/mL (n=5). The atomized feed contained approximately 1700 bacterial cells. If all bacterial cells remained viable and distributed to a single droplet, 277 viable bacteria-laden droplets would indicate that 16% of the generated droplets reach the impactor and are collected.

Additionally, we collected 2197±435 viable bacteria-laden droplets from the atomization of 0.17 mL of 1×10^5 CFU/mL (n=5). The atomized feed contained approximately 17000 bacterial cells. Assuming each bacterial cell remained viable and distributed to a single droplet, 2200 droplets indicate that 13% of the generated droplets reach the impactor and are collected. Lastly, we collected 13339±133 viable bacteria-laden droplets from the atomization of 0.17 mL of 1×10^6 CFU/mL. The atomized volume contained approximately 170000 bacterial cells. If the same assumption is applied, 13339 droplets represent 7.8% of the generated droplets.

The total viable bacteria-laden droplet counts representing less than 16% fraction would suggest the presence of more than one viable bacterial cell within collected droplets. Based on the above estimations, the number of bacterial cells per droplet is likely increasing from 1 cell per droplet in 1×10^4 CFU/mL condition to >1 cell per droplet for 1×10^5 CFU/mL condition and approximately two cells per droplet for 1×10^6 CFU/mL condition. However, a fraction of the droplets in the 1×10^5 and 1×10^6 CFU/mL conditions likely contain a single viable bacterial cell, while other droplets contain 2-4 bacterial cells.

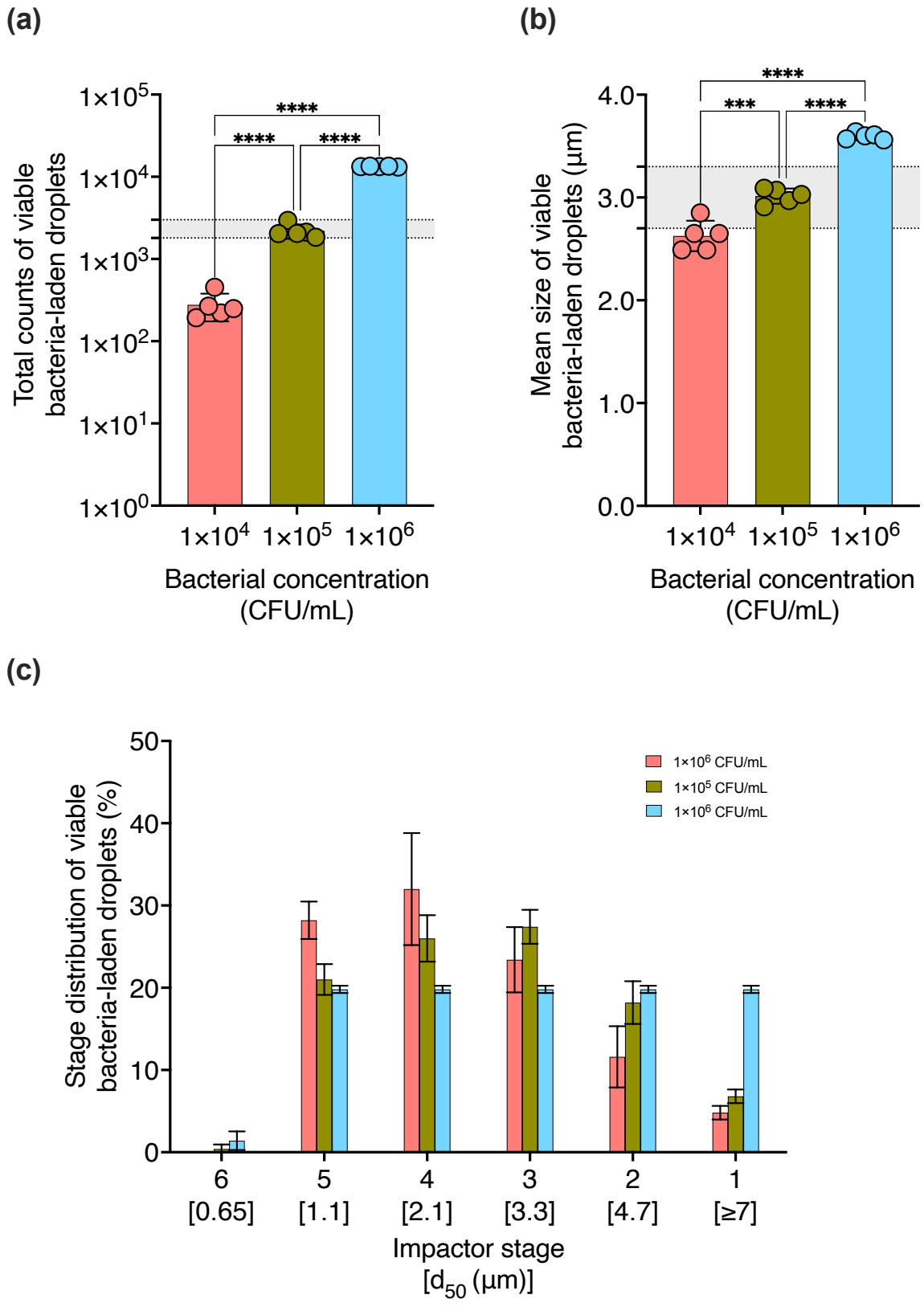
(a)
Total counts of viable bacteria-laden droplets
1×10^5
1×10^4
1×10^3
1×10^2
1×10^1
1×10^0
****
****
****
1×10^4
1×10^5
1×10^6
Bacterial concentration (CFU/mL)
(b)
Mean size of viable bacteria-laden droplets (µm)
4.0
3.0
2.0
1.0
0.0
****
***
****
1×10^4
1×10^5
1×10^6
Bacterial concentration (CFU/mL)
(c)
Stage distribution of viable bacteria-laden droplets (%)
50
40
30
20
10
0
1×10^6 CFU/mL
1×10^5 CFU/mL
1×10^6 CFU/mL
6 [0.65]
5 [1.1]
4 [2.1]
3 [3.3]
2 [4.7]
1 [≥7]
Impactor stage [d50 (µm)]

Figure 4. Effect of bacterial concentration on the mean size, total counts, and stage distribution of viable bacteria-laden droplets. The impact of varying bacterial concentration on **(a)** mean size, **(b)** total count, and **(c)** stage distribution of viable bacteria-laden droplets is shown (n=5). All other operating variables for aerosol generation were kept constant according to **Table S11** as bacterial concentration was varied. The remaining parameters were adjusted as specified in **Table 1**. Regions shaded in grey indicate ASTM standard F2101-19 specified range for **(a)** mean size and **(b)** total count of viable bacteria-laden droplets. Asterisks indicate statistically significant differences, defined as *p-value<0.05, ** p-value <0.01, *** p-value <0.001, **** p-value <0.0001.

The increased mean size of viable bacteria-laden droplets with increasing bacterial concentration might arise from the diffusional mixing rate of bacteria within.[30] The diffusivity constant of a particle D_i (cm^2/s) can be calculated using **Equation 8**, where k_B (dyn•cm/K) is the Boltzmann's constant, T (K) is the temperature in Kelvin, u_i (Pa•s) is the viscosity of the solvent medium, and r_i (cm) is the radius of the diffusing particle.[30]

$$D_i = \frac{k_B T}{6\pi u_i r_i} \qquad \textbf{Equation 8}$$

According to the Stokes-Einstein equation, an inverse relationship exists between the diffusional mixing rate of a particle within a suspended droplet (which is proportional to the diffusivity, D_i) and the radius of the diffusing particle (r_i). Staphylococci, with an approximate size of 1 μm, will exhibit much slower rates of diffusional mixing within droplets than smaller water molecules and dissolved solutes.[31] As the droplet surface recedes, bacterial cells become concentrated near the droplet surface, while water molecules (assumed to be 0.2 nm in size) readily diffuse inwards.[32] Consequently, bacterial cells may act as a barrier, impeding evaporative moisture loss by limiting the droplet surface area in contact with the environment.[33,34] Thus, the observed increase in the mean size of viable bacteria-laden droplets with bacterial concentration may be attributed to the moisture retention within droplets containing a higher bacterial load (**Figure 4a**).

In addition, the kinetic coagulation of aerosol droplets is another mechanism that may contribute to the increase in the mean size of viable bacteria-laden droplets. Coagulation is a process by which droplets collide to produce a larger droplet, and kinematic coagulation describes a process governed by forces in addition to Brownian diffusion (as is the case within our system).[35] It is likely that both the kinematic coagulation process and higher bacterial load within droplets lead to the observed increase in the mean size of viable bacteria-laden droplets generated from the more concentrated feed suspensions (**Figure 4**).

The increase in viable bacteria-laden droplet count with logarithmic increases in bacterial concentration (**Figure 4b**) can be explained, in part, by an increasing number of bacteria-containing droplets, leading to a higher count of droplets detected through culture methods. Fernandez *et al.* investigated the correlation between the bacterial feed concentration and the number of bacterial cells contained within generated droplets.[33] **Equation 9** shows the probability distribution function (PDF), representing the likelihood of occurrence of a certain number of bacterial cells within aerosol droplets, where k is the number of cells contained in a droplet and λ is the Poisson distribution coefficient (average of cells per droplet for the bacterial feed concentration loaded into the droplet generator).[33]

$$\text{PDF}\ (\kappa) = \frac{\lambda^{-\kappa}}{\kappa!} e^{-\lambda} \qquad \textbf{Equation 9}$$

Equation 9 represents a log-linear model supported by empirical data, illustrating that an increase in bacterial feed concentration raises the probability of droplets containing more than one bacterial cell. The research conducted by Liang *et al.* complements this equation, presenting evidence that bacterial viability within aerosol droplets is positively affected by an increased density of bacterial cells.[34] The authors propose that a higher number of cells aid in mitigating the osmotic stress experienced by bacteria within the aerosol droplet, ultimately contributing to enhanced bacterial viability, termed the population effect.[34] This effect could lead to more droplets harbouring more than one bacterial cell and a corresponding increase in total counts of viable bacteria-laden droplets (**Figure 4**).

4.5.4. Effect of atomizer airflow rate on viable bacteria-laden aerosol properties

Given the absence of a specific aerosol generation module in the ASTM standard, we opted for the Blaustein single-jet module operated in atomizer mode to generate bacteria-laden droplets. The aerosol generation mechanism of the Blaustein atomizer does not involve recirculation and concentration of the feed over time, which ensures a controlled and consistent output of bacterial aerosols.[36] The Blaustein atomizer can operate at airflow rates ranging from 0.5 to 3.6 L/min and feed flow rates from 100 µL/min to 6 mL/min.[36] To investigate the impact of airflow rate on aerosol properties, we generated droplets using airflow rates of 0.5, 1.5, and 2.5 L/min (**Figure 5**). **Table S15** provides the operating values held constant during these trials. **Tables S16-S18** provide stage-specific viable bacteria-laden droplet count data using varied bacterial feed suspensions.

The mean size of viable bacteria-laden droplets showed a significant decrease with increasing flow rates over a range of 4.01±0.16, 3.13±0.10, and 2.74±0.04 µm (**Figure 5a**). Viable bacteria-laden droplet counts increased from 560±143, 2232±346, to 3309±653 for 0.5, 1.5, and 2.5 L/min airflow rates, respectively (**Figure 5b**). **Figure 5c** presents the percentage of viable bacteria-laden droplets collected below each stage under varied atomizer airflow rates. The highest percentages of viable bacteria-laden droplets generated using a 0.5 L/min atomizer airflow rate were collected below stages two and three with cut-off diameters of 4.7 and 3.3 µm, respectively (**Figure 5c**). Meanwhile, the highest percentages of viable bacteria-laden droplets generated using a 1.5 L/min atomizer airflow rate were collected below stages three and four with cut-off diameters of 3.3 and 2.1 µm, respectively (**Figure 5c**). Lastly, the highest percentages of viable bacteria-laden droplets generated using a 2.5 L/min atomizer airflow rate were collected below stages four and five cut-off diameters of 2.1 and 1.1 µm, respectively (**Figure 5c**). Thus, as the atomizer airflow rate increases, viable bacteria-laden droplets are left-skewed and collect primarily on stages with lower cut-off values (**Figure 5c**). Notably, an atomizer airflow rate of 1.5 L/min was the only condition that produced viable bacteria-laden droplets with mean size and count within the ASTM-specified range, as indicated by the shaded regions in **Figures 5a** and **5b**, respectively.

Increases in atomizer airflow rates were associated with a decrease in mean size (**Figure 5a**) and a corresponding increase in the total count of viable bacteria-laden droplets (**Figure 5b**). These trends align with prior reports in the literature, highlighting an inverse relationship between droplet size and airflow rates during jet atomization.[37] The Weber number governs the process of liquid jet atomization by high-velocity gas streams.[38] The non-dimensional Weber number is the ratio between the deforming force created by the gas stream and the restoring surface tension force of

the liquid stream.[38] The aerodynamic Weber number W_e, for low-viscosity liquids, can be calculated according to **Equation 10**, where ρ_g (Pa·s) is the gas density, U_g (m/s) is the gas velocity, D_l (m) is the diameter of the liquid jet, and σ (N/m) is the surface tension of the liquid.[38]

$$W_e = \frac{\rho_g U_g^2 D_l}{\sigma} \qquad \textbf{Equation 10}$$

Higher airflow velocities (U_g) produce significant deformations in the liquid stream, corresponding to a higher Weber number and finer droplet sizes.[38] As discussed previously, smaller droplets are less likely to be removed by impaction and sedimentation, which explains the corresponding increase in droplet counts with decreased droplet size (**Figure 5**).

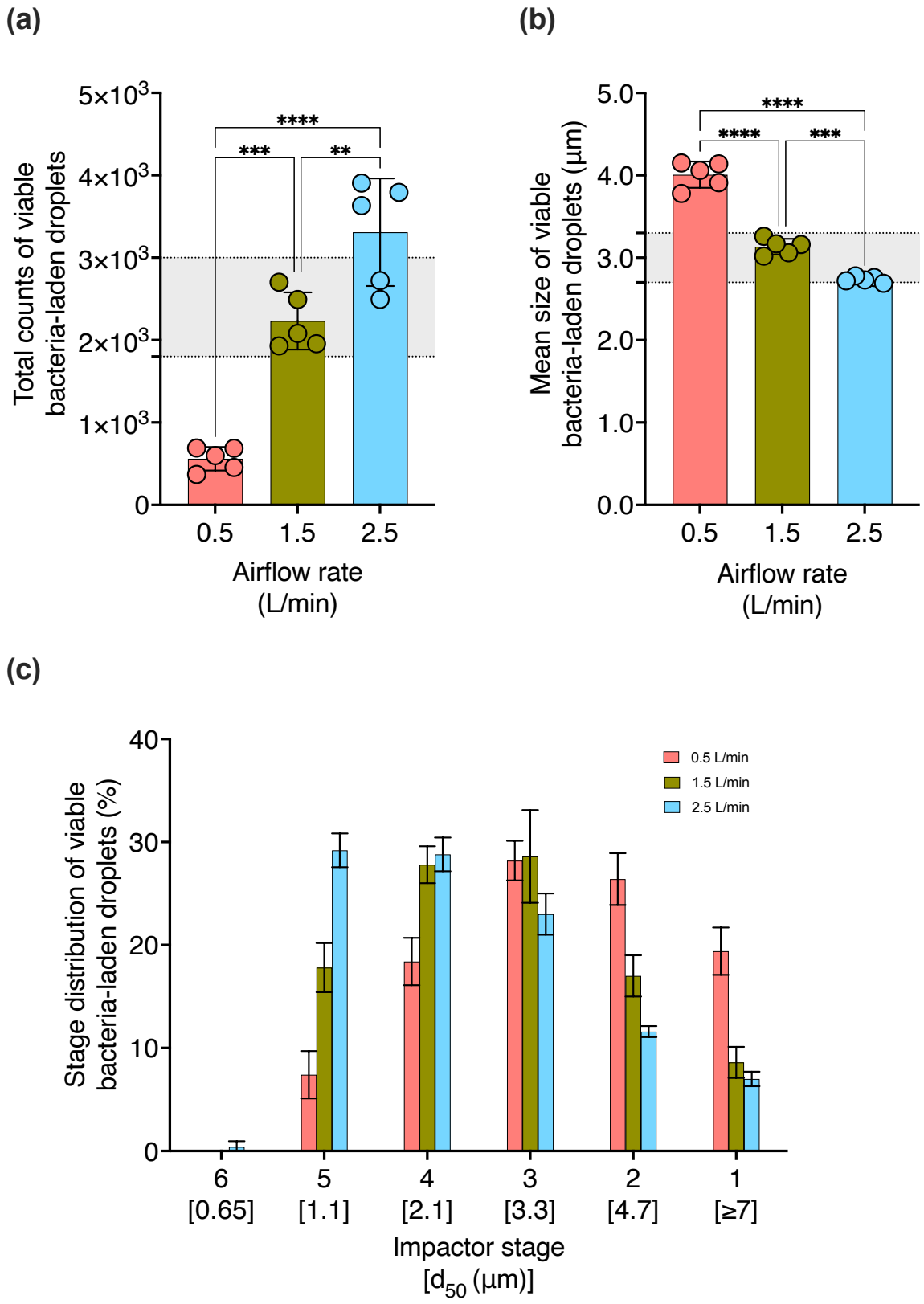
(a)
Total counts of viable bacteria-laden droplets
5×10^3
4×10^3
3×10^3
2×10^3
1×10^3
0
****
***
**
0.5
1.5
2.5
Airflow rate (L/min)
(b)
Mean size of viable bacteria-laden droplets (µm)
5.0
4.0
3.0
2.0
1.0
0.0
****
****
***
0.5
1.5
2.5
Airflow rate (L/min)
(c)
Stage distribution of viable bacteria-laden droplets (%)
40
30
20
10
0
0.5 L/min
1.5 L/min
2.5 L/min
6 [0.65]
5 [1.1]
4 [2.1]
3 [3.3]
2 [4.7]
1 [≥7]
Impactor stage [d50 (µm)]

Figure 5. Effect of atomizer airflow rate on mean size, total counts, and stage distribution of viable bacteria-laden droplets. The impact of varying atomizer airflow rates on **(a)** mean size, **(b)** total counts, and **(c)** stage distribution of viable bacteria-laden droplets is shown (n=5). All other operating variables for aerosol generation were kept constant according to **Table S15** as the atomizer airflow rate was varied. The remaining parameters were adjusted as specified in **Table 1**. Regions shaded in grey indicate ASTM standard F2101-19 specified range for **(a)** mean size and **(b)** total count of viable bacteria-laden droplets. Asterisks indicate statistically significant differences, defined as *p-value<0.05, ** p-value <0.01, *** p-value <0.001, **** p-value <0.0001.

4.5.5. Effect of atomizer feed flow rate on viable bacteria-laden aerosol properties

To investigate the impact of bacterial feed delivery rate on aerosol properties, we generated droplets using feed flow rates of under 100, 170, and 240 µL/min (**Figure 6**). **Table S19** provides the operating values held constant during these trials. **Tables S20-S22** provide stage-specific viable bacteria-laden droplet count data under varied atomizer feed flow rates. The mean size of viable bacteria-laden droplets ranged from 3.18±0.22, 3.03±0.16, to 3.09±0.06 µm for 100, 170, and 240 µL/min flow rate, respectively, showing no significant change (**Figure 6a**). The total count of viable bacteria-laden droplets showed an increase in the range of 1123±269, 2615±181, and 3619±276 for 100, 170, and 240 µL/min flow rate, respectively (**Figure 6b**). **Figure 6c** presents the stage distribution of viable bacteria-laden droplets. The generation of droplets under the three feed flow rates all produce similar stage distribution patterns, with the highest fraction of viable bacteria-laden droplets collected below stages three and four (**Figure 6c**). Among the three conditions tested, an atomizer feed flow rate of 170 µL/min produced viable bacteria-laden aerosols within ASTM-specified size and count range, as indicated by the shaded regions in **Figure 6a** and **6b**, respectively. Under an increased feed flow rate, atomization of a larger volume of the bacterial suspension generates more droplets (**Figure 6b**). Our findings are consistent with data reported by Yi *et al.* [39], showing an increase in the viable droplet counts with an increase in the feed flow rate from 0.1 mL/min to 0.9 mL/min.

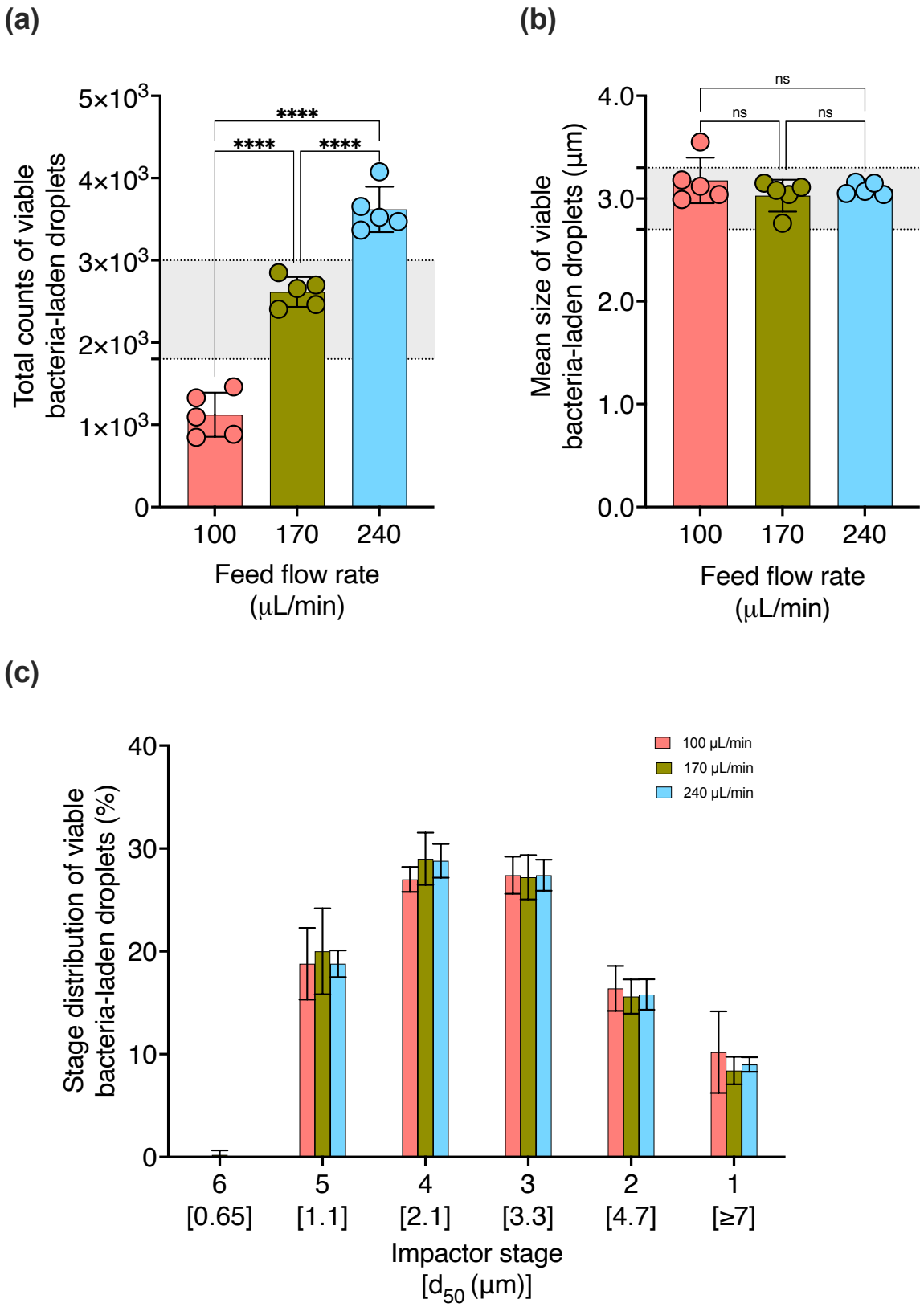
(a)
Total counts of viable bacteria-laden droplets
5×10³
4×10³
3×10³
2×10³
1×10³
0
****
****
****
100
170
240
Feed flow rate (µL/min)
(b)
Mean size of viable bacteria-laden droplets (µm)
4.0
3.0
2.0
1.0
0.0
ns
ns
ns
100
170
240
Feed flow rate (µL/min)
(c)
Stage distribution of viable bacteria-laden droplets (%)
40
30
20
10
0
100 µL/min
170 µL/min
240 µL/min
6 [0.65]
5 [1.1]
4 [2.1]
3 [3.3]
2 [4.7]
1 [≥7]
Impactor stage [d50 (µm)]

Figure 6. Effect of atomizer feed flow rates on mean size, total counts, and stage distribution of viable bacteria-laden droplets. The impact of varying atomizer feed flow rate on **(a)** mean size, **(b)** total count, and **(c)** stage distribution of viable bacteria-laden droplets is shown (n=5). All other operating variables for aerosol generation were kept constant according to **Table S19** as the atomizer feed flow rate was varied. The remaining parameters were adjusted as specified in **Table 1**. Regions shaded in grey indicate ASTM standard F2101-19 specified range for **(a)** mean size and **(b)** total count of viable bacteria-laden droplets. Asterisks indicate statistically significant differences, defined as *p-value<0.05, ** p-value <0.01, *** p-value <0.001, **** p-value <0.0001.

4.5.6. Bacterial filtration efficiency and breathability of test materials

We applied our findings to generate a bacterial aerosol challenge with the ASTM-specified size and count range to perform BFE testing of selected materials (**Tables S23-S30**). Specifically, the following test values consistently produced between 1700 to 3000 viable bacteria-laden droplets with a mean aerodynamic size range of 2.7 to 3.3 µm across 25 aerosol trials conducted over 12 months: 1.5% w/v peptone water concentration, ≥80% relative humidity at 24±2°C, 1×10^5 CFU/mL bacterial feed suspension concentration, 1.5 L/min atomizer airflow rate, and 170 µL/min feed flow rate (**Table S30, Figure S3**). The microscopic fibre arrangements of three mask materials, visualized by scanning electron microscopy, are shown in **Figure 7a**. **Figure 7b** shows the size and quantity of bacterial droplets detected in the presence and absence of mask materials. The BFE was calculated using the measured droplet counts for the 1-ply bandana, 3-ply mask, and N95 FFR, resulting in values of 15.76±13.27%, 99.86±0.11%, and 100.00%, respectively (**Figure 7c**). Microbial growth was absent on all negative control plates conducted at the end of the experimental period. Additionally, the average pressure drop across the 1-ply bandana, 3-ply mask, and N95 FFR at an airflow velocity of 27.2 cm/s was also measured, resulting in resistance values of 0.52±0.05, 7.00±0.37, and 11.04±0.05 mmH_2O/cm^2, respectively (**Figure 7d**).

The effectiveness of face masks in safeguarding against airborne transmission hinges on the filtration quality of the material. The 1-ply cotton bandana exhibited poor filtration efficiency, with an average BFE value of 15.76±13.27% (**Figure 7c**). The BFE results for the 1-ply bandana align with the findings of others, including Konda *et al.* [40], who reported a filtration efficiency of 14% for single-layer cotton material with a low thread count when challenged with sodium chloride particles 0.3 to 6 µm in size.[35] The bandana demonstrated high breathability (**Figure 7d**), which is expected based on the large mesh size observed in the electron micrograph images (**Figure 7a**). In contrast, the filtration performance of 3-ply masks was excellent, with an average BFE of 99.86±0.11% (**Figure 7c**), albeit with a moderately high-pressure drop of 7.00±0.37 mmH_2O/cm^2 (**Figure 7d**). ASTM barrier level 1 designation identifies masks with BFE ≥95% and pressure differential <5.1 mmH_2O/cm^2, while barrier level 2 and 3 designations are for masks with BFE ≥98% and pressure differential <6.1 mmH_2O/cm^2.[6] The 3-ply masks evaluated in this study fulfilled the filtration requirement but failed to meet the pressure differential for ASTM barrier designations.

The N95 FFRs were used to benchmark superior mask filtration performance. NIOSH-approved N95 FFRs, designed to filter out at least 95% of 0.3 µm-sized sodium chloride particles, represent a more stringent test than the BFE method.[17] Our filtration test results for N95 FFRs align with expectations for BFE, consistent with previously reported values obtained using the ASTM platform.[17,41] The breathability of the N95 FFR material was poor as compared to the other samples; however, the measured pressure differential of 11.04±0.05 mmH_2O/cm^2 is within the

accepted maximum values of 35 and 25 mmH_2O/cm^2 during inhalation and exhalation, respectively.[6]

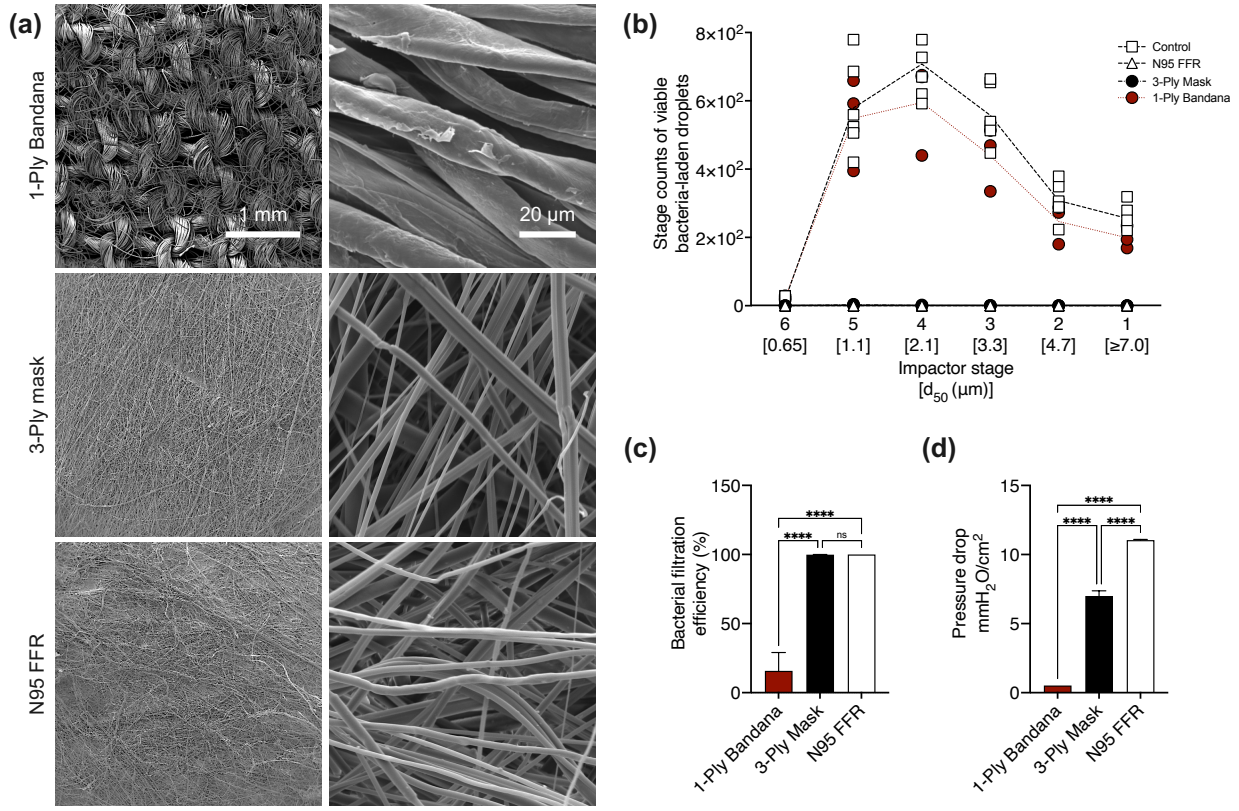

Figure 7. Dependence of bacterial filtration efficiency and breathability on test material. (a) Scanning electron microscope images of 1-ply bandana, 3-ply mask (filter layer), and N95 face filtering respirator (filter layer). **(b)** Bacteria-laden droplets collected below impactor stages in the presence and absence of test materials are shown (n=3). Dotted lines are added to guide the eye and have no scientific significance. **(c)** Bacterial filtration efficiency, and **(d)** pressure differential of test materials (n=3). Significance was defined as *p<0.05, **p<0.01, ***p<0.001, ****p<0.0001. These operating values generate bacterial challenge consisting of 1700 to 3000 viable bacteria-laden droplets with a mean size of 2.7 to 3.3 µm: ≥80% relative humidity, 1.5% w/v peptone water concentration, 1×10^5 CFU/mL bacterial concentration, 1.5 L/min and 170 µL/min atomizer airflow and feed flow rates.

4.6. IMPLICATIONS

Reliable testing of mask filtration quality requires infectious droplet generation of realistic size and number that wearers might encounter in the environment. Aerodynamic size dictates whether infectious aerosol droplets reach the airways of a potential host.[42,43] Larger droplets, with increased settling velocities, are less likely to be inhaled to mediate airborne disease transmission.[42,44] For instance, 1, 5, and 10 µm droplets falling from a height of 2 meters will reach the ground in 18.5 hours, 45 minutes, and 11 minutes, respectively.[42] Consequently, droplets in the 1 to 5 µm size range are more likely to be inhaled due to their longer airborne residence time. The ASTM-

specified size range falls within these calculated bounds, underscoring the relevance of the bacterial aerosol challenge size range for simulating airborne transmission scenarios.[8]

Regarding infectious droplet counts, studies have reported an elevation in exhaled droplet counts from SARS-CoV-2 patients.[45,46] Specifically, PCR-positive SARS-CoV-2 patients exhaled 1490 droplets per litre (d/L), while PCR-negative individuals exhaled only 252 d/L.[45] Despite the observed increase in total exhaled droplets during an active SARS-CoV-2 infection, it remains unclear what fraction of these droplets are infectious. The average ventilation rate for humans at rest is approximately 6 L/min.[47] An estimated 2700 infectious droplets are exhaled over two minutes if we assume 10% are infectious. This theoretical estimate, based on clinical evidence, aligns with the ASTM-specified droplet count range used to establish filtration efficiencies of mask materials.[8]

Our findings highlight the range of operating conditions for aerosol generation that successfully produce aerosols within the size and count range specified by the ASTM Guidance document. Inadequate control of the test conditions can lead to erroneous BFE measurements and inconsistent results between labs. Manipulating operating variables, including suspension media concentration, relative humidity, bacterial concentration, atomizer airflow and feed flow rates, revealed trends in bacterial aerosol size and counts. We identified established theories to support the mechanisms proposed for the changes in droplet size and count with parameter changes, as summarized in **Figure S4**. Certain variables, such as RH, are dictated by environmental conditions and geographical location and may be beyond the control of a standard test or a research laboratory unless they invest in an environmentally controlled room or biological safety cabinet. Consistent aerosol generation achieved using optimized test parameters led to BFE values consistent with existing literature, indicating our ability to ensure reproducibility under standard conditions.

4.7. REFERENCES

1. Zhang, R., Li, Y., Zhang, A. L., Wang, Y. & Molina, M. J. Identifying airborne transmission as the dominant route for the spread of COVID-19. *Proceedings of the National Academy of Sciences* **117**, 14857 LP – 14863 (2020).
2. Lyu, W. & Wehby, G. L. Community use of face masks and COVID-19: Evidence from a natural experiment of state mandates in the US. *Health Aff* **39**, 1419–1425 (2020).
3. Leung, N. H. L. *et al.* Respiratory virus shedding in exhaled breath and efficacy of face masks. *Nat Med* **26**, 676–680 (2020).
4. Asadi, S. *et al.* Efficacy of masks and face coverings in controlling outward aerosol particle emission from expiratory activities. *Scientific Reports 2020 10:1* **10**, 1–13 (2020).
5. Ueki, H. *et al.* Effectiveness of Face Masks in Preventing Airborne Transmission of SARS-CoV-2. *mSphere* **5**, (2020).
6. Jones, R. M. & Rempel, D. Standards for Surgical Respirators and Masks: Relevance for Protecting Healthcare Workers and the Public During Pandemics. *Ann Work Expo Health* **65**, 495–504 (2021).
7. Standard Specification for Performance of Materials Used in Medical Face Masks 1. doi:10.1520/F2100-23.
8. ASTM F2101. Standard Test Method for Evaluating the Bacterial Filtration Efficiency (BFE) of Medical Face Mask Materials , Using a Biological Aerosol of Staphylococcus aureus. *American Society for Testing and Materials* **i**, (2019).
9. Tessarolo, F. *et al.* Testing Surgical Face Masks in an Emergency Context: The Experience of Italian Laboratories during the COVID-19 Pandemic Crisis. *Int J Environ Res Public Health* **18**, 1–19 (2021).
10. Pourchez, J. *et al.* New insights into the standard method of assessing bacterial filtration efficiency of medical face masks. *Scientific Reports 2021 11:1* **11**, 1–11 (2021).
11. Dvaid L. Swift. Aerosol characterization and generation. in *Aerosols in Medicine. Principles, Diagnosis, and Therapy* (eds. Morén, F., Dolovich, M. B., Newhouse, M. T. & Newhouse, S. P.) 61–83 (Elsevier Science Publishers B. V. (Biomedical Division), Amsterdam, 1993).
12. Macher, J. M. Positive-Hole Correction of Multiple-Jet Impactors for Collecting Viable Microorganisms. *Am Ind Hyg Assoc J* **50**, (1989).
13. Andersen, A. A. New sampler for the collection, sizing, and enumeration of viable airborne particles. *J Bacteriol* **76**, (1958).
14. ATCC. Staphylococcus aureus subsp. aureus Rosenbach - 6538 | ATCC. https://www.atcc.org/products/6538.
15. Tishe Environmental. *Cascade Impactor Series 10-8XX Viable (Microbial) Particle Sizing Instruments Operations Manual*.
16. Ramachandran, G. & Cooper, D. W. Size Distribution Data Analysis and Presentation. in *Aerosol Measurement* 479–506 (John Wiley & Sons, Inc., Hoboken, NJ, USA, 2011). doi:10.1002/9781118001684.ch22.
17. Rengasamy, S., Shaffer, R., Williams, B. & Smit, S. A comparison of facemask and respirator filtration test methods. *J Occup Environ Hyg* **14**, (2017).
18. F2100 Standard Specification for Performance of Materials Used in Medical Face Masks. https://www.astm.org/f2100-23.html.

19. BSI (British Standard Institute). BS EN 14683: Medical face masks. Requirements and test metho. 26 (2019).
20. Hill, D. B. *et al.* A biophysical basis for mucus solids concentration as a candidate biomarker for airways disease. *PLoS One* **9**, (2014).
21. Hill, D. B., Button, B., Rubinstein, M. & Boucher, R. C. PHYSIOLOGY AND PATHOPHYSIOLOGY OF HUMAN AIRWAYMUCUS. *Physiol Rev* **102**, 1757–1836 (2022).
22. Song, D., Cahn, D. & Duncan, G. A. Mucin biopolymers and their barrier function at airway surfaces. *Langmuir* **36**, (2020).
23. Boucher, R. C. Muco-Obstructive Lung Diseases. *New England Journal of Medicine* **380**, (2019).
24. Huynh, E. *et al.* Evidence for a semisolid phase state of aerosols and droplets relevant to the airborne and surface survival of pathogens. *Proc Natl Acad Sci U S A* **119**, (2022).
25. Božič, A. & Kanduč, M. Relative humidity in droplet and airborne transmission of disease. *Journal of Biological Physics* vol. 47 Preprint at https://doi.org/10.1007/s10867-020-09562-5 (2021).
26. Darquenne, C. Deposition Mechanisms. *J Aerosol Med Pulm Drug Deliv* **33**, (2020).
27. Zuo, Y. Y., Uspal, W. E. & Wei, T. Airborne Transmission of COVID-19: Aerosol Dispersion, Lung Deposition, and Virus-Receptor Interactions. *ACS Nano* **14**, 16502–16524 (2020).
28. Crowder, T. M., Rosati, J. A., Schroeter, J. D., Hickey, A. J. & Martonen, T. B. Fundamental effects of particle morphology on lung delivery: Predictions of Stokes' law and the particular relevance to dry powder inhaler formulation and development. *Pharmaceutical Research* vol. 19 Preprint at https://doi.org/10.1023/A:1014426530935 (2002).
29. Tavakoli, F. & Olfert, J. S. An instrument for the classification of aerosols by particle relaxation time: Theoretical models of the aerodynamic aerosol classifier. *Aerosol Science and Technology* **47**, (2013).
30. Archer, J., Walker, J. S., Gregson, F. K. A., Hardy, D. A. & Reid, J. P. Drying kinetics and particle formation from dilute colloidal suspensions in aerosol droplets. *Langmuir* **36**, (2020).
31. Ranklin, F. & Owy, D. L. Staphylococcus aureus Infections. *https://doi-org.libaccess.lib.mcmaster.ca/10.1056/NEJM199808203390806* **339**, 520–532 (1998).
32. Davies, J. F., Haddrell, A. E., Miles, R. E. H., Bull, C. R. & Reid, J. P. Bulk, surface, and gas-phase limited water transport in aerosol. *Journal of Physical Chemistry A* **116**, (2012).
33. Fernandez, M. O. *et al.* Assessing the airborne survival of bacteria in populations of aerosol droplets with a novel technology. *J R Soc Interface* **16**, (2019).
34. Liang, Z. *et al.* Inactivation of Escherichia coli in droplets at different ambient relative humidities: Effects of phase transition, solute and cell concentrations. *Atmos Environ* **280**, 119066 (2022).
35. Hinds, W. C. Physical and Chemical Processes in Aerosol Systems. *Aerosol Measurement: Principles, Techniques, and Applications: Third Edition* 31–40 (2011) doi:10.1002/9781118001684.CH3.
36. CH Technologies. *Blaustein Atomizer (BLAM) Single-Jet Model User's Manual Revision 2*.
37. Clay, M. M., Pavia, D., Newman, T. P. & Clarke, S. W. Factors influencing the size distribution of aerosols from jet nebulisers. *Thorax* **38**, (1983).

38. Varga, C. M., Lasheras, J. C. & Hopfinger, E. J. Initial breakup of a small-diameter liquid jet by a high-speed gas stream. *J Fluid Mech* **497**, 405–434 (2003).
39. Yi, Y., Shi, D., He, C., Liu, K. & He, Q. The Influence Factors of Mean Particle Size and Positive Control of Bacterial Filtration Efficiency System. *Fortune Journal of Health Sciences* **6**, 450–456.
40. Konda, A. *et al.* Aerosol Filtration Efficiency of Common Fabrics Used in Respiratory Cloth Masks. *ACS Nano* **14**, (2020).
41. Teo, J. Y. *et al.* Exploring Reusability of Disposable Face Masks: Effects of Disinfection Methods on Filtration Efficiency, Breathability, and Fluid Resistance. *Global Challenges* **5**, (2021).
42. Scheuch, G. Breathing Is Enough: For the Spread of Influenza Virus and SARS-CoV-2 by Breathing only. *J Aerosol Med Pulm Drug Deliv* **33**, (2020).
43. Wang, C. C. *et al.* Airborne transmission of respiratory viruses. *Science* vol. 373 Preprint at https://doi.org/10.1126/science.abd9149 (2021).
44. Wells, W. F. On air-borne infection: Study II. Droplets and droplet nuclei. *Am J Epidemiol* **20**, 611–618 (1934).
45. Gutmann, D. *et al. Aerosol Measurement Identifies SARS-CoV 2 PCR Positive Adults Compared with Healthy Controls*. *medRxiv* (2022).
46. Edwards, D., Salzman, J., Devlin, T. & Langer, R. Nasal Calcium-Rich Salts for Cleaning Airborne Particles from the Airways of Essential Workers, Students, and a Family in Quarantine. *Mol Front J* **04**, 36–45 (2020).
47. Morawska, L. & Buonanno, G. The physics of particle formation and deposition during breathing. *Nature Reviews Physics* vol. 3 Preprint at https://doi.org/10.1038/s42254-021-00307-4 (2021).

4.8. SUPPORTING INFORMATION

SECTION S1. MEAN AERODYNAMIC SIZE AND TOTAL COUNT DETERMINATION OF VIABLE BACTERIA-LADEN AEROSOLS

The six-stage viable cascade impactor was selected as the bioaerosol sampler for use within the test setup to determine the total counts and mean aerodynamic size of viable bacteria-laden droplets because the ASTM standard F2101-19 refers to this instrument **(Table 1)**.[1] Moreover, among agar-based impaction systems for bioaerosol sampling, the Andersen six-stage viable cascade impactor has become a commonly used reference sampler since its introduction in 1958.[2]

Mean aerodynamic size of viable bacteria-laden droplets

The aerodynamic size reflects the behaviour of the droplet in a gaseous medium such as air and results from the size, shape, and density.[3] Each impactor stage contains 400 perforations, forming 11 concentric rings. Agar plates are positioned beneath each stage to collect droplets through impaction. Aerosols that travel through perforations will either maintain a downward trajectory until they strike the plate or follow the air currents around the glass Petri dishes to the next stage. Aerosols with sufficient momentum cannot deviate from the downward trajectory and impact the collection medium. Conversely, smaller aerosols deviate from their initial downward trajectory and follow a curved trajectory around the plates towards lower stages.

Stage cut-off diameter indicates the size of droplets collected with 50% efficiency below a given stage. Collection efficiencies increase above 50% for larger droplets and decrease below 50% for smaller droplets relative to the stage cut-off diameter. Notably, the diameter of stage perforations decreases from the first to the sixth stage: 1.18, 0.91, 0.71, 0.53, 0.34, and 0.25 mm.[4] Consequently, airflow velocity through lower stage perforations must increase proportionally for the volumetric flow rate to remain constant within the impactor. Smaller droplets that escape collection gain momentum with higher airflow velocities experienced on lower stages. Stage cut-off diameter decreases from the first to the sixth stage: 7.0, 4.7, 3.3, 2.1, 1.1, and 0.65 μm.[4] Thus, smaller aerosols are collected beneath lower stages as they require higher velocities to achieve sufficient momentum for impaction. Conversely, larger aerosols with sufficient momentum collect below the upper stages.

Total counts of viable bacteria-laden droplet

Viable bacterial-laden droplet counts reflect the colonies-forming units (CFU) detected on tryptic soy agar (Figure S1). Viable bacteria-laden droplets that impact the agar medium produce colonies. Droplets travel through one of 400 stage perforations to impact the collection medium below. An underestimate of the number of viable bacteria-laden droplets can result from multiple viable bacteria-laden droplets entering through the same perforation to produce a single colony. Therefore, a correction was applied to the 'raw' colony counts, accounting for the masking effect of multiple viable bacteria-laden droplets impacting the same region.[5,6] Reliable estimation of viable bacteria-laden droplet counts is only possible when there are less than 400 bacterial colonies per plate. Trials performed with 1×10^6 CFU/mL suspensions produced 400 colonies on five of the six collection plates; therefore, the viable bacteria-laden droplet counts presented could be an underestimation of the actual value.

Aerosol trials performed in this work
5 parameters x 3 test value per parameter = 15 conditions
15 conditions x 5 replicates per condition = 75 runs performed, analysed, and graphed (excluding 3 replicate BFE trials)

Aerosol trials required for all permutations
5 parameters with 3 test value = 3^5 total permutations = 243 conditions
243 conditions x 3 replicates = 729 runs required
243 conditions x 5 replicates = 1215 runs required

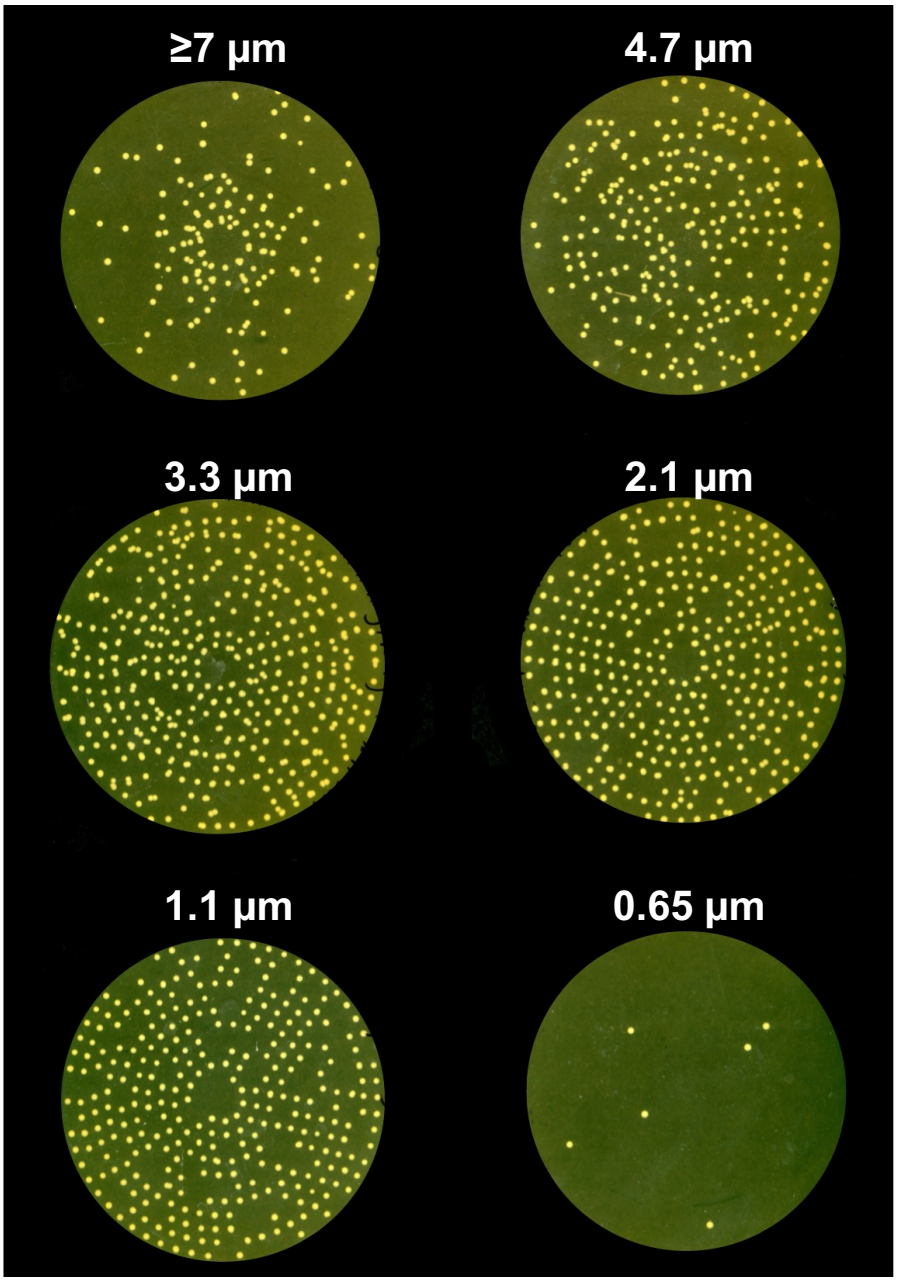

Figure S1. Scan of single aerosol run collection plate.

SECTION S2. OPERATING CONDITIONS

Preparation and delivery of bacterial feed suspension

Bacterial culture preparation used 10 µL of 25% v/v *S. aureus* glycerol stock stored at -80°C, introduced with an inoculation loop (VWR 89126-870), into 3 mL of fresh TSB media in a snap cap culture tube (Fisherbrand 14-956-9B). Bacteria were grown for 18 h at 37°C in a shaking incubator set to perform 180 rotations per minute. Bacterial cultures were stored at 4ºC before use and were discarded one week after preparation. An appropriate volume of the bacterial culture, with a concentration of 1×10^9 CFU/mL, was added to 10 mL aliquot of peptone water solution to prepare the feed suspension (1×10^4, 1×10^5, or 1×10^6 CFU/mL).

Bacterial suspension in peptone water was dispensed from a 5 mL syringe (BD 309646) and delivered to the atomizer using a 1/16'' x 3/16'' ID/OD silicone tubing (McMaster-Carr 51135K608). Feed was delivered to the atomizer at a controlled feed flow rate (100, 170, or 240 µL/min) for 1 min using a syringe pump (Fisherbrand 780100I). Bacterial feed concentration was verified using the dilution plating method. Briefly, the feed suspension was serially diluted in 900 µL aliquots of 0.9% (w/v) saline, followed by the plating of 100 µL aliquots from an appropriate dilution on TSA plates in triplicates. Plates were incubated at 37°C for 24 h to allow for colony formation. Average colony counts from the three plates were used to verify the concentration of the bacterial feed used to generate viable bacteria-laden aerosol droplets.

Test values selected for unspecified operating conditions

For the unspecified operating conditions highlighted in **Table 1**, we investigated the effect of three test values on the quality of the generated bacterial aerosol. The ambient temperature within the biosafety cabinet (BSC), housing the aerosol exposure platform, was monitored and remained relatively stable over a year-long period ranging between 22.4 and 25.6°C. We could not freely manipulate the temperature within the BSC, which excluded this variable from our investigation. We examined three relative humidity ranges: low (≤20%), intermediary (40-60%), and high (≥80%), at ambient temperature conditions between 22.4 to 25.6°C. The bacterial suspension concentration, starting at 1×10^4 CFU/mL, was increased by 1-log increments up to 1×10^6 CFU/mL. The lowest atomizer airflow and feed flow values investigated reflect the minimum operating requirements for the Blaustein single-jet atomizer module. The airflow rate was increased by 1 L/min increments in 3 steps starting from 0.5 L/min. Meanwhile, the feed flow rate, starting at 100 µL/min, was increased by 70 µL/min in 3-step increments.

The relative humidity of the makeup air controls the relative humidity within the aerosol platform. The makeup air (27.8, 26.8, 25.8 L/min) is filtered room air that is passed through an inline HEPA capsule filter (TSI 1602051) before being drawn into the 60-cm-high glass aerosol mixing chamber and mixes with aerosol droplets before being drawn into the impactor by the downstream vacuum pump (**Figure 1**). We performed the ≤20% RH runs during winter when ambient RH conditions were low, producing ≤20% RH airflows within the platform. We performed the 40-60% RH runs during the summer with intermediate RH conditions, producing airflow with a 40-60% RH within the platform. For the ≥80 RH runs, we passed filtered room air through an inline water-to-air humidifier before it entered the 60-cm-high aerosol mixing chamber, and airflow within the platform reached ≥80% RH. We confirmed the RH of the airflow within the platform by placing the SensorPush device between the stages of an assembled impactor without the agar plates (just

assembled stages) and conducting an airflow-only run (without atomizing the bacterial feed) before each trial.

Differential pressure testing conditions

The differential pressure (DP) test assesses resistance to airflow across the test material. Potassium sulphate was dissolved in 500 mL of deionized water to prepare a saturated salt solution and placed inside a sealed bag with the test materials. A PushSensor thermometer-hygrometer (HT.w 16794383) placed inside the sealed bag was used to ensure masks were conditioned for a minimum of 4 h at 85±5% RH at 21±5ºC before DP or BFE tests. DP tests measure the change in pressure across the material under constant airflow. The differential pressure tests, performed according to standard specifications, subjects the material to 27 cm/s airflow velocity, while the BFE testing subjects the material to 9.6 cm/s airflow velocity.[1,7,8] A device was constructed according to specification in British Standard BS EN 14683:2019 + AC:2019 to measure DP across test materials.[7,8] The conditioned test material was placed within the device holder with an area of 4.9 cm^2 and oriented to simulate exhalation. DP was measured using a differential manometer (Dwyer Instruments 2310) at an airflow rate of 8 L/min across the material. An average of five DP values from different regions of each test material provides a representative value.

SECTION S3. LOSS QUANTIFICATION WITHIN THE SYSTEM

Table S1. Values of operating conditions for loss quantification trial

Peptone water concentration (% w/v)	Relative humidity (%)	Fluorescein concentration (mg/mL)	Atomizer airflow rate (L/min)	Atomizer feed flow rate (µL/min)
1.5, 3, 6	≤20	1	1.5	170

A droplet loss quantification trial was performed using 1 mg/mL sodium fluorescein (Sigma-Aldrich F6377-100G) added to 1.5, 3, and 6% w/v peptone water solutions free of bacteria and atomized under ≤20% RH humidity conditions. A 170 µL volume of the fluorescein-containing peptone water solution was atomized over one minute using 1.5 LPM of compressed airflow. Foils were placed over 27 mL tryptic soy agar-containing glass Petri dishes to collect the droplets. The deposits were removed by washing the foils in 5 mL ultrapure water. Spectrophotometric readings of fluoresceine samples were taken at excitation and emission wavelengths of 490±5 and 515±5 nm, respectively (Biotek Synergy Neo2) of 200 µL of wash samples in 96-well microplates (Greiner Bio-One 655086).

Due to the difficulty in removing the fluorescein dye from the inner surfaces of the system (impactor stages, 60-cm-high glass aerosol mixing chamber, atomizer nozzle), additional trials were not pursued. The data demonstrate that 18%, 13%, and 6.5% of the fluorescein-containing feed, introduced into the system via atomization, was recovered from below the impactor stages. The loss within the system for the 6% w/v peptone water solution is more than double that of the 1.5% w/v peptone water solution.

Table S2. Nominal doses (%) of fluoresceine-containing peptone water solutions

Stage	Cut-off (µm)	Recovered dose 1.5% w/v	Recovered dose 3% w/v	Recovered dose 6% w/v
1	≥7	2.17	2.27	1.21
2	4.7	2.01	1.92	0.94
3	3.3	1.97	2.03	2.01
4	2.1	0.82	2.98	0.64
5	1.1	5.33	2.67	1.25
6	0.65	5.96	1.15	0.44
Recovered (%)		18.26	13.01	6.49
Loss (%)		81.74	86.99	93.51

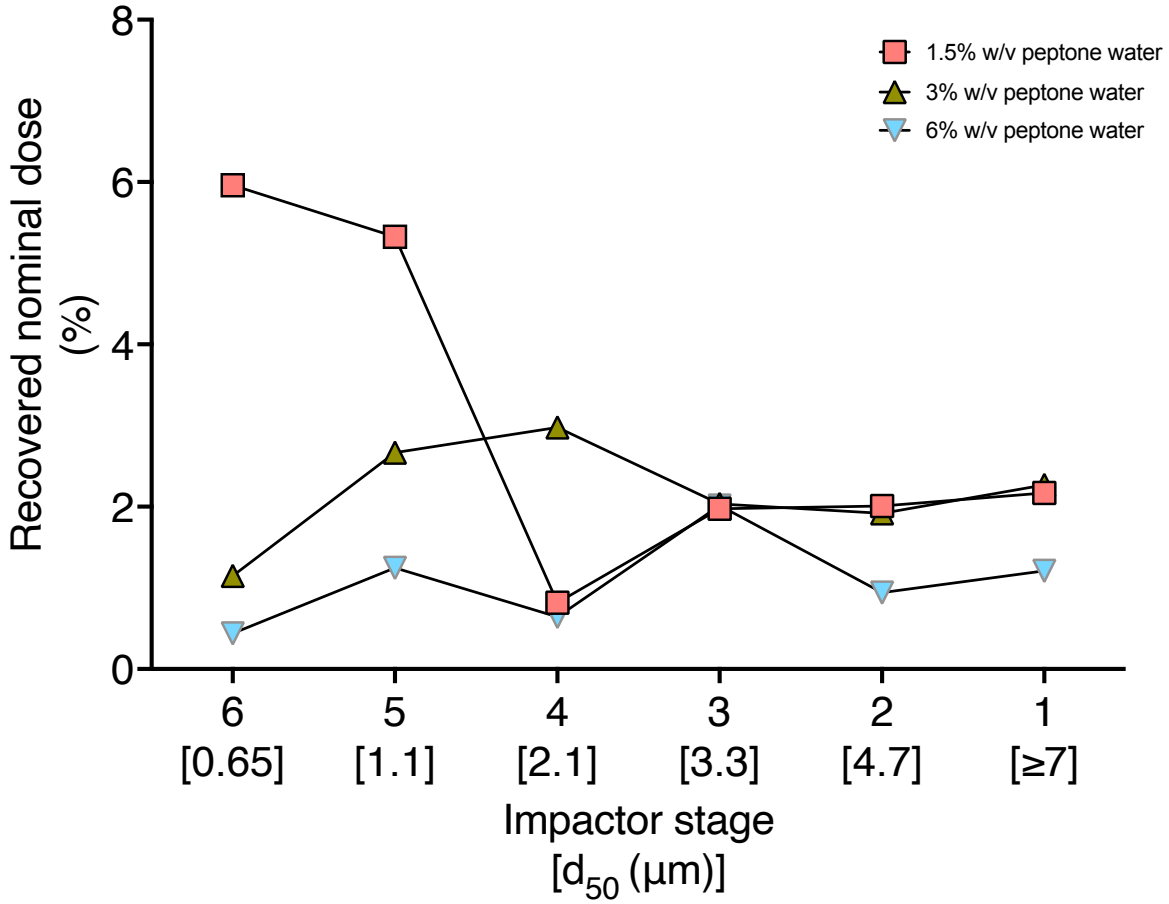

Figure S2. Stage distribution of the nominal doses of fluorescein-containing droplets.

SECTION S4. PEPTONE WATER CONCENTRATION EFFECTS ON VIABLE BACTERIA-LADEN AEROSOL PROPERTIES

Table S3. Figure 2: Values for operating parameters under varied peptone water concentration

Peptone water concentration (% w/v)	Relative humidity (%)	Bacterial concentration (CFU/mL)	Atomizer airflow rate (L/min)	Atomizer feed flow rate (µL/min)
1.5, 3, 6	≥80	1×10^5	1.5	170

Table S4. Figure 2 Data Set A: Droplet counts for five independent aerosol trials performed with 1.5% w/v peptone water suspension media

d_{50}	N_R	$\mathbf{N_{CC}}$	N_R	N_{CC}	N_R	N_{CC}	N_R	N_{CC}	N_R	N_{CC}
7	176	**232**	170	221	135	165	129	156	132	160
4.7	268	**444**	215	308	233	349	251	395	248	387
3.3	321	**649**	312	606	260	420	318	634	307	584
2.1	343	**779**	331	703	328	686	326	675	314	615
1.1	341	**766**	344	786	274	462	288	509	292	524
0.65	25	**26**	24	25	4	4	4	4	2	2
MPS		**2.88**		2.78		2.94		2.96		2.96
Total		**2896**		2649		2086		2373		2272

d_{50} = Stage cut-off diameter; N_R = Raw counts; N_C = Coincidence-correct counts; MPS = Mean particle size (µm)

S2 - Sample calculations

$$Mean\ droplet\ size, \bar{D}_{ae} = \frac{\sum_{i=1}^{6} d_{50,i} \times N_{c,i}}{N_T}$$

$$= \frac{[7 \times 232 + 4.7 \times 444 + 3.3 \times 649 + 2.1 \times 779 + 1.1 \times 766 + 0.65 \times 26]}{[232 + 444 + 649 + 779 + 766 + 26]}$$

$$= 2.88\ \mu m$$

$$N_T = \sum_{i=1}^{6} N_{c,i}$$

$$Total\ droplet\ counts, N_T = 232 + 444 + 649 + 779 + 766 + 26$$

$$= 2896$$

Table S5. Figure 2 Data Set B: Droplet counts for five independent aerosol trials performed with 3% w/v peptone water suspension media

d_{50}	N_R	N_C	N_R	N_C	N_R	N_C	N_R	N_C	N_R	N_C
7	188	254	205	287	186	250	188	254	186	250
4.7	292	524	298	547	274	462	287	506	268	444
3.3	340	759	367	998	336	733	343	779	340	759
2.1	353	857	354	865	326	675	326	675	327	680
1.1	248	387	238	362	229	340	240	367	205	287
0.65	1	1	1	1	3	3	2	2	1	1
MPS		3.22		3.30		3.30		3.31		3.34

Total		2782		3060		2463		2583		2421

Table S6. Figure 2 Data Set C: Droplet counts for five independent aerosol trials performed with 6% w/v peptone water suspension media

d_{50}	N_R	N_C	N_R	N_C	N_R	N_C	N_R	N_C	N_R	N_C
7	178	236	182	243	192	262	176	232	176	232
4.7	279	478	300	555	301	559	280	482	284	495
3.3	326	675	327	680	327	680	328	686	330	697
2.1	282	488	288	509	308	588	261	423	287	506
1.1	89	101	149	186	182	243	60	65	100	115
0.65	0	0	0	0	0	0	0	0	0	0
MPS		3.67		3.60		3.52		3.77		3.64
Total		1978		2173		2332		1888		2045

SECTION S5. RELATIVE HUMIDITY EFFECTS ON VIABLE BACTERIA-LADEN AEROSOL PROPERTIES

Table S7. Figure 3: Values for operating parameters under varied relative humidity

Peptone water concentration (% w/v)	Relative humidity (%)	Bacterial concentration (CFU/mL)	Atomizer airflow rate (L/min)	Atomizer feed flow rate (µL/min)
1.5	≤20,40-60, ≥80	1×10^5	1.5	170

Table S8. Figure 3 Data Set A: Droplet counts for five independent aerosol trials performed at ≤20% relative humidity

d_{50}	N_R	N_C	N_R	N_C	N_R	N_C	N_R	N_C	N_R	N_C
7	216	311	207	292	206	289	232	347	239	364
4.7	262	426	308	588	315	620	300	555	334	721
3.3	300	555	362	942	358	902	350	832	375	1109
2.1	380	1198	383	1263	387	1371	391	1518	397	1961
1.1	374	1093	383	1263	383	1263	393	1619	394	1681
0.65	55	59	49	52	65	71	82	92	88	99
MPS		2.68		2.73		2.71		2.58		2.63
Total		3642		4400		4516		4963		5935

Table S9. Figure 3 Data Set B: Droplet counts for five independent aerosol trials performed at 40-60% relative humidity

d_{50}	N_R	N_C	N_R	N_C	N_R	N_C	N_R	N_C	N_R	N_C
7	202	281	196	269	166	214	185	248	176	232
4.7	326	675	317	629	268	444	291	520	288	509
3.3	365	975	368	975	326	675	343	779	329	692
2.1	376	1125	372	1064	347	809	342	772	344	786
1.1	359	911	374	1093	331	703	353	857	341	766
0.65	12	12	12	12	15	15	20	21	18	18

MPS		2.95		2.85		2.90		2.92		2.93
Total		3979		4042		2860		3197		3003

Table S10. Figure 3 Data Set C: Droplet counts for five independent aerosol trials performed at ≥80% relative humidity

d_{50}	N_R	N_C	N_R	N_C	N_R	N_C	N_R	N_C	N_R	N_C
7	120	143	127	153	146	182	157	199	177	234
4.7	264	432	229	340	257	411	259	417	268	444
3.3	307	584	319	639	326	675	346	801	338	746
2.1	323	659	323	659	342	772	358	902	361	931
1.1	291	520	304	571	316	624	333	715	287	506
0.65	4	4	6	6	7	7	11	11	4	4
MPS		2.95		2.87		2.90		2.85		3.04
Total		2342		2368		2671		3045		2865

SECTION S6. PATHOGEN CONCENTRATION EFFECTS ON VIABLE BACTERIA-LADEN AEROSOL PROPERTIES

Table S11. Figure 4: Values for operating parameters under varied bacterial concentration

Peptone water concentration (% w/v)	Relative humidity (%)	Bacterial concentration (CFU/mL)	Atomizer airflow rate (L/min)	Atomizer feed flow rate (μL/min)
1.5	≥80	1×10^4, 1×10^5, 1×10^6	1.5	170

Table S12. Figure 4 Data Set A: Droplet counts for five independent aerosol trials performed with 1×10^4 CFU/mL with bacterial concentration

d_{50}	N_R	N_C	N_R	N_C	N_R	N_C	N_R	N_C	N_R	N_C
7	20	21	11	11	12	12	12	12	10	10
4.7	68	75	20	21	27	28	18	18	24	25
3.3	114	134	44	47	43	46	55	59	46	49
2.1	93	106	51	55	64	70	93	106	81	91
1.1	100	115	55	59	59	64	66	72	67	73
0.65	2	2	0	0	1	1	0	0	1	1
MPS		2.85		2.65		2.65		2.49		2.49
Total		453		193		221		267		249

Table S13. Figure 4 Data Set B: Droplet counts for five independent aerosol trials performed with 1×10^5 CFU/mL with bacterial concentration

d_{50}	N_R	N_C	N_R	N_C	N_R	N_C	N_R	N_C	N_R	N_C
7	168	218	103	119	104	120	124	148	123	147
4.7	294	531	270	450	251	395	214	306	214	306
3.3	355	874	301	559	312	606	288	509	280	482
2.1	333	715	286	502	284	495	311	601	294	531
1.1	310	597	250	392	283	492	277	472	242	372

0.65	18	18	12	12	9	9	6	6	3	3
MPS		3.07		3.09		2.97		2.91		3.03
Total		2953		2034		2117		2042		1841

Table S14. Figure 4 Data Set C: Droplet counts for five independent aerosol trials performed with 1×10^6 CFU/mL with bacterial concentration

d_{50}	N_R	N_C	N_R	N_C	N_R	N_C	N_R	N_C	N_R	N_C
7	400	2628	400	2628	400	2628	400	2628	400	2628
4.7	400	2628	400	2628	400	2628	400	2628	400	2628
3.3	400	2628	400	2628	400	2628	400	2628	400	2628
2.1	400	2628	400	2628	400	2628	400	2628	400	2628
1.1	400	2628	400	2628	400	2628	400	2628	400	2628
0.65	16	16	143	177	122	146	231	345	217	313
MPS		3.64		3.60		3.61		3.56		3.57
Total		13156		13317		13286		13485		13453

SECTION S7. ATOMIZER AIR FLOW RATE EFFECTS ON VIABLE BACTERIA-LADEN AEROSOL PROPERTIES

Table S15. Figure 5: Values for operating parameters under varied atomizer airflow rate

Peptone water concentration (% w/v)	Relative humidity (%)	Bacterial concentration (CFU/mL)	Atomizer airflow rate (L/min)	Atomizer feed flow rate (µL/min)
1.5	≥80	1×10^5	0.5, 1.5, 2.5	170

Table S16. Figure 5 Data Set A: Droplet counts for five independent aerosol trials performed at 0.5 L/min atomizer airflow rate

d_{50}	N_R	N_C	N_R	N_C	N_R	N_C	N_R	N_C	N_R	N_C
7	113	133	86	97	73	81	98	112	99	114
4.7	160	204	107	125	88	99	135	165	121	144
3.3	144	179	112	131	89	101	165	213	135	165
2.1	104	120	68	75	64	70	109	127	110	129
1.1	48	51	26	27	19	19	67	73	44	47
0.65	0	0	0	0	0	0	1	1	0	0
MPS		4.06		4.15		4.14		3.78		3.91
Total		687		455		370		691		599

Table S17. Figure 5 Data Set B: Droplet counts for five independent aerosol trials performed at 1.5 L/min atomizer airflow rate

d_{50}	N_R	N_C	N_R	N_C	N_R	N_C	N_R	N_C	N_R	N_C
7	139	171	144	179	138	169	136	166	209	296
4.7	252	398	202	281	277	472	209	296	272	456
3.3	328	686	319	639	313	610	301	559	320	644
2.1	297	543	286	502	340	759	300	555	343	779
1.1	203	283	224	328	279	478	245	379	293	527

0.65	0	0	1	1	4	4	0	0	0	0
MPS		3.26		3.16		3.02		3.06		3.17
Total		2081		1930		2492		1955		2702

Table S18. Figure 5 Data Set C: Droplet counts for five independent aerosol trials performed at 2.5 L/min atomizer airflow rate

d_{50}	N_R	N_C	N_R	N_C	N_R	N_C	N_R	N_C	N_R	N_C
7	183	245	154	194	158	201	196	269	194	265
4.7	280	482	221	322	199	275	258	414	273	459
3.3	365	975	322	654	310	597	347	809	342	772
2.1	378	1160	332	709	333	715	370	1036	376	1125
1.1	370	1036	349	824	330	697	373	1078	378	1160
0.65	8	8	18	18	9	9	25	26	11	11
MPS		2.76		2.73		2.78		2.72		2.69
Total		3906		2721		2494		3632		3792

SECTION S8. ATOMIZER FEED FLOW RATE EFFECTS ON VIABLE BACTERIA-LADEN AEROSOL PROPERTIES

Table S19. Figure 6: Values for operating parameters under varied atomizer feed flow rate

Peptone water concentration (% w/v)	Relative humidity (%)	Bacterial concentration (CFU/mL)	Atomizer airflow rate (L/min)	Atomizer feed flow rate (µL/min)
1.5	≥80	1×10^5	1.5	100, 170, 240

Table S20. Figure 6 Data Set A: Droplet counts for five independent aerosol trials performed at 100 µL/min atomizer feed flow rate

d_{50}	N_R	N_C	N_R	N_C	N_R	N_C	N_R	N_C	N_R	N_C
7	116	137	188	254	73	81	61	66	74	82
4.7	158	201	172	225	111	130	120	143	168	218
3.3	250	392	258	414	178	236	167	216	207	292
2.1	240	367	240	367	185	248	174	228	209	296
1.1	175	230	158	201	151	190	153	193	161	206
0.65	0	0	0	0	0	0	2	2	0	0
MPS		2.85		2.65		2.65		2.49		2.49
Total		453		193		221		267		249

Table S21. Figure 6 Data Set B: Droplet counts for five independent aerosol trials performed at 170 µL/min atomizer feed flow rate

d_{50}	N_R	N_C	N_R	N_C	N_R	N_C	N_R	N_C	N_R	N_C
7	140	172	168	218	166	214	175	230	190	258
4.7	231	345	234	352	256	409	267	440	273	459
3.3	330	697	313	610	336	733	343	779	335	727
2.1	334	721	342	772	332	709	328	686	356	883

1.1	335	727	270	450	251	395	291	520	291	520
0.65	36	38	4	4	2	2	3	3	3	3
MPS		2.76		3.04		3.15		3.11		3.08
Total		2700		2406		2462		2658		2850

Table S22. Figure 6 Data Set C: Droplet counts for five independent aerosol trials performed at 240 µL/min atomizer feed flow rate

d_{50}	N_R	N_C	N_R	N_C	N_R	N_C	N_R	N_C	N_R	N_C
7	247	384	222	324	212	302	215	308	234	352
4.7	333	715	299	551	288	509	286	502	300	555
3.3	371	1050	357	892	358	902	372	1064	368	1010
2.1	382	1241	367	998	365	975	375	1109	361	931
1.1	328	686	330	697	326	675	325	670	325	670
0.65	1	1	10	10	5	5	2	2	4	4
MPS		3.16		3.07		3.05		3.04		3.15
Total		4077		3472		3368		3655		3522

SECTION S9. BACTERIAL FILTRATION EFFICIENCY EVALUATIONS OF THREE TEST MATERIALS

Table S23. Figure 7: Values of optimized operating conditions

Peptone water concentration (% w/v)	Relative humidity (%)	Bacterial concentration (CFU/mL)	Atomizer airflow rate (L/min)	Atomizer feed flow rate (µL/min)
1.5	≥80	1×10^5	1.5	170

Table S24. Figure 7b,7c Data Set A: Control aerosol trials

d_{50}	N_R Positive control A	**N_C Positive control A**	N_R Positive control B	**N_C Positive control B**	N_R Negative control A	N_C Negative control A
7	201	**279**	175	**230**	0	0
4.7	171	**223**	211	**300**	0	0
3.3	322	**654**	293	**527**	0	0
2.1	343	**779**	315	**620**	0	0
1.1	292	**524**	301	**559**	0	0
0.65	14	**14**	13	**13**	0	0
MPS		**2.98**		**2.97**		-
Total		**2473**		**2249**		0
MPS	2.97					
Total	**2361**					

S24 - Sample calculation

$$Total\ droplet\ counts, N_{\mathrm{T}} = \sum_{i=1}^{6} N_{\mathrm{c},i}$$

$$Total\ droplet\ counts, N_{T,A} = 279 + 223 + 527 + 620 + 559 + 13 = 2473$$

$$Total\ droplet\ counts, N_{T,B} = 230 + 300 + 654 + 779 + 524 + 14 = 2249$$

$$Average\ positive\ control\ droplet\ counts, N_{Avg} = \frac{2473 + 2249}{2} = 2361$$

Table S25. Figure 7b,7c Data Set A: Bacterial filtration efficiency trials

d_{50}	N_R Bandana	**N_C Bandana**	N_R 3-Ply Mask	N_C 3-Ply Mask	N_R N95 Respirator	N_C N95 Respirator
7	177	**234**	0	0	0	0
4.7	198	**273**	0	0	0	0
3.3	289	**513**	0	0	0	0
2.1	326	**675**	0	0	0	0
1.1	309	**592**	1	1	0	0
0.65	21	**22**	0	0	0	0
MPS		**2.9**		1.1	-	-
Total		**2309**		1	0	0
BFE (%)		**2.20**		99.96		100

BFE = Bacterial filtration efficiency (%)

S25 - Sample calculation

$$Bandana\ bacterial\ filtration\ efficiency = \left[1 - \frac{[Droplets\ in\ the\ presence\ of\ test\ material]}{[Average\ positve\ control\ droplets\ (absence\ of\ test\ material)]}\right] \times 100$$

$$Bandana\ bacterial\ filtration\ efficiency = \left[1 - \frac{[2309]}{2361}\right] \times 100 = 2.2\%$$

Table S26. Figure 7b,7c Data Set B: Control aerosol trials

d_{50}	N_R Positive control A	N_C Positive control A	N_R Positive control B	N_C Positive control B	N_R Negative control A	N_C Negative control A
7	178	236	170	221	0	0
4.7	214	306	233	349	0	0
3.3	296	539	269	447	0	0
2.1	325	670	309	592	0	0
1.1	287	506	260	420	0	0
0.65	9	9	14	14	0	0

MPS		3.02		3.12		-
Total		2266		2043		0
MPS	3.07					
Total	2155					

Table S27. Figure 7b,7c Data Set B: Bacterial filtration efficiency trials

d_{50}	N_R Bandana	N_C Bandana	N_R 3-Ply Mask	N_C 3-Ply Mask	N_R N95 Respirator	N_C N95 Respirator
7	138	169	0	0	0	0
4.7	145	180	0	0	0	0
3.3	227	335	0	0	0	0
2.1	267	440	0	0	0	0
1.1	251	395	3	3	0	0
0.65	17	17	0	0	0	0
MPS		2.93		1.1	-	-
Total		1536		3	0	0
BFE (%)		28.71		99.86		100

Table S28. Figure 7b,7c Data Set C: Control trials

d_{50}	N_R Positive control A	N_C Positive control A	N_R Positive control B	N_C Positive control B	N_R Negative control A	N_C Negative control A
7	220	319	186	250	0	0
4.7	245	379	206	289	0	0
3.3	324	664	289	513	0	0
2.1	353	857	335	727	0	0
1.1	343	779	328	686	0	0
0.65	28	29	27	28	0	0
MPS		2.93		2.85		-
Total		3027		2493		0
MPS	2.89					
Total	2760					

Table S29. Figure 7b,7c Data Set C: Bacterial filtration efficiency trials

d_{50}	N_R Bandana	N_C Bandana	N_R 3-Ply Mask	N_C 3-Ply Mask	N_R N95 Respirator	N_C N95 Respirator
7	154	194	0	0	0	0
4.7	205	287	0	0	0	0
3.3	276	469	1	1	0	0
2.1	325	670	2	2	0	0
1.1	323	659	4	4	0	0
0.65	28	29	0	0	0	0
MPS		2.78		1.7	-	-
Total		2308		7	0	0

BFE (%)		16.38		99.75		100

BFE material testing was performed in accordance with ASTM F2101-19.[5]

SECTION S10. STAGE DISTRIBUTION OF VIABLE BACTERIA-LADEN DROPLETS UNDER OPTIMIZED TEST CONDITIONS

Table S30. Stage distribution of viable bacteria-laden aerosol droplets

Stage	Cut-off (µm)	Counts	SD	Trials
1	≥7	193	50	25
2	4.7	368	73	25
3	3.3	608	104	25
4	2.1	673	122	25
5	1.1	530	137	25
6	**0.65**	**10**	**9**	**25**

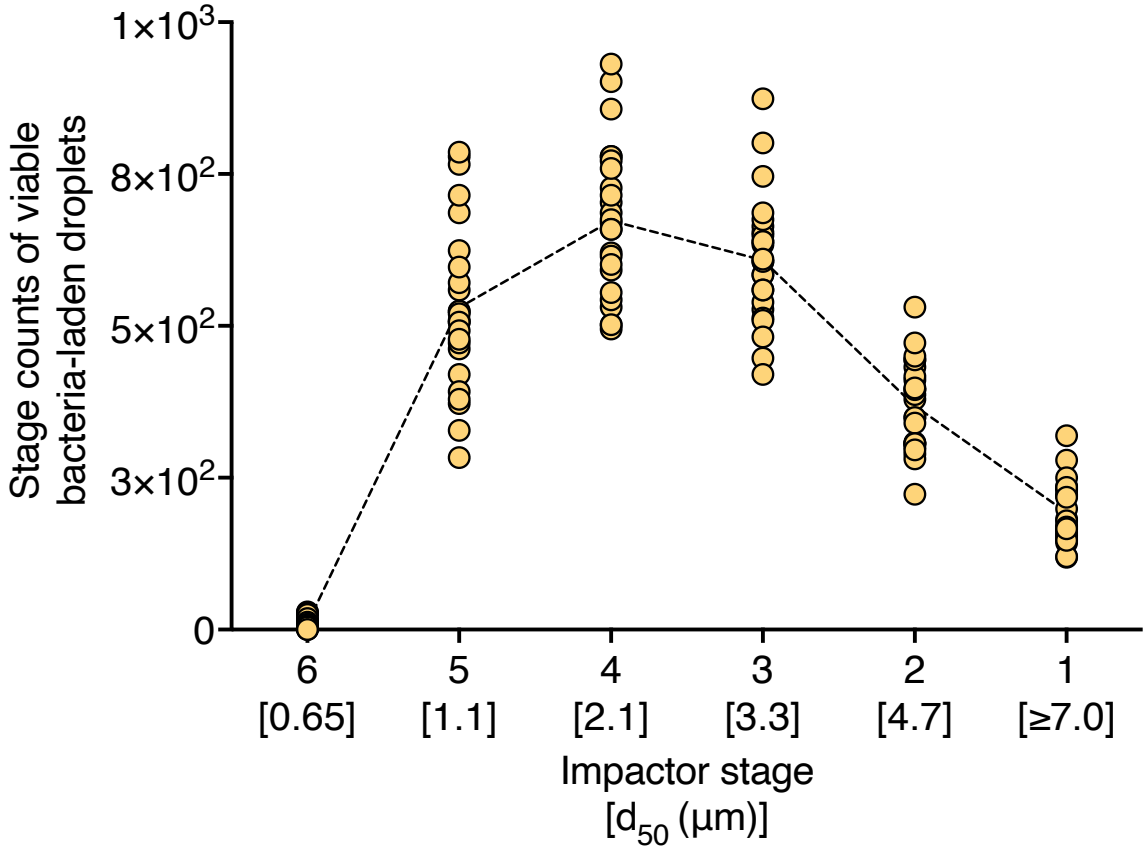

Figure S3. Stage distribution of viable bacteria-laden aerosol droplets (n=25).

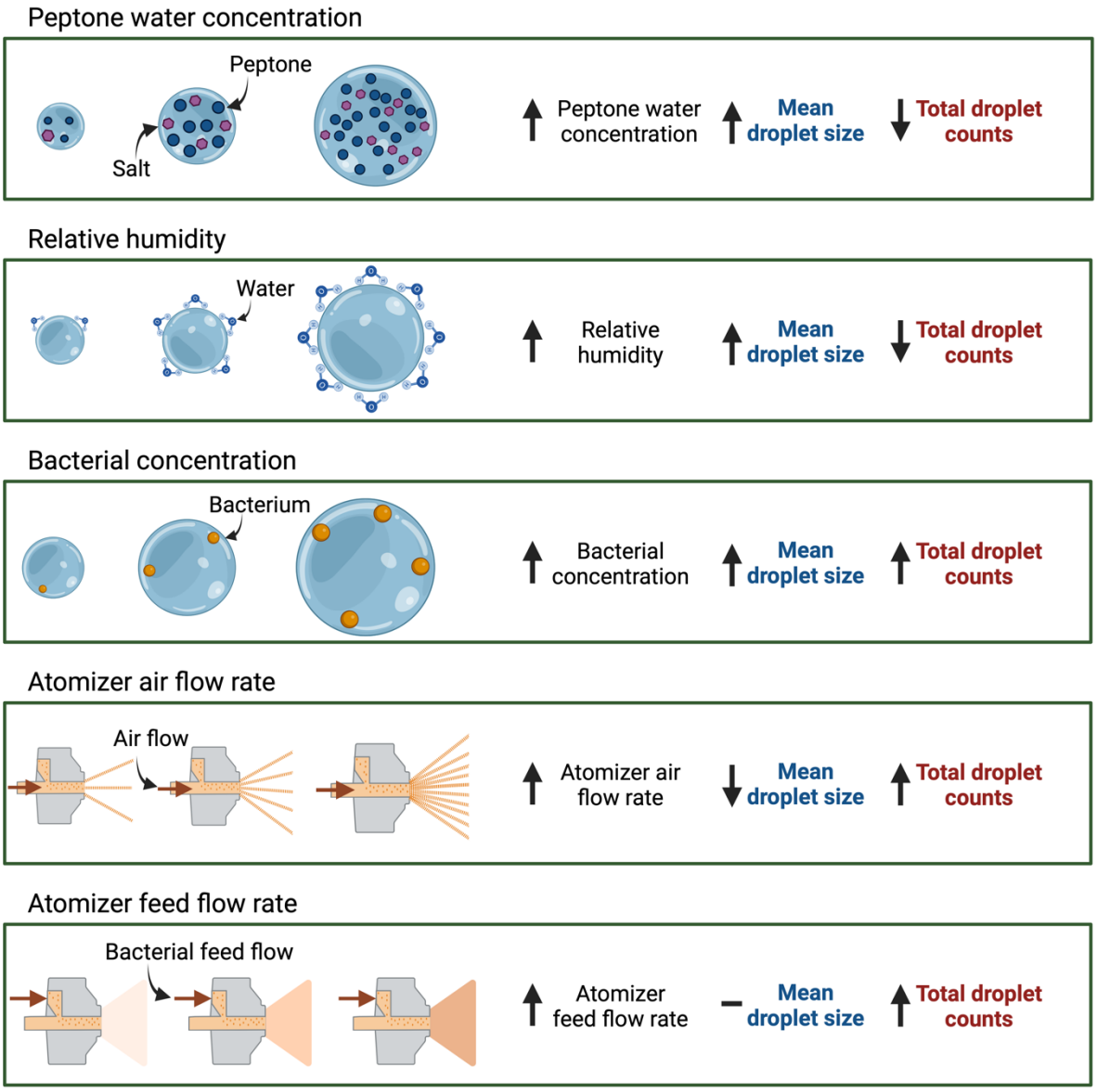

Figure S4. The illustration depicts potential mechanisms impacting viable bacteria-laden droplet size and count.

4.9. REFERENCES

1. ASTM F2101. Standard Test Method for Evaluating the Bacterial Filtration Efficiency (BFE) of Medical Face Mask Materials , Using a Biological Aerosol of Staphylococcus aureus. *American Society for Testing and Materials* **i**, (2019).
2. Mainelis, G. Bioaerosol sampling: Classical approaches, advances, and perspectives. *Aerosol Science and Technology* **54**, 496–519 (2020).
3. Crowder, T. M., Rosati, J. A., Schroeter, J. D., Hickey, A. J. & Martonen, T. B. Fundamental effects of particle morphology on lung delivery: Predictions of Stokes' law and the particular relevance to dry powder inhaler formulation and development. *Pharmaceutical Research* vol. 19 Preprint at https://doi.org/10.1023/A:1014426530935 (2002).
4. Tishe Environmental. *Cascade Impactor Series 10-8XX Viable (Microbial) Particle Sizing Instruments Operations Manual*.
5. Macher, J. M. Positive-Hole Correction of Multiple-Jet Impactors for Collecting Viable Microorganisms. *Am Ind Hyg Assoc J* **50**, (1989).
6. Andersen, A. A. New sampler for the collection, sizing, and enumeration of viable airborne particles. *J Bacteriol* **76**, (1958).
7. F2100 Standard Specification for Performance of Materials Used in Medical Face Masks. https://www.astm.org/f2100-23.html.
8. BSI (British Standard Institute). BS EN 14683: Medical face masks. Requirements and test metho. 26 (2019).

Chapter 5. An impactor-based aerosol platform for probing indoor, short-range transmission dynamics: a Phi6 bacteriophage study

Preface. This chapter discusses the use of the aerosol platform to model changes in virus viability within aerosol droplets in indoor environments during winter and summer in temperate zones across two different pathogen concentrations and three different suspension matrix compositions. ***The results and conclusions presented in this chapter are valid under specific conditions and assumptions outlined in the study. Therefore, the accuracy and reliability of the findings depend on defined test conditions. These results may not be applicable under all circumstances or in different environments. Users of this information should exercise caution and consider additional factors relevant to their specific context before applying these results to describe and interpret real-world phenomena.***

Contributions. I performed all aerosol experiments and wrote and incorporated edits from coauthors for all manuscript drafts. Dr. Mellissa Gomez helped to process the samples from the wash trials (**Figure S1, Tables S7-S18**), assisted with conducting the aerosol trials (**Figures 3-9, Tables S34-S36**), and edited all manuscript drafts. Ekaterina Kvitka performed multiple rounds of washing and autoclave sterilization of silicone tubing and plates; preparation and autoclave sterilization of agar media used in a subset of the aerosol trials; scanned plates (**Figures 3-9, Tables S34-S36**); contributed to editing the final manuscript draft; and helped design the graphical abstract. Kyle Jackson edited multiple versions of the manuscript. Rod G. Rhem constructed the aerosol platform and provided input to troubleshoot issues and optimize operational parameters. Dr. Zeinab Hosseinidoust and Prof. Myrna B. Dolovich were responsible for funding acquisition, methods development, project administration, supervision, weekly meetings, and review and scientific editing of the final manuscript drafts. Paul Gatt, Justin Bernar, John Colenbrander from the Chemical and Mechanical Engineering Machine Shop and Doug Keller were instrumental in helping to design and build the aerosol platform.

Citation. This chapter is under review, Environment Science and Technology.
Thirugnanasampanthar, M., Gomez, M., Kvitka, E., Jackson, K., Rhem, R. G., Dolovich, M. B., & Hosseinidoust, Z. (2024). An impactor-based aerosol platform for probing indoor, short-range transmission dynamics: a Phi6 bacteriophage study.

5.1. ABSTRACT

This study explored the effects of droplet size range, solute content, and virus concentration on viable virus-laden droplet counts following short timescales of exposure to indoor environmental conditions using an aerosol platform. The platform can generate and equilibrate droplets to set environmental conditions (<20 seconds exposure to 24±1.6°C and 15±5% or 50±5% relative humidity) within a 60-cm-high glass aerosol mixing chamber and collect size-resolved droplets within a six-stage viable cascade impactor, enabling the sizing and enumeration of viable virus-laden droplets. SARS-CoV-2 surrogate bacteriophage Phi6 titers were selected to reflect sputum viral loads and suspended in solutions formulated to reflect the solute content of the airway lining fluid. Most droplet size fractions generated from 1×10^5 plaque-forming units per millilitre (PFU/mL) virus suspensions containing 1.5% w/v solute content and equilibrated to low humidity conditions resulted in significantly fewer droplets compared to those containing 6% w/v solute content and equilibrated to intermediate humidity condition. However, droplets generated from concentrated phage suspensions (5×10^5 PFU/mL) remained comparable in counts regardless of solute content and equilibration to low or intermediate humidity conditions. The results suggest heterogeneities in sputum solute content and viral loads may alter virus stability within airborne droplets and indoor close-range transmission dynamics.

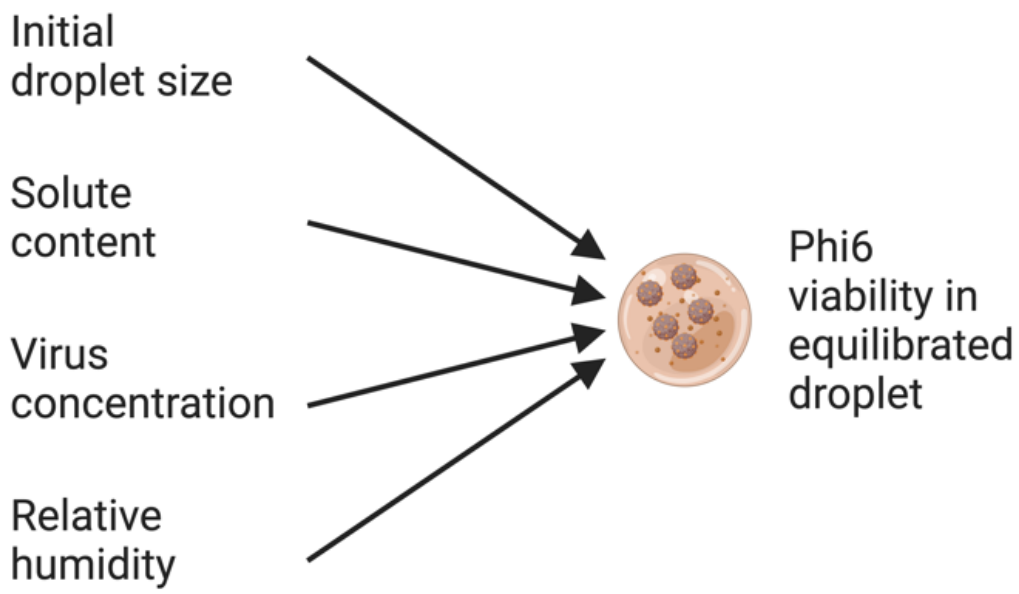

Graphical abstract – The illustration depicts the experimental design to study virus viability changes within aerosol droplets based on initial droplet size, solute content, virus concentration, and indoor relative humidity.

5.2. INTRODUCTION

The complex interplay between environmental and biological (host- and pathogen-related) factors dictates the survival of pathogens within aerosol droplets and the potential for airborne transmission of respiratory infections.[1] SARS-CoV-2 transmission primarily occurs indoors, attributable to increased exposure to infectious droplets.[2] Indoor spaces are the site of frequent and prolonged close-range interactions, increasing exposure to infectious droplets that are more concentrated nearer to the source.[3] Moreover, poor ventilation can lead to the accumulation of infectious droplets within enclosed spaces.[4] Evidence suggests indoor temperature and humidity conditions can prolong the infectiousness of airborne pathogens.[5–7] Furthermore, SARS-CoV-2 infection rates reliably peak during temperate winter and wane during temperate summer months.[4,8] Low relative humidity conditions during the winter can promote evaporative moisture loss from droplets, reducing the size and increasing the airborne residence time of infectious droplets.[4] Additionally, time spent indoors may contribute to this variation by increasing the frequency and duration of close contact interactions in winter.[4] Consequently, behavioural changes combined with slower rates of pathogen inactivation and removal may increase the risk of transmission indoors during winter months.

In addition to environmental factors, biological factors related to the infectious host and pathogen, including the size, composition, and quantity of pathogen-laden respiratory droplets, may alter SARS-CoV-2 transmissibility.[9,10] Airborne transmission of SARS-CoV-2 occurs when infectious aerosols are generated and expelled from the airways, remain suspended in the environment, and then inhaled by a susceptible individual.[11] Infectious respiratory droplets originate from the airway lining fluid (ALF) during respiratory activities.[12,13,14] Individuals known as 'super spreaders' constitute 20% of the population but account for at least 80% of transmission events.[15,16] Studies by Edwards *et al.* suggest compositional differences within the ALF of super-spreaders infected with SARS-CoV-2 could account for a disproportionately high 80% of total transmission events.[17,16] The composition of the ALF dictates the solute content of droplets, which can influence the survival of enclosed pathogens during the physicochemical transformation of droplets expelled from the airways and into the external environment. [17,18,19] In addition to host factors, pathogen-related factors, such as an evolved SARS-CoV-2 variant of concern, can produce higher sputum viral loads with consequences for transmissibility.[20]

The initial size and composition of respiratory droplets depend on the site of origin within the airways.[12,18] Respiratory droplets with initial diameters of 20 μm or less can equilibrate rapidly to indoor environments due to a large surface-to-volume and remain suspended in the air. These airborne droplets have the potential to participate in airborne transmission events.[21] Conversely, droplets with an initial size ≥100 μm tend to follow a ballistic trajectory and settle on surfaces to contribute to the fomite transmission events.[22] In addition to size, respiratory droplet composition changes during the transport from the airways into the environment.[23] The rate of these changes will have consequences for the airborne residence period of respiratory droplets, the survival of encapsulated pathogens, and the site of deposition if inhaled into the airways of a secondary host.[19]

Investigations of the effects of environmental and biological factors on pathogen survival within aerosol droplets commonly utilize rotating Goldberg drums and particle levitation platforms.[6,24] Goldberg drums studies examine pathogen decay kinetics over long timescales.[5–7,24] A limitation of Goldberg drums is the inability to perform infectious droplet size measurements at the endpoint. Endpoint droplet size measurements are critical to estimate airborne residence time and deposition efficiency once inhaled into the airways.[25,26] Another drawback of this model is the

inability to provide information regarding viability changes over short timescales to probe short-range transmission dynamics. Transmission risk studies conducted during the COVID-19 pandemic revealed the importance of short-range transmission events mediated by high concentrations of infectious droplets found proximate to the source.[16,3,25,27] Thus, pathogen decay kinetics over short timescales is needed to understand short-range transmission events.[28,29] Droplet levitation models are used to investigate short-range airborne transmission dynamics.[28] Oswin *et al.* used a levitation platform to monitor viral decay within a 25 µm radius droplet over short timescales.[6] They reported a near-instantaneous loss in SARS-CoV-2 infectivity in over 50% of droplets exposed to <50% RH environment.[6] Recent work by French *et al.* demonstrated viral decay rates under varied RH conditions to be dependent on initial droplet volume.[19,30] Biological droplets are inherently polydisperse with pathogen decay rates varying with initial droplet volume.[13,30] Thus, changes in viability within physiologically relevant droplet sizes over short timescales are needed to model short-range transmission dynamics.[3]

We developed an aerosol platform to address the limitations of the existing models for studying virus survival within aerosol droplets (**Figure 1a**). Using this model, we equilibrated droplets with initial sizes ranging from 1.73 to ≥20.28 µm under low (15±5%) and intermediate (50±5%) indoor relative humidity (RH) conditions at 24±1.6°C. Phi6, a bacteriophage surrogate for SARS-CoV-2, was a model virus to detect viable virus-laden droplets post-equilibration.[31] Trials were conducted during the summer and winter months to simulate the range of indoor relative humidity extremes.[4] Virus suspensions were prepared in 1.5%, 3%, or 6% weight-per-volume (w/v) peptone water solutions to reflect the solute content of ALF in normal and muco-obstructive airway disease states.[32] Phi6 concentrations of 1×10^5 PFU/mL and 5×10^5 PFU/mL were selected to reflect sputum RNA concentrations reported in infectious SARS-CoV-2 patients.[33] The number of viable virus-laden droplets collected under each set of conditions was determined using the standard plaque assay method (**Figure 1b, 1c**).

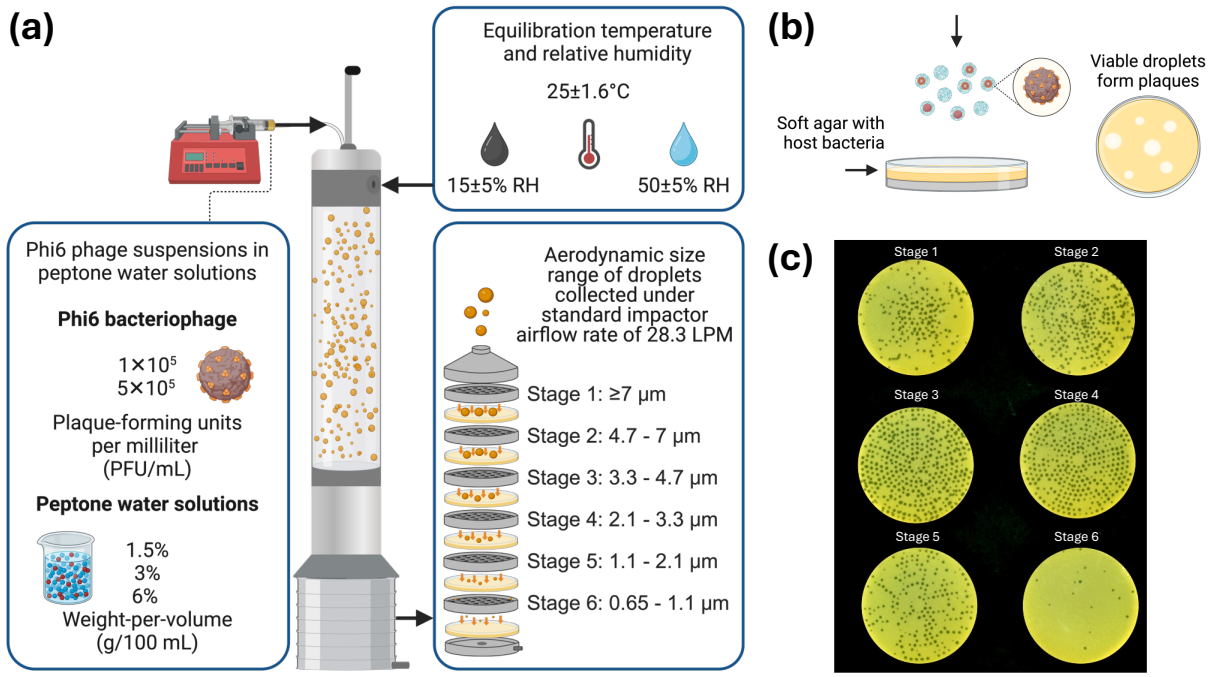

Figure 1. Schematic of the aerosol platform and the experimental workflow. (**a**) The platform

contains three main components: the Blaustein single-jet atomizer, a 60-cm-high aerosol mixing chamber, and a 6-stage viable cascade impactor. Phi6 concentrations 1×10^5 and 5×10^5 plaque-forming units per millilitre (PFU/mL) were selected to reflect sputum RNA concentrations reported in infectious SARS-CoV-2 patients. Virus suspensions in peptone water reflect solute concentrations in the airway lining fluid in healthy (1.5% w/v) and disease (3.0% and 6.0% w/v) states. Low (15±5%) and intermediate (50±5%) relative humidity at 24±1.6°C reflects seasonal fluctuations in indoor environments. (**b**) The schematic depicts the viable virus-laden droplet detection method. The deposition of Phi6 on soft agar containing the host bacteria *Pseudomonas syringae* results in plaque formation owing to lytic phage activity. (**c**) Scanned image of six collection plates with plaques at the site of impaction of infective Phi6 aerosol droplets. Plaque counts were converted to coincidence-corrected whole number values and used to calculate total droplet counts and the size range of viral aerosols. Schematics created with Biorender.

5.3. MATERIALS AND METHODS

5.3.1. Solutions preparation

Tryptic soy broth (TSB) contains 30 g of tryptic soy broth (BD B211825) in 1 L of deionized water. Tryptic soy agar (TSA) contains 30 g of tryptic soy broth (BD B211825) and 15 g of agar (Fisher BioReagents BP1423-500) in 1 L of deionized water. Tryptic soy broth with yeast extract and magnesium sulphate (TSBY+) contains 30 g of tryptic soy broth (BD B211825), 6 g of yeast extract (Amresco J850-500G), and 0.6 g of magnesium sulphate (Amresco E797-500) in 1 L of deionized water. Tryptic soy agar with yeast extract and magnesium sulphate (TSAY+) contains 30 g of tryptic soy broth (BD B211825), 6 g of yeast extract (Amresco J850-500G), 6 g of agar (Fisher BioReagents BP1423500), and 0.6 g of magnesium sulphate (Amresco E797-500) in 1 L of deionized water. Peptone water solutions contain 15 g, 30 g, and 60 g of peptone water (Thermo Scientific CM0009) in 1 L of ultrapure water. All solutions were sterilized by autoclaving (Yamato Steam Sterilizer SM301) at 121°C for 20 minutes.

5.3.2. Phage aerosol generation and size-resolved sampling

The aerosol platform depicted in **Figure 1a** consists of a single-jet Blaustein atomizer (CH Technologies ARGBLM2), a 60-cm-high glass mixing chamber, and a six-stage viable cascade impactor (Tisch Environmental TE-10-800). The atomizer, fitted with a 10-40 expansion plate (CH Technologies ARGBLM0031), generated polydisperse phage aerosols for one minute. Phage suspension was dispensed from a 5 mL syringe (BD 309646) and delivered to the atomizer through 1/16'' x 3/16'' ID/OD silicone tubing (McMaster-Carr 51135K608). The liquid feed flow rate of 170 µL/min was maintained using a syringe pump (Fisherbrand 780100I). The compressed airflow rate of 1.5 L/min was maintained using a pressure gauge (IMI NORGREN R72G-2AT-RFG). Filtered room air at a volumetric airflow rate of 26.8 L/min entered the platform. The volumetric airflow rate of 28.3 L/min was maintained within the system using a vacuum pump (GAST 0823-101Q-G608NEX). Monitoring upstream and downstream airflow rates utilized OMEGA (FMA-A2317) and TSI (5300 series) flow meters, respectively. The ASTM International standard F2101-19 guided the initial design and operation of the platform.[34]

The intermediate and low humidity trials occurred on days when ambient relative humilities were 50±5% and 15±5%. Humidity and temperature within the platform were measured using a SensorPush device (HT.w 16859565) before the start of each trial. Droplets experience a six-

second flight time under the standard impactor airflow rate of 28.3 L/min within the chamber before reaching the impactor, followed by size-fractioning and collection.[35]

5.3.3. Aerosol distribution profile

Phage-free, peptone water solutions (1.5%, 3%, and 6% w/v) containing 1 mg/mL fluorescein sodium salt (Sigma-Aldrich F6377-100G) were aerosolized for 1 minute using 1.5 L/min of airflow. Foil substrates were placed on 27 mL agar-containing plates to collect the droplets. 5 mL of ultrapure water removed the deposited material from the foils. Spectrophotometric measurements of fluorescein in 200 µL samples, added in triplicates to 96-well microplates (Greiner Bio-One 655086), used $\lambda_{ex}/\lambda_{em}$ of 490±5 and 515±5 nm (Biotek Synergy Neo2).

5.3.4. Bacteria and bacteriophage

Pseudomonas bacteriophage Phi6 (DSM 21518) is an accepted surrogate for SARS-CoV-2 that we propagated in the host bacterial strain, *Pseudomonas syringae* (DSM 21482).[36] Culturing of *P. syringae* for Phi6 propagation and detection used previously established methods with minor modifications.[31] *P. syringae* was grown in TSBY media for 48 h at 25°C in a shaking incubator. *P. syringae* subculture was prepared by diluting 80 µL of the overnight culture in 4 mL of fresh TSBY broth, followed by incubation at 25ºC under agitation for six hours. A single Phi6 plaque isolate was introduced into the subculture and incubated for 14 hours. The resultant suspension was centrifuged at 7000×g for 20 minutes at 4ºC. The supernatant was passed through a 0.22-µm-pore-sized filter to sterilize the stock Phi6 suspension, stored at 4ºC.

5.3.5. Preparation of bacteriophage feed solution

1×10^5 PFU/mL and 5×10^5 PFU/mL Phi6 suspensions in peptone water solutions (1.5%, 3.0%, or 6.0% w/v) used the phage stock suspension (3×10^{10} PFU/mL). The standard dilution plating method confirmed the concentration of Phi6 in peptone water suspensions.[37] Briefly, the phage suspension was serially diluted in 900 µL aliquots of TSBY broth. An appropriate dilution was plated (100 µL) on bacterial agar plates in triplicates. The plates incubated at 25°C for 24 hours produced countable plaques used to calculate the titer of the suspension.

5.3.6. Preparation of agar collection plates

Bacterial agar plates were prepared to collect and quantify viable virus-laden droplets. Sterile glass Petri dishes (Pyrex 3160-100) contained 20 mL of TSA medium in the bottom layer plus 7 mL of *P. syringae* overnight culture (15 mL) mixed with liquid TSAY media (100 mL) in the top layer, bringing the total volume to 27 mL.[26]

5.3.7. Phage aerosol detection and quantification

Bacterial agar plates positioned below each stage collected size-fractioned aerosol droplets within the impactor. Collection plates were incubated for 36 - 48 hours at 25°C to allow plaques to form. Plaque counts on each plate were corrected for coincidence errors and rounded to the nearest whole number (**Figure 1c**).[38,39]

5.3.8. Statistical analysis and data visualization

Statistical analyses and data visualisations used GraphPad PRISM 10 software. Viable droplet counts collected below impactor stages were analysed using ordinary one-way ANOVA followed by Tukey's multiple comparisons test. Nominal doses of fluorescein droplets collected below

individual impactor stages were analysed using one-way ANOVA followed by Šídák's multiple comparisons test. Significance was defined as * - p<0.05, ** - p<0.01, *** - p<0.001, **** - p<0.0001.

5.4. THEORY AND MODEL DEVELOPMENT

5.4.1. Overview

Respiratory droplets expelled from the airways must retain the viability of encapsulated pathogens and remain airborne to mediate airborne disease transmission. Droplets ≤20 µm in size can rapidly equilibrate to indoor environmental conditions due to a large surface-to-volume ratio and remain airborne for prolonged periods.[40] For example, a 1 µm droplet will equilibrate more rapidly (~ 20 ms) than a 10 µm droplet (~ 200 ms) at 50% RH.[41] Thus, droplets ≤20 µm in size are relevant when evaluating airborne transmission risks. Droplets with different initial solute concentrations in the process of equilibrating droplet phase water activity with the environment will tend towards the same final solute content but different equilibrated sizes under ideal mixing conditions.[41,42] Consequently, equilibrated droplet size will increase with solute content and RH.[42,43] The transformation of the expelled droplet, influenced by the initial size, chemical composition, and environmental conditions, can have consequences for the viability of encapsulated pathogens.[30,18] Additionally, the capacity of encapsulated pathogens to remain viable during droplet equilibration may also depend on the pathogen load.[36]

5.4.2. Initial and equilibrated droplet diameters

This work aimed to investigate the effects of droplet composition, pathogen load, and environmental conditions on viable virus-laden droplet counts to model indoor short-range transmission risk in the winter and summer months using an aerosol platform (**Figure 1**). Polydisperse aerosol droplets generated by the atomizer experience ~ 6 seconds of exposure to temperature and humidity conditions within the 60-cm-high glass aerosol mixing chamber before encountering the collection plates within the viable six-stage impactor, the volumetric airflow within the system is 28.3 L/min. The size of droplets generated by the atomizer changes as they traverse the length of the 60-cm-high aerosol mixing chamber. The six-stage viable cascade impactor size-fractions and collects equilibrated droplets. The impactor, operated under the standard volumetric airflow rate of 28.3 LPM, collects droplets within the following aerodynamic size fractions: 0.65-1.1, 1.1-2.1, 2.1-3.3, 3.3-4.7, 4.7-7, and ≥7 µm.

As discussed, the equilibrated size of droplets depends on initial droplet size, solute content, and relative humidity. The initial diameter of droplets, d_o in µm, can be calculated according to **Equation 1** where d_{50} is equilibrated droplet diameter in µm, C is the solute concentration in g/L, ρ is the density of water in g/L, and RH is the relative humidity.[41,44,45] The d_{50} value is the reference cut-off range for the impactor stage.

Initial droplet diameter

$$d_o = d_{50} \Big/ \sqrt[3]{\frac{(C/\rho)}{(1-(\frac{RH}{100}))}} \qquad \textbf{Equation 1}$$

As illustrated by **Equation 1** and **Figure S1**, the initial size (d_o) of droplets will differ depending on the stage cut-off value (d_{50}), the solute content (1.5, 3, or 6% w/v peptone water

concentration), and equilibration condition (15±5% or 50±5% relative humidity at 24±1.6°C) within the 60-cm-high aerosol mixing chamber. For example, droplets collected on the second stage of the impactor with a 4.7 µm cut-off value will have an initial size of 18.05 µm if generated from 1.5% w/v peptone water solution and equilibrated at 15±5% RH or an initial size of 9.53 µm if generated from 6% w/v peptone water solution and equilibrated at 50±5% RH conditions (**Figure S1**).

5.4.3. Use of varied impactor airflow rates to collect equilibrated droplets with similar initial size ranges

For a given stage, i, the cut-off diameter, d_{50}, specifies the aerodynamic size of droplets collected with 50% efficiency.[46] The impactor stage cut-off values are dependent on the airflow rate. Stage cut-off diameters for reference airflow rates, $d_{50,\chi,i}$, can be calculated according to **Equation 2,** where χ is the reference airflow rate, i is the impactor stage, and $d_{50,28.3,i}$, is the stage cut-off diameter under the standard airflow rate of 28.3 LPM.[46,47]

Reference cut-off

$$d_{50,\chi,i} = d_{50,28.3,i} \times \sqrt{\frac{28.3}{\chi}} \qquad \textbf{Equation 2}$$

Aerosol droplets possessing the same initial size, generated from three different peptone water solutions and equilibrated under two different relative humidity conditions, can be collected below each stage by adjusting the impactor airflow rate (**Figure S2**). To collect equilibrated droplets with similar initial sizes generated across three different peptone water concentrations and two relative humidity conditions at 24±1.6°C, impactor airflow rates were modified according to **Equation 2** (**Tables S1-S6)**. This methodology enabled the collection of droplets of the same initial size range below each impactor stage (under varied airflow rates) regardless of variations in peptone water concentration and relative humidity (**Figure S2**). The equilibration of droplets with initial sizes of ≤20 µm occurs rapidly, and the 3.4 to 12-second exposure period (depending on impactor airflow rates) provides adequate time for equilibration of collected droplets.[45,40] Equilibrated droplet size ranges were derived from the reference cut-off ranges for corresponding impactor stages.[46]

5.4.4. Quantifying viable virus-laden droplets with similar initial size ranges

Within droplets possessing a similar initial size range, humidity-, solute-, and pathogen-load-dependent changes in viable virus-laden droplet counts were analyzed. Viable Phi6 bacteriophage-containing droplets impinging on the bacterial lawn plates produce plaques after 24-36 hours of incubation at room temperature (**Figure 1c**), converted to coincidence-corrected plaque counts, $N_{c,i}$, for a given impactor stage, I.[39]

5.5. RESULTS

5.5.1. Effect of solute content, relative humidity conditions, and varied impactor airflow rates on nominal dose deposition profiles

To attribute variations in viable virus-laden droplet counts collected under different conditions (solute content, relative humidities, and impactor airflow rates) to changes in virus stability rather than delivery, we had to confirm that the operating conditions do not affect the amount of material deposited below each stage. Consequently, the system was operated under each set of conditions

using fluorescein-containing peptone water solutions. The fluorescein collected below each stage was quantified to determine the nominal dose delivered under varied impactor airflow rates, relative humidity conditions, and peptone water solutions. Peptone water solutions containing 1 mg/mL of sodium fluorescein were aerosolized, and size-fractioned droplets were collected and quantified (**Tables S7-S12**). The results presented in **Figure S3** show no significant differences in the nominal dose of aerosolized solution recovered from below each stage despite variations in solute content, relative humidity conditions, and impactor airflow rates to collect droplets with roughly the same initial size range (**Tables S13-S18**). These results indicate that the nominal dose reaching the collection plates is comparable despite the differences in solute content, relative humidities, and impactor airflow rates. Consequently, differences in the counts of viable virus-laden droplets below each stage are likely the result of viability changes and not due to different fractions of the aerosol reaching the collection plates.

5.5.2. Viable virus-laden droplets collected below the first impactor stage with an initial size range of ≥18.65 to ≥20.28 µm (cut-off range of ≥6 of ≥8.22 µm)

Figures 2a and 2b present the viable virus-laden droplet counts collected below the first impactor stage with an initial size range of ≥18.65 to ≥20.28 µm and an equilibrated size range of ≥6 to ≥8.22 µm. Counts of viable droplets generated from 1×10^5 PFU/mL phage suspensions were unaffected by solute content or exposure to low versus intermediate RH (**Figure 2a; Tables S19-S29, S37**). However, the counts of viable droplets generated from 5×10^5 PFU/mL phage suspension containing 6% w/v solute content and exposed to 50±5% RH were significantly higher compared to droplets generated from 1.5% solute suspensions and exposed to 50±5% RH and droplets generated from 1.5% and 6% w/v solute suspensions and exposed to 15±5% RH (**Figure 2b; Tables S30-S36, S38**). The results indicate that increased solute content and exposure to intermediate RH increase virus stability within droplets with an initial size range of ≥18.65 to ≥20.28 µm generated from 5×10^5 PFU/mL phage suspensions.

5.5.3. Viable virus-laden droplets collected below the second impactor stage with an initial size range of 12.52 to ≥20.28 µm (cut-off range of 4.03 to ≥8.22 µm)

Figures 2c and 2d present the viable virus-laden droplet counts collected below the second impactor stage with an initial size range of 12.52 to ≥20.28 µm and an equilibrated size range of 4.03 to ≥8.22 µm. Counts of viable droplets generated from 1×10^5 PFU/mL phage suspensions containing 1.5% w/v solute content and exposed to 15±5% RH were significantly higher compared to droplets generated from 6% w/v solute suspension and exposed to 15±5% RH or droplets generated from 3% and 6% w/v solute suspensions exposed to 50±5% RH (**Figure 2c; Tables S19-S29, S39**). Conversely, counts of viable droplets generated from the 5×10^5 PFU/mL phage suspensions were unaffected by solute content or exposure to low and intermediate RH (**Figure 2d; Tables S30-S36, S40**).

5.5.4. Viable virus-laden droplets collected below the third impactor stage with an initial size range of 8.79 to 13.62 µm (cut-off range of 2.83 to 5.52 µm)

Figures 2e and 2f present the viable virus-laden droplet counts collected below the third impactor stage with an initial size range of 8.79 to 13.62 µm and an equilibrated size range of 2.83 to 5.52 µm. Counts of viable droplets generated from 1×10^5 PFU/mL phage suspensions containing 1.5% w/v solute content and exposed to 15±5% RH were significantly higher compared to droplets generated from 6% w/v solute suspension and exposed to 15±5% RH and droplets generated from

3% and 6% w/v solute suspensions exposed to 50±5% RH (**Figure 2e; Tables S19-S29, S41**). Moreover, droplets generated from 3% w/v solute content and exposed to 15±5% RH were significantly higher compared to droplets generated from 6% w/v solute suspension and exposed to 50±5% RH (**Figure 2e; Tables S19-S29, S41**). Lastly, droplets generated from 1.5% w/v solute content and exposed to 50±5% RH were significantly higher compared to droplets generated from 6% w/v solute suspension and exposed to 50±5% RH (**Figure 2e; Tables S19-S29, S41**). Conversely, the counts of viable virus-laden droplets generated from 5×10^5 PFU/mL phage suspension were unaffected by solute content or exposure to low and intermediate RH (**Figure 2f; Tables S30-S36, S42**).

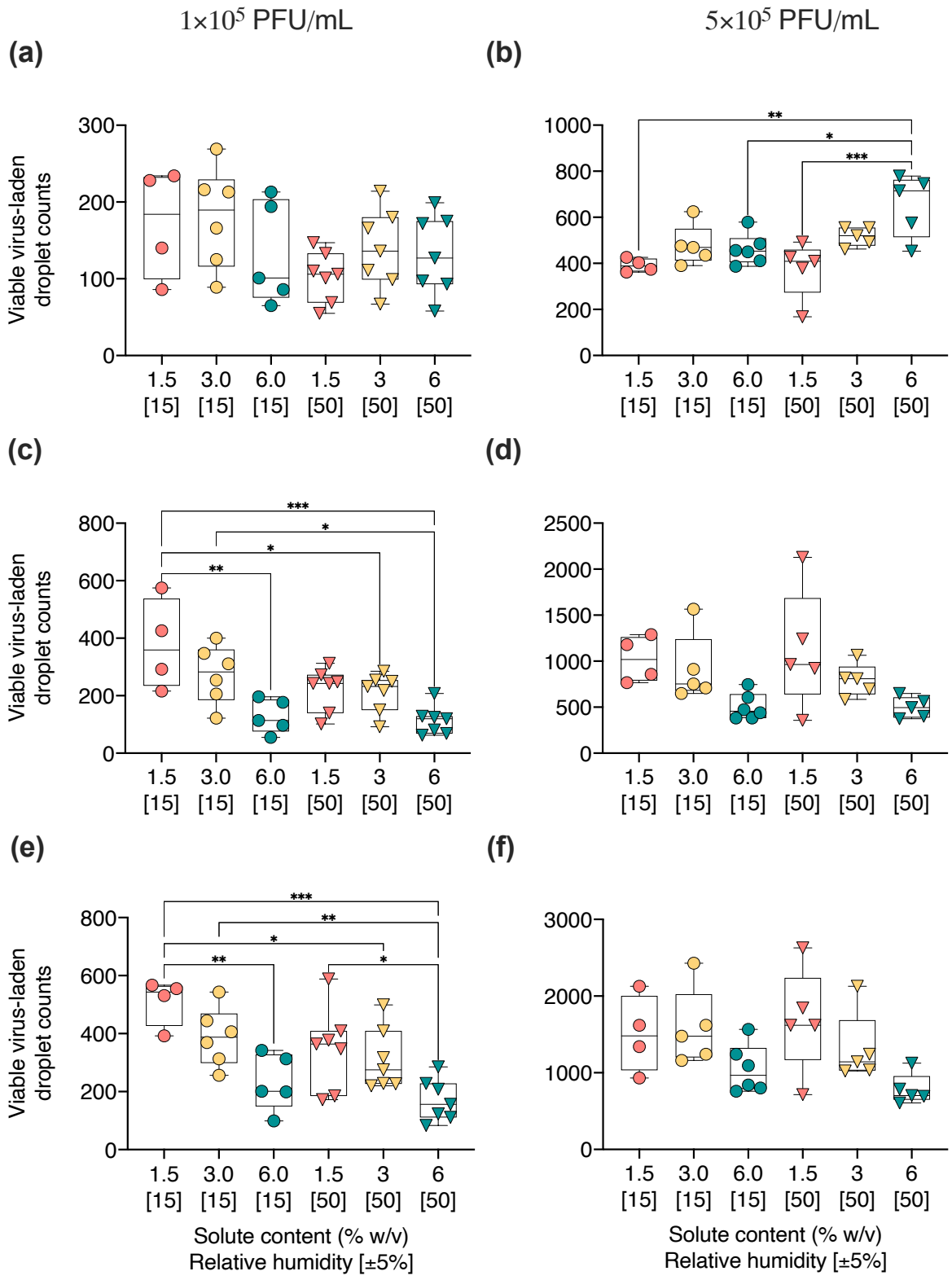

Figure 2. Effect of solute content on viable virus-laden droplet counts, collected under low and intermediate relative humidity conditions and varying virus concentrations, below the

first (initial size range of ≥18.65 to ≥20.28 µm), second (initial size range of 12.52 to ≥18.65 µm), and third (initial size range of 8.79 to 13.62 µm) impactor stages. Phi6 bacteriophage suspensions with concentrations of (**a,c,e**) 1×10^5 PFU/mL and (**b,d,f**) 5×10^5 PFU/mL were prepared in 1.5% (**coral**), 3% (**yellow**), and 6% (**turquoise**) w/v peptone water solutions and aerosolized into 15±5% (**circles**) and 50±5% (**inverted triangles**) relative humidity conditions at 24±1.6°C. Graphs present coincidence-corrected viable droplet counts collected below the (**a,b**) first, (**c,d**) second, (**e,f**) third impactor stages. Significance was determined using one-way ANOVA followed by Tukey's multiple comparisons test * - $p<0.05$, ** - $p<0.01$, *** - $p<0.001$.

5.5.5. Viable virus-laden droplets collected below the fourth impactor stage with an initial size range of 5.59 to 9.56 µm (cut-off range of 1.80 to 3.88 µm)

Figures 3a and 3b present the viable virus-laden droplet counts collected below the fourth impactor stage with an initial size range of 5.59 to 9.56 µm and an equilibrated size range of 1.80 to 3.88 µm. Viable droplets generated from 1×10^5 PFU/mL phage suspensions containing 1.5% w/v solute content and exposed to 15±5% RH were significantly higher compared to droplets generated from 6% w/v solute suspension and exposed to 15±5% RH and those generated from 1.5, 3, and 6% w/v solute suspensions and exposed to 50±5% RH (**Figure 3a; Tables S19-S29, S43**). Moreover, droplets generated from 3% w/v solute content and exposed to 15±5% RH were significantly higher compared to droplets generated from 6% w/v solute suspension and exposed to 50±5% RH (**Figure 3a; Tables S19-S29, S43**). Conversely, viable droplets generated from 5×10^5 PFU/mL phage suspensions were unaffected by solute content or exposure to low and intermediate RH (**Figure 3b; Tables S30-S36, S44**).

5.5.6. Viable virus-laden droplets collected below the fifth impactor stage with an initial size range of 2.93 to 6.09 µm (cut-off range of 0.94 to 2.47 µm)

Figures 3c and 3d present the viable virus-laden droplet counts collected below the fifth impactor stage with an initial size range of 2.93 to 6.09 µm and an equilibrated size range of 0.94 to 2.47 µm. Viable droplets generated from 1×10^5 PFU/mL phage suspensions containing 1.5% w/v solute content and exposed to 15±5% RH were significantly higher compared to droplets generated from 6% w/v solute suspension and exposed to 50±5% RH (**Figure 3c; Tables S19-S29, S45**). Conversely, viable droplets generated from 5×10^5 PFU/mL phage suspensions were unaffected by solute content or exposure to low and intermediate RH (**Figure 3d; Tables S30-S36, S46**).

5.5.7. Viable virus-laden droplets collected below the sixth impactor stage with an initial size range of 1.73 to 3.19 µm (cut-off range of 0.56 to 1.29 µm)

Figures 3e and 3f present the viable virus-laden droplet counts collected below the sixth impactor stage with an initial size range of 1.73 to 3.19 µm and an equilibrated size range of 0.56 to 1.29 µm. Viable droplets generated from 1×10^5 PFU/mL phage suspensions containing 1.5% w/v solute content and exposed to 15±5% RH were significantly higher compared to droplets generated from 1.5, 3, and 6% w/v solute suspensions and exposed to 50±5% RH (**Figure 3e; Tables S19-S29, S47**). Conversely, viable droplets generated from 5×10^5 PFU/mL phage suspensions were unaffected by solute content or exposure to low and intermediate RH (**Figure 3f; Tables S30-S36, S48**).

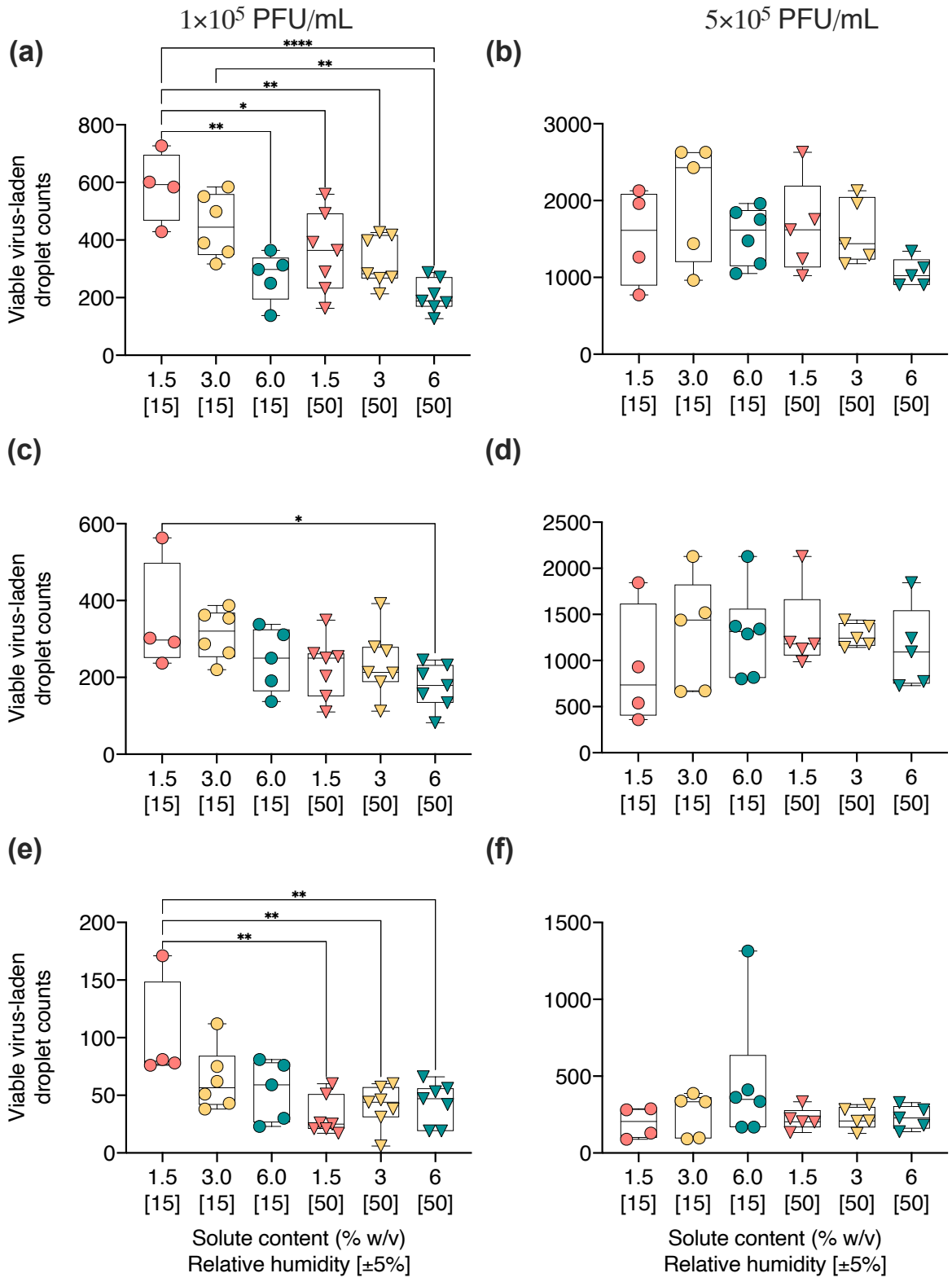

Figure 3. Effect of solute content on viable virus-laden droplet counts, collected under low and intermediate relative humidity conditions and varying virus concentrations, below the

fourth (initial size range of 5.59 to 9.56 µm), fifth (initial size range of 2.93 to 6.09 µm) and sixth (initial size range of 1.73 to 3.19 µm) impactor stages. Phi6 bacteriophage suspensions with concentrations of (**a,c,e**) 1×10^5 PFU/mL and (**b,d,f**) 5×10^5 PFU/mL were prepared in 1.5% (**coral**), 3% (**yellow**), and 6% (**turquoise**) w/v peptone water solutions and aerosolized into 15±5% (**circles**) and 50±5% (**inverted triangles**) relative humidity conditions at 24±1.6°C. Graphs present coincidence-corrected viable droplet counts collected below the (**a,b**) fourth, (**c,d**) fifth, and (**e,f**) sixth impactor stage. Significance was determined using one-way ANOVA followed by Tukey's multiple comparisons test * - $p<0.05$, ** - $p<0.01$, **** - $p<0.0001$.

5.6. DISCUSSION

The results of this work demonstrate the interplay between initial droplet size range, solute content, and virus concentration produces variations in viable virus-laden droplet counts following short timescales of exposure to indoor relative humidity conditions (**Figures 2 and 3**). The general trends (as highlighted in **Figures S4 and S5**) indicate that low-humidity conditions lead to higher counts of viable virus-laden droplets. Exposure to low-humidity environments can trigger rapid evaporation and reduce droplet-phase water activity, concentrating non-volatile solutes such as salts and proteins.[6] Under these conditions, salts can become sequestered within crystalline structures, excluding free diffusion of these ions and circumventing salt toxicity-induced virus inactivation.[6,24,48] However, salts remain in solution in droplets exposed to higher RH conditions (increased droplet-phase water activity), contributing to increased viral inactivation.[24]

Higher counts of viable virus-laden droplets generated from low solute suspensions and exposed to low humidity conditions are consistent with the hypothesized mechanism of enhanced virus viability due to salt crystallization.[48] Sodium chloride is present within the airway lining fluid (ALF), the source of exhaled biological aerosols. Heterogeneity in the composition of the ALF can arise due to age, disease course, and genetic makeup.[10,17,32] Studies have implicated individual heterogeneity in airway mucus composition with altered potential for airborne transmission.[9,10,17,49] The results of this work indicate low solute content (salts and proteins) within the ALF may increase transmission potential in low-humidity environments.

Airborne transmission occurs when the number of viable pathogens deposited within the airways of a susceptible host reaches or surpasses the minimal infectious dose.[29] The likelihood of reaching this threshold will increase with the number of infectious droplets in the environment. As discussed previously, droplet size will fluctuate until droplet phase water activity reaches equilibrium with the gas phase water activity (% RH).[35] Equilibrated droplets under ideal mixing conditions will tend towards the same final solute content at a given RH.[42] Droplet settling velocity increases with size (gravitational force outweighs the viscous drag force acting on the droplet).[14,24] Evaporative moisture loss at low humidity reduces the size of viable droplets.[24,37] Consequently, the decreased size of equilibrated droplets containing low solute content and exposure to low humidity increases the airborne residence time and subsequent risk of inhalation. Higher counts of equilibrated droplets of a smaller size experience longer airborne residence periods, providing insight into epidemiological trends of increased transmission rates in temperate-zone winters.[4]

Significantly, the number of viable virus-laden droplets generated from 5×10^5 PFU/mL phage suspensions with initial size ranges of 12.52 to ≥20.28 µm (**Figure 2d**), 8.79 to 13.62 µm (**Figure 2f**), 5.59 to 9.56 µm (**Figure 3b**), 2.93 to 6.09 µm (**Figure 3d**), and 1.73 to 3.19 µm (**Figure 3f**) were comparable despite differences in solute content and equilibration at low or intermediate RH conditions. These results suggest a higher pathogen load might function as a buffer against solute-

and humidity-dependent changes in viable droplet counts. Our findings are consistent with an earlier study that reported slower decay of Phi6 as phage concentration increased.[50] Virus aggregation increases with concentration[51] and may enhance virus viability within aerosolized droplets. Clinical data indicates evolved SARS-CoV-2 variants Omicron and Delta, compared to ancestral strains, lead to higher peak sputum viral loads.[20] Our results suggest a higher viral load may enhance virus survival within droplets with an initial size range of 1.73 to 20.28 μm containing 6% w/v solute content, mimicking the solute content within the ALF of those diagnosed with moderate to severe muco-obstructive airway diseases.[32,52] A higher viral load may also enhance virus survival within aerosol droplets under intermediate relative humidity conditions during summer, leading to increased transmission rates.

5.7. IMPLICATIONS

Contact-tracing data gathered during the 2019 coronavirus disease pandemic demonstrates that SARS-CoV-2 transmission varies significantly across seasons, persons, environments, and seasons, indicative of transmission heterogeneities.[16,4] The duration and closeness of the interaction increase the likelihood of transmission as the concentration of infectious droplets is highest nearer to the source and shortly after expulsion.[40] The inactivation of viruses within droplets expelled from an infected individual over short timescales (immediately after being expelled from the airways) is relevant for understanding close-contact/short-range transmission events.[21] Respiratory droplets with initial diameters of 20 μm or less will equilibrate rapidly due to a large surface-to-volume ratio to remain suspended in the air.[40] Clinical evidence has demonstrated the presence of SARS-CoV-2 RNA in airborne droplets <5 μm in aerodynamic size.[35,36] However, *in vitro* models allowing for investigations of assessing virus viability within clinically relevant droplet size ranges after equilibration to indoor environments are presently lacking.

Viable droplets containing the bacteriophage Phi6 were size-fractioned and collected using an impactor-based aerosol platform. Droplets generated from 1×10^5 PFU/mL bacteriophage suspensions with initial size ranges of 12.52 to ≥20.28, 8.79 to 13.62, 5.59 to 9.56, 2.93 to 6.09, and 1.73 to 3.19 μm and containing a 1.5% w/v solute content when equilibrated under low humidity conditions resulted in significantly higher counts compared to droplets with 6% w/v solute content and equilibrated under intermediate humidity conditions. These results indicate that low solute content and equilibration at low humidity increase viable virus-laden droplet counts generated from 1×10^5 PFU/mL phage suspensions. The findings are consistent with increases in viral transmission events during winter months coinciding with low relative humidity conditions.[4] Droplets with these initial size ranges when generated from 5-fold concentrated phage suspensions (5×10^5 PFU/mL), the droplet counts remained comparable regardless of solute content and exposure to low or intermediate humidity conditions. Thus, a higher pathogen load may mask the effects of solute- and relative humidity-dependent effects on virus stability within specific size fractions of viable virus-laden droplets. The findings suggest that the effects of heterogeneities in airway mucus solute content on virus stability within size fractions of droplets may occur in a humidity- and pathogen-load-dependent manner.

In summary, the developed aerosol platform supports investigations of viability changes in clinically relevant droplet size ranges following 3 to 12 seconds of exposure (depending on impactor airflow rate) to low and intermediate humidity conditions in indoor environments during temperate summer and winter. The significance of this work lies in the demonstration of the utility

of the aerosol platform to model the viability of virus-containing droplets exposed for short timescales (3 to 12 seconds) to indoor environmental conditions in winter (low humidity) and summer (intermediate humidity), using a high and low concentration suspensions of the bacteriophage Phi6 (a surrogate for SARS-CoV-2) to reflect sputum virus concentration during infection and three suspension media formulations to reflect sputum solute content in healthy and disease states.

5.8. REFERENCES

1. Leung, N. H. L. Transmissibility and transmission of respiratory viruses. *Nature Reviews Microbiology* (2021) doi:10.1038/s41579-021-00535-6.
2. Greenhalgh, T. *et al.* Ten scientific reasons in support of airborne transmission of SARS-CoV-2. *The Lancet* **397**, 1603–1605 (2021).
3. Peng, Z. *et al.* Practical Indicators for Risk of Airborne Transmission in Shared Indoor Environments and Their Application to COVID-19 Outbreaks. *Environ. Sci. Technol.* **56**, 1125–1137 (2022).
4. Moriyama, M., Hugentobler, W. J. & Iwasaki, A. Seasonality of Respiratory Viral Infections. *Annual Review of Virology* **7**, 83–101 (2020).
5. Dabisch, P. *et al.* The influence of temperature, humidity, and simulated sunlight on the infectivity of SARS-CoV-2 in aerosols. *Aerosol Science and Technology* **55**, (2021).
6. Oswin, H. P. *et al.* The Dynamics of SARS-CoV-2 Infectivity with Changes in Aerosol Microenvironment. doi:10.1101/2022.01.08.22268944.
7. Biryukov, J. *et al.* Increasing Temperature and Relative Humidity Accelerates Inactivation of SARS-CoV-2 on Surfaces. *mSphere* **5**, (2020).
8. Božič, A. & Kanduč, M. Relative humidity in droplet and airborne transmission of disease. *J Biol Phys* **47**, 1–29 (2021).
9. Qian, Z. *et al.* Variability in Donor Lung Culture and Relative Humidity Impact the Stability of 2009 Pandemic H1N1 Influenza Virus on Nonporous Surfaces. *Applied and Environmental Microbiology* **89**, e00633-23 (2023).
10. Edwards, D., Salzman, J., Devlin, T. & Langer, R. Nasal Calcium-Rich Salts for Cleaning Airborne Particles from the Airways of Essential Workers, Students, and a Family in Quarantine. *Molecular Frontiers Journal* **04**, 36–45 (2020).
11. Pöhlker, M. L. *et al.* Respiratory aerosols and droplets in the transmission of infectious diseases. *Rev. Mod. Phys.* **95**, 045001 (2023).
12. Morawska, L., Buonanno, G., Mikszewski, A. & Stabile, L. The physics of respiratory particle generation, fate in the air, and inhalation. *Nature Reviews Physics* **4**, 723–734 (2022).
13. Bagheri, G. *et al.* Size, concentration, and origin of human exhaled particles and their dependence on human factors with implications on infection transmission. *Journal of Aerosol Science* **168**, 106102 (2023).
14. Fiegel, J., Clarke, R. & Edwards, D. A. Airborne infectious disease and the suppression of pulmonary bioaerosols. *Drug Discov Today* **11**, 51–57 (2006).
15. Majra, D., Benson, J., Pitts, J. & Stebbing, J. SARS-CoV-2 (COVID-19) superspreader events. *Journal of Infection* vol. 82 36–40 (2021).
16. Sun, K. *et al.* Transmission heterogeneities, kinetics, and controllability of SARS-CoV-2. *Science* **371**, eabe2424 (2021).
17. Edwards, D. A. *et al.* Exhaled aerosol increases with COVID-19 infection, age, and obesity. *Proceedings of the National Academy of Sciences of the United States of America* **118**, (2021).
18. Santarpia, J. L., Reid, J. P., Wu, C.-Y., Lednicky, J. A. & Oswin, H. P. The aerobiological pathway of natural respiratory viral aerosols. *TrAC Trends in Analytical Chemistry* **172**, 117557 (2024).
19. Oswin, H. P. *et al.* The dynamics of SARS-CoV-2 infectivity with changes in aerosol microenvironment. *Proc Natl Acad Sci U S A* **119**, e2200109119 (2022).

20. Puhach, O., Meyer, B. & Eckerle, I. SARS-CoV-2 viral load and shedding kinetics. *Nat Rev Microbiol* **21**, 147–161 (2023).
21. Zhang, N. *et al.* Close contact behavior in indoor environment and transmission of respiratory infection. *Indoor Air* **30**, 645–661 (2020).
22. Hardy, D. A. *et al.* Accurate Measurements and Simulations of the Evaporation and Trajectories of Individual Solution Droplets. *J. Phys. Chem. B* **127**, 3416–3430 (2023).
23. Löndahl, J. & Alsved, M. Abrupt decreases in infectivity of SARS-CoV-2 in aerosols. *Proceedings of the National Academy of Sciences* **119**, e2208742119 (2022).
24. Lin, K. & Marr, L. C. Humidity-Dependent Decay of Viruses, but Not Bacteria, in Aerosols and Droplets Follows Disinfection Kinetics. *Environmental Science and Technology* **54**, (2020).
25. Wang, C. C. *et al.* Airborne transmission of respiratory viruses. *Science* vol. 373 (2021).
26. Haddrell, A. E., Davies, J. F. & Reid, J. P. Dynamics of Particle Size on Inhalation of Environmental Aerosol and Impact on Deposition Fraction. *Environ. Sci. Technol.* **49**, 14512–14521 (2015).
27. Morris, D. H. *et al.* Mechanistic theory predicts the effects of temperature and humidity on inactivation of sars-cov-2 and other enveloped viruses. *eLife* **10**, (2021).
28. Löndahl, J. & Alsved, M. Abrupt decreases in infectivity of SARS-CoV-2 in aerosols. *Proceedings of the National Academy of Sciences of the United States of America* **119**, e2208742119 (2022).
29. Brosseau, L. M. *et al.* Severe Acute Respiratory Syndrome Coronavirus 2 (SARS-CoV-2) Dose, Infection, and Disease Outcomes for Coronavirus Disease 2019 (COVID-19): A Review. *Clinical Infectious Diseases* **75**, e1195–e1201 (2022).
30. French, A. J. *et al.* Environmental Stability of Enveloped Viruses Is Impacted by Initial Volume and Evaporation Kinetics of Droplets. *mBio* **14**, e03452-22 (2023).
31. Fedorenko, A., Grinberg, M., Orevi, T. & Kashtan, N. Survival of the enveloped bacteriophage Phi6 (a surrogate for SARS-CoV-2) in evaporated saliva microdroplets deposited on glass surfaces. *Scientific Reports* **10**, (2020).
32. Hill, D. B. *et al.* A biophysical basis for mucus solids concentration as a candidate biomarker for airways disease. *PLoS ONE* **9**, (2014).
33. Pan, Y., Zhang, D., Yang, P., Poon, L. L. M. & Wang, Q. Viral load of SARS-CoV-2 in clinical samples. *The Lancet Infectious Diseases* vol. 20 (2020).
34. F2101, A. Standard Test Method for Evaluating the Bacterial Filtration Efficiency (BFE) of Medical Face Mask Materials , Using a Biological Aerosol of Staphylococcus aureus 1. *American Society for Testing and Materials* **i**, (2019).
35. Haddrell, A. E. *et al.* Pulmonary aerosol delivery and the importance of growth dynamics. *Therapeutic Delivery* **8**, (2017).
36. Bangiyev, R., Chudaev, M., Schaffner, D. W. & Goldman, E. Higher Concentrations of Bacterial Enveloped Virus Phi6 Can Protect the Virus from Environmental Decay. *Appl Environ Microbiol* **87**, e0137121 (2021).
37. Kropinski, A. M., Mazzocco, A., Waddell, T. E., Lingohr, E. & Johnson, R. P. Enumeration of Bacteriophages by Double Agar Overlay Plaque Assay BT - Bacteriophages: Methods and Protocols, Volume 1: Isolation, Characterization, and Interactions. *Methods in molecular biology (Clifton, N.J.)* **501**, 69–76 (2009).
38. ANDERSEN, A. A. New sampler for the collection, sizing, and enumeration of viable airborne particles. *Journal of bacteriology* **76**, (1958).

39. Macher, J. M. Positive-Hole Correction of Multiple-Jet Impactors for Collecting Viable Microorganisms. *American Industrial Hygiene Association Journal* **50**, (1989).
40. Poydenot, F. *et al.* Risk assessment for long- and short-range airborne transmission of SARS-CoV-2, indoors and outdoors. *PNAS Nexus* **1**, pgac223 (2022).
41. Božič, A. & Kanduč, M. Relative humidity in droplet and airborne transmission of disease. *Journal of Biological Physics* vol. 47 (2021).
42. Fernandez, M. O., Thomas, R. J., Oswin, H., Haddrell, A. E. & Reid, J. P. Transformative Approach To Investigate the Microphysical Factors Influencing Airborne Transmission of Pathogens. *Applied and Environmental Microbiology* **86**, (2020).
43. Davies, J. F., Haddrell, A. E. & Reid, J. P. Time-Resolved Measurements of the Evaporation of Volatile Components from Single Aerosol Droplets. *http://dx.doi.org/10.1080/02786826.2011.652750* **46**, 666–677 (2012).
44. Li, X., Shang, Y., Yan, Y., Yang, L. & Tu, J. Modelling of evaporation of cough droplets in inhomogeneous humidity fields using the multi-component Eulerian-Lagrangian approach. *Building and Environment* **128**, 68–76 (2018).
45. Nicas, M., Nazaroff, W. W. & Hubbard, A. Toward understanding the risk of secondary airborne infection: Emission of respirable pathogens. *Journal of Occupational and Environmental Hygiene* **2**, (2005).
46. ENVIRONMENTAL, T. Cascade Impactor Series 10-8XX Viable (Microbial) Particle Sizing Instruments OPERATIONS MANUAL.
47. Yoshida, H., Kuwana, A., Shibata, H., Izutsu, K. & Goda, Y. Comparison of Aerodynamic Particle Size Distribution Between a Next Generation Impactor and a Cascade Impactor at a Range of Flow Rates. *AAPS PharmSciTech* **18**, 646–653 (2017).
48. Huynh, E. *et al.* Evidence for a semisolid phase state of aerosols and droplets relevant to the airborne and surface survival of pathogens. *Proceedings of the National Academy of Sciences of the United States of America* **119**, (2022).
49. Edwards, D. A. *et al.* Inhaling to mitigate exhaled bioaerosols. *Proceedings of the National Academy of Sciences of the United States of America* **101**, (2004).
50. Bangiyev, R., Chudaev, M., Schaffner, D. W. & Goldman, E. Higher Concentrations of Bacterial Enveloped Virus Phi6 Can Protect the Virus from Environmental Decay. *Applied and environmental microbiology* **87**, e0137121 (2021).
51. Gerba, C. P. & Betancourt, W. Q. Viral Aggregation: Impact on Virus Behavior in the Environment. *Environ. Sci. Technol.* **51**, 7318–7325 (2017).
52. Boucher, R. C. Muco-Obstructive Lung Diseases. *New England Journal of Medicine* **380**, (2019).

5.9. SUPPORTING INFORMATION

SECTION S1. STAGE CUT-OFF DIAMETERS, EQUILIBRATED, AND INITIAL DROPLET SIZE CALCULATIONS

d_{50} = Cut-off diameter
d_{eq} = Equilibrated droplet diameter
d_o = Initial droplet diameter

Table S1. Equilibrated and initial droplet size calculation for 1.5% w/v peptone water suspensions collected under 15±5% RH at 52.8 LPM impactor airflow rate

Stage	$\mathbf{d_{50}}$ **52.8 LPM**	$\mathbf{d_o}$ **10% RH**	d_o 15% RH	d_o 20% RH	$\frac{d_{eq}}{d_{o,15\%}}$
1	**5.12**	**20.06**	19.68	19.29	0.26
2	3.44	13.47	13.22	12.95	0.26
3	2.42	9.46	9.28	9.09	0.26
4	1.54	6.02	5.91	5.79	0.26
5	0.81	3.15	3.09	3.03	0.26
6	0.48	1.86	1.83	1.79	0.26

$d_{50,28.3,i}$ = 7, 4.7, 3.3, 2.1, 1.1, 0.65 for stages 1 to 6, respectively.

S1 - Sample calculation

$$d_{50,\chi,i} = d_{50,28.3,i} \times \sqrt{\frac{28.3}{\chi}}$$

$$= 7 \times \sqrt{\frac{28.3}{52.8}}$$

$$= 5.12\ \mu m$$

$$d_o = d_{eq} \Big/ \sqrt[3]{\frac{(C/\rho)}{(1-(\frac{RH}{100})}}$$

$$= 5.12 \Big/ \sqrt[3]{\frac{(15/1000)}{\left[1-\left(\frac{10}{100}\right)\right]}}$$

$$= 20.04\ \mu m$$

Table S2. Equilibrated and initial droplet size calculation for 3% w/v peptone water suspensions collected under 15±5% RH at 33 LPM impactor airflow rate

Stage	d_{50} 33 LPM	d_o 10% RH	d_o 15% RH	d_o 20% RH	$\frac{d_{50}}{d_{o,15\%}}$
1	6.48	20.14	19.76	19.37	0.33
2	4.35	13.52	13.27	13.00	0.33
3	3.06	9.50	9.32	9.13	0.33
4	1.94	6.04	5.93	5.81	0.33
5	1.02	3.17	3.11	3.04	0.33
6	0.60	1.87	1.84	1.80	0.33

Table S3. Equilibrated and initial droplet size calculation for 6% w/v peptone water suspensions collected under 15±5% RH at 20.5 LPM impactor airflow rate

Stage	d_{50} 20.5 LPM	d_o 10% RH	d_o 15% RH	d_o 20% RH	$\frac{d_{50}}{d_{o,15\%}}$
1	8.22	20.28	19.90	19.50	0.41
2	5.52	13.62	13.36	13.09	0.41
3	3.88	9.56	9.38	9.19	0.41
4	2.47	6.09	5.97	5.85	0.41
5	1.29	3.19	3.13	3.06	0.41
6	0.76	1.88	1.85	1.81	0.41

Table S4. Equilibrated and initial droplet size calculation for 1.5% w/v peptone water suspensions collected under 50±5% RH at 38.5 LPM impactor airflow rate

Stage	d_{50} 38.5 LPM	d_o 45% RH	d_o 50% RH	d_o 55% RH	$\frac{d_{50}}{d_{o,50\%}}$
1	6.00	19.94	19.31	18.65	0.31
2	4.03	13.39	12.97	12.52	0.31
3	2.83	9.40	9.11	8.79	0.31
4	1.80	5.98	5.79	5.59	0.31
5	0.94	3.13	3.04	2.93	0.31
6	0.56	1.85	1.79	1.73	0.31

Table S5. Equilibrated and initial droplet size calculation for 3% w/v peptone water suspensions collected under 50±5% RH at 24.2 LPM impactor airflow rate

Stage	d_{50} 24.2 LPM	d_o 45% RH	d_o 50% RH	d_o 55% RH	$\frac{d_{50}}{d_{o,50\%}}$
1	7.57	19.96	19.34	18.67	0.39
2	5.08	13.40	12.98	12.53	0.39
3	3.57	9.41	9.12	8.80	0.39
4	2.27	5.99	5.80	5.60	0.39
5	1.19	3.14	3.04	2.93	0.39
6	0.70	1.85	1.80	1.73	0.39

Table S6. Equilibrated and initial droplet size calculation for 6% w/v peptone water suspensions collected under 50±5% RH at 15 LPM impactor airflow rate

Stage	d_{50} 15 LPM	d_o 45% RH	d_o 50% RH	d_o 55% RH	$\frac{d_{50}}{d_{o,50\%}}$
1	9.61	20.12	19.49	18.82	0.49
2	6.46	13.51	13.09	12.64	0.49
3	4.53	9.49	9.19	8.87	0.49
4	2.88	6.04	5.85	5.65	0.49
5	1.51	3.16	3.06	2.96	0.49
6	0.89	1.87	1.81	1.75	0.49

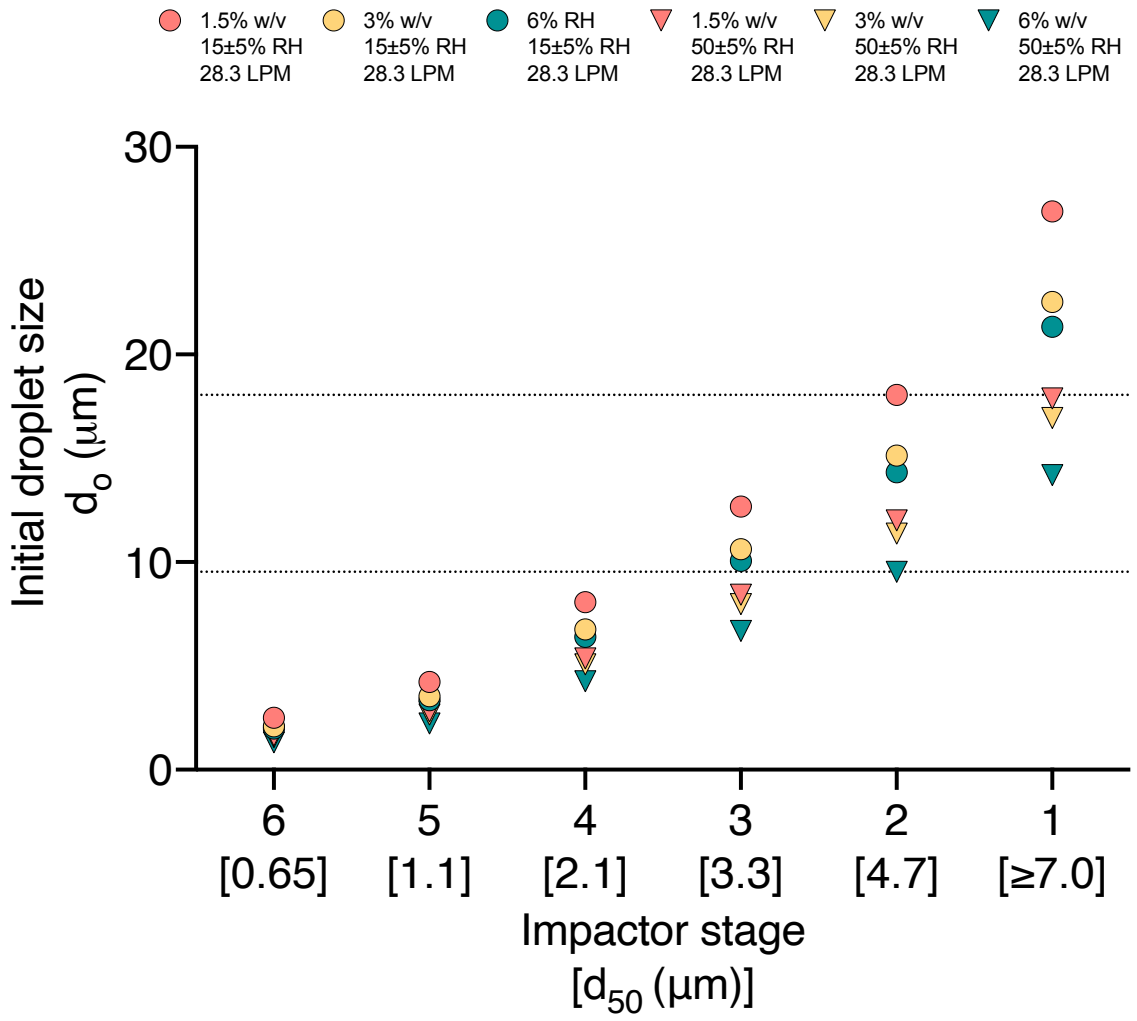

Figure S1. Initial droplet size calculation for an impactor airflow rate of 28.3 LPM. The initial size of droplets, collected below each impactor stage under the standard impactor airflow rate of 28.3 LPM, will vary depending on the solute content (1.5, 3, and 6% w/v) and equilibration conditions (15±5% or 50±5% relative humidity at 24±1.6°C) within the 60-cm-high aerosol mixing chamber. The dotted lines indicate the initial size of 18.05 µm for droplets generated from

1.5% w/v peptone water solution and equilibrated at 15±5% RH (top) and initial size of 9.53 µm for droplets generated from 6% w/v peptone water solution and equilibrated at 50±5% RH (bottom) collected below the second stage of the impactor with a 4.7 µm cut-off value under an impactor airflow rate of 28.3 LPM.

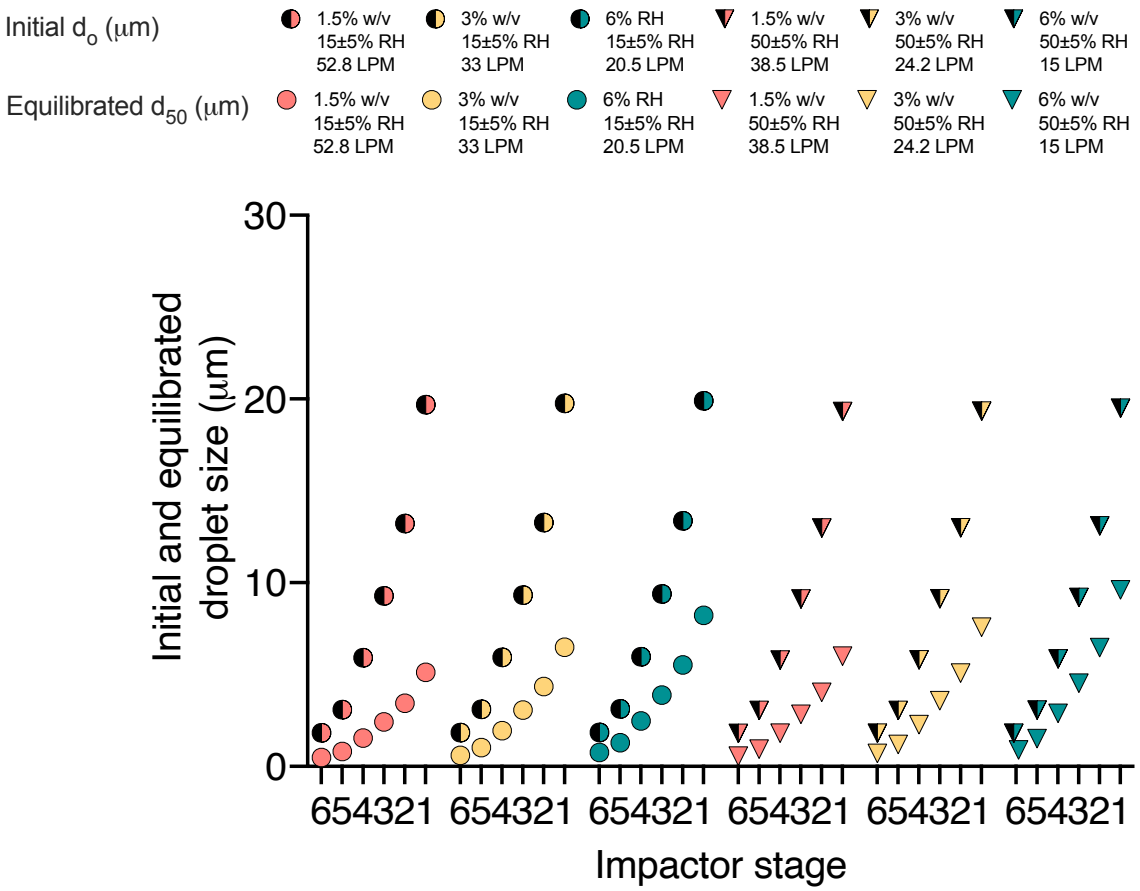

Figure S2. Effect of varied impactor airflow rates on initial and equilibrated droplet sizes. The graph illustrates similar initial size ranges of droplets generated from three different peptone water solutions (1.5, 3, and 6% w/v) and equilibrated under two different environmental conditions (15±5% or 50±5% relative humidity at 24±1.6°C) within the 60-cm-high aerosol mixing chamber and collected under varied impactor airflow rates.

SECTION S2. SPECTROPHOTOMETRIC DETECTION OF 1.5, 3, AND 6% W/V PEPTONE WATER SOLUTIONS CONTAINING 1 MG/ML FLUORESCEIN, AEROSOLIZED AND COLLECTED BELOW EACH IMPACTOR STAGE UNDER 15±5% RH CONDITIONS

Table S7. Inert aerosol droplets generated from 1.5% w/v peptone water solutions, collected under 52.8 LPM impactor airflow rate

Stage	$\lambda_{ex}/\lambda_{em}$, 490±5/520±5 nm	Avg	Percent

1	**3549**	**3461**	**3498**	**3503**	2.50
2	3357	3215	3160	3244	2.32
3	3174	3214	3180	3189	2.28
4	1296	1303	1366	1322	0.94
5	8330	8739	8741	8603	6.14
6	9739	9534	9615	9629	6.88
1	2018	2081	2075	2058	1.47
2	2218	2213	2166	2199	1.57
3	1826	1817	1819	1821	1.30
4	1816	1814	1829	1820	1.30
5	919	848	810	859	0.61
6	1529	1414	1423	1455	1.04
1	2213	2092	2122	2142	1.53
2	3323	3489	3476	3429	2.45
3	3079	3141	3143	3121	2.23
4	1681	1586	1715	1661	1.19
5	1742	1680	1749	1724	1.23
6	2167	2307	2231	2235	1.60

Maximum fluorescence signal 1.5% peptone water solution containing 1 mg/mL fluorescein – 700098.75

S7 - Sample calculation

$$Percent\ fluorescein\ deposition\ \ (\lambda_{ex}/\lambda_{em}, 490 \pm 5/520 \pm 5\ \text{nm})$$
$$= \left[\frac{3503 \times 5}{700098.75}\right] \times 100\%$$
$$= 2.5\%$$

Table S8. Inert aerosol droplets generated from 3% w/v peptone water solutions, collected under 33 LPM impactor airflow rate

Stage	$\lambda_{ex}/\lambda_{em}$, 490±5/520±5 nm			Avg	Percent
1	**4501**	**4552**	**4353**	**4469**	**2.94**
2	3787	3795	3762	3781	2.49
3	4144	3929	3946	4006	2.63
4	5808	5868	5920	5865	3.86
5	5414	5321	5029	5255	3.46
6	2262	2208	2309	2260	1.49
1	2349	2329	2285	2321	1.53
2	2358	2258	2300	2305	1.52
3	2251	2252	2267	2257	1.48
4	2864	2842	2791	2832	1.86
5	3300	3280	3316	3299	2.17
6	1713	1720	1742	1725	1.13

1	2549	2513	2501	2521	1.66
2	2748	2768	2871	2796	1.84
3	4142	4183	4079	4135	2.72
4	3128	3117	3291	3179	2.09
5	642	613	643	633	0.42
6	1347	1280	1385	1337	0.88

Maximum fluorescence signal 3% peptone water solution containing 1 mg/mL fluorescein – 760437.5

S8 - Sample calculation

$$Percent\ fluorescein\ deposition\ \ (\lambda_{ex}/\lambda_{em}, 490 \pm 5/520 \pm 5\ \text{nm}) = \left[\frac{4469 \times 5}{760437.5}\right] \times 100\% = 2.94\%$$

Table S9. Inert aerosol droplets generated from 6% w/v peptone water solutions, collected under 20.5 LPM impactor airflow rate

Stage	$\lambda_{ex}/\lambda_{em}$, 490±5/520±5 nm			Avg	Percent
1	**2631**	**2586**	**2720**	**2646**	**1.69**
2	2080	2067	2026	2058	1.32
3	4349	4462	4407	4406	2.82
4	1374	1412	1436	1407	0.90
5	2613	2863	2703	2726	1.75
6	924	961	999	961	0.62
1	2227	2276	2174	2226	1.43
2	1902	1904	1951	1919	1.23
3	2681	2679	2651	2670	1.71
4	4080	3969	3937	3995	2.56
5	3153	2985	3153	3097	1.98
6	1070	1016	1053	1046	0.67
1	2687	2639	2587	2638	1.69
2	2657	2719	2739	2705	1.73
3	2950	3050	3007	3002	1.92
4	2713	2792	2810	2772	1.78
5	4257	4251	4332	4280	2.74
6	1148	1209	1192	1183	0.76

Maximum fluorescence signal 3% peptone water solution containing 1 mg/mL fluorescein – 780500

S8 - Sample calculation

$$Fluorescein\ deposition\ \ (\lambda_{ex}/\lambda_{em}, 490 \pm 5/520 \pm 5\ \text{nm})$$

$$= \left[\frac{2646 \times 5}{780500}\right] \times 100\%$$
$$= 1.69\%$$

SECTION S3. SPECTROPHOTOMETRIC DETECTION OF 1.5, 3, AND 6% W/V PEPTONE WATER SOLUTIONS CONTAINING 1 MG/ML FLUORESCEIN, AEROSOLIZED AND COLLECTED BELOW EACH IMPACTOR STAGE UNDER 50±5% RH CONDITIONS

Table S10. Inert aerosol droplets generated from 1.5% w/v peptone water solutions, collected under 38.5 LPM impactor airflow rate

Stage	$\lambda_{ex}/\lambda_{em}$, 490±5/520±5 nm			Avg	Percent
1	884	943	858	895	0.80
2	1216	1223	1229	1223	1.09
3	2093	2096	2062	2084	1.86
4	3361	3283	3310	3318	2.96
5	3883	3849	3738	3823	3.41
6	1070	1071	1077	1073	0.96
1	761	746	705	737	0.67
2	1169	1218	1187	1191	1.07
3	3783	3931	3767	3827	3.45
4	4169	4024	4412	4202	3.79
5	4576	4623	4454	4551	4.11
6	2189	2181	2157	2176	1.96
1	725	753	701	726	0.64
2	1316	1328	1379	1341	1.18
3	2524	2581	2459	2521	2.23
4	3197	3057	3277	3177	2.81
5	6011	5892	6040	5981	5.28
6	996	969	927	964	0.85

Table S11. Inert aerosol droplets generated from 3% w/v peptone water solutions, collected under 24.2 LPM impactor airflow rate

Stage	$\lambda_{ex}/\lambda_{em}$, 490±5/520±5 nm			Avg	Percent
1	3217	3158	3022	3132	2.55
2	2757	2781	2763	2767	2.26
3	3776	3759	3719	3751	3.06
4	5762	5742	5930	5811	4.74
5	8972	8965	8787	8908	7.27
6	1547	1454	1480	1494	1.22
1	1052	1013	1012	1026	0.83
2	645	680	664	663	0.54
3	1782	1837	1789	1803	1.46

4	1729	1749	1852	1777	1.44
5	2060	2102	2051	2071	1.68
6	896	887	875	886	0.72
1	691	587	594	624	0.51
2	845	771	809	808	0.66
3	566	566	544	559	0.46
4	1415	1437	1433	1428	1.17
5	2156	2268	1957	2127	1.74
6	736	725	700	720	0.59

Table S12. Inert aerosol droplets generated from 6% w/v peptone water solutions, collected under 15 LPM impactor airflow rate

Stage	$\lambda_{ex}/\lambda_{em}$, 490±5/520±5 nm			Avg	Percent
1	2512	2530	2431	2491	1.76
2	1472	1434	1467	1458	1.03
3	1985	2026	2047	2019	1.43
4	2862	2890	2850	2867	2.03
5	5901	5844	5915	5887	4.17
6	1746	1796	1730	1757	1.24
1	901	816	834	850	0.60
2	693	744	747	728	0.51
3	1163	1129	1107	1133	0.80
4	1691	1864	1711	1755	1.24
5	2299	2271	2253	2274	1.61
6	1007	1081	1059	1049	0.74
1	1664	1638	1581	1628	1.18
2	938	1026	985	983	0.71
3	1653	1703	1693	1683	1.22
4	3955	3933	4075	3988	2.90
5	5018	5016	4953	4996	3.63
6	1879	1933	1920	1911	1.39

SECTION S4. TWO-WAY ANOVA FOLLOWED BY ŠÍDÁK MULTIPLE COMPARISONS TEST RESULTS FOR DOSES OF 1.5, 3, AND 6% W/V PEPTONE WATER SOLUTIONS CONTAINING 1 MG/ML FLUORESCEIN COLLECTED BELOW EACH IMPACTOR STAGE

Table S13. Dose deposited below the first impactor stage

Šídák's multiple comparisons test	Mean Diff.	95.00% CI of diff.	Below threshold?	Summary	Adjusted P Value
1.5 [15±5] vs. 3.0 [15±5]	-0.2068	-3.132 to 2.719	No	ns	>0.9999
1.5 [15±5] vs. 6.0 [15±5]	0.2303	-2.695 to 3.156	No	ns	>0.9999

1.5 [15±5] vs. 1.5 [50±5]	1.132	-1.793 to 4.058	No	ns	0.9853
1.5 [15±5] vs. 3 [50±5]	0.5348	-2.391 to 3.460	No	ns	>0.9999
1.5 [15±5] vs. 6 [50±5]	0.6508	-2.275 to 3.576	No	ns	>0.9999
3.0 [15±5] vs. 6.0 [15±5]	0.4372	-2.488 to 3.363	No	ns	>0.9999
3.0 [15±5] vs. 1.5 [50±5]	1.339	-1.587 to 4.265	No	ns	0.9389
3.0 [15±5] vs. 3 [50±5]	0.7417	-2.184 to 3.667	No	ns	0.9999
3.0 [15±5] vs. 6 [50±5]	0.8577	-2.068 to 3.783	No	ns	0.9992
6.0 [15±5] vs. 1.5 [50±5]	0.9019	-2.024 to 3.827	No	ns	0.9986
6.0 [15±5] vs. 3 [50±5]	0.3045	-2.621 to 3.230	No	ns	>0.9999
6.0 [15±5] vs. 6 [50±5]	0.4205	-2.505 to 3.346	No	ns	>0.9999
1.5 [50±5] vs. 3 [50±5]	-0.5974	-3.523 to 2.328	No	ns	>0.9999
1.5 [50±5] vs. 6 [50±5]	-0.4814	-3.407 to 2.444	No	ns	>0.9999
3 [50±5] vs. 6 [50±5]	0.1160	-2.810 to 3.042	No	ns	>0.9999

Table S14. Dose deposited below the second impactor stage

Šídák's multiple comparisons test	Mean Diff.	95.00% CI of diff.	Below threshold?	Summary	Adjusted P Value
1.5 [15±5] vs. 3.0 [15±5]	-2.760 to 3.091	No	ns	>0.9999	-2.760 to 3.091
1.5 [15±5] vs. 6.0 [15±5]	-2.240 to 3.611	No	ns	>0.9999	-2.240 to 3.611
1.5 [15±5] vs. 1.5 [50±5]	-1.930 to 3.921	No	ns	0.9958	-1.930 to 3.921
1.5 [15±5] vs. 3 [50±5]	-1.966 to 3.886	No	ns	0.9972	-1.966 to 3.886
1.5 [15±5] vs. 6 [50±5]	-1.567 to 4.284	No	ns	0.9320	-1.567 to 4.284
3.0 [15±5] vs. 6.0 [15±5]	-2.406 to 3.446	No	ns	>0.9999	-2.406 to 3.446
3.0 [15±5] vs. 1.5 [50±5]	-2.095 to 3.756	No	ns	0.9994	-2.095 to 3.756
3.0 [15±5] vs. 3 [50±5]	-2.131 to 3.720	No	ns	0.9997	-2.131 to 3.720

3.0 [15±5] vs. 6 [50±5]	-1.733 to 4.118	No	ns	0.9764	-1.733 to 4.118
6.0 [15±5] vs. 1.5 [50±5]	-2.615 to 3.236	No	ns	>0.9999	-2.615 to 3.236
6.0 [15±5] vs. 3 [50±5]	-2.651 to 3.200	No	ns	>0.9999	-2.651 to 3.200
6.0 [15±5] vs. 6 [50±5]	-2.253 to 3.598	No	ns	>0.9999	-2.253 to 3.598
1.5 [50±5] vs. 3 [50±5]	-2.961 to 2.890	No	ns	>0.9999	-2.961 to 2.890
1.5 [50±5] vs. 6 [50±5]	-2.563 to 3.288	No	ns	>0.9999	-2.563 to 3.288
3 [50±5] vs. 6 [50±5]	-2.527 to 3.324	No	ns	>0.9999	-2.527 to 3.324

Table S15. Dose deposited below the third impactor stage

Šídák's multiple comparisons test	Mean Diff.	95.00% CI of diff.	Below threshold?	Summary	Adjusted P Value
1.5 [15±5] vs. 3.0 [15±5]	-0.3432	-3.269 to 2.582	No	ns	>0.9999
1.5 [15±5] vs. 6.0 [15±5]	-0.2165	-3.142 to 2.709	No	ns	>0.9999
1.5 [15±5] vs. 1.5 [50±5]	-0.5769	-3.502 to 2.349	No	ns	>0.9999
1.5 [15±5] vs. 3 [50±5]	0.2765	-2.649 to 3.202	No	ns	>0.9999
1.5 [15±5] vs. 6 [50±5]	0.7840	-2.142 to 3.710	No	ns	0.9997
3.0 [15±5] vs. 6.0 [15±5]	0.1267	-2.799 to 3.052	No	ns	>0.9999
3.0 [15±5] vs. 1.5 [50±5]	-0.2337	-3.159 to 2.692	No	ns	>0.9999
3.0 [15±5] vs. 3 [50±5]	0.6197	-2.306 to 3.545	No	ns	>0.9999
3.0 [15±5] vs. 6 [50±5]	1.127	-1.798 to 4.053	No	ns	0.9859
6.0 [15±5] vs. 1.5 [50±5]	-0.3604	-3.286 to 2.565	No	ns	>0.9999
6.0 [15±5] vs. 3 [50±5]	0.4930	-2.433 to 3.419	No	ns	>0.9999
6.0 [15±5] vs. 6 [50±5]	1.001	-1.925 to 3.926	No	ns	0.9956
1.5 [50±5] vs. 3 [50±5]	0.8534	-2.072 to 3.779	No	ns	0.9992
1.5 [50±5] vs. 6 [50±5]	1.361	-1.565 to 4.287	No	ns	0.9310

3 [50±5] vs. 6 [50±5]	0.5075	-2.418 to 3.433	No	ns	>0.9999

Table S16. Dose deposited below the fourth impactor stage

Šídák's multiple comparisons test	Mean Diff.	95.00% CI of diff.	Below threshold?	Summary	Adjusted P Value
1.5 [15±5] vs. 3.0 [15±5]	-1.460	-4.385 to 1.466	No	ns	0.8868
1.5 [15±5] vs. 6.0 [15±5]	-0.6024	-3.528 to 2.323	No	ns	>0.9999
1.5 [15±5] vs. 1.5 [50±5]	-2.042	-4.968 to 0.8837	No	ns	0.4409
1.5 [15±5] vs. 3 [50±5]	-1.307	-4.232 to 1.619	No	ns	0.9495
1.5 [15±5] vs. 6 [50±5]	-0.9139	-3.839 to 2.012	No	ns	0.9983
3.0 [15±5] vs. 6.0 [15±5]	0.8574	-2.068 to 3.783	No	ns	0.9992
3.0 [15±5] vs. 1.5 [50±5]	-0.5822	-3.508 to 2.343	No	ns	>0.9999
3.0 [15±5] vs. 3 [50±5]	0.1531	-2.772 to 3.079	No	ns	>0.9999
3.0 [15±5] vs. 6 [50±5]	0.5459	-2.380 to 3.472	No	ns	>0.9999
6.0 [15±5] vs. 1.5 [50±5]	-1.440	-4.365 to 1.486	No	ns	0.8969
6.0 [15±5] vs. 3 [50±5]	-0.7043	-3.630 to 2.221	No	ns	>0.9999
6.0 [15±5] vs. 6 [50±5]	-0.3115	-3.237 to 2.614	No	ns	>0.9999
1.5 [50±5] vs. 3 [50±5]	0.7353	-2.190 to 3.661	No	ns	0.9999
1.5 [50±5] vs. 6 [50±5]	1.128	-1.798 to 4.054	No	ns	0.9858
3 [50±5] vs. 6 [50±5]	0.3928	-2.533 to 3.318	No	ns	>0.9999

Table S17. Dose deposited below the fifth impactor stage

Šídák's multiple comparisons test	Mean Diff.	95.00% CI of diff.	Below threshold?	Summary	Adjusted P Value
1.5 [15±5] vs. 3.0 [15±5]	0.6496	-2.276 to 3.575	No	ns	>0.9999
1.5 [15±5] vs. 6.0 [15±5]	0.5055	-2.420 to 3.431	No	ns	>0.9999
1.5 [15±5] vs. 1.5 [50±5]	-1.603	-4.529 to 1.323	No	ns	0.7990

1.5 [15±5] vs. 3 [50±5]	-0.8991	-3.825 to 2.026	No	ns	0.9986
1.5 [15±5] vs. 6 [50±5]	-0.4735	-3.399 to 2.452	No	ns	>0.9999
3.0 [15±5] vs. 6.0 [15±5]	-0.1441	-3.070 to 2.781	No	ns	>0.9999
3.0 [15±5] vs. 1.5 [50±5]	-2.253	-5.178 to 0.6730	No	ns	0.2895
3.0 [15±5] vs. 3 [50±5]	-1.549	-4.474 to 1.377	No	ns	0.8353
3.0 [15±5] vs. 6 [50±5]	-1.123	-4.049 to 1.803	No	ns	0.9863
6.0 [15±5] vs. 1.5 [50±5]	-2.108	-5.034 to 0.8171	No	ns	0.3893
6.0 [15±5] vs. 3 [50±5]	-1.405	-4.330 to 1.521	No	ns	0.9131
6.0 [15±5] vs. 6 [50±5]	-0.9790	-3.905 to 1.947	No	ns	0.9965
1.5 [50±5] vs. 3 [50±5]	0.7038	-2.222 to 3.629	No	ns	>0.9999
1.5 [50±5] vs. 6 [50±5]	1.129	-1.796 to 4.055	No	ns	0.9856
3 [50±5] vs. 6 [50±5]	0.4257	-2.500 to 3.351	No	ns	>0.9999

Table S18. Dose deposited below the sixth impactor stage

Šídák's multiple comparisons test	Mean Diff.	95.00% CI of diff.	Below threshold?	Summary	Adjusted P Value
1.5 [15±5] vs. 3.0 [15±5]	2.004	-0.9212 to 4.930	No	ns	0.4712
1.5 [15±5] vs. 6.0 [15±5]	2.490	-0.4361 to 5.415	No	ns	0.1659
1.5 [15±5] vs. 1.5 [50±5]	1.914	-1.012 to 4.840	No	ns	0.5469
1.5 [15±5] vs. 3 [50±5]	2.329	-0.5968 to 5.254	No	ns	0.2442
1.5 [15±5] vs. 6 [50±5]	2.046	-0.8799 to 4.971	No	ns	0.4379
3.0 [15±5] vs. 6.0 [15±5]	0.4851	-2.441 to 3.411	No	ns	>0.9999
3.0 [15±5] vs. 1.5 [50±5]	-0.09050	-3.016 to 2.835	No	ns	>0.9999
3.0 [15±5] vs. 3 [50±5]	0.3244	-2.601 to 3.250	No	ns	>0.9999
3.0 [15±5] vs. 6 [50±5]	0.04127	-2.884 to 2.967	No	ns	>0.9999

6.0 [15±5] vs. 1.5 [50±5]	-0.5756	-3.501 to 2.350	No	ns	>0.9999
6.0 [15±5] vs. 3 [50±5]	-0.1607	-3.086 to 2.765	No	ns	>0.9999
6.0 [15±5] vs. 6 [50±5]	-0.4438	-3.369 to 2.482	No	ns	>0.9999
1.5 [50±5] vs. 3 [50±5]	0.4149	-2.511 to 3.340	No	ns	>0.9999
1.5 [50±5] vs. 6 [50±5]	0.1318	-2.794 to 3.057	No	ns	>0.9999
3 [50±5] vs. 6 [50±5]	-0.2831	-3.209 to 2.643	No	ns	>0.9999

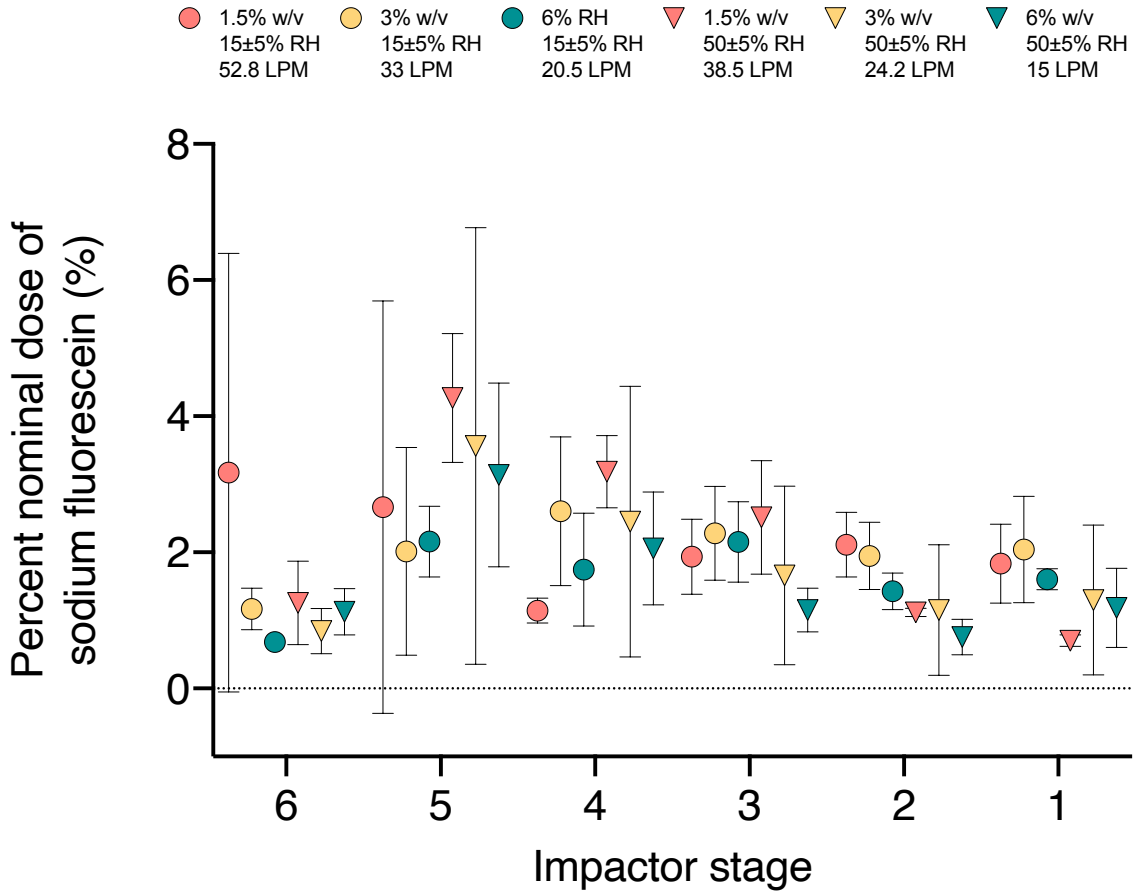

Figure S3. Effect of varied peptone water concentration, relative humidity conditions, and impactor airflow rates on the nominal dose of fluorescein-laden droplets collected below impactor stages. Solutions containing 1 mg/mL sodium fluorescein, prepared in 1.5% (**coral**), 3% (**yellow**), and 6% (**turquoise**) w/v peptone water solutions, were atomized into 15±5% (**circles**) and 50±5% (**inverted triangles**) relative humidity conditions at 24±1.6°C. The graph presents the percentage nominal dose average from three trials conducted for the six conditions (n=3). Spectrophotometric measurements of fluorescein wash samples were performed under excitation

and emission wavelengths of 490±5 and 515±5 nm, respectively. Doses recovered below each impactor stage across the six conditions, analysed using two-way ANOVA followed by Tukey's multiple comparisons, were found to be non-significant, ns - p>0.05.

SECTION S5. VIABLE VIRUS-LADEN DROPLETS GENERATED FROM 1×10^5 PFU/ML PHAGE SUSPENSION COLLECTED UNDER 15±5% RH

N_R = Raw counts
N_C = Coincidence-correct counts
MDS = Mean droplet size (µm)

Table S19. Viable virus-laden droplet counts generated from 1.5% w/v peptone water suspension, collected under 52.8 LPM impactor airflow rate

d_{50}	N_R	**N_C**	N_R	N_C	N_R	N_C	N_R	N_C
5.12	118	**140**	77	86	174	228	177	234
3.44	262	**426**	167	216	207	292	305	575
2.42	294	**531**	250	392	300	555	303	567
1.54	311	**601**	335	727	263	429	307	584
0.81	179	**237**	302	563	207	292	212	302
0.48	71	**78**	139	171	69	76	73	81
Total		**2013**		2155		1872		2343
MDS		**2.29**		1.76		2.37		2.44

S19 - Sample calculations

$$Mean\ droplet\ size, \overline{D}_{\mathrm{ae,C}} = \frac{\sum_{i=1}^{6} d_{50,i} \times N_{\mathrm{c},i}}{N_{\mathrm{T}}}$$

$$= \frac{[7 \times 140 + 4.7 \times 426 + 3.3 \times 531 + 2.1 \times 601 + 1.1 \times 237 + 0.65 \times 78]}{[140 + 426 + 531 + 601 + 237 + 78]}$$

$$= 2.29\ \mu m$$

$$Total\ droplet\ counts, N_{\mathrm{T}} = \sum_{i=1}^{6} N_{\mathrm{c},i}$$

$$Total\ droplet\ counts, N_{\mathrm{T,A}} = 140 + 426 + 531 + 601 + 237 + 78$$

$$= 2013$$

Table S20. Dataset 1- Viable virus-laden droplet counts generated from 3% w/v peptone water suspension, collected under 33 LPM impactor airflow rate

d_{50}	N_R	N_C	N_R	N_C	N_R	N_C
6.48	136	166	165	213	80	89
4.35	188	254	216	311	105	122
3.06	255	406	241	369	189	256

1.94	249	390	307	584	237	359
1.02	248	387	193	264	238	362
0.60	41	43	36	38	98	112
Total		1646		1779		1300
MPS		2.80		2.97		2.33

Table S21. Dataset 2 - Viable aerosol droplets generated from 3% w/v peptone water suspension, collected under 33 LPM impactor airflow rate

d_{50}	N_R	N_C	N_R	N_C	N_R	N_C
6.48	107	125	167	216	196	269
4.35	161	206	232	347	253	400
3.06	217	313	297	543	268	444
1.94	219	317	299	551	285	499
1.02	169	220	235	354	205	287
0.60	48	51	68	75	57	62
Total		1232		2086		1961
MPS		2.87		2.90		3.13

Table S22. Dataset 1 - Viable virus-laden droplet counts generated from 6% w/v peptone water suspension, collected under 20.5 LPM impactor airflow rate

d_{50}	N_R	N_C	N_R	N_C	N_R	N_C
8.22	154	194	60	65	77	86
5.52	155	196	51	55	99	114
3.88	230	342	88	99	157	199
2.47	239	364	117	138	186	250
1.29	228	338	116	137	152	191
0.76	73	81	29	30	22	23
Total		1515		524		863
MPS		3.56		3.36		3.46

Table S23. Dataset 2 - Viable virus-laden droplet counts generated from 6% w/v peptone water suspension, collected under 20.5 LPM impactor airflow rate

d_{50}	N_R	N_C	N_R	N_C
8.22	89	101	165	213
5.52	86	97	143	177
3.88	158	201	217	313
2.47	210	298	217	313
1.29	186	250	216	311
0.76	55	59	69	76
Total		1006		1403
MPS		3.23		3.69

SECTION S6. VIABLE VIRUS-LADEN DROPLET COUNTS GENERATED FROM 1×10^5 PFU/ML PHAGE SUSPENSION COLLECTED UNDER 50±5% RH

Table S24. Dataset 1 - Viable virus-laden droplet counts generated from 1.5% w/v peptone water suspension, collected under 38.5 LPM impactor airflow rate

d_{50}	N_R	N_C	N_R	N_C	N_R	N_C	N_R	N_C
6.00	63	69	123	147	113	133	51	55
4.03	118	140	182	243	217	313	90	102
2.83	140	172	256	409	308	588	148	185
1.80	134	163	283	492	301	559	176	232
0.94	96	110	192	262	233	349	126	151
0.56	20	21	56	60	48	51	17	17
Total		675		1613		1993		742
MPS		2.78		2.59		2.55		2.47

Table S25. Dataset 2 – Viable virus-laden droplet counts generated from 1.5% w/v peptone water suspension, collected under 38.5 LPM impactor airflow rate

d_{50}	N_R	N_C	N_R	N_C	N_R	N_C
6.00	96	110	89	101	93	106
4.03	182	243	185	248	198	273
2.83	239	364	232	347	244	377
1.80	239	364	206	289	250	392
0.94	188	254	159	203	186	250
0.56	24	25	25	26	21	22
Total		1360		1214		1420
MPS		2.63		2.73		2.65

Table S26. Dataset 1 - Viable virus-laden droplet counts generated from 3% w/v peptone water suspension, collected under 24.2 LPM impactor airflow rate

d_{50}	N_R	N_C	N_R	N_C	N_R	N_C	N_R	N_C
7.57	62	67	145	180	166	214	97	111
5.08	176	232	204	285	168	218	82	92
3.57	173	227	256	409	285	499	174	228
2.27	165	213	259	417	252	398	197	271
1.19	98	112	196	269	250	392	150	188
0.70	6	6	53	57	42	44	30	31
Total		857		1617		1765		921
MPS		3.64		3.45		3.35		3.24

Table S27. Dataset 2 - Viable virus-laden droplet counts generated from 1×10^5 PFU/mL phage suspension in 3% w/v peptone water, collected under 24.2 LPM impactor airflow rate

d_{50}	N_R	N_C	N_R	N_C	N_R	N_C
7.57	88	99	115	136	136	166
5.08	125	150	186	250	188	254

3.57	169	220	199	275	219	317
2.27	195	267	203	283	262	426
1.19	165	213	164	211	201	279
0.70	36	38	43	46	56	60
Total		987		1201		1502
MPS		3.23		3.50		3.34

Table S28. Dataset 1 - Viable virus-laden droplet counts generated from 6% w/v peptone water suspension, collected under 15 LPM impactor airflow rate

d_{50}	N_R	N_C	N_R	N_C	N_R	N_C	N_R	N_C
9.61	109	127	54	58	140	172	86	97
6.46	162	208	63	69	104	120	73	81
4.53	204	285	75	83	129	156	106	123
2.88	138	169	150	188	165	213	147	183
1.51	114	134	163	209	130	157	144	179
0.89	19	19	40	42	44	47	52	56
Total		942		649		865		719
MPS		4.84		3.51		4.66		3.98

Table S29. Dataset 2 - Viable virus-laden droplet counts generated from 6% w/v peptone water suspension, collected under 15 LPM impactor airflow rate

d_{50}	N_R	N_C	N_R	N_C	N_R	N_C
9.61	83	93	157	199	142	175
6.46	58	63	110	129	107	125
4.53	97	111	162	208	174	228
2.88	109	127	205	287	197	271
1.51	74	82	176	232	183	245
0.89	19	19	61	66	50	53
Total		495		1121		1097
MPS		4.67		4.39		4.30

SECTION S7. VIABLE VIRUS-LADEN DROPLET COUNTS GENERATED FROM 5×10^5 PFU/ML PHAGE SUSPENSION COLLECTED UNDER 15±5% RH

Table S30. Viable virus-laden droplet counts generated from 1.5% w/v peptone water suspension, collected under 52.8 LPM impactor airflow rate

d_{50}	N_R	N_C	N_R	N_C	N_R	N_C	N_R	N_C
5.12	254	403	243	374	262	426	238	362
3.44	353	857	341	766	384	1288	379	1179
2.42	361	931	386	1341	393	1619	398	2128
1.54	342	772	383	1263	398	2128	397	1961
0.81	237	359	296	539	396	1844	361	931
0.48	80	89	110	129	202	281	205	287

Total		3411		4412		7586		6848
MPS		2.57		2.32		2.03		2.18

Table S31. Viable virus-laden droplet counts generated from 3% w/v peptone water suspension, collected under 33 LPM impactor airflow rate

d_{50}	N_R	N_C	N_R	N_C	N_R	N_C	N_R	N_C	N_R	N_C
6.48	265	435	249	390	316	624	276	469	278	475
4.35	332	709	321	649	392	1565	359	911	339	752
3.06	378	1160	382	1241	399	2428	390	1476	393	1619
1.94	389	1438	364	963	400	2628	400	2628	399	2428
1.02	324	664	325	670	398	2128	389	1438	391	1518
0.60	82	92	87	98	248	387	228	338	226	333
Total		4498		4011		9760		7260		7125
MPS		2.89		2.93		2.64		2.52		2.49

Table S32. Viable virus-laden droplet counts generated from 6% w/v peptone water suspension, collected under 20.5 LPM impactor airflow rate

d_{50}	N_R	N_C	N_R	N_C	N_R	N_C
8.22	270	450	306	579	272	456
5.52	277	472	312	606	246	382
3.88	340	759	374	1093	382	1241
2.47	371	1050	379	1179	397	1961
1.29	346	801	348	816	386	1341
0.76	137	168	137	168	238	362
Total		3700		4441		5743
MPS		3.51		3.70		3.05

Table S33. Viable virus-laden droplet counts generated from 6% w/v peptone water suspension, collected under 20.5 LPM impactor airflow rate

d_{50}	N_R	N_C	N_R	N_C	N_R	N_C
8.22	257	411	248	387	281	485
5.52	246	382	267	440	338	746
3.88	346	801	351	840	392	1565
2.47	396	1844	390	1476	395	1754
1.29	387	1371	384	1288	398	2128
0.76	227	335	257	411	285	1314
Total		5144		4842		7992
MPS		2.95		2.99		2.79

SECTION S8. VIABLE VIRUS-LADEN DROPLET COUNTS GENERATED FROM 5×10^5 PFU/ML PHAGE SUSPENSION COLLECTED UNDER 50±5% RH

Table S34. Viable virus-laden droplet counts generated from 1.5% w/v peptone water suspension, collected under 38.5 LPM impactor airflow rate

d_{50}	N_R	N_C	N_R	N_C	N_R	N_C	N_R	N_C	N_R	N_C
6.00	256	409	245	379	283	492	137	168	262	426
4.03	364	963	382	1241	398	2128	236	357	360	921
2.83	396	1844	393	1619	400	2628	333	715	393	1619
1.80	395	1754	393	1619	400	2628	369	1023	382	1241
0.94	380	1198	379	1179	398	2128	376	1125	366	986
0.56	159	203	158	201	226	333	171	223	113	133
Total		6371		6238		10337		3611		5326
MPS		2.50		2.56		2.50		2.08		2.64

Table S35. Viable virus-laden droplet counts generated from 3% w/v peptone water suspension, collected under 24.2 LPM impactor airflow rate

d_{50}	N_R	N_C	N_R	N_C	N_R	N_C	N_R	N_C	N_R	N_C
7.57	274	462	300	555	283	492	291	520	300	555
5.08	330	697	372	1064	348	816	347	809	307	584
3.57	369	1023	398	2128	377	1142	382	1241	370	1036
2.27	379	1179	397	1961	398	2128	389	1438	384	1288
1.19	382	1241	389	1438	387	1371	379	1179	377	1142
0.70	161	206	218	315	203	283	162	208	109	127
Total		4808		7461		6232		5395		4732
MDS		3.12		3.16		2.99		3.21		3.22

Table S36. Viable virus-laden droplet counts generated from 6% w/v peptone water suspension, collected under 15 LPM impactor airflow rate

d_{50}	N_R	N_C	N_R	N_C	N_R	N_C	N_R	N_C	N_R	N_C
9.61	333	715	338	746	343	779	305	575	271	453
6.46	284	495	302	563	321	649	243	374	253	400
4.53	344	786	329	692	376	1125	331	703	312	606
2.88	369	1023	376	1125	386	1341	358	902	358	902
1.51	374	1093	382	1241	396	1844	342	772	335	727
0.89	174	228	202	281	224	328	145	180	117	138
Total		4340		4648		6066		3506		3226
MDS		4.25		4.16		3.91		4.30		4.19

SECTION S9. ORDINARY ONE-WAY ANOVA FOLLOWED BY TUKEY'S MULTIPLE COMPARISON TESTS OF VIABLE VIRUS-LADEN DROPLET COUNTS

Table S37. 1×10^5 PFU/mL - Viable virus-laden droplet counts collected below the first stage

Tukey's multiple comparisons test	Mean Diff.	95.00% CI of diff.	Below threshold?	Summary	Adjusted P Value
1.5 [15±5] vs. 3.0 [15±5]	-7.667	-117.2 to 101.8	No	ns	>0.9999
1.5 [15±5] vs. 6.0 [15±5]	40.20	-73.61 to 154.0	No	ns	0.8876

1.5 [15±5] vs. 1.5 [50±5]	69.00	-37.33 to 175.3	No	ns	0.3802
1.5 [15±5] vs. 3 [50±5]	33.00	-73.33 to 139.3	No	ns	0.9316
1.5 [15±5] vs. 6 [50±5]	40.43	-65.91 to 146.8	No	ns	0.8534
3.0 [15±5] vs. 6.0 [15±5]	47.87	-54.86 to 150.6	No	ns	0.7166
3.0 [15±5] vs. 1.5 [50±5]	76.67	-17.72 to 171.1	No	ns	0.1652
3.0 [15±5] vs. 3 [50±5]	40.67	-53.72 to 135.1	No	ns	0.7770
3.0 [15±5] vs. 6 [50±5]	48.10	-46.29 to 142.5	No	ns	0.6361
6.0 [15±5] vs. 1.5 [50±5]	28.80	-70.54 to 128.1	No	ns	0.9480
6.0 [15±5] vs. 3 [50±5]	-7.200	-106.5 to 92.14	No	ns	>0.9999
6.0 [15±5] vs. 6 [50±5]	0.2286	-99.11 to 99.57	No	ns	>0.9999
1.5 [50±5] vs. 3 [50±5]	-36.00	-126.7 to 54.68	No	ns	0.8298
1.5 [50±5] vs. 6 [50±5]	-28.57	-119.3 to 62.11	No	ns	0.9274
3 [50±5] vs. 6 [50±5]	7.429	-83.25 to 98.11	No	ns	0.9999

Table S38. 5×10^5 PFU/mL - Viable virus-laden droplet counts collected below the first stage

Tukey's multiple comparisons test	Mean Diff.	95.00% CI of diff.	Below threshold?	Summary	Adjusted P Value
1.5 [15±5] vs. 3.0 [15±5]	-87.35	-275.5 to 100.8	No	ns	0.7059
1.5 [15±5] vs. 6.0 [15±5]	-70.08	-251.1 to 110.9	No	ns	0.8339
1.5 [15±5] vs. 1.5 [50±5]	16.45	-171.7 to 204.6	No	ns	0.9998
1.5 [15±5] vs. 3 [50±5]	-125.6	-313.7 to 62.57	No	ns	0.3385
1.5 [15±5] vs. 6 [50±5]	-262.4	-450.5 to -74.23	Yes	**	0.0029
3.0 [15±5] vs. 6.0 [15±5]	17.27	-152.5 to 187.1	No	ns	0.9995
3.0 [15±5] vs. 1.5 [50±5]	103.8	-73.56 to 281.2	No	ns	0.4786
3.0 [15±5] vs. 3 [50±5]	-38.20	-215.6 to 139.2	No	ns	0.9841

3.0 [15±5] vs. 6 [50±5]	-175.0	-352.4 to 2.360	No	ns	0.0546
6.0 [15±5] vs. 1.5 [50±5]	86.53	-83.28 to 256.3	No	ns	0.6214
6.0 [15±5] vs. 3 [50±5]	-55.47	-225.3 to 114.3	No	ns	0.9101
6.0 [15±5] vs. 6 [50±5]	-192.3	-362.1 to -22.46	Yes	*	0.0201
1.5 [50±5] vs. 3 [50±5]	-142.0	-319.4 to 35.36	No	ns	0.1712
1.5 [50±5] vs. 6 [50±5]	-278.8	-456.2 to -101.4	Yes	***	0.0008
3 [50±5] vs. 6 [50±5]	-136.8	-314.2 to 40.56	No	ns	0.2011

Table S39. 1×10^5 PFU/mL - Viable virus-laden droplet counts collected below the second stage

Tukey's multiple comparisons test	Mean Diff.	95.00% CI of diff.	Below threshold?	Summary	Adjusted P Value
1.5 [15±5] vs. 3.0 [15±5]	103.9	-62.16 to 270.0	No	ns	0.4199
1.5 [15±5] vs. 6.0 [15±5]	249.5	76.86 to 422.0	Yes	**	0.0016
1.5 [15±5] vs. 1.5 [50±5]	154.1	-7.157 to 315.4	No	ns	0.0676
1.5 [15±5] vs. 3 [50±5]	165.7	4.415 to 326.9	Yes	*	0.0413
1.5 [15±5] vs. 6 [50±5]	263.7	102.4 to 424.9	Yes	***	0.0003
3.0 [15±5] vs. 6.0 [15±5]	145.5	-10.26 to 301.3	No	ns	0.0779
3.0 [15±5] vs. 1.5 [50±5]	50.19	-92.95 to 193.3	No	ns	0.8907
3.0 [15±5] vs. 3 [50±5]	61.76	-81.38 to 204.9	No	ns	0.7760
3.0 [15±5] vs. 6 [50±5]	159.8	16.62 to 302.9	Yes	*	0.0218
6.0 [15±5] vs. 1.5 [50±5]	-95.34	-246.0 to 55.31	No	ns	0.4074
6.0 [15±5] vs. 3 [50±5]	-83.77	-234.4 to 66.88	No	ns	0.5478
6.0 [15±5] vs. 6 [50±5]	14.23	-136.4 to 164.9	No	ns	0.9997
1.5 [50±5] vs. 3 [50±5]	11.57	-126.0 to 149.1	No	ns	0.9998

1.5 [50±5] vs. 6 [50±5]	109.6	-27.95 to 247.1	No	ns	0.1805
3 [50±5] vs. 6 [50±5]	98.00	-39.53 to 235.5	No	ns	0.2822

Table S40. 5×10^5 PFU/mL - Viable virus-laden droplet counts collected below the second stage

Tukey's multiple comparisons test	Mean Diff.	95.00% CI of diff.	Below threshold?	Summary	Adjusted P Value
1.5 [15±5] vs. 3.0 [15±5]	105.3	-591.7 to 802.3	No	ns	0.9969
1.5 [15±5] vs. 6.0 [15±5]	517.8	-152.9 to 1189	No	ns	0.2003
1.5 [15±5] vs. 1.5 [50±5]	-99.50	-796.5 to 597.5	No	ns	0.9976
1.5 [15±5] vs. 3 [50±5]	228.5	-468.5 to 925.5	No	ns	0.9088
1.5 [15±5] vs. 6 [50±5]	526.3	-170.7 to 1223	No	ns	0.2194
3.0 [15±5] vs. 6.0 [15±5]	412.5	-216.7 to 1042	No	ns	0.3570
3.0 [15±5] vs. 1.5 [50±5]	-204.8	-862.0 to 452.4	No	ns	0.9250
3.0 [15±5] vs. 3 [50±5]	123.2	-534.0 to 780.4	No	ns	0.9915
3.0 [15±5] vs. 6 [50±5]	421.0	-236.2 to 1078	No	ns	0.3815
6.0 [15±5] vs. 1.5 [50±5]	-617.3	-1247 to 11.86	No	ns	0.0566
6.0 [15±5] vs. 3 [50±5]	-289.3	-918.5 to 339.9	No	ns	0.7140
6.0 [15±5] vs. 6 [50±5]	8.467	-620.7 to 637.7	No	ns	>0.9999
1.5 [50±5] vs. 3 [50±5]	328.0	-329.2 to 985.2	No	ns	0.6412
1.5 [50±5] vs. 6 [50±5]	625.8	-31.37 to 1283	No	ns	0.0684
3 [50±5] vs. 6 [50±5]	297.8	-359.4 to 955.0	No	ns	0.7260

Table S41. 1×10^5 PFU/mL - Viable virus-laden droplet counts collected below the third stage

Tukey's multiple comparisons test	Mean Diff.	95.00% CI of diff.	Below threshold?	Summary	Adjusted P Value
1.5 [15±5] vs. 3.0 [15±5]	122.8	-82.81 to 328.3	No	ns	0.4710

1.5 [15±5] vs. 6.0 [15±5]	280.5	66.82 to 494.1	Yes	**	0.0048
1.5 [15±5] vs. 1.5 [50±5]	162.4	-37.21 to 362.0	No	ns	0.1639
1.5 [15±5] vs. 3 [50±5]	200.5	0.9316 to 400.1	Yes	*	0.0484
1.5 [15±5] vs. 6 [50±5]	340.7	141.1 to 540.3	Yes	***	0.0002
3.0 [15±5] vs. 6.0 [15±5]	157.7	-35.14 to 350.5	No	ns	0.1600
3.0 [15±5] vs. 1.5 [50±5]	39.64	-137.5 to 216.8	No	ns	0.9828
3.0 [15±5] vs. 3 [50±5]	77.79	-99.39 to 255.0	No	ns	0.7634
3.0 [15±5] vs. 6 [50±5]	217.9	40.75 to 395.1	Yes	**	0.0092
6.0 [15±5] vs. 1.5 [50±5]	-118.1	-304.5 to 68.41	No	ns	0.4070
6.0 [15±5] vs. 3 [50±5]	-79.91	-266.4 to 106.6	No	ns	0.7808
6.0 [15±5] vs. 6 [50±5]	60.23	-126.2 to 246.7	No	ns	0.9200
1.5 [50±5] vs. 3 [50±5]	38.14	-132.1 to 208.4	No	ns	0.9827
1.5 [50±5] vs. 6 [50±5]	178.3	8.063 to 348.5	Yes	*	0.0359
3 [50±5] vs. 6 [50±5]	140.1	-30.08 to 310.4	No	ns	0.1549

Table S42. 5×10^5 PFU/mL - Viable virus-laden droplet counts collected below the third stage

Tukey's multiple comparisons test	Mean Diff.	95.00% CI of diff.	Below threshold?	Summary	Adjusted P Value
1.5 [15±5] vs. 3.0 [15±5]	-80.05	-1042 to 881.8	No	ns	0.9998
1.5 [15±5] vs. 6.0 [15±5]	454.9	-470.6 to 1380	No	ns	0.6555
1.5 [15±5] vs. 1.5 [50±5]	-180.3	-1142 to 781.6	No	ns	0.9915
1.5 [15±5] vs. 3 [50±5]	190.8	-771.1 to 1153	No	ns	0.9890
1.5 [15±5] vs. 6 [50±5]	722.4	-239.5 to 1684	No	ns	0.2241
3.0 [15±5] vs. 6.0 [15±5]	535.0	-333.3 to 1403	No	ns	0.4232
3.0 [15±5] vs. 1.5 [50±5]	-100.2	-1007 to 806.6	No	ns	0.9993

3.0 [15±5] vs. 3 [50±5]	270.8	-636.0 to 1178	No	ns	0.9366
3.0 [15±5] vs. 6 [50±5]	802.4	-104.4 to 1709	No	ns	0.1044
6.0 [15±5] vs. 1.5 [50±5]	-635.2	-1503 to 233.1	No	ns	0.2479
6.0 [15±5] vs. 3 [50±5]	-264.2	-1132 to 604.1	No	ns	0.9317
6.0 [15±5] vs. 6 [50±5]	267.4	-600.8 to 1136	No	ns	0.9283
1.5 [50±5] vs. 3 [50±5]	371.0	-535.8 to 1278	No	ns	0.8004
1.5 [50±5] vs. 6 [50±5]	902.6	-4.227 to 1809	No	ns	0.0516
3 [50±5] vs. 6 [50±5]	531.6	-375.2 to 1438	No	ns	0.4769

Table S43. 1×10^5 PFU/mL - Viable virus-laden droplet counts collected below the fourth stage

Tukey's multiple comparisons test	Mean Diff.	95.00% CI of diff.	Below threshold?	Summary	Adjusted P Value
1.5 [15±5] vs. 3.0 [15±5]	135.3	-66.32 to 336.8	No	ns	0.3443
1.5 [15±5] vs. 6.0 [15±5]	312.7	103.2 to 522.1	Yes	**	0.0011
1.5 [15±5] vs. 1.5 [50±5]	229.4	33.67 to 425.1	Yes	*	0.0143
1.5 [15±5] vs. 3 [50±5]	260.3	64.53 to 456.0	Yes	**	0.0042
1.5 [15±5] vs. 6 [50±5]	379.8	184.1 to 575.5	Yes	****	<0.0001
3.0 [15±5] vs. 6.0 [15±5]	177.4	-11.69 to 366.5	No	ns	0.0758
3.0 [15±5] vs. 1.5 [50±5]	94.14	-79.58 to 267.9	No	ns	0.5747
3.0 [15±5] vs. 3 [50±5]	125.0	-48.73 to 298.7	No	ns	0.2726
3.0 [15±5] vs. 6 [50±5]	244.6	70.84 to 418.3	Yes	**	0.0022
6.0 [15±5] vs. 1.5 [50±5]	-83.26	-266.1 to 99.59	No	ns	0.7354
6.0 [15±5] vs. 3 [50±5]	-52.40	-235.2 to 130.4	No	ns	0.9504
6.0 [15±5] vs. 6 [50±5]	67.17	-115.7 to 250.0	No	ns	0.8703
1.5 [50±5] vs. 3 [50±5]	30.86	-136.1 to 197.8	No	ns	0.9927

1.5 [50±5] vs. 6 [50±5]	150.4	-16.48 to 317.3	No	ns	0.0963
3 [50±5] vs. 6 [50±5]	119.6	-47.34 to 286.5	No	ns	0.2769

Table S44. 5×10^5 PFU/mL - Viable virus-laden droplet counts collected below the fourth stage

Tukey's multiple comparisons test	Mean Diff.	95.00% CI of diff.	Below threshold?	Summary	Adjusted P Value
1.5 [15±5] vs. 3.0 [15±5]	-486.0	-1575 to 602.8	No	ns	0.7380
1.5 [15±5] vs. 6.0 [15±5]	-13.00	-1061 to 1035	No	ns	>0.9999
1.5 [15±5] vs. 1.5 [50±5]	-122.0	-1211 to 966.8	No	ns	0.9993
1.5 [15±5] vs. 3 [50±5]	-67.80	-1157 to 1021	No	ns	>0.9999
1.5 [15±5] vs. 6 [50±5]	472.4	-616.4 to 1561	No	ns	0.7597
3.0 [15±5] vs. 6.0 [15±5]	473.0	-509.8 to 1456	No	ns	0.6747
3.0 [15±5] vs. 1.5 [50±5]	364.0	-662.6 to 1391	No	ns	0.8780
3.0 [15±5] vs. 3 [50±5]	418.2	-608.4 to 1445	No	ns	0.8032
3.0 [15±5] vs. 6 [50±5]	958.4	-68.15 to 1985	No	ns	0.0770
6.0 [15±5] vs. 1.5 [50±5]	-109.0	-1092 to 873.8	No	ns	0.9993
6.0 [15±5] vs. 3 [50±5]	-54.80	-1038 to 928.0	No	ns	>0.9999
6.0 [15±5] vs. 6 [50±5]	485.4	-497.4 to 1468	No	ns	0.6511
1.5 [50±5] vs. 3 [50±5]	54.20	-972.4 to 1081	No	ns	>0.9999
1.5 [50±5] vs. 6 [50±5]	594.4	-432.2 to 1621	No	ns	0.4901
3 [50±5] vs. 6 [50±5]	540.2	-486.4 to 1567	No	ns	0.5897

Table S45. 1×10^5 PFU/mL - Viable virus-laden droplet counts collected below the fifth stage

Tukey's multiple comparisons test	Mean Diff.	95.00% CI of diff.	Below threshold?	Summary	Adjusted P Value
1.5 [15±5] vs. 3.0 [15±5]	36.17	-130.5 to 202.8	No	ns	0.9850
1.5 [15±5] vs. 6.0 [15±5]	103.1	-70.08 to 276.3	No	ns	0.4743

1.5 [15±5] vs. 1.5 [50±5]	122.9	-38.88 to 284.7	No	ns	0.2212
1.5 [15±5] vs. 3 [50±5]	110.8	-51.02 to 272.6	No	ns	0.3230
1.5 [15±5] vs. 6 [50±5]	171.6	9.833 to 333.5	Yes	*	0.0326
3.0 [15±5] vs. 6.0 [15±5]	66.93	-89.39 to 223.3	No	ns	0.7814
3.0 [15±5] vs. 1.5 [50±5]	86.76	-56.86 to 230.4	No	ns	0.4584
3.0 [15±5] vs. 3 [50±5]	74.62	-69.01 to 218.2	No	ns	0.6172
3.0 [15±5] vs. 6 [50±5]	135.5	-8.150 to 279.1	No	ns	0.0733
6.0 [15±5] vs. 1.5 [50±5]	19.83	-131.3 to 171.0	No	ns	0.9986
6.0 [15±5] vs. 3 [50±5]	7.686	-143.5 to 158.8	No	ns	>0.9999
6.0 [15±5] vs. 6 [50±5]	68.54	-82.62 to 219.7	No	ns	0.7387
1.5 [50±5] vs. 3 [50±5]	-12.14	-150.1 to 125.8	No	ns	0.9998
1.5 [50±5] vs. 6 [50±5]	48.71	-89.28 to 186.7	No	ns	0.8879
3 [50±5] vs. 6 [50±5]	60.86	-77.13 to 198.8	No	ns	0.7601

Table S46. 5×10^5 PFU/mL - Viable virus-laden droplet counts collected below the fifth stage

Tukey's multiple comparisons test	Mean Diff.	95.00% CI of diff.	Below threshold?	Summary	Adjusted P Value
1.5 [15±5] vs. 3.0 [15±5]	-365.4	-1381 to 650.4	No	ns	0.8716
1.5 [15±5] vs. 6.0 [15±5]	-372.6	-1350 to 604.8	No	ns	0.8425
1.5 [15±5] vs. 1.5 [50±5]	-405.0	-1421 to 610.8	No	ns	0.8167
1.5 [15±5] vs. 3 [50±5]	-356.0	-1372 to 659.8	No	ns	0.8831
1.5 [15±5] vs. 6 [50±5]	-217.2	-1233 to 798.6	No	ns	0.9846
3.0 [15±5] vs. 6.0 [15±5]	-7.233	-924.1 to 909.7	No	ns	>0.9999
3.0 [15±5] vs. 1.5 [50±5]	-39.60	-997.3 to 918.1	No	ns	>0.9999
3.0 [15±5] vs. 3 [50±5]	9.400	-948.3 to 967.1	No	ns	>0.9999

3.0 [15±5] vs. 6 [50±5]	148.2	-809.5 to 1106	No	ns	0.9965
6.0 [15±5] vs. 1.5 [50±5]	-32.37	-949.3 to 884.5	No	ns	>0.9999
6.0 [15±5] vs. 3 [50±5]	16.63	-900.3 to 933.5	No	ns	>0.9999
6.0 [15±5] vs. 6 [50±5]	155.4	-761.5 to 1072	No	ns	0.9946
1.5 [50±5] vs. 3 [50±5]	49.00	-908.7 to 1007	No	ns	>0.9999
1.5 [50±5] vs. 6 [50±5]	187.8	-769.9 to 1145	No	ns	0.9895
3 [50±5] vs. 6 [50±5]	138.8	-818.9 to 1096	No	ns	0.9974

Table S47. 1×10^5 PFU/mL - Viable virus-laden droplet counts collected below the sixth stage

Tukey's multiple comparisons test	Mean Diff.	95.00% CI of diff.	Below threshold?	Summary	Adjusted P Value
1.5 [15±5] vs. 3.0 [15±5]	38.00	-10.87 to 86.87	No	ns	0.2007
1.5 [15±5] vs. 6.0 [15±5]	47.70	-3.085 to 98.48	No	ns	0.0753
1.5 [15±5] vs. 1.5 [50±5]	69.93	22.48 to 117.4	Yes	**	0.0013
1.5 [15±5] vs. 3 [50±5]	61.21	13.76 to 108.7	Yes	**	0.0057
1.5 [15±5] vs. 6 [50±5]	58.36	10.91 to 105.8	Yes	**	0.0092
3.0 [15±5] vs. 6.0 [15±5]	9.700	-36.14 to 55.54	No	ns	0.9866
3.0 [15±5] vs. 1.5 [50±5]	31.93	-10.19 to 74.05	No	ns	0.2232
3.0 [15±5] vs. 3 [50±5]	23.21	-18.90 to 65.33	No	ns	0.5570
3.0 [15±5] vs. 6 [50±5]	20.36	-21.76 to 62.48	No	ns	0.6851
6.0 [15±5] vs. 1.5 [50±5]	22.23	-22.10 to 66.56	No	ns	0.6514
6.0 [15±5] vs. 3 [50±5]	13.51	-30.81 to 57.84	No	ns	0.9363
6.0 [15±5] vs. 6 [50±5]	10.66	-33.67 to 54.99	No	ns	0.9764
1.5 [50±5] vs. 3 [50±5]	-8.714	-49.18 to 31.75	No	ns	0.9855
1.5 [50±5] vs. 6 [50±5]	-11.57	-52.04 to 28.89	No	ns	0.9508

3 [50±5] vs. 6 [50±5]	-2.857	-43.32 to 37.61	No	ns	>0.9999

Table S48. 5×10^5 PFU/mL - Viable virus-laden droplet counts collected below the sixth stage

Tukey's multiple comparisons test	Mean Diff.	95.00% CI of diff.	Below threshold?	Summary	Adjusted P Value
1.5 [15±5] vs. 3.0 [15±5]	-53.10	-498.4 to 392.2	No	ns	0.9990
1.5 [15±5] vs. 6.0 [15±5]	-263.2	-691.7 to 165.3	No	ns	0.4267
1.5 [15±5] vs. 1.5 [50±5]	-22.10	-467.4 to 423.2	No	ns	>0.9999
1.5 [15±5] vs. 3 [50±5]	-31.30	-476.6 to 414.0	No	ns	>0.9999
1.5 [15±5] vs. 6 [50±5]	-34.50	-479.8 to 410.8	No	ns	0.9999
3.0 [15±5] vs. 6.0 [15±5]	-210.1	-612.0 to 191.9	No	ns	0.5966
3.0 [15±5] vs. 1.5 [50±5]	31.00	-388.8 to 450.8	No	ns	>0.9999
3.0 [15±5] vs. 3 [50±5]	21.80	-398.0 to 441.6	No	ns	>0.9999
3.0 [15±5] vs. 6 [50±5]	18.60	-401.2 to 438.4	No	ns	>0.9999
6.0 [15±5] vs. 1.5 [50±5]	241.1	-160.9 to 643.0	No	ns	0.4523
6.0 [15±5] vs. 3 [50±5]	231.9	-170.1 to 633.8	No	ns	0.4941
6.0 [15±5] vs. 6 [50±5]	228.7	-173.3 to 630.6	No	ns	0.5089
1.5 [50±5] vs. 3 [50±5]	-9.200	-429.0 to 410.6	No	ns	>0.9999
1.5 [50±5] vs. 6 [50±5]	-12.40	-432.2 to 407.4	No	ns	>0.9999
3 [50±5] vs. 6 [50±5]	-3.200	-423.0 to 416.6	No	ns	>0.9999

Table S49. 1×10^5 PFU/mL - Viable virus-laden droplet counts collected below all impactor stages

Tukey's multiple comparisons test	Mean Diff.	95.00% CI of diff.	Below threshold?	Summary	Adjusted P Value
1.5 [15±5] vs. 3.0 [15±5]	428.4	-270.4 to 1127	No	ns	0.4423
1.5 [15±5] vs. 6.0 [15±5]	1034	307.3 to 1760	Yes	**	0.0019

1.5 [15±5] vs. 1.5 [50±5]	807.6	129.0 to 1486	Yes	*	0.0125
1.5 [15±5] vs. 3 [50±5]	831.5	152.9 to 1510	Yes	**	0.0095
1.5 [15±5] vs. 6 [50±5]	1255	576.0 to 1933	Yes	****	<0.0001
3.0 [15±5] vs. 6.0 [15±5]	605.1	-50.46 to 1261	No	ns	0.0837
3.0 [15±5] vs. 1.5 [50±5]	379.2	-223.2 to 981.5	No	ns	0.4132
3.0 [15±5] vs. 3 [50±5]	403.0	-199.3 to 1005	No	ns	0.3472
3.0 [15±5] vs. 6 [50±5]	826.2	223.8 to 1429	Yes	**	0.0030
6.0 [15±5] vs. 1.5 [50±5]	-225.9	-859.9 to 408.0	No	ns	0.8839
6.0 [15±5] vs. 3 [50±5]	-202.1	-836.0 to 431.9	No	ns	0.9240
6.0 [15±5] vs. 6 [50±5]	221.1	-412.9 to 855.0	No	ns	0.8929
1.5 [50±5] vs. 3 [50±5]	23.86	-554.9 to 602.6	No	ns	>0.9999
1.5 [50±5] vs. 6 [50±5]	447.0	-131.7 to 1026	No	ns	0.2066
3 [50±5] vs. 6 [50±5]	423.1	-155.6 to 1002	No	ns	0.2569

Table S50. 5×10^5 PFU/mL - Viable virus-laden droplet counts collected below all impactor stages

Tukey's multiple comparisons test	Mean Diff.	95.00% CI of diff.	Below threshold?	Summary	Adjusted P Value
1.5 [15±5] vs. 3.0 [15±5]	-966.6	-4733 to 2800	No	ns	0.9659
1.5 [15±5] vs. 6.0 [15±5]	253.9	-3370 to 3878	No	ns	>0.9999
1.5 [15±5] vs. 1.5 [50±5]	-812.4	-4579 to 2954	No	ns	0.9840
1.5 [15±5] vs. 3 [50±5]	-161.4	-3928 to 3605	No	ns	>0.9999
1.5 [15±5] vs. 6 [50±5]	1207	-2559 to 4973	No	ns	0.9164
3.0 [15±5] vs. 6.0 [15±5]	1220	-2179 to 4620	No	ns	0.8725
3.0 [15±5] vs. 1.5 [50±5]	154.2	-3397 to 3705	No	ns	>0.9999

3.0 [15±5] vs. 3 [50±5]	805.2	-2746 to 4356	No	ns	0.9800
3.0 [15±5] vs. 6 [50±5]	2174	-1377 to 5725	No	ns	0.4303
6.0 [15±5] vs. 1.5 [50±5]	-1066	-4466 to 2334	No	ns	0.9231
6.0 [15±5] vs. 3 [50±5]	-415.3	-3815 to 2985	No	ns	0.9989
6.0 [15±5] vs. 6 [50±5]	953.1	-2447 to 4353	No	ns	0.9508
1.5 [50±5] vs. 3 [50±5]	651.0	-2900 to 4202	No	ns	0.9923
1.5 [50±5] vs. 6 [50±5]	2019	-1532 to 5570	No	ns	0.5093
3 [50±5] vs. 6 [50±5]	1368	-2183 to 4919	No	ns	0.8365

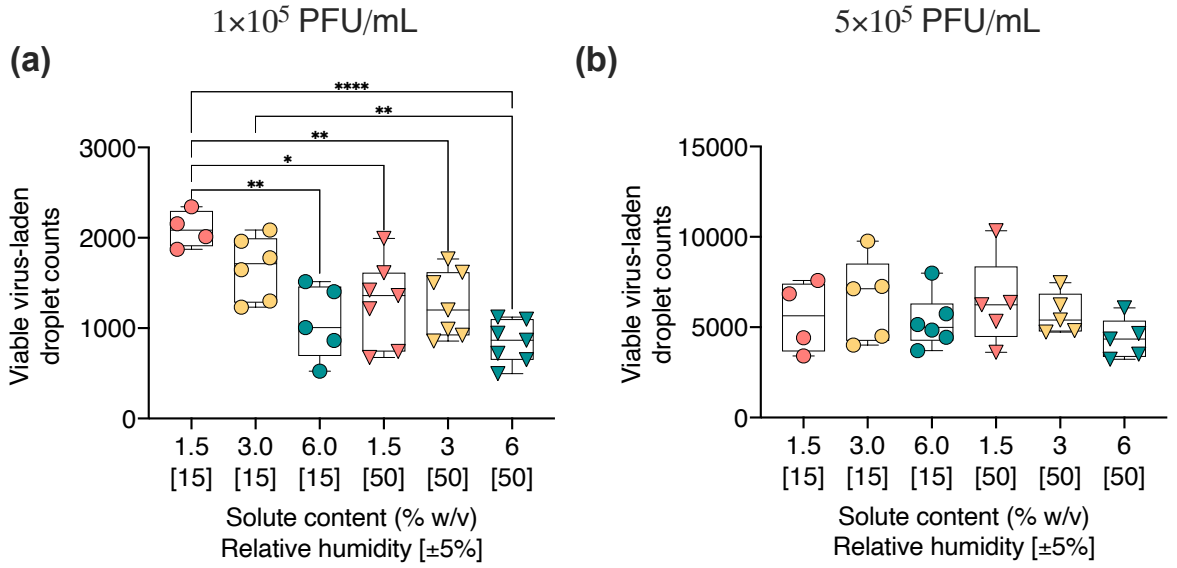

Figure S4. **Effect of virus concentration, solute content, and relative humidity on viable droplet counts with initial size range of 1.73 to ≥20.28 µm.** Phi6 bacteriophage suspensions with concentrations of 1×10^5 PFU/mL (**a,b**) and 5×10^5 PFU/mL (**c,d**) were prepared in 1.5% (**salmon**), 3% (**grey**), and 6% (**turquoise**) w/v peptone water solutions and aerosolized into 15±5% (**circles**) and 50±5% (**triangles**) relative humidity conditions at 24±1.6°C. Graphs present coincidence-corrected viable droplet counts collected below all impactor stages. Significance determined using ordinary one-way ANOVA followed by Tukey's multiple comparisons test defined as * - $p<0.05$, ** - $p<0.01$, **** - $p<0.0001$.

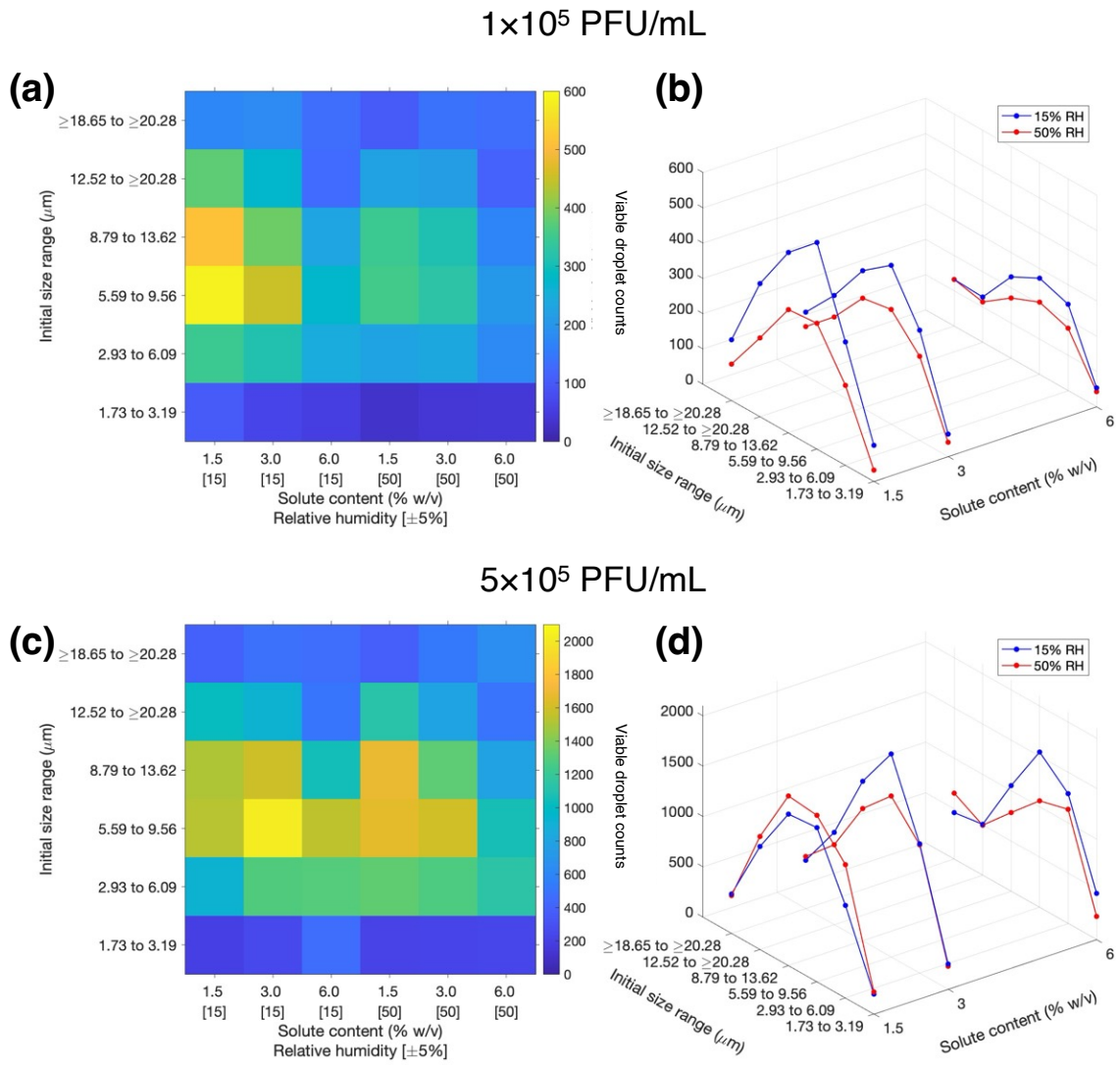

Figure S5. Initial size range influences solute-, relative humidity-, and virus concentration-dependent changes in viable virus-laden droplet counts. (a,c) Intensity maps and **(b,d)** 3D plots present viable virus-laden droplet counts with initial size range of 1.73 to ≥20.28 μm generated from Phi6 suspensions with concentrations of **(a,b)** 1×10^5 PFU/mL and **(c,d)** 5×10^5 PFU/mL prepared in 1.5%, 3%, and 6% w/v peptone water solutions and aerosolized into 15±5% and 50±5% relative humidity conditions at 24±1.6°C.

Chapter 6. An *in vitro* exposure platform for investigating bacterial and epithelial cell responses to aerosolized phage challenge

Preface. This chapter explores the multi-functionality of the aerosol platform, by re-purposing the system to study inhaled therapeutic delivery. The cell-integrated exposure platform can be utilized to evaluate cellular responses (viability, permeability, and inflammatory response) to aerosolized pathogens, allergens, or therapeutics. ***The results and conclusions presented in this chapter are valid under specific conditions and assumptions outlined in the study. Therefore, the accuracy and reliability of the findings depend on defined test conditions. These results may not be applicable under all circumstances or in different environments. Users of this information should exercise caution and consider additional factors relevant to their specific context before applying these results to describe and interpret real-world phenomena.***

Contributions. I conceived the study design, developed and optimized experimental techniques for data acquisition, performed the bulk of the experimentation, formal data analysis, troubleshooting, and data visualization, and wrote the original manuscript drafts. Michelle Feng was an undergraduate student whom I trained extensively on Calu-3 culture techniques and helped maintain cell cultures. Michelle was instrumental in troubleshooting and standardizing Calu-3 culture assay protocols. Michelle helped me perform the permeability (Figure 2b) and Live/Dead assays (Figure 3a) and wrote parts of the introduction to the 2022 conference proceeding. Mellissa Gomez helped to write, edit, and revise significant portions of the 2023 conference proceeding and performed TEM imaging of phage virion (Figure 4b) and the SEM imaging of ciprofloxacin flakes (Figure 4c). Fereshteh Bayat performed SEM imagining of bacterial cells (Figure 1c) and TEM imaging of phage virion (Figure 1d). Rod G. Rhem constructed the aerosol exposure platform. Prof. Myrna B. Dolovich and Dr. Zeinab Hosseinidoust were responsible for project supervision and reviewing and editing the final draft manuscript drafts. Paul Gatt, Justin Bernar, and John Colenbrander from the Chemical and Mechanical Engineering Machine Shop and Doug Keller were instrument in helping to design and building the aerosol platform.

Citation. This chapter contains the contents of two 4-page research papers peer-reviewed and accepted in the 2022 and 2023 Drug Delivery to the Lungs conference proceedings. This chapter is under review, ACS Omega.

1. **Thirugnanasampanthar, M.**, Feng, M., Gomez, M., Bayat, F., Rhem, R. G., Dolovich, M. B., & Hosseinidoust, Z. (2024). An *in vitro* exposure platform for investigating bacterial and epithelial cell responses to aerosolized phage challenge.
2. **Thirugnanasampanthar, M.**, Gomez, M., Dolovich, M. B., & Hosseinidoust, Z. (2023). Anti-biofilm activity of aerosolized phage vs. ciprofloxacin using an *in vitro* lung deposition platform. Drug Delivery to the Lungs Conference. 34: 324-327.
3. **Thirugnanasampanthar, M.**, Feng, M., Bayat, F., Rhem, R. G., Dolovich, M. B., & Hosseinidoust, Z. (2022). An *in vitro* exposure platform for investigating bacterial and epithelial cell responses to aerosolized phage challenge. Drug Delivery to the Lungs Conference. 33: 352-355.

6.1. ABSTRACT

Pseudomonas aeruginosa is a bacterial pathogen frequently implicated in recurrent, antibiotic-resistant airway infections in cystic fibrosis patients. Bacteriophages (phages) are viruses that exclusively infect bacteria. Phage therapy describes the treatment of bacterial infections, more specifically, antibiotic-resistant infections, with bacterial viruses. Investigations with aerosolized phage are limited, focusing on proof-of-concept demonstrations with animal models. *In vitro* models are needed to conduct comprehensive, mechanistic research. We report the development and use of an impactor-based *in vitro* exposure platform for evaluating the responses of *P. aeruginosa* biofilms and Calu-3 human airway epithelial cells to aerosolized bacteriophage-laden droplets. We observed significant reductions in the metabolic activity and viability of *P. aeruginosa* biofilms after exposure to phage aerosol droplets, indicative of phage-mediated lysis of bacterial cells. We further probed the effects of exposure to size-fractioned aerosol droplets of phage or the fluoroquinolone antibiotic ciprofloxacin on *P. aeruginosa* biofilm cultures using a modified configuration of the aerosol exposure platform. Exposure to aerosolized phage challenge, regardless of the dose delivered by size-fractioned droplets, resulted in a significant reduction of free-floating and adherent bacteria compared to negative control samples. Conversely, the antibacterial efficacy of ciprofloxacin exhibited a strong dose dependence. This work demonstrates the promise of inhaled delivery of lytic phages for tackling persistent deep lung infections compared to conventional antibiotics.

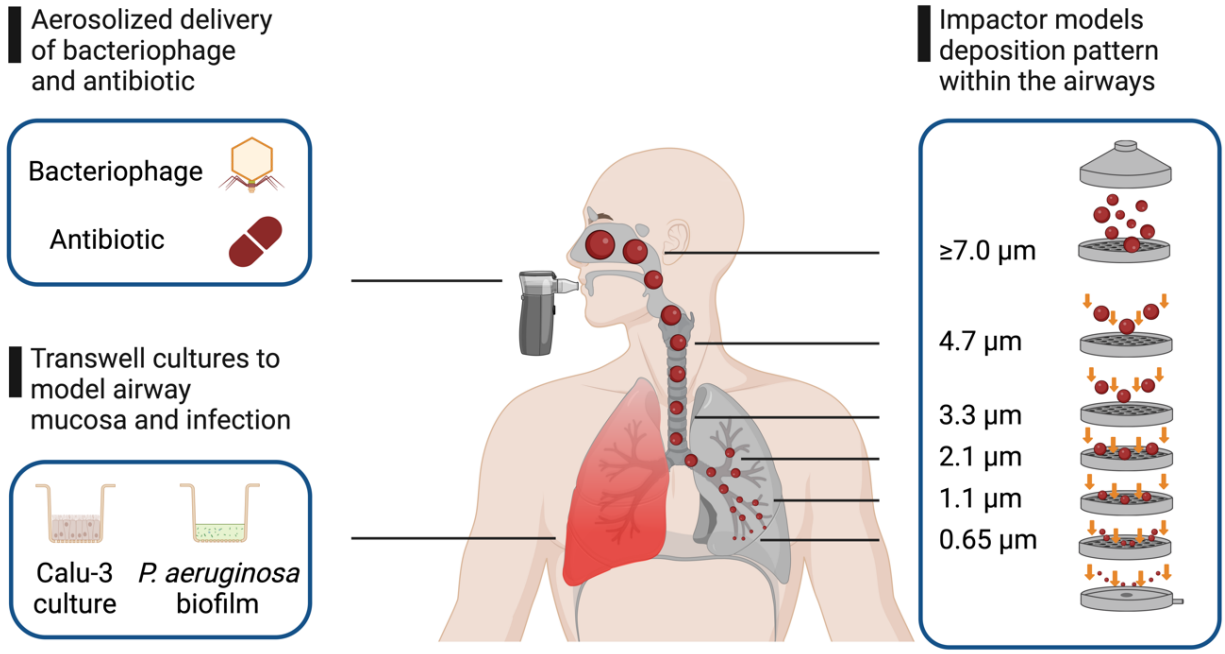

Graphical abstract – The illustration depicts aerosol droplet generation via atomization, the use of transwell cultures of epithelial cells and *P. aeruginosa* biofilms to model airway infections, and the use of the impactor to model size-dependent airways deposition pattern.

6.2. INTRODUCTION

1.5 million deaths were attributed to antimicrobial resistance (AMR) development in lower respiratory tract infections in 2019.[1] The gram-negative bacterial pathogen, *P. aeruginosa*, is one of the most common species implicated in AMR-related mortalities[2] and identified among the most common causes of nosocomial infections exhibiting broad antibiotic resistance.[3] Biofilm growth, wherein bacteria reside within a hydrated exopolysaccharide matrix, allows pathogens to evade host immune surveillance, resist bactericidal agents, and establish chronic airway infections.[4] Biofilms not only prevent antibacterial compounds from reaching embedded bacteria, but bacteria residing within these matrices may exhibit intrinsic resistance to antimicrobial agents.[4] Cystic fibrosis (CF) is a genetic disorder caused by recessive mutations within the CF transmembrane conductance regulator gene, which encodes for a transmembrane chloride channel expressed across multiple organs.[5] Disease manifestations in cystic fibrosis patients are characterized by chronic lung infections leading to inflammation, pneumonia, respiratory failure, and mortality.[6] Notably, multi-drug-resistant *P. aeruginosa* infections contribute to high mortality rates among CF patients.[6]

Phages are bacterial viruses that exhibit targeted antibacterial activity, low inherent toxicity, and the capacity to propagate in the presence of host bacterial cells.[7] The effectiveness of phage therapy has been demonstrated in several *in vivo* studies showing improved survival in animal models experimentally infected with lethal doses of *P. aeruginosa* strains isolated from CF patients.[8,9] Phage therapy has been proposed to target multi-drug-resistant strains of *P. aeruginosa* infecting CF patients.[10] The route of administration is a determinant of treatment efficacy.[11] Studies have shown that intravenous delivery of phages leads to rapid immune clearance.[12] For respiratory infections, inhaled delivery of phage aerosol droplets can directly target biofilms on mucosal surfaces of the airways.

Relevant *in vitro* test platforms are needed to evaluate cellular responses following phage delivery. In this work, we utilized two different configurations of an aerosol exposure platform to examine the effects of aerosolized phage-laden droplets on *P. aeruginosa* biofilms and human airway epithelial cell cultures. Furthermore, we compare the antibacterial efficacy of aerosolized phage-laden droplets to that of ciprofloxacin-laden droplets against *P. aeruginosa* biofilm cultures. Lastly, the dose distribution profiles of phage- and ciprofloxacin-laden droplets were quantified and compared to antibacterial efficacy.

6.3. RESULTS AND DISCUSSION

6.3.1. Experimental setup for the exposure of Calu-3 ALI cultures and PAO1 biofilms to airflow or 0.65 – 1.1 µm sized phage-laden droplets

The first set of experiments was carried out using the configuration of the aerosol exposure platform depicted in **Figure 1a** and incorporates the 60-cm-high glass mixing chamber. Transwells containing air-liquid interface (ALI) cultures of Calu-3 cells (**Figure 1b**) or biofilm cultures of *P. aeruginosa* cells (**Figure 1c)** experience exposure to airflow or phage-laden droplets (**Figure 1d**) below the sixth stage of the cascade impactor. Airflow velocity increases from the first to the last impactor stage to capture droplets that tend to deposit within the lower airways (**Figure 1e**). Samples below the last impactor stage experience an airflow velocity of 24 m/s. An in-line humidifier maintained the humidity above 70-80% to prevent desiccation of bacterial and epithelial cell cultures during exposure. Assays performed 24 hours later were used to determine

the effect of exposure to airflow and phage aerosol droplets on *P. aeruginosa* biofilms and Calu-3 ALI cultures.

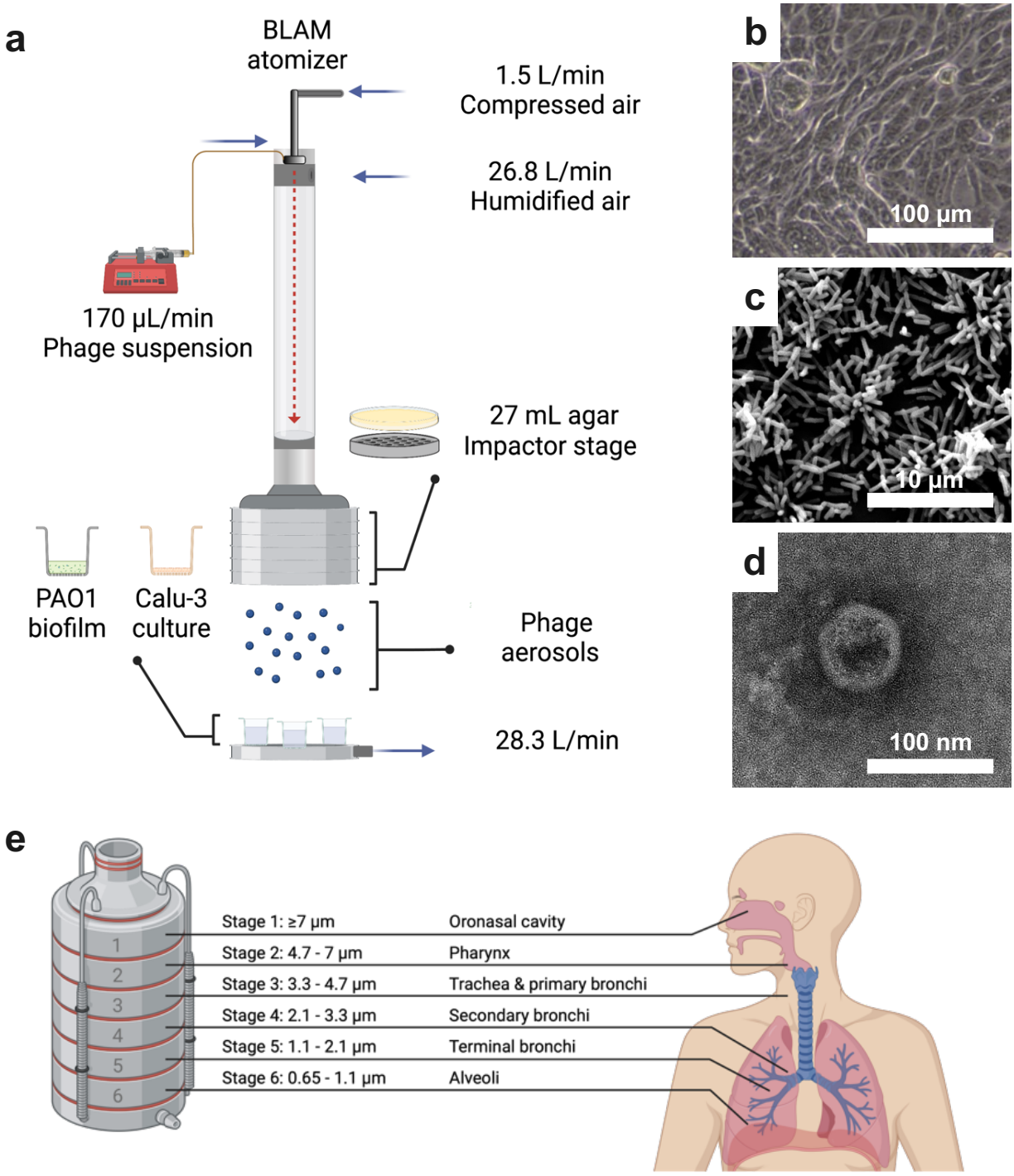

Figure 1. The illustration depicts the platform configuration for exposing *P. aeruginosa* biofilms and Calu-3 airway epithelial cell cultures to airflow or aerosolized phage droplets. **(a)** Aerosol exposure platform; **(b)** Calu-3 cells under 10x Magnification; **(c)** SEM image of Pa

bacterial cells; **(d)** TEM image of Pseudomonas phage vB_Pae-TbilisiM32; **(e)** 6-stage viable cascade impactor simulates deposition pattern within the human respiratory tract.

6.3.2. Post-exposure junctional integrity of Calu-3 cultures and metabolic activity of PAO1 biofilm cultures

FITC-dextran is a fluorescent molecule commonly used to assess permeability across confluent cell layers. The leakage of FITC-dextran from empty transwell inserts defined the maximum permeability value. Leakage from Calu-3-containing transwells, presented as a fraction of the leakage from empty transwells, was used to assess the tight-junctional barrier integrity of Calu-3 cells following exposure to airflow or phage aerosol droplets. Mean permeability values for unexposed, airflow-exposed, and phage aerosol-exposed samples were 0.51±0.17%, 0.8±0.73%, and 2.91±4.39%, respectively (**Figure 2a, Table S1**). Thus, the mean permeability values of <5% for Calu-3-containing transwells from the unexposed, airflow-exposed, and phage-exposed conditions indicate airflow and phage exposure have negligible effects on tight-junctional barrier integrity.

The XTT assay is a colorimetric assay used to quantify the metabolic activity of viable cells. Yellow tetrazolium salt, the main component of the XTT assay, is reduced to the orange formazan compound in the presence of live cells. Formazan absorbs 490nm wavelengths of light, with greater absorbance corresponding to the high metabolic activity of viable cells. The mean absorbance value was 2.20±0.40 for bacterial cells exposed to airflow, comparable to the absorbance value of 2.21±0.30 calculated for unexposed samples (**Figure 2b, Table S2**). Similar absorbance as the unexposed condition suggests the metabolic activity of bacterial cells is unaffected following exposure to airflow within the platform. A significantly lower mean absorbance value of 1.03±0.19 was observed in phage-exposed samples (**Figure 2b, Table S2**). These results indicate that while airflow has negligible effects, phage exposure produces significant reductions in the metabolic activity of bacterial cells.

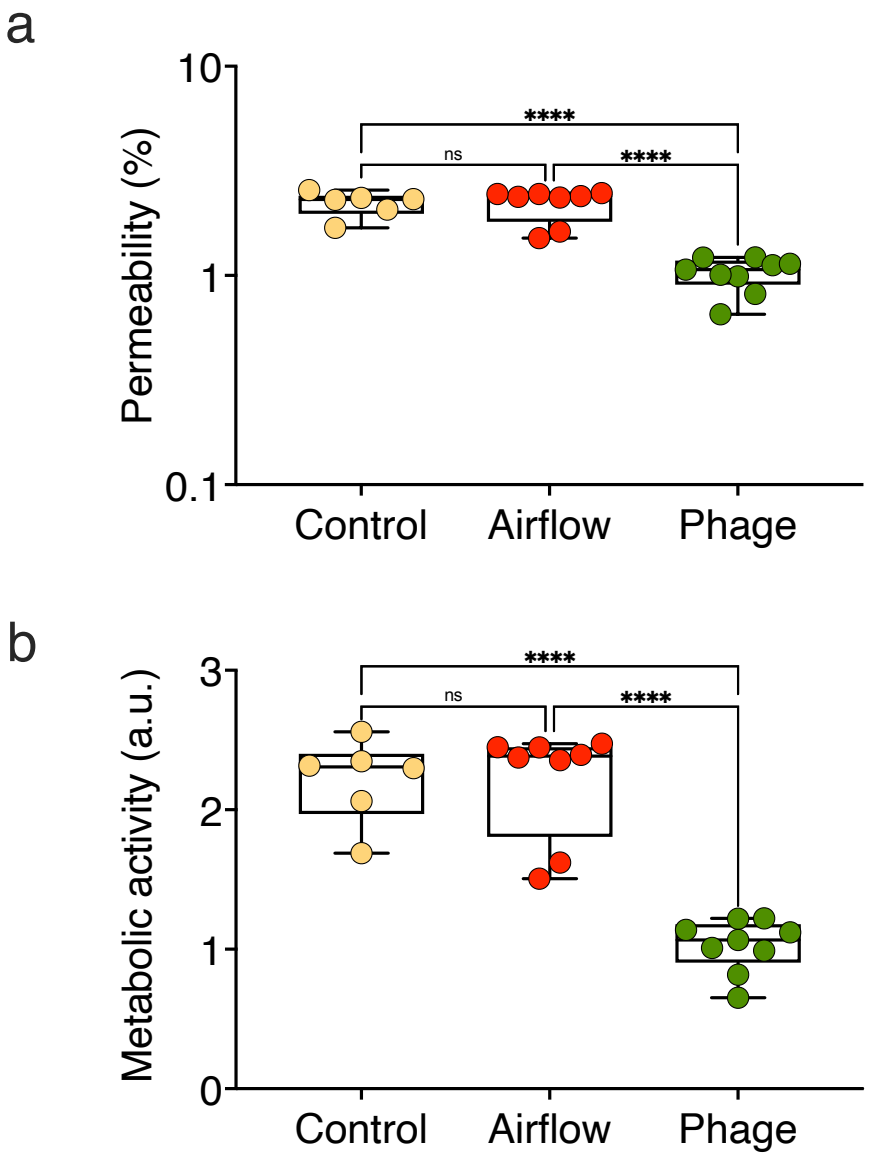

Figure 2. Effect of airflow and phage exposure on (a) Calu-3 barrier integrity and (b) *P. aeruginosa* metabolic activity. (a) FITC-dextran permeability across Calu-3 cells exposed to airflow and phage did not significantly differ from unexposed cells, indicating cell barrier integrity was uncompromised by airflow or phage exposure. **(b)** The absorbance of 490 nm wavelength of light reflects the metabolic activity of viable *P. aeruginosa* cells; absorbance values of *P. aeruginosa* cells exposed to phage were significantly lower than unexposed or airflow-exposed cells, indicating phage-mediated killing of bacterial cells has occurred. Phage = exposure to phage aerosol droplets, Airflow = airflow exposure within the platform, and Control = unexposed samples. Results from 3-4 replicate trials are shown, with each data point representing an individual transwell insert (n=5-10). One-way ANOVA followed by Tukey's post-hoc test was used to analyse data sets (****$p<0.0001$).

6.3.3. Post-exposure viability of Calu-3 and PAO1 cells

Calu-3 cells were stained with DAPI and NucGreen dyes to visualize live and dead cells. In agreement with permeability results, fluorescent staining results show similar quantities of live and dead cells in unexposed, airflow-exposed, and phage-exposed conditions (**Figure 3a**). These results indicate the deposition of approximately 1×10^5 PFU of aerosolized phage aerosol droplets does not impair the barrier integrity or viability of Calu-3 cells. Syto9 staining of viable bacterial cells indicates airflow-exposed and unexposed samples have similar densities of live cells (**Figure 3b**). However, significantly fewer viable bacterial cells were present in phage-exposed samples (**Figure 3b**).

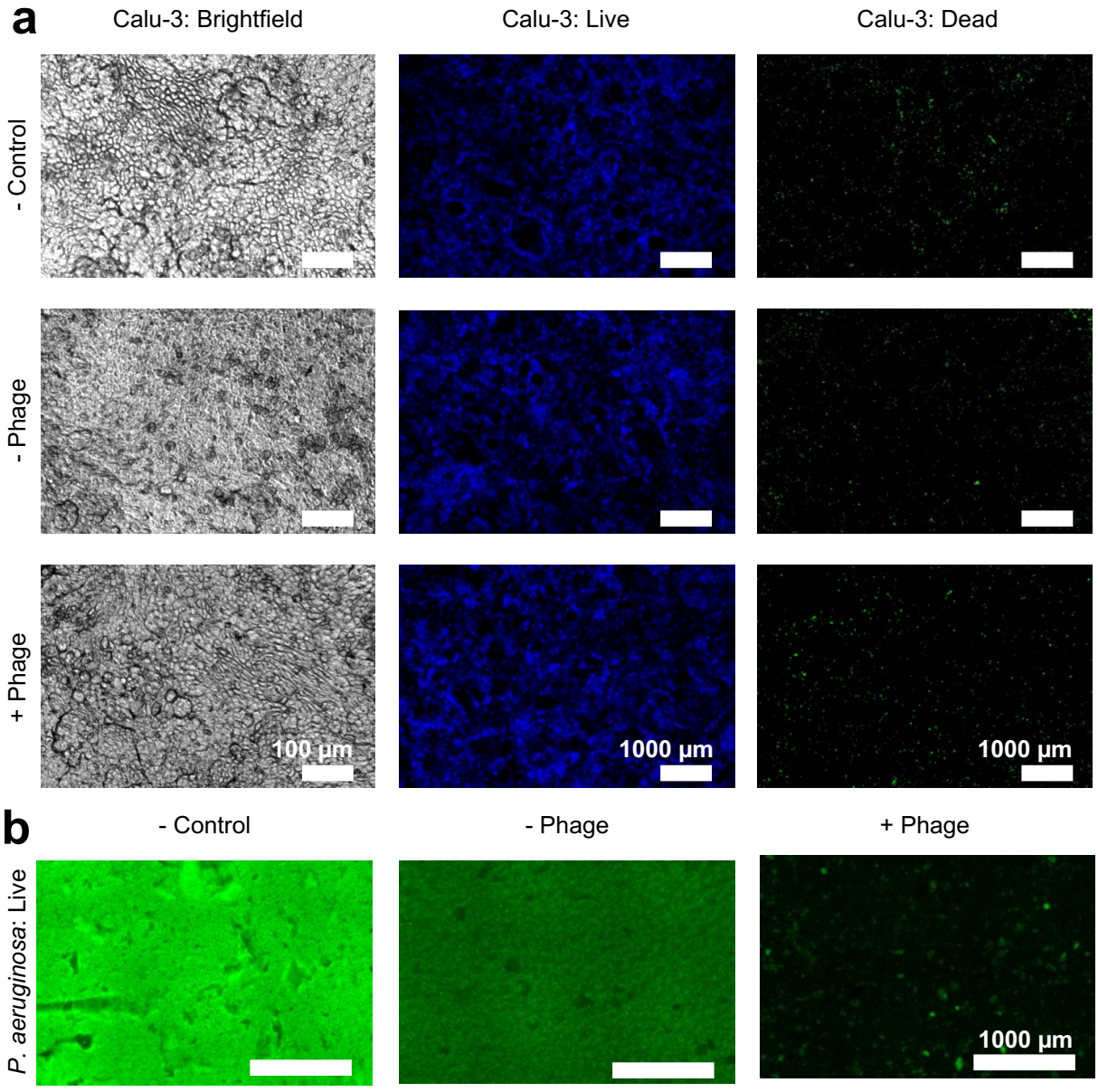

Figure 3. Effect of airflow and phage exposure on the viability of (a) Calu-3 and (b) *P. aeruginosa* cells. (a) DAPI- and NucGreen-stained Calu-3 cells. **(b)** Syto9- and propidium iodide-

stained bacterial cells. **(a)** Fluorescent images show airflow and phage exposure did not reduce the viability of Calu-3 cells as the number of live cells stained in blue and dead cells stained in green are comparable to the unexposed condition. **(b)** Live *P. aeruginosa* cells were stained green by Syto9, and fluorescent images show similar densities of live cells in airflow-exposed and unexposed conditions but significantly fewer live cells in the phage-exposed condition, indicative of phage-mediated lysis of bacterial cells. (+) Phage = phage exposure, (-) Phage = airflow exposure, (-) Control = unexposed.

Results from the first set of experiments indicate exposure to high-velocity airflow within the *in vitro* exposure platform has negligible effects on *P. aeruginosa* biofilms and Calu-3 ALI cultures. The leakage of FITC-dextran across airflow-exposed Calu-3 cells was comparable to leakage across unexposed Calu-3 cultures (**Figure 2a)**. Additionally, absorbance values indicate the metabolic activities of airflow-exposed and unexposed bacterial samples are similar (**Figure 2b**). Furthermore, fluorescent images of Calu-3 (**Figure 3a**) and *P. aeruginosa* cells (**Figure 3b**) exposed to high-velocity airflows were indistinguishable from unexposed samples. Assays performed on biofilms and Calu-3 ALI cultures exposed to viable phage-laden droplets demonstrate phage exposure has negligible effects on Calu-3 cells (**Figures 2a, 3a**) but significantly depletes biofilm bacterial cells (**Figures 2b, 3b**).

6.3.4. Experimental setup for the exposure of PAO1 biofilms to size-fractioned phage-laden, phage-free-carrier-laden, ciprofloxacin-laden, and ciprofloxacin-free-carrier-laden droplets

A second set of experiments was conducted with a modified configuration of the aerosol exposure platform using a 10-cm-high aerosol mixing chamber (**Figure 4a**). Using this platform, we investigated the dose distribution profiles and antibacterial efficacies of aerosolized droplets of phage or ciprofloxacin. Exposed to size-fractioned droplets of phage (**Figure 4b**) or ciprofloxacin (**Figure 4c**) involved the placement of foil-lined (**Figure 4e**) or biofilm-containing (**Figure 4f**) transwell inserts below odd or even numbered impactor stages in triplicates (**Figure 4d**). Metabolic activity assays were performed 24 hours after exposure to determine the viability of planktonic (free-floating) and sessile (adherent) bacterial cells.

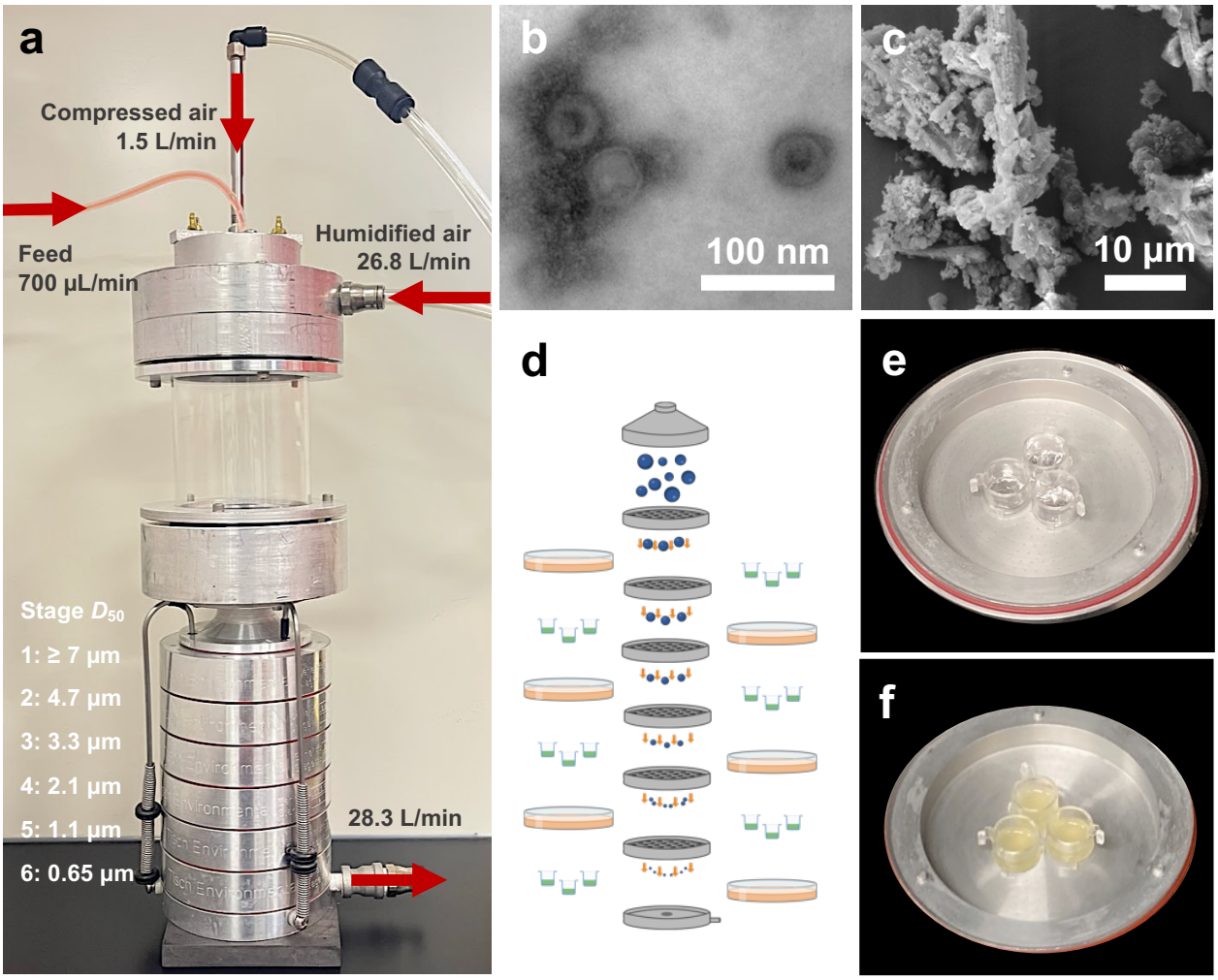

Figure 4. Platform configuration for exposing *P. aeruginosa* biofilms to size-fractioned droplets of aerosolized phage suspension and antibiotic solution. (a) The aerosol exposure platform consists of a 10-cm-high aerosol mixing chamber and a 6-stage viable cascade impactor, which separates droplets according to aerodynamic cut-off size. **(b)** TEM image of anti-Pseudomonas phage virions. **(c)** SEM image of ciprofloxacin flakes. **(d-f)** Transwell inserts lined with foil or containing biofilm cultures were placed below alternate stages of the impactor and exposed to droplets generated from the aerosolization of phage suspension (7×10^8 PFU/mL) or ciprofloxacin solution (7.5 mg/mL).

6.3.5. Dose deposition profiles and bactericidal efficacy of aerosolized ciprofloxacin- and phage-laden droplets

The stock antibiotic solution (10 mg/mL) was prepared using equal parts 0.1 M HCl and ultrapure water due to the pH-dependent solubility of ciprofloxacin (increased solubility at low pH)[16]. Carrier medium, consisting of 25% TSB and 75% ultrapure water, was used to prepare the phage suspension (7×10^8 PFU/mL) and the ciprofloxacin solution (7.5 mg/mL). The antibiotic solution had a final pH of 3.15, while the phage suspension had a pH of 7.4. Consequently, a ciprofloxacin-free carrier (pH of 3.15) and a phage-free carrier (pH of 7.4) solution were prepared separately as negative controls. A fluorescent tracer added to phage-free and ciprofloxacin-free

carrier solutions allowed us to spectrofluorimetrically quantify the carrier recovered from foil-lined transwell inserts and determine the dose distribution profiles of the inert carriers (**Figure 5a, Tables S3-S6)**. The distribution profiles of inert carrier droplets were similar (**Figure 5a**).

We can calculate plaque-forming-units of phage (5×10^8 PFU) and mass of ciprofloxacin (5.25 mg) introduced via atomization into the exposure platform using the concentration of the bactericidal suspension or solution (7×10^8 PFU/mL or 7.5 mg/mL), the feed flow rate (700 µL/minute), and duration of atomization (1 minute). However, only small fractions of the total dose introduced into the system reach transwell inserts placed below each impactor stage. Quantitative dose distribution profiles of bactericidal droplets were determined using the plaque assay method to detect infectious phage virions and the spectrofluorimetric method to detect ciprofloxacin (**Figure 5b, Tables S7-S10**). The percentage nominal doses of phage and ciprofloxacin deposited into transwells placed within the impactor were unequal across the stages (**Figure 5b**). The nominal dose of ciprofloxacin recovered from transwells exposed below impactor stages 2, 3, and 5 was significantly higher than nominal doses of infectious phage virions (**Figure 5b**). Lower than expected phage dose distribution can result from damage incurred during nebulization, as previously reported in the literature.[17]

Biofilms exposed below the first and fourth impactor stages received the highest and lowest phage doses of 1×10^4 PFU and 2×10^2 PFU, respectively (**Figure 5b, Tables S7, S8**). Despite a 50-fold reduction in phage dose, antibacterial efficacy was comparable in samples that received the highest dose below the first impactor stage (**Figure 5c,5e, Tables S11-S20**). The results reflect the ability of lytic phages to undergo on-site amplification and eradicate bacteria in a dose-independent manner. Our results agree with the *in vivo* study using a murine *P. aeruginosa* lung infection model.[18] However, the study did not investigate aerosolized delivery or biofilm eradication as the phage was administered intratracheally via pipette only two hours after bacterial infection. In comparison, our work illustrates the dose-independent activity of aerosolized phage droplets against established biofilm cultures.

Biofilms exposed below the first impactor stage, representing infection sites within the oral and nasal cavities, received the highest antibiotic dose of 2.5 µg (**Figure 5b**). This dose significantly depleted planktonic (**Figure 5d, Tables S21-S27)** and sessile cell fractions (**Figure 5f, Tables S28-S34**). Biofilms exposed below the sixth stage, representing the distal-most airway region, only received 0.5 µg of ciprofloxacin (**Figure 5b**). The reduced antibiotic dose failed to deplete the planktonic or the sessile bacterial fraction (**Figure 5d,5f**). The effective ciprofloxacin dose of 5 µg/mL, calculated using the seeding volume of 0.5 mL, is consistent with previously reported antibiotic concentrations that reduced biofilm biomass formed by clinical strains of P. aeruginosa by ≥90%.[19] These results indicate the approximate dose of antibiotic carried to lower airway infection sites by droplets generated from the tested atomizer in the 1-minute dosing period, as predicted by the *in vitro* test setup, would be ineffective against established biofilms.

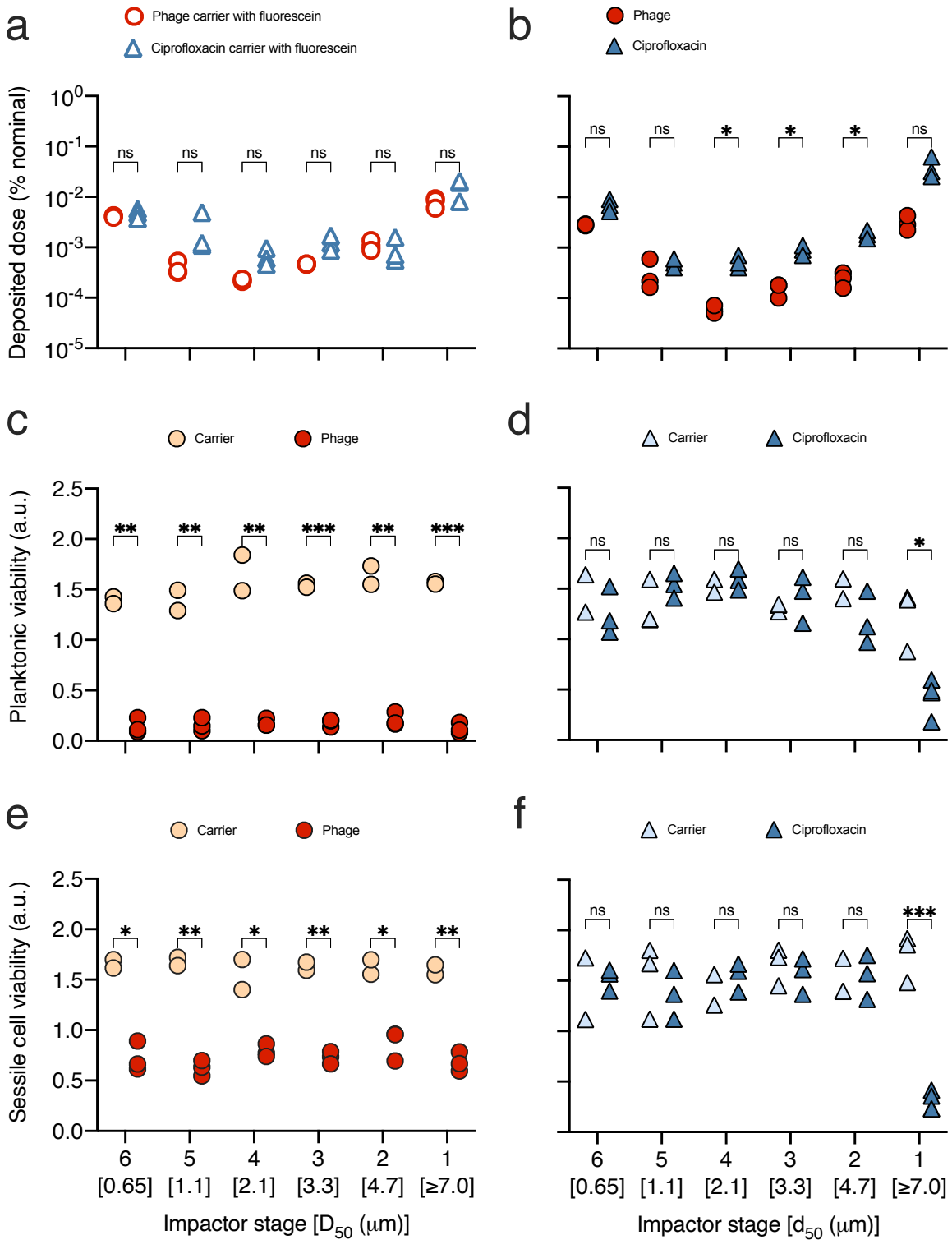

Figure 5. Dose distribution profiles and antibacterial efficacy of aerosol droplets. (a) Dose distribution profiles of phage- and ciprofloxacin-free carrier solutions containing 10 mg/mL of fluorescein were determined using the spectrofluorimetric method ($\lambda_{ex}/\lambda_{em}$ 490±5/515±5 nm). **(b)** Dose distribution profiles of phage and ciprofloxacin were determined using the plaque assay and

spectrofluorimetric method, respectively ($\lambda_{ex}/\lambda_{em}$ 270±5/445±5 nm). Viability of planktonic biofilm bacteria quantified 24 hours after exposure to size-fractioned droplets of **(c)** phage and phage-free carrier or **(d)** ciprofloxacin and ciprofloxacin-free carrier. Viability of sessile biofilm bacteria quantified 24 hours after exposure to size-fractioned droplets of **(e)** phage and phage-free carrier or **(f)** ciprofloxacin and ciprofloxacin-free carrier. Metabolic activity was measured using the XTT assay (λ_{abs} 490 nm), where high absorbance corresponds to high metabolic activity of viable cells. Multiple unpaired t-tests: ns indicates insignificant, *– $p<0.05$, **– $p\leq0.01$, and ***– $p\leq0.001$. Each symbol represents a technical replicate data point. Stages 1-6 cut-off values: ≥7, 4.7, 3.3, 2.1, 1.1, 0.65 μm.

6.4. CONCLUSIONS

We investigated the responses of both bacterial and airway epithelial cells to aerosolized phage and airflow exposure within a viable cascade impactor. Phage exposure had negligible effects on epithelial cell viability and barrier integrity. In contrast, we observed significant reductions in the metabolic activity and viability of *P. aeruginosa* biofilms following the phage challenge. Aerosolized treatments for lower respiratory tract infections should include fine droplets <5 μm in aerodynamic size that can effectively penetrate and deposit at distal sites within the lungs. We modelled different sites of infection within the airways using a six-stage viable cascade impactor fitted with transwell inserts containing *P. aeruginosa* biofilms. We then challenged these biofilms with size-fractioned aerosol droplets containing lytic phage or ciprofloxacin. Despite dose differences, a significant reduction in bacterial viability was noted 24 hours after the phage challenge. Conversely, only the highest dose of ciprofloxacin significantly reduced biofilm loads.

High-efficiency devices or longer dosing times may be required to deliver effective antibiotic doses to lower airway infection sites, increasing treatment duration and expense. Exposure to sub-inhibitory doses of antibiotics can increase the risk of AMR development. The on-site, self-amplifying nature of phages allows doses as small as a few hundred infectious virions to deplete biofilm bacterial loads. Aerosolized delivery of lytic phages can be a promising strategy for treating distal airway infections where minimum effective antibiotic concentration is difficult to achieve. The self-replicating ability of phages offers a clear advantage compared to dose-dependent antibiotics.

6.5. EXPERIMENTAL SECTION

6.5.1. Solution preparation

Tryptic soy broth (TSB) contains 30 g tryptic soy broth (BD B211825) in 1 L of deionized water. Tryptic soy agar (TSA) contains 30 g of tryptic soy broth (BD B211825) and 15 g of agar (Fisher BioReagents BP1423500) in 1 L of deionized water. The saline solution contains 9 g of sodium chloride (Fisher Chemicals S271500) in 1 L of deionized water. Phosphate buffered saline (PBS) solution contains one tablet (Fisher BioReagents BP2944100) in 200 mL of deionized water. Agar solution for transwell coating contains 15 g/L agar (Fisher BioReagents BP1423500) in ultrapure water. TSB, TSA, PBS, saline, and agar solutions were sterilized by autoclaving at 121°C for 20 minutes.

10 mg/mL ciprofloxacin solution contains 1 g of ciprofloxacin (Enzo Life Sciences ALX380287G025) in equal parts mix of 0.1 M HCL (LabChem LC152202) and ultrapure water. 7.5 mg/mL ciprofloxacin contains 0.25 mL of TSB and 0.75 mL of 10 mg/mL ciprofloxacin

solution. Phage and ciprofloxacin carrier media contain 25% and 75% v/v mix of TSB and ultrapure water, respectively. Ciprofloxacin carrier media was modified to a pH of 3.15 using 6N hydrochloric acid (VWR BDH7204-1) to match the pH of the ciprofloxacin solution. 10 mg/mL fluorescein-containing carrier solutions contain 10 mg of sodium fluorescein (Sigma-Aldrich F6377) in 10 mL of phage-free and ciprofloxacin-free carrier media.

The 1 mg/mL XTT solution contains 1 mg XTT (Sigma-Aldrich X4626) in 1 mL PBS solution. A 10 mM menadione solution contains 18 mg of menadione (Thermo Scientific AC127181000) in 10 mL of 100% acetone (VWR BDH1101). The XTT reaction solution is 79% v/v of TSB, 20% v/v of 1 mg/mL XTT solution in PBS and 1% v/v of 10 mM menadione in acetone. A 1 mg/mL fluorescein isothiocyanate dextran (FITC-dextran) solution contains 1 mg of 10 kDa FITC-dextran (Sigma 60842468) in 1 mL of complete cell culture medium. Ciprofloxacin, XTT, and FITC-dextran solutions were sterilized by passing through 0.22-um-pore-sized filters (Thermo Fisher Scientific 13100106) and stored protected from light. Aliquots of ciprofloxacin and XTT solutions are frozen (-20°C), FITC-dextran solution is refrigerated (4°C), and the menadione solution is at room temperature, all protected from light.

6.5.2. Experimental setup for the exposure of Calu-3 ALI cultures and PAO1 biofilms to airflow or 0.65-µm-sized phage-laden droplets

The aerosol platform (depicted in **Figure 1a**) reflects the specifications of the ASTM standard F2101-19.[13] An in-line humidifier delivers humidified air into the glass aerosol mixing chamber at a rate of 26.8 LPM. Compressed air is delivered via the atomizer into the glass aerosol mixing chamber at a rate of 1.5 LPM. A vacuum pump draws air through the system at 28.3 LPM. Airflow within the platform continues for two minutes before aerosol generation begins. Blaustein Atomizer single-jet module operated with the 10-40 expansion plate generates aerosol droplets for one minute. Phage suspension, with a concentration of 1×10^{11} PFU/mL, is delivered to the atomizer at a feed flow rate of 170 µL/min, controlled using a syringe pump. The 6-stage viable impactor size-fractions droplets into six size ranges. Glass Petri dishes with 27 mL of TSA were inserted beneath impactor stages 1 to 5. Three transwell inserts were positioned below the sixth impactor stage to collect size-fractioned aerosol droplets through impaction.

6.5.3. Experimental setup for the exposure of PAO1 biofilm cultures to size-fractioned phage-laden, phage-free-carrier-laden, ciprofloxacin-laden, and ciprofloxacin-free-carrier-laden droplets

In the platform configuration depicted in **Figure 4a,** aerosol droplets were generated using the single-jet Blaustein fitted with the 10-40 expansion plate and operated in atomizer mode (Similar to **Figure 1a**). Feed flow rate of 700 µL/min, compressed airflow rate of 1.5 L/min, and humidified airflow rate of 26.8 L/min remained constant across all trials. The placement of transwell inserts (foil-lined or biofilm-containing) within the impactor followed an odd-even arrangement with glass Petri dishes containing 27 mL of agar (**Figure 4d**) and remained constant across all trials.

6.5.4. *Pseudomonas aeruginosa* PAO1 biofilm cultures exposed to airflow or 0.65-µm-sized phage-laden droplets

Pseudomonas aeruginosa strain PAO1 (DSM 25641) was cultured for 18-24 hours in TSB at 37°C and 180 rotations per minute. 400 µL of 1.5% w/v agar was added to transwell inserts to solidify before bacterial addition. Transwells are seeded with 500 µL of bacteria, diluted in TSB,

to a concentration of 1×10^7 CFU/mL. The receiving wells had 1 mL of TSB to maintain the humidity. *P. aeruginosa* biofilms were cultured at 37°C and 120 rpm for 24 hours.

6.5.5. *Pseudomonas aeruginosa* PAO1 biofilm cultures exposed to size-fractioned phage-laden, phage-free-carrier-laden, ciprofloxacin-laden, and ciprofloxacin-free-carrier-laden droplets

P. aeruginosa strain PAO1 (DSM 25641) is cultured in TSB for 18 hours at 37°C under agitation (180 rotations per minute or rpm) and stored at 4ºC. Overnight bacterial culture was diluted 1:100 in fresh TSB. Transwell inserts (BRAND 782730) received 500 µL aliquots of bacterial suspension at a concentration of 5×10^7 CFU/mL. Transwells were placed into 12-well plates (VWR 10861-556) and incubated for 24 hours (37°C, 120 rpm). Spent media was removed (250 µL) from biofilms before aerosol exposure. Exposed biofilms received fresh media (250 µL) and returned to the incubator for 24 hours.

6.5.6. Calu-3 cell culture

Dr. Jeremy Hirota kindly provided Calu-3 cells (HTB-55). Cell culture medium contains 50 mL of heat-inactivated fetal bovine serum (Gibco A3840301), 10 mL of Penicillin-Streptomycin (Gibco 15630106), and 10 mL of HEPES buffer (Sigma 83264) adjusted to a pH of 7.4, and 500 mL of Alpha Minimum Essential Medium (Corning 10022CV). Passage 28-32 cells cultured in 75cm^2 flasks for 4-5 days until they reached 80% confluence at 37°C, 95% humidity, and 5% CO_2 (ThermoScientific Forma Series II Water-Jacketed CO2 Incubator 3110). The spent medium was removed from confluent flasks and washed twice with 10 mL of Dulbecco's phosphate-buffered saline or DPBS (Gibco 14190144). After the wash, the flask received 5 mL of 0.05% trypsin-EDTA solution (Gibco 25300054) and incubated for 10 minutes at 37°C, 95% humidity, and 5% CO_2.

500 µL of cell suspension with a concentration of 5×10^5 cells/mL was added to apical compartments of transwell inserts with an area of 1.38 cm^2 (BRAND 782730) with 1.8×10^5 cells/cm^2. Seeded transwells were placed into 12-well plates (VWR 10861556) and cultured for one week in a liquid-liquid interface until a confluent monolayer formation followed by two weeks of culturing under an air-liquid interface. Liquid-liquid interface cultures received 500 µL of apical and 1 mL of basolateral media, refreshed every 48 hours. Cultures were lifted into an air-liquid interface in the second week by removing 500 µL apical media and providing only 1 mL of basolateral media, refreshed every 48 hours. During the third week of culture, transwells were hooked and received 2 mL of fresh basolateral media, refreshed every 48 hours.

6.5.7. FITC-Dextran permeability assay

Empty and Calu-3-containing transwells received 500 µL of FITC-dextran. The receiving wells contained fresh culture medium (1 mL/well). The 12-well plates were incubated, protected from light, at 37°C for an hour. Following the incubation period, the solution from the receiving wells was added (200 µL/ well) to a black, flat-bottom 96-well microplate (Greiner Bio-One 655086). Fluorescence intensity was measured at $\lambda_{ex}/\lambda_{em}$ of 490±5 nm and 520±5 nm using a multi-plate reader (BioTek Synergy Neo2). Normalized values subtract the fluorescence due to the culture medium. Fluorescence readings from empty transwell samples were the greatest. The permeability values for the cell-containing well are a fraction of the leakage from the empty well.

6.5.8. Live-Dead staining of Calu-3 cells

Calu-3 cultures were stained using the ReadyProbes™ Cell Viability Imagining Kit (Invitrogen R37609). The staining solution contains 30 µL of DAPI, 30 µL of NucGreen™, and 200 µL of culture medium was added to transwells and incubated for 45 minutes at 37°C, 95% humidity, and 5% CO_2. The Nikon Eclipse Ti2 inverted microscope imaged the cells under the DAPI filter ($\lambda_{ex}/\lambda_{em}$ maxima of 360/460 nm) to visualize live cells and under the FITC filter ($\lambda_{ex}/\lambda_{em}$ maxima of 504/523 nm) to visualize cells with compromised plasma membranes.

6.5.9. Live-Dead staining of PAO1 cells

The staining solution contains 30 µL of Component A (1.67 mM Syto9/1.67mMPropidium iodide) in 10 mL of 0.9% w/v saline solution. Contents of *P. aeruginosa*-containing transwells were centrifuged (5752×g for 20 minutes). The pellet was resuspended in 10 mL of staining solution and incubated in the dark at room temperature for 15 minutes. After the incubation, the solution was centrifuged (5752×g for 20 minutes); the pellet was dispersed (1 mL of 0.9% w/v saline solution). 250 µL of dispersed bacteria were added to a black, clear-bottom 96-well microplate and spun down at 402×g for 20 minutes. A Nikon Eclipse Ti2 inverted microscope captured fluorescent-stained *P. aeruginosa* cells in wells.

6.5.10. Metabolic activity assay of biofilm bacteria (planktonic and sessile)

P. aeruginosa-containing transwells were transferred into 10 mL of 0.9% w/v saline solution and centrifuged at 5752×g for 20 minutes. The pellet was resuspended in 5 mL of XTT solution and incubated at 37°C at 180 RPM for an hour, protected from light. XTT solution consisted of 39.5 mL of TSB, 10 mL of 1% w/v XTT, and 500 µL of 10 mM menadione dissolved in 100% acetone. After incubation, the solution was vortexed, and 200 µL samples were added to a black, clear-bottom 96-well microplate for absorbance reading at 490 nm. The absorbance values of sample-containing wells incubated with the reaction solution minus the absorbance due to bacteria-free reaction solution give normalized values.

6.5.11. Metabolic activity assay of planktonic versus sessile biofilm bacteria

The metabolic activity of bacteria was quantitated 24 hours after exposure. Free-floating bacteria (planktonic) in the liquid portions were transferred into 10 mL of 0.9% (w/v) saline, vortexed to disperse the bacteria, and centrifuged at 7000×g for 20 minutes. The bacterial pellets were isolated by decanting the supernatant. The reaction solution (4 mL), added to planktonic and sessile bacterial fractions (adherent bacteria on the transwell membrane), was incubated at 37°C and 120 rpm for 1 hour. After the incubation, 200 µL of the samples were added to a 96-well microplate (Greiner Bio-One 655090) in triplicate and measured at λ_{abs} of 490 nm (Biotek Synergy Neo2). Absorbance values from sample incubation with the XTT reaction solution were normalized (deduction of the absorbance of the reaction solution alone).

6.5.12. Dose distribution profiles of phage-laden and ciprofloxacin-laden droplets

Transwell inserts, lined with foil substrates, were used to collect aerosol droplets of phage (**Tables S3, S4**), ciprofloxacin (**Tables S5, S6**) or inert carrier solutions (**Tables S7-S10**), deposited below each impactor stage. Nominal doses of the inert carrier-laden droplets represent the doses recovered following the atomization of phage-free and ciprofloxacin-free carrier solutions (containing 10 mg/mL of sodium fluorescein tracer) for 1 minute. Nominal doses of infectious phage-laden droplets represent the doses recovered following the atomization of phage suspension (1×10^9 PFU/mL) for two minutes. Nominal doses of ciprofloxacin-laden droplets represent the

doses recovered following the atomization of ciprofloxacin solution (7.5 mg/mL) for two minutes. The duration of atomization, extended from one to two and three minutes, improved the detection of phage-laden and ciprofloxacin-laden droplets without a fluorescent tracer. Foil substrates were removed from transwell inserts and placed into Eppendorf tubes containing 1 mL of ultrapure water (fluorescein or ciprofloxacin) or 1 mL of TSB (phage) and vortexed. Fluorescein wash samples were added to a black, 96-well microplate (Greiner Bio-One 655086) in triplicates (200 µL/well) and detected at a gain of 100 and $\lambda_{ex}/\lambda_{em}$ of 490±5/515±5 nm (Biotek Synergy Neo2). Detection of ciprofloxacin required $\lambda_{ex}/\lambda_{em}$ of 270±5/445±5 nm at a gain of 150.[14] Percent ciprofloxacin dose deposited into each transwell was calculated (**Table S4**). Phage wash samples were diluted (in TSB as needed) and plated on bacterial lawn plates (100 µL). Plaque counts were used to determine the nominal dose of infectious phage deposited into each transwell (**Table S6**).

6.5.13. Phage propagation and enumeration

Overnight cultures of P. aeruginosa were diluted 1:100 in fresh TSB and incubated for 4 hours at 37°C and 180 rpm. A single plaque of vB_Pae-Tbilisi32 (DSM 25635) was introduced to the subculture and incubated for 3 hours. The supernatant from the centrifuged crude lysate (20 minutes at 7000×g) is sterile-filtered. The concentration of the phage suspension was determined using a standard plaque assay method.[15]

6.5.14. Transmission electron microscopy (TEM)

Phage virion was imagined by adding a small volume of phage suspension with a concentration of 1×10^9 PFU/mL onto plasma-cleaned, carbon-coated copper grids, stained with 1% uranyl acetate, and imaged at 92000×magnification using Talos L120C electron microscope (**Figure 1d**). Phage virion was obtained by staining a phage stock sample with 1% uranyl acetate on a copper-coated formvar grid and imaged at 300000× magnification and under 80kV accelerating voltage (**Figure 4b**).

6.5.15. Scanning electron microscopy (SEM)

Bacteria grown on steel coupons were fixed in 30% glutaraldehyde for 30 minutes at 4°C. Samples were submerged in ethanol (10%, 30%, 50%, 70%, 90%, 100%) for 10 minutes each, and subjected to critical point drying. Samples were then coated with 20 nm of gold using a sputter coater. Images were obtained under 10kV beam voltage and 5000× magnification using a Tecan VEGA microscope (**Figure 1c**). Ciprofloxacin flakes on a copper-taped aluminium stub, gold sputter coated to 15 nm and imaged via scanning electron microscopy (**Figure 4c**).

6.5.16. Statistical analysis

Data analyses included one-way ANOVA followed by Tukey's post-hoc multiple comparisons test (Figure 2) and multiple unpaired t-tests (Figure 5) performed on GraphPad PRISM 9 software; a p-value ≤ 0.05 was considered statistically significant.

6.5.17. Data Availability

The data generated in this study are in the Source Data file, provided as online supplementary information.

6.6. REFERENCES

1. Murray CJ, Ikuta KS, Sharara F, et al. Global burden of bacterial antimicrobial resistance in 2019: a systematic analysis. *The Lancet*. 2022;399(10325). doi:10.1016/S0140-6736(21)02724-0
2. Boucher HW, Talbot GH, Bradley JS, et al. Bad bugs, no drugs: No ESKAPE! An update from the Infectious Diseases Society of America. *Clinical Infectious Diseases*. 2009;48(1). doi:10.1086/595011
3. Mulani MS, Kamble EE, Kumkar SN, Tawre MS, Pardesi KR. Emerging strategies to combat ESKAPE pathogens in the era of antimicrobial resistance: A review. *Front Microbiol*. 2019;10(APR). doi:10.3389/fmicb.2019.00539
4. Stewart PS, Costerton JW. Antibiotic resistance of bacteria in biofilms. *Lancet*. 2001;358(9276). doi:10.1016/S0140-6736(01)05321-1
5. Lyczak JB, Cannon CL, Pier GB. Lung infections associated with cystic fibrosis. *Clin Microbiol Rev*. 2002;15(2):194-222. doi:10.1128/CMR.15.2.194-222.2002
6. Hassett DJ, Korfhagen TR, Irvin RT, et al. Pseudomonas aeruginosa biofilm infections in cystic fibrosis: Insights into pathogenic processes and treatment strategies. *Expert Opin Ther Targets*. 2010;14(2). doi:10.1517/14728220903454988
7. Chan BK, Abedon ST, Loc-Carrillo C. Phage cocktails and the future of phage therapy. *Future Microbiol*. 2013;8(6):769-783. doi:10.2217/FMB.13.47/ASSET/IMAGES/LARGE/FIGURE2.JPEG
8. Morello E, Saussereau E, Maura D, Huerre M, Touqui L, Debarbieux L. Pulmonary bacteriophage therapy on pseudomonas aeruginosa cystic fibrosis strains: First steps towards treatment and prevention. *PLoS One*. 2011;6(2). doi:10.1371/journal.pone.0016963
9. Debarbieux L, Leduc D, Maura D, et al. Bacteriophages can treat and prevent pseudomonas aeruginosa lung infections. *Journal of Infectious Diseases*. 2010;201(7):1096-1104. doi:10.1086/651135
10. Alemayehu D, Casey PG, Mcauliffe O, et al. Bacteriophages φMR299-2 and φNH-4 can eliminate Pseudomonas aeruginosa in the murine lung and on cystic fibrosis lung airway cells. *mBio*. 2012;3(2). doi:10.1128/mBio.00029-12
11. Wang X, Xie Z, Zhao J, Zhu Z, Yang C, Liu Y. Prospects of Inhaled Phage Therapy for Combatting Pulmonary Infections. *Front Cell Infect Microbiol*. 2021;11. doi:10.3389/fcimb.2021.758392
12. Düzgüneş N, Sessevmez M, Yildirim M. Bacteriophage Therapy of Bacterial Infections: The Rediscovered Frontier. *Pharmaceuticals 2021, Vol 14, Page 34*. 2021;14(1):34. doi:10.3390/PH14010034
13. ASTM F2101. Standard Test Method for Evaluating the Bacterial Filtration Efficiency (BFE) of Medical Face Mask Materials , Using a Biological Aerosol of Staphylococcus aureus. *American Society for Testing and Materials*. 2019;i(February).
14. Navalón A, Ballesteros O, Blanc R, Vílchez JL. Determination of ciprofloxacin in human urine and serum samples by solid-phase spectrofluorimetry. *Talanta*. 2000;52(5):845-852. doi:10.1016/S0039-9140(00)00437-9
15. Ács N, Gambino M, Brøndsted L. Bacteriophage Enumeration and Detection Methods. *Front Microbiol*. 2020;11. doi:10.3389/fmicb.2020.594868
16. Ross DL, Riley CM. Aqueous solubilities of some variously substituted quinolone antimicrobials. *Int J Pharm*. 1990;63(3):237-250. doi:10.1016/0378-5173(90)90130-V

17. Leung SSY, Carrigy NB, Vehring R, et al. Jet nebulization of bacteriophages with different tail morphologies – Structural effects. *Int J Pharm*. 2019;554:322-326. doi:10.1016/J.IJPHARM.2018.11.026
18. Chang RYK, Chow MYT, Wang Y, et al. The effects of different doses of inhaled bacteriophage therapy for Pseudomonas aeruginosa pulmonary infections in mice. *Clin Microbiol Infect*. 2022;28(7):983-989. doi:10.1016/j.cmi.2022.01.006
19. Chang RYK, Das T, Manos J, Kutter E, Morales S, Chan HK. Bacteriophage PEV20 and Ciprofloxacin Combination Treatment Enhances Removal of Pseudomonas aeruginosa Biofilm Isolated from Cystic Fibrosis and Wound Patients. *AAPS Journal*. 2019;21(3). doi:10.1208/s12248-019-0315-0

6.7. SUPPORTING INFORMATION

SECTION S1: SPECTROPHOTOMETRIC DETECTION OF FITC-DEXTRAN

Table S1. Spectrophotometric detection of FITC-dextran in basolateral transwell compartments (leakage from apical compartments)

Date	Condition	$\lambda_{ex}/\lambda_{em}$, 490±20/520±20 nm		Avg	Percent
2022-06-28	**Empty**	**75514**	**75716**	**75615**	
	Unexposed	**632**	**1628**	**1130**	**1.494412**
	Airflow	1641	1646	1643.5	2.173511
	Phage	10170	10060	10115	13.37698
2022-07-02	Empty		77990		
	Unexposed		1764		2.261828
	Unexposed		1880		2.410565
	Airflow		1802		2.310553
	Airflow		2882		3.695346
	Phage		1849		2.370817
	Phage		2198		2.81831
2022-07-10	Empty		344290		
	Unexposed	2572	2506	2539	0.73746
	Unexposed	2300	1975	2137.5	0.620843
	Airflow	2593	2568	2580.5	0.749513
	Airflow	2372	1490	1931	0.560864
	Airflow	2518	1765	2141.5	0.622005
	Phage	6569	6497	6533	1.897528
	Phage	16	2310	1163	0.337797

Avg = average.

S1 - Sample calculation

$$Permeability\ (\%) = \frac{Empty_{\mathrm{Avg}}}{Unexposed_{\mathrm{Avg}}} \times 100\%$$
$$= \frac{[1130]}{[75615]} \times 100\%$$
$$= 1.49\%$$

SECTION S2: SPECTROPHOTOMETRIC DETECTION OF BACTERIAL METABOLIC ACTIVITY

Table S2. Spectrophotometric detection of metabolic activity of biofilm bacteria

Date	Condition	λ_{abs}, 490			Avg	Avg - BG
2022-06-24	**Unexposed**	**2.54**	**2.54**	**2.522**	**2.534**	**2.388333**
	Unexposed	2.472	2.453	2.579	2.501333	2.355667
	Airflow	2.544	2.558	2.579	2.560333	2.414667

	Phage	1.142	1.219	1.167	1.176	1.030333
	Phage	0.997	1.031	0.982	1.003333	0.857667
	Phage	1.376	1.447	1.39	1.404333	1.258667
2022-06-25	Airflow	2.577	2.711	2.689	2.659	2.473333
	Airflow	2.608	2.603	2.528	2.579667	2.394
	Airflow	2.592	2.672	2.636	2.633333	2.447666
	Phage	1.184	1.24	1.162	1.195333	1.009666
	Phage	1.405	1.379	1.437	1.407	1.221333
2022-07-08	Unexposed	2.733	2.663	2.716	2.704	2.558333
	Unexposed	2.433	2.47	2.429	2.444	2.298333
	Airflow	2.46	2.522	2.522	2.501333	2.355667
	Airflow	2.562	2.565	2.652	2.593	2.447333
	Phage	0.797	0.806	0.792	0.798333	0.652667
	Phage	1.229	1.217	1.191	1.212333	1.066667
2022-07-10	Unexposed	2.154	2.152	2.249	2.185	2.062333
	Unexposed	1.797	1.825	1.81	1.810667	1.688
	Airflow	1.621	1.627	1.638	1.628667	1.506
	Phage	1.716	1.755	1.762	1.744333	1.621667
	Phage	1.201	1.229	1.302	1.244	1.121333
	Phage	1.252	1.269	1.264	1.261667	1.139

Background (BG) = 0.1856667 [2022-06-24, 2022-06-25]; 0.145667 [2022-07-08]; 0.122666667 [2022-07-10]

S2 - Sample calculation

$$Metabolic\ activity\ (\lambda\text{abs}, 490) = [Unexposed_{\text{Avg}} - BG]$$
$$= 2.534 - 0.185667$$
$$= 2.388333$$

SECTION S3: SPECTROPHOTOMETRIC DETECTION OF PHAGE-FREE-CARRIER-LADEN DROPLETS WITH 10 MG/ML SODIUM FLUORESCEIN

Table S3. Spectrophotometric detection of dilutions of phage-free carrier (pH 7.4) containing 10 mg/mL sodium fluorescein

DF	$\lambda_{ex}/\lambda_{em}$, 490±5/515±5 nm	Signal x DF
-3	50218	50218000
-4	4367	43670000
-5	407	40700000
44862667		

Table S4. Spectrophotometric detection of fluorescein in wash samples recovered from transwells exposed to phage-free carrier droplets

Stage	$\lambda_{ex}/\lambda_{em}$, 490±5/515±5 nm			Avg	Percent
1	4044	4152	4162	4119.333	9.18E-3
	3795	3841	3844	3826.667	8.53E-3

	2755	2605	2649	2669.667	5.95E-3
2	466	470	473	469.6667	1.05E-3
	605	628	605	612.6667	1.37E-3
	404	382	391	392.3333	8.75E-4
3	209	190	217	205.3333	4.58E-4
	197	205	225	209	4.66E-4
	223	207	203	211	4.70E-4
4	102	99	96	99	2.21E-4
	93	98	92	94.33333	2.10E-4
	100	115	99	104.6667	2.33E-4
5	258	236	220	238	5.31E-4
	150	140	139	143	3.19E-4
	140	154	151	148.3333	3.31E-4
6	1992	1834	1799	1875	4.18E-3
	1941	1850	1909	1900	4.24E-3
	1767	1713	1827	1769	3.94E-3

S8 - Sample calculation

$$Phage - free\ carrier\ with\ fluorescein\ deposition\ \ (\lambda_{ex}/\lambda_{em}, 490 \pm 5/515 \pm 5\ \text{nm}) = \left[\frac{4116.33}{44862667}\right] \times 100\% = 0.009183\%$$

SECTION S4: SPECTROPHOTOMETRIC DETECTION OF CIRPOFLOXACIN-FREE-CARRIER-LADEN DROPLETS WITH 10 MG/ML SODIUM FLUORESCEIN

Table S5. Fluorescence signal of dilutions of ciprofloxacin-free carrier (pH 3.15) containing 10 mg/mL sodium fluorescein

DF	$\lambda_{ex}/\lambda_{em}$, 490±5/515±5 nm			Avg x DF
-3	34665	40736	42034	39145000
-4	6276	6136	3078	51633333
-5	283	274	289	28200000
39659444				

Table S6. Detection of fluorescein in wash samples recovered from transwells exposed to ciprofloxacin-free carrier droplets.

Stage	$\lambda_{ex}/\lambda_{em}$, 490±5/515±5 nm			Avg	Percent
1	2468	2415	4753	4119.333	8.06E-03
	6375	8280	8389	3826.667	1.93E-02
	8544	8548	7331	2669.667	2.04E-02
2	212	225	219	469.6667	5.49E-04
	284	275	277	612.6667	6.99E-04
	622	592	636	392.3333	1.55E-03
3	445	452	545	205.3333	1.21E-03

	651	685	687	209	1.69E-03
	338	350	343	211	8.62E-04
4	360	408	365	99	9.47E-04
	293	213	207	94.33333	5.96E-04
	170	184	189	104.6667	4.54E-04
5	1855	1927	2062	238	4.89E-03
	534	401	378	143	1.10E-03
	477	471	491	148.3333	1.20E-03
6	2212	2441	2143	1875	5.68E-03
	2132	1817	1728	1900	4.75E-03
	1483	1438	1457	1769	3.66E-03

SECTION S5: PLAQUE-ASSAY DETECTION OF THE PHAGE-LADEN DROPLETS

Table S7. Phage feed concentrations

Concentration (PFU/mL)	Volume atomized (mL)	Duration (min)	PFU
7×10^8	0.7	1	4.9×10^8
1×10^9	**0.7**	**2**	**1.4×10^9**

Table S8. Plaque-forming units (PFUs) detected in wash samples recovered from transwells exposed to aerosol droplets generated from 1×10^9 PFU/mL phage suspension for two minutes

Stage	PFUs	DF	mL	PFU/mL	Fraction	Percent	PFU
1	**40**	**E2**	**E-1**	**4E4**	**2.86E-5**	**2.86E-3**	**14000**
	31	E2	E-1	3.1E4	2.21E-5	2.21E-3	10850
	60	E2	E-1	6E4	4.29E-5	4.29E-3	21000
2	44	E1	E-1	4.4E3	3.14E-6	3.14E-4	1540
	35	E1	E-1	3.5E3	2.50E-6	2.50E-4	1225
	22	E1	E-1	2.2E3	1.57E-6	1.57E-4	770
3	25	E1	E-1	2.5E3	1.79E-6	1.79E-4	875
	14	E1	E-1	1.4E3	1.00E-6	1.00E-4	490
	25	E1	E-1	2.5E3	1.79E-6	1.79E-4	875
4	8	E1	E-1	8E2	5.71E-7	5.71E-5	280
	7	E1	E-1	7E2	5.00E-7	5.00E-5	245
	10	E1	E-1	1E3	7.14E-7	7.14E-5	350
5	30	E1	E-1	3E3	2.14E-6	2.14E-4	1050
	83	E1	E-1	8.3E3	5.93E-6	5.93E-4	2905
	23	E1	E-1	2.3E3	1.64E-6	1.64E-4	805
6	38	E2	E-1	3.8E4	2.71E-5	2.71E-3	13300
	40	E2	E-1	4E4	2.93E-5	2.93E-3	14350
	41	E2	E-1	4.1E4	2.86E-5	2.86E-3	14000

S6 - Sample calculation

$$Percent\ aerosolized\ phage\ deposition\ over\ two\ minutes\ (\%) = \left[\frac{4 \times 10^4 \frac{PFU}{mL}}{1.4 \times 10^9 \frac{PFU}{mL}}\right] \times 100\% = 0.00286\%$$

$$Phage\ deposition\ over\ one\ minute\ (PFU) = 0.0000286\ \times 4.9 \times 10^8\ PFU = 14000\ \text{PFU}$$

SECTION S6: SPECTROPHOTOMETRIC DETECTION OF CIPROFLOXACIN-LADEN DROPLETS

Table S9. Ciprofloxacin fluorescence signal intensity

DF	$\lambda_{ex}/\lambda_{em}$, 270±5/445±5 nm				MeanxDF
-3	5941	5315	5046	5362	5628000
-4	438	639	541	620	5385000
5506500					

Table S10. Spectrophotometric detection of ciprofloxacin recovered from transwells exposed to aerosol droplets of 7.5 mg/mL ciprofloxacin solution for three minutes

Stage	$\lambda_{ex}/\lambda_{em}$, 270±5/445±5 nm			Avg	Avg/3	Percent
1	**5327**	**5849**	**4952**	**5376**	**1792**	**0.0325**
	10806	9652	10781	10413	3471	0.0630
	4154	4502	4060	4239	1413	0.0257
2	268	266	366	300	100	0.0018
	370	305	410	362	121	0.0022
	195	308	257	253	84	0.0015
3	201	126	125	151	50	0.0009
	206	145	176	176	59	0.0011
	92	132	146	123	41	0.0007
4	108	95	146	116	39	0.0007
	83	66	54	68	23	0.0004
	47	108	86	80	27	0.0005
5	37	129	100	89	30	0.0005
	85	96	37	73	24	0.0004
	67	144	85	99	33	0.0006
6	1634	1645	1208	1496	499	0.0091
	1134	1102	1180	1139	380	0.0069
	828	865	885	859	286	0.0052

S4 - Sample calculation

$$Ciprofloxacin\ dose\ deposition\ per\ minute\ (\lambda_{ex}/\lambda_{em}, 270 \pm 5/445 \pm 5\ \text{nm}) = \left[\frac{1792}{5506500}\right] \times 100\% = 0.0325\%$$

SECTION S7: SPECTROPHOTOMETRIC DETECTION OF METABOLIC ACTIVITY OF PLANKTONIC CELLS POST-EXPOSURE TO PHAGE-LADEN DROPLETS

Table S11. Dataset 1 - Metabolic activity of planktonic cells 24 hours post-exposure to phage-laden droplets

Stage	λ_{abs}, 490			Avg	Avg - BG	
1	0.415	0.424	0.426	0.421667	0.069167	
	0.445	0.443	0.444	0.444	0.0915	
	0.429	0.439	0.44	0.436	0.0835	0.081389
2	0.527	0.543	0.543	0.537667	0.185167	
	0.424	0.434	0.432	0.43	0.0775	
	0.585	0.591	0.588	0.588	0.2355	0.166056
3	0.381	0.395	0.397	0.391	0.105333	
	0.406	0.419	0.413	0.412667	0.127	
	0.471	0.467	0.456	0.464667	0.179	0.137111
4	0.526	0.537	0.543	0.535333	0.182833	
	0.556	0.572	0.571	0.566333	0.213833	
	0.416	0.43	0.425	0.423667	0.071167	0.155944
5	0.368	0.378	0.384	0.376667	0.091	
	0.408	0.411	0.418	0.412333	0.126666	
	0.363	0.367	0.369	0.366333	0.080666	0.099444
6	0.416	0.429	0.43	0.425	0.0725	
	0.437	0.446	0.444	0.442333	0.089833	
	0.449	0.464	0.458	0.457	0.1045	0.088944

Background (BG) = 0.2856667 [Stages 3, 5]; 0.3525 [Stages 1,2,4,6]

Table S12. Dataset 2 - Metabolic activity of planktonic cells 24 hours post-exposure to phage-laden droplets

Stage	λ_{abs}, 490			Avg	Avg - BG	
1	0.408	0.399	0.403	0.403333	0.190133	
	0.466	0.461	0.455	0.460667	0.247467	
	0.328	0.32	0.316	0.321333	0.108133	0.181911
2	0.432	0.44	0.438	0.436667	0.223467	
	0.451	0.456	0.456	0.454333	0.241133	
	0.601	0.607	0.613	0.607	0.3938	0.286133
3	0.409	0.414	0.411	0.411333	0.198133	
	0.411	0.415	0.409	0.411667	0.198467	
	0.411	0.411	0.41	0.410667	0.197467	0.198022
4	0.328	0.334	0.332	0.331333	0.118133	

	0.408	0.414	0.409	0.410333	0.197133	
	0.561	0.568	0.569	0.566	0.3528	0.222689
5	0.332	0.338	0.343	0.337667	0.124467	
	0.37	0.368	0.373	0.370333	0.157133	
	0.371	0.379	0.372	0.374	0.1608	0.147467
6	0.433	0.439	0.442	0.438	0.2248	
	0.405	0.409	0.409	0.407667	0.194467	
	0.486	0.482	0.485	0.484333	0.271133	0.230133

Background (BG) = 0.2132 [Stages 1-6]

Table S13. Dataset 3 - Metabolic activity of planktonic cells 24 hours post-exposure to phage-laden droplets

Stage	λ_{abs}, 490			Avg	Avg - BG	
1	0.242	0.245	0.247	0.244667	0.090667	
	0.269	0.277	0.276	0.274	0.12	
	0.26	0.264	0.267	0.263667	0.109667	0.106778
2	0.37	0.376	0.372	0.372667	0.218667	
	0.313	0.32	0.324	0.319	0.165	
	0.298	0.304	0.302	0.301333	0.147333	0.177
3	0.258	0.263	0.265	0.262	0.108	
	0.554	0.568	0.569	0.563667	0.409667	
	0.245	0.25	0.249	0.248	0.094	0.203889
4	0.307	0.302	0.303	0.304	0.15	
	0.351	0.357	0.359	0.355667	0.201667	
	0.27	0.275	0.274	0.273	0.119	0.156889
5	0.365	0.37	0.371	0.368667	0.214667	
	0.39	0.399	0.401	0.396667	0.242667	
	0.382	0.386	0.39	0.386	0.232	0.229778
6	0.26	0.267	0.268	0.265	0.111	
	0.3	0.306	0.303	0.303	0.149	
	0.224	0.229	0.227	0.226667	0.072667	0.110889

Background (BG) = 0.154 [Stages 1-6]

SECTION S8: SPECTROPHOTOMETRIC DETECTION OF METABOLIC ACTIVITY OF PLANKTONIC CELLS POST-EXPOSURE TO PHAGE-FREE-CARRIER-LADEN DROPLETS

Table S14. Dataset 1 - Metabolic activity of planktonic cells 24 hours post-exposure to phage-free-carrier-laden droplets

Stage	λ_{abs}, 490			Avg	Avg - BG	
1	1.846	1.871	1.815	1.844	1.59778	
	1.758	1.747	1.786	1.763667	1.517447	
	1.788	1.783	1.797	1.789333	1.543113	1.55278
2	2.041	2.093	2.149	2.094333	1.7825	

	1.864	1.876	1.907	1.882333	1.5705	
	2.107	2.206	2.162	2.158333	1.8465	1.733167
3	1.758	1.782	1.771	1.770333	1.524113	
	1.754	1.738	1.77	1.754	1.50778	
	1.738	1.768	1.835	1.780333	1.534113	1.522002
4	2.157	2.211	2.123	2.163667	1.851834	
	2.148	2.15	2.142	2.146667	1.834834	
	2.147	2.156	2.145	2.149333	1.8375	1.841389
5	1.694	1.718	1.729	1.713667	1.467447	
	1.862	1.872	1.89	1.874667	1.628447	
	1.624	1.632	1.63	1.628667	1.382447	1.49278
6	1.371	1.429	1.463	1.421	1.109167	
	1.68	1.74	1.694	1.704667	1.392834	
	2.088	2.085	2.098	2.090333	1.7785	1.426834

Background (BG) = 0.246222 [Stages 1,3,5]; 0.3118333 [Stages 2,4,6]

Table S15. Dataset 2 - Metabolic activity of planktonic cells 24 hours post-exposure to phage-free-carrier-laden droplets

Stage	λ_{abs}, 490			Avg	Avg - BG	
1	1.802	1.787	1.74	1.776333	1.572583	
	1.748	1.792	1.797	1.779	1.57525	
	1.726	1.824	1.83	1.793333	1.589583	1.579139
2	1.794	1.795	1.806	1.798333	1.594583	
	1.779	1.778	1.791	1.782667	1.578917	
	1.676	1.672	1.693	1.680333	1.476583	1.550028
3	1.751	1.774	1.779	1.768	1.56425	
	1.756	1.766	1.778	1.766667	1.562917	
	1.78	1.765	1.743	1.762667	1.558917	1.562028
4	1.804	1.729	1.745	1.759333	1.555583	
	1.509	1.562	1.55	1.540333	1.336583	
	1.786	1.776	1.768	1.776667	1.572917	1.488361
5	1.663	1.65	1.678	1.663667	1.459917	
	1.229	1.241	1.28	1.25	1.04625	
	1.586	1.559	1.566	1.570333	1.366583	1.290917
6	1.343	1.385	1.402	1.376667	1.172917	
	1.672	1.68	1.691	1.681	1.47725	
	1.632	1.652	1.614	1.632667	1.428917	1.359694

Background (BG) = 0.20375 [Stages 1-6]

SECTION S9: SPECTROPHOTOMETRIC DETECTION OF THE METABOLIC ACTIVITY OF SESSILE CELLS POST-EXPOSURE TO PHAGE-LADEN DROPLETS

Table S16. Dataset 1 - Metabolic activity of sessile cells 24 hours post-exposure to phage-laden droplets

Stage	λ_{abs}, 490			Avg	Avg - BG	
1	1.02	1.006	1.01	1.012	0.57175	
	1.023	1.05	1.043	1.038667	0.598417	
	1.051	1.061	1.058	1.056667	0.616417	0.595528
2	1.252	1.269	1.292	1.271	0.83075	
	0.975	0.971	0.971	0.972333	0.532083	
	1.149	1.159	1.172	1.16	0.71975	0.694194
3	0.916	0.962	0.953	0.943667	0.658	
	1.13	1.159	1.153	1.147333	0.861666	
	1.009	1.006	1.012	1.009	0.723333	0.747666
4	1.202	1.225	1.244	1.223667	0.783417	
	1.192	1.065	1.07	1.109	0.66875	
	1.328	1.293	1.293	1.304667	0.864417	0.772194
5	0.74	0.75	0.753	0.747667	0.462	
	0.963	0.96	0.967	0.963333	0.677666	
	0.81	0.821	0.827	0.819333	0.533666	0.557777
6	0.957	0.972	0.977	0.968667	0.528417	
	1.082	1.059	1.061	1.067333	0.627083	
	1.143	1.137	1.102	1.127333	0.687083	0.614194

Background (BG) = 0.44025 [Stages 1,2,4,6]; 0.2976667 [Stages 3,5]

Table S17. Dataset 2 - Metabolic activity of sessile cells 24 hours post-exposure to phage-laden droplets

Stage	λ_{abs}, 490			Avg	Avg - BG	
1	1.209	1.2	1.263	1.224	1.006	
	0.792	0.793	0.789	0.791333	0.573333	
	0.986	0.986	0.997	0.989667	0.771667	0.783667
2	1.312	1.344	1.334	1.33	1.112	
	1.009	0.994	0.989	0.997333	0.779333	
	1.188	1.203	1.222	1.204333	0.986333	0.959222
3	1.039	1.028	1.094	1.053667	0.835667	
	0.949	0.948	0.949	0.948667	0.730667	
	1.009	1.036	0.996	1.013667	0.795667	0.787333
4	0.886	0.887	0.902	0.891667	0.673667	
	1.24	1.247	1.244	1.243667	1.025667	
	1.109	1.113	1.109	1.110333	0.892333	0.863889
5	0.714	0.71	0.718	0.714	0.496	
	0.9	0.903	0.911	0.904667	0.686667	
	0.946	0.932	0.932	0.936667	0.718667	0.633778
6	1.302	1.314	1.328	1.314667	1.096667	
	0.954	0.944	0.954	0.950667	0.732667	
	1.071	1.056	1.064	1.063667	0.845667	0.891667

Background (BG) = 0.218 [Stages 1-6]

Table S18. Dataset 3 - Metabolic activity of sessile cells 24 hours post-exposure to phage-laden droplets

Stage	λ_{abs}, 490			Avg	Avg - BG	
1	0.767	0.777	0.777	0.773667	0.616667	
	0.82	0.822	0.825	0.822333	0.665333	
	0.872	0.877	0.883	0.877333	0.720333	0.667444
2	1.068	1.071	1.053	1.064	0.907	
	1.158	1.154	1.168	1.16	1.003	
	1.095	1.118	1.126	1.113	0.956	0.955333
3	0.98	0.998	0.988	0.988667	0.831667	
	0.549	0.555	0.556	0.553333	0.396333	
	0.931	0.92	0.925	0.925333	0.768333	0.665444
4	1.096	1.111	1.086	1.097667	0.934067	
	0.688	0.679	0.676	0.681	0.5174	
	0.902	0.942	0.947	0.930333	0.766733	0.7394
5	0.948	0.963	0.963	0.958	0.7944	
	0.759	0.781	0.763	0.767667	0.604067	
	0.862	0.861	0.859	0.860667	0.697067	0.698511
6	0.688	0.703	0.686	0.692333	0.528733	
	0.782	0.791	0.787	0.786667	0.623067	
	1.015	0.982	1.008	1.001667	0.838067	0.663289

Background (BG) = 0.157 [Stages 1-3]; 0.1636 [Stages 4-6]

SECTION S10: SPECTROPHOTOMETRIC DETECTION OF THE METABOLIC ACTIVITY OF SESSILE CELLS POST-EXPOSURE TO PHAGE-FREE-CARRIER-LADEN DROPLETS

Table S19. Dataset 1 - Metabolic activity of sessile cells 24 hours post-exposure to phage-free-carrier-laden droplets

Stage	λ_{abs}, 490			Avg	Avg - BG	
1	1.873	1.903	1.828	1.868	1.662667	
	1.817	1.854	1.841	1.837333	1.632	1.647334
	1.816	1.845	1.936	1.865667	1.553834	
2	1.98	2.003	1.987	1.99	1.678167	
	1.735	1.765	1.724	1.741333	1.4295	1.553834
	1.856	1.971	1.891	1.906	1.700667	
3	1.788	1.789	1.82	1.799	1.593667	
	1.871	1.899	1.923	1.897667	1.692334	1.662223
	1.574	1.56	1.603	1.579	1.267166	
4	1.728	1.744	1.734	1.735333	1.423499	
	1.841	1.849	1.782	1.824	1.512166	1.400944
	1.824	1.871	1.89	1.861667	1.656334	
5	1.813	1.835	1.839	1.829	1.623667	
	1.859	1.85	1.821	1.843333	1.638	1.639334

	2.43	2.122	2.143	2.231667	1.919834	
6	1.962	1.979	1.951	1.964	1.652167	
	1.868	1.791	1.854	1.837667	1.525834	1.699278

Background (BG) = 0.2053333[Stages 1,3,5]; 0.3118333 [Stages 2,4,6]

Table S20. Dataset 2 - Metabolic activity of sessile cells 24 hours post-exposure to phage-free-carrier-laden droplets

Stage	λ_{abs}, 490			Avg	Avg - BG	
1	1.693	1.862	1.841	1.798667	1.546778	
	1.796	1.808	1.808	1.804	1.552111	
	1.812	1.774	1.811	1.799	1.547111	1.548667
2	2.034	2.029	1.928	1.997	1.745111	
	1.939	1.969	1.745	1.884333	1.632444	
	2.025	1.973	1.897	1.965	1.713111	1.696889
3	1.806	1.834	1.875	1.838333	1.586444	
	1.768	1.899	1.824	1.830333	1.578444	
	1.786	1.902	1.909	1.865667	1.613778	1.592889
4	1.927	1.924	1.928	1.926333	1.674444	
	2.243	1.929	1.902	2.024667	1.772778	
	1.93	1.914	1.871	1.905	1.653111	1.700111
5	1.985	2.026	2.021	2.010667	1.758778	
	1.982	2.023	1.958	1.987667	1.735778	
	1.915	1.94	1.906	1.920333	1.668444	1.721
6	1.877	1.871	1.954	1.900667	1.648778	
	1.836	1.835	1.847	1.839333	1.587444	
	1.816	1.876	1.887	1.859667	1.607778	1.614667

Background (BG) = 0.2518889[Stages 1-6]

SECTION S11: SPECTROPHOTOMETRIC DETECTION OF THE METABOLIC ACTIVITY OF PLANKTONIC CELLS POST-EXPOSURE TO CIPROFLOXACIN-LADEN DROPLETS

Table S21. Dataset 1 - Metabolic activity of planktonic cells 24 hours post-exposure to ciprofloxacin-laden droplets

Stage	λ_{abs}, 490			Avg	Avg - BG	
1	0.764	0.782	0.779	0.775	0.542667	
	0.691	0.702	0.7	0.697667	0.465334	
	0.624	0.644	0.64	0.636	0.403667	0.470556
2	1.161	1.189	1.19	1.18	0.947667	
	1.469	1.496	1.472	1.479	1.246667	
	1.418	1.418	1.397	1.411	1.178667	1.124334
4	1.77	1.805	1.831	1.802	1.569667	
	1.878	1.882	1.89	1.883333	1.651	

	1.736	1.783	1.767	1.762	1.529667	1.583445
6	1.017	1.048	1.046	1.037	0.804667	
	1.458	1.446	1.445	1.449667	1.217334	
	1.394	1.438	1.424	1.418667	1.186334	1.069445

Background (BG) = 0.2323333[Stages 1,2,4,6]

Table S22. Dataset 2 - Metabolic activity of planktonic cells 24 hours post-exposure to ciprofloxacin-laden droplets

Stage	λ_{abs}, 490			Avg	Avg - BG	
1	1.031	1.095	1.113	1.079667	0.833445	
	0.527	0.552	0.538	0.539	0.292778	
	0.582	0.598	0.599	0.593	0.346778	0.491
3	0.924	0.97	0.972	0.955333	0.709111	
	1.502	1.568	1.546	1.538667	1.292445	
	1.711	1.738	1.709	1.719333	1.473111	1.158222
5	1.694	1.749	1.706	1.716333	1.470111	
	1.48	1.526	1.481	1.495667	1.249445	
	1.728	1.75	1.767	1.748333	1.502111	1.407222

Background (BG) = 0.2462222[Stages 1,3,5]

Table S23. Dataset 3 - Metabolic activity of planktonic cells 24 hours post-exposure to ciprofloxacin-laden droplets

Stage	λ_{abs}, 490			Avg	Avg - BG	
1	0.594	0.608	0.613	0.605	0.319	
	0.946	0.984	0.987	0.972333	0.686333	
	1.027	1.08	1.105	1.070667	0.784667	0.596667
2	1.766	1.798	1.789	1.784333	1.498333	
	1.682	1.747	1.758	1.729	1.443	
	1.729	1.781	1.814	1.774667	1.488667	1.476667
3	1.715	1.756	1.763	1.744667	1.458667	
	1.713	1.77	1.763	1.748667	1.462667	
	1.741	1.793	1.848	1.794	1.508	1.476444
4	1.718	1.762	1.74	1.74	1.454	
	1.803	1.822	1.818	1.814333	1.528333	
	1.73	1.769	1.805	1.768	1.482	1.488111
5	1.793	1.836	1.857	1.828667	1.542667	
	1.777	1.813	1.831	1.807	1.521	
	1.805	1.859	1.885	1.849667	1.563667	1.542444
6	1.782	1.819	1.809	1.803333	1.517333	
	1.747	1.775	1.801	1.774333	1.488333	
	1.82	1.854	1.86	1.844667	1.558667	1.521444

Background (BG) = 0.286[Stages 1-6]

Table S24. Dataset 4 - Metabolic activity of planktonic cells 24 hours post-exposure to ciprofloxacin-laden droplets

Stage	λ_{abs}, 490			Avg	Avg - BG	
1	0.149	0.151	0.153	0.151	0.013	
	0.642	0.658	0.649	0.649667	0.511667	
	0.154	0.156	0.155	0.155	0.017	0.180556
2	0.672	0.689	0.692	0.684333	0.546333	
	0.819	0.834	0.838	0.830333	0.692333	
	1.784	1.821	1.815	1.806667	1.668667	0.969111
3	1.641	1.682	1.679	1.667333	1.529333	
	1.797	1.825	1.833	1.818333	1.680333	
	1.737	1.783	1.785	1.768333	1.630333	1.613333
4	1.832	1.864	1.85	1.848667	1.710667	
	1.795	1.837	1.824	1.818667	1.680667	
	1.817	1.853		1.835	1.697	1.696111
5	1.819	1.829	1.818	1.822	1.684	
	1.718	1.752	1.745	1.738333	1.600333	
	1.797	1.824		1.8105	1.6725	1.652278
6	0.383	0.392	0.393	0.389333	0.251333	
	1.782	1.825	1.817	1.808	1.67	
	1.754	1.773		1.7635	1.6255	1.182278

Background (BG) = 0.138[Stages 1-6]

SECTION S12: SPECTROPHOTOMETRIC DETECTION OF THE METABOLIC ACTIVITY OF PLANKTONIC CELLS POST-EXPOSURE TO CIPROFLOXACIN-FREE-CARRIER-LADEN DROPLETS

Table S25. Dataset 1 - Metabolic activity of planktonic cells 24 hours post-exposure to ciprofloxacin-free-carrier-laden droplets

Stage	λ_{abs}, 490			Avg	Avg - BG	
1	1.846	1.862	1.863	1.857	1.652	
	1.486	1.548	1.525	1.519667	1.314667	
	1.462	1.483	1.484	1.476333	1.271333	1.412667
3	1.44	1.47	1.478	1.462667	1.257667	
	1.526	1.587	1.572	1.561667	1.356667	
	1.556	1.65	1.617	1.607667	1.402667	1.339
5	1.184	1.183	1.19	1.185667	0.980667	
	1.487	1.528	1.542	1.519	1.314	
	1.483	1.521	1.476	1.493333	1.288333	1.194333

Background (BG) = 0.205[Stages 1,3,5]

Table S26. Dataset 2 - Metabolic activity of planktonic cells 24 hours post-exposure to ciprofloxacin-free-carrier-laden droplets

Stage	λ_{abs}, 490	Avg	Avg - BG	

1	1.12	1.126	1.126	1.124	0.866889	
	1.162	1.195	1.159	1.172	0.914889	
	1.079	1.134	1.113	1.108667	0.851556	0.877778
2	1.801	1.832	1.836	1.823	1.565889	
	1.826	1.874	1.887	1.862333	1.605222	
	1.852	1.915	1.873	1.88	1.622889	1.598
3	1.623	1.642	1.648	1.637667	1.380556	
	1.328	1.353	1.343	1.341333	1.084222	
	1.601	1.622	1.612	1.611667	1.354556	1.273111
4	1.8	1.797	1.823	1.806667	1.549556	
	1.856	1.864	1.838	1.852667	1.595556	
	1.868	1.91	1.891	1.889667	1.632556	1.592556
5	1.928	1.932	1.94	1.933333	1.676222	
	1.776	1.797	1.796	1.789667	1.532556	
	1.804	1.826	1.847	1.825667	1.568556	1.592444
6	1.82	1.843	1.833	1.832	1.574889	
	1.916	1.96	1.942	1.939333	1.682222	
	1.879	1.99	1.879	1.916	1.658889	1.638667

Background (BG) = 0.2571111[Stages 1-6]

Table S27. Dataset 3 - Metabolic activity of planktonic cells 24 hours post-exposure to ciprofloxacin-free-carrier-laden droplets

Stage	λ_{abs}, 490			Avg	Avg - BG	
1	1.678	1.688	1.683	1.683	1.414833	
	1.638	1.618	1.593	1.616333	1.348167	
	1.665	1.663	1.706	1.678	1.409833	1.390944
2	1.683	1.647	1.656	1.662	1.393833	
	1.653	1.637	1.738	1.676	1.407833	
	1.622	1.673	1.728	1.674333	1.406167	1.402611
3	1.656	1.667	1.665	1.662667	1.3945	
	1.651	1.628	1.646	1.641667	1.3735	
	1.532	1.557	1.514	1.534333	1.266167	1.344722
4	1.756	1.979	1.989	1.908	1.639833	
	1.675	1.605	1.629	1.636333	1.368167	
	1.632	1.665	1.679	1.658667	1.3905	1.466167
5	1.681	1.717	1.696	1.698	1.429833	
	1.495	1.503	1.513	1.503667	1.2355	
	1.205	1.192	1.212	1.203	0.934833	1.200056
6	1.567	1.595	1.599	1.587	1.318833	
	1.57	1.664	1.577	1.603667	1.3355	
	1.41	1.429	1.425	1.421333	1.153167	1.269167

Background (BG) = 0.2681667[Stages 1-6]

SECTION S13: SPECTROPHOTOMETRIC DETECTION OF THE METABOLIC ACTIVITY OF SESSILE CELLS POST-EXPOSURE TO CIPROFLOXACIN-LADEN DROPLETS

Table S28. Dataset 1 - Metabolic activity of sessile cells 24 hours post-exposure to ciprofloxacin-laden droplets

Stage	λ_{abs}, 490			Avg	Avg - BG	
1	0.677	0.681	0.686	0.681333	0.420333	
	0.649	0.653	0.652	0.651333	0.390333	
	0.694	0.697	0.696	0.695667	0.434667	0.415111
2	1.794	1.816	1.837	1.815667	1.554667	
	1.776	1.84	1.829	1.815	1.554	
	1.848	1.855	1.89	1.864333	1.603333	1.570667
4	1.828	1.898	1.844	1.856667	1.595667	
	1.834	1.82	1.841	1.831667	1.570667	
	1.86	1.864	1.912	1.878667	1.617667	1.594667
6	1.808	1.824	1.837	1.823	1.562	
	1.834	1.847	1.835	1.838667	1.577667	
	1.824	1.826	1.822	1.824	1.563	1.567556

Background (BG) = 0.261[Stages 1,2,4,6]

Table S29. Dataset 2 - Metabolic activity of sessile cells 24 hours post-exposure to ciprofloxacin-laden droplets

Stage	λ_{abs}, 490			Avg	Avg - BG	
1	0.562	0.611	0.564	0.579	0.373667	
	0.556	0.533	0.543	0.544	0.338667	0.356167
3	1.875	1.85	1.852	1.859	1.653667	
	1.774	1.806	1.73	1.77	1.564667	
	1.835	1.81	1.815	1.82	1.614667	1.611
5	1.807	1.853	1.821	1.827	1.621667	
	1.767	1.806	1.814	1.795667	1.590334	
	1.783	1.763	1.838	1.794667	1.589334	1.600445

Background (BG) = 0.2053333[Stages 1,3,5]

Table S30. Dataset 3 - Metabolic activity of sessile cells 24 hours post-exposure to ciprofloxacin-laden droplets

Stage	λ_{abs}, 490			Avg	Avg - BG	
1	0.513	0.524	0.533	0.523333	0.256333	
	0.438	0.42	0.418	0.425333	0.158333	
	0.551	0.558	0.562	0.557	0.29	0.234889
2	1.601	1.587	1.636	1.608	1.341	
	1.555	1.55	1.573	1.559333	1.292333	
	1.573	1.585	1.576	1.578	1.311	1.314778
3	1.58	1.582	1.625	1.595667	1.328667	

	1.722	1.736	1.71	1.722667	1.455667	
	1.515	1.57	1.649	1.578	1.311	1.365111
4	1.844	1.858	1.827	1.843	1.576	
	1.611	1.629	1.641	1.627	1.36	
	1.489	1.492	1.514	1.498333	1.231333	1.389111
5	1.543	1.53	1.501	1.524667	1.257667	
	1.486	1.516	1.532	1.511333	1.244333	
	1.124	1.116	1.122	1.120667	0.853667	1.118556
6	1.669	1.727	1.698	1.698	1.431	
	1.56	1.541	1.593	1.564667	1.297667	
	1.719	1.74	1.742	1.733667	1.466667	1.398444

Background (BG) = 0.267[Stages 1-6]

Table S31. Dataset 4 - Metabolic activity of sessile cells 24 hours post-exposure to ciprofloxacin-laden droplets

Stage	λ_{abs}, 490			Avg	Avg - BG	
1	0.233	0.238	0.233	0.234667	0.089778	
	0.61	0.732	0.61	0.650667	0.505778	
	0.236	0.239	0.239	0.238	0.093111	0.229555
2	1.859	2.009	1.901	1.923	1.778111	
	1.878	1.921	1.904	1.901	1.756111	
	1.874	1.857	1.871	1.867333	1.722444	1.752222
3	1.875	1.879	1.848	1.867333	1.722444	
	1.855	1.867	1.876	1.866	1.721111	
	1.858	1.858	1.845	1.853667	1.708778	1.717444
4	1.882	1.831	1.827	1.846667	1.701778	
	1.766	1.79	1.712	1.756	1.611111	
	1.884	1.807	1.797	1.829333	1.684444	1.665778
5	1.825	1.806	1.807	1.812667	1.667778	
	1.835	1.805	1.867	1.835667	1.690778	
	0.878	0.888	0.883	0.883	0.738111	1.365555
6	1.837	1.819	1.805	1.820333	1.675444	
	1.786	1.833	1.817	1.812	1.667111	
	1.804	1.54	1.505	1.616333	1.471444	1.604667

Background (BG) = 0.1448889[Stages 1-6]

SECTION S14: SPECTROPHOTOMETRIC DETECTION OF THE METABOLIC ACTIVITY OF SESSILE CELLS POST-EXPOSURE TO CIPROFLOXACIN-FREE-CARRIER-LADEN DROPLETS

Table S32. Dataset 1 - Metabolic activity of sessile cells 24 hours post-exposure to ciprofloxacin-free-carrier-laden droplets

Stage	λ_{abs}, 490			Avg	Avg - BG	
1	1.951	2.021	2.546	2.172667	1.946667	

	2.068	2.23	2.054	2.117333	1.891333	1.919
3	2.001	2.013	2.047	2.020333	1.794333	
	2.01	2.037	2.038	2.028333	1.802333	
	2.034	2.052	2.032	2.039333	1.813333	1.803333
5	2.01	2.012	2.05	2.024	1.798	
	1.973	2.003	2.007	1.994333	1.768333	
	2.046	2.037	2.114	2.065667	1.839667	1.802

Background (BG) = 0.226[Stages 1,3,5]

Table S33. Dataset 2 - Metabolic activity of sessile cells 24 hours post-exposure to ciprofloxacin-free-carrier-laden droplets

Stage	λ_{abs}, 490			Avg	Avg - BG	
1	1.803	1.875	1.789	1.822333	1.531	
	1.779	1.796	1.819	1.798	1.506667	
	1.71	1.682	1.713	1.701667	1.410333	1.482667
2	1.627	1.641	1.62	1.629333	1.338	
	1.686	1.696	1.704	1.695333	1.404	
	1.754	1.76	1.698	1.737333	1.446	1.396
3	1.771	1.762	1.784	1.772333	1.481	
	1.685	1.665	1.645	1.665	1.373667	
	1.791	1.801	1.772	1.788	1.496667	1.450444
4	1.567	1.556	1.565	1.562667	1.271333	
	1.53	1.553	1.53	1.537667	1.246333	
	1.563	1.569	1.525	1.552333	1.261	1.259556
5	1.477	1.545	1.537	1.519667	1.228333	
	1.349	1.306	1.315	1.323333	1.032	
	1.414	1.375	1.376	1.388333	1.097	1.119111
6	1.457	1.509	1.505	1.490333	1.199	
	1.323	1.332	1.315	1.323333	1.032	
	1.451	1.387	1.389	1.409	1.117667	1.116222

Background (BG) = 0.2913333[Stages 1-6]

Table S34. Dataset 3 - Metabolic activity of sessile cells 24 hours post-exposure to ciprofloxacin-free-carrier-laden droplets

Stage	λ_{abs}, 490			Avg	Avg - BG	
1	1.87	2.679	2.067	2.205333	1.896	
	1.892	1.905	1.872	1.889667	1.580333	
	3	2.329	1.87	2.399667	2.090333	1.855556
2	2.104	2.103	1.898	2.035	1.725667	
	1.912	2.829	1.918	2.219667	1.910333	
	1.814	1.893	1.821	1.842667	1.533333	1.723111
3	1.85	1.883	1.893	1.875333	1.566	
	2.932	1.843	1.862	2.212333	1.903	
	2.032	2.178	1.891	2.033667	1.724333	1.731111

4	2.376	1.864	1.791	2.010333	1.701	
	1.785	1.761	1.792	1.779333	1.47	
	1.799	1.818	1.849	1.822	1.512667	1.561222
5	1.858	2.66	1.875	2.131	1.821667	
	1.885	2.163	1.909	1.985667	1.676333	
	1.788	1.832	1.834	1.818	1.508667	1.668889
6	1.824	1.91	2.935	2.223	1.913667	
	1.832	1.866	1.833	1.843667	1.534333	
	2.103	2.112	1.91	2.041667	1.732333	1.726778

Background (BG) = 0.3093333[Stages 1-6]

Chapter 7. Concluding remarks and future directions

This thesis explored three research objectives using an in-house aerosol platform designed according to the American Society for Testing and Materials (ASTM) standard F2101-19.[1] The first objective was to develop an optimized protocol for reproducible quality control assessments of facemask materials. The second objective was to probe the effects of initial droplet size, suspension matrix composition, pathogen load, and indoor environmental conditions on viable virus droplet counts. The third objective was to adapt the platform to model the inhaled delivery of bactericidal agents to the lungs. This chapter summarizes key findings, significance, and future directions for these research objectives.

7.1. BACTERIAL AEROSOL DROPLETS

Summary of key findings – **Chapters 3 and 4** explored the first thesis objective: to identify and investigate ambiguous aspects of the ASTM standard and develop optimized procedures to evaluate the bacterial filtration efficiencies of facemask materials. **Chapter 3** provides the optimized protocol for operating the in-house setup and conducting BFE testing of facemask materials. **Chapter 4** discusses five unspecified parameters involved in platform operation and examines how varying the input values for these parameters impacts viable bacterial aerosol size and counts. The standard requires facemask materials to be challenged with 1700 to 3000 viable bacterial aerosols with a mean aerodynamic size of 3.0±0.3 μm. Based on our results, the following values generate bacterial aerosol challenge within ASTM specified count and size range: 1×10^5 CFU/mL bacterial concentration, 1.5% w/v peptone water concentration, 1.5 L/min atomizer airflow and 170 μL/min feed flow rates, and ≥80% relative humidity.

Significance – The significance of the work includes improved understanding, time optimization, improved testing accuracy, and practical applications. Many of the limitations of the ASTM standard F2101-19, identified by Rengasamy et al.[2], were addressed by this work. Procedures that clarify ambiguous aspects of the standard can improve the efficiency and accuracy of BFE test results. These chapters also provide detailed insight into the operation of atomizers, impactors, and airflow meters alongside knowledge of the aerodynamic behaviour of pathogen-containing aerosol droplets. This information provides valuable foundational knowledge for investigators without a background in aerosol research. A clear and detailed protocol minimizes the time lost for future investigators by circumventing a trial-and-error approach to arrive at optimized parameter values. Furthermore, identifying and understanding the impact of unspecified parameters on viable bacterial aerosol size and counts helps ensure reliable and consistent filtration efficiency results. Lastly, pressure-drop test results of facemask materials supported BFE test results.

Future directions – The testing procedures rely on 1700 to 3000 viable bacterial aerosol droplets, sized 2.7 to 3.3 μm, delivered over two minutes to evaluate facemask materials. This method is not suitable for assessing the antiviral properties of facemasks or fabric materials. Future work can develop protocols for generating viable virus aerosol droplets of relevant size and count range. Additionally, using agar plates to detect viable bacterial droplets may not be suitable for evaluating high-performance mask materials; the agar collection medium would dry out and compromise the detection of viable droplets during long challenge periods. Instead, inert fluorescent droplets

collected on a foil substrate for fluorescence intensity measurements would be a more suitable approach for long filtration challenges.

7.2. VIRUS AEROSOL DROPLETS

Summary of key findings – **Chapter 5** explored the second thesis objective, which utilized the aerosol platform to examine the impact of droplet size ranges, suspension matrix, relative humidity, and pathogen load on viable virus aerosol droplets after brief exposure to indoor environmental conditions in summer and winter. Initial droplet size calculations used an equation incorporating equilibrated droplet size, RH, and solute concentration to estimate the values. Droplets generated by the atomizer were subjected to 3 to 12 seconds of exposure to 15±5% or 50±5% RH at 24±1.6°C within the 60-cm-high glass mixing chamber before collection within the impactor. Under varied impactor airflow rates, droplets with an initial size range of ≥20.28 to 1.82 µm were collected (despite differing RH conditions and solute concentrations). The selected size ranges are relevant as respiratory droplets with initial diameters of 20 µm or less will equilibrate rapidly, due to a large surface-to-volume, to remain suspended in the air.[3]

The findings indicate the effects of heterogeneities in suspension matrix solids content on virus stability within aerosol droplets may occur in a humidity- and pathogen-load-dependent manner. Droplets generated from phage suspensions with a concentration of 1×10^5 PFU/mL with initial sizes of 12.52 to ≥20.28, 8.79 to 13.62, 5.59 to 9.56, 2.93 to 6.09, and 1.73 to 3.19 µm, exposure to low humidity conditions and a 1.5% w/v solute content resulted in significantly higher counts compared to 6% w/v solute content and exposure to intermediate humidity conditions. Droplets with these initial sizes and generated from 5-fold concentrated phage suspensions (5×10^5 PFU/mL), viable droplet counts remained comparable regardless of solute content and exposure to low or intermediate humidity conditions. Thus, a higher pathogen load may mask the effects of solute content and relative humidity on pathogen stability within aerosol droplets.

Significance – Contact-tracing data gathered during the 2019 coronavirus disease pandemic demonstrates that SARS-CoV-2 transmission varies significantly across persons, environments, and seasons, indicative of transmission heterogeneities.[4,5] The duration and closeness of the interaction increase the likelihood of transmission as the viability and concentration of pathogen-containing droplets are highest nearer to the source and shortly after expulsion.[3] The inactivation of viruses within droplets expelled from an infected individual over short time scales (immediately after being expelled from the airways) is relevant for understanding close-contact/short-range transmission events. Additionally, 80% of secondary infections were linked to 15% of infectious persons, indicating a small population of individuals possess an increased capacity to transmit the infection.[4] Compositional differences in the airway lining fluid may be a potential driver of individual transmission heterogeneities in airborne respiratory diseases.[6–8] The significance of this work lies in the demonstration of the utility of the aerosol platform to model the viability of virus-containing droplets exposed for short timescales (3 to 12 seconds) to indoor environmental conditions in winter (low humidity) and summer (intermediate humidity), using a high and low concentration suspensions of the bacteriophage Phi6 (a surrogate for SARS-CoV-2) to reflect sputum pathogen load during infection course, and three suspension media formulations to reflect sputum solids content.

Future directions – Estimated initial droplet size ranges, the use of a surrogate organism in place of the mammalian virus, and the use of peptone water as the suspension matrix are limitations of the study. Future work can utilize a laser diffraction system to assess how droplets equilibrate to ambient humidity conditions in winter and summer. This information can corroborate calculated estimates of initial droplet size based on equilibrated droplets collected using the six-stage viable cascade impactor. Secondly, aerosolization of an attenuated mammalian virus and collection on susceptible cell culture surfaces can increase the biological relevance of study findings. Lastly, in place of peptone water, saliva or airway lining fluid can be the suspension matrix for a surrogate or attenuated virus.

7.3. BACTERICIDAL AEROSOL DROPLETS

Summary of key findings – **Chapter 6** explored the last objective using the aerosol platform to investigate *in vitro* safety, effectiveness, and dosage of aerosolized bactericidal agents. *Pseudomonas aeruginosa* is a common bacterial pathogen responsible for recurring, antibiotic-resistant airway infections. Air-liquid interface (ALI) cultures of Calu-3 cells and biofilms in transwell inserts were placed below the last stage of the impactor and exposed to airflow or 0.65-µm-sized aerosol droplets containing anti-Pseudomonas bacteriophage. The barrier integrity and viability of Calu-3 cells were unaffected by exposure to high-velocity airflow or phage droplets within the platform. Metabolic activity assays demonstrated phage exposure significantly depletes biofilm bacterial cells. A second set of experiments was conducted with a modified configuration of the aerosol platform using a 10-cm-high aerosol mixing chamber. Aerosolized bacteriophage suspension and the fluoroquinolone antibiotic ciprofloxacin solution were size-fractioned and deposited onto biofilm cultures. Significantly lower fractions of the nominal phage dose, compared to the nominal ciprofloxacin dose, were delivered by aerosol droplets. Loss of phage infectivity could be a consequence of the stress of nebulization. Despite lower relative dose deposition, phage doses (4×10^2 – 2×10^4 PFU/mL) significantly reduced the viability of planktonic and sessile bacterial fractions. The highest ciprofloxacin dose (4.96 µg/mL), delivered by ≥7 µm droplets, significantly reduced the bacterial viability. Lower antibiotic doses (0.06 − 0.87 µg/mL) delivered by 0.65 − 4.7 µm droplets were ineffective.

Significance – The significance of this work lies in repurposing the aerosol platform as an *in vitro* lung deposition platform to investigate targeted delivery, safety, and dosing of aerosolized bactericidal agents as a strategy to combat antibiotic resistance. This work builds on transwell-integrated impactor models for inhaled drug delivery studies.[9–11] The results show aerosolized delivery of lytic phages, with the ability to self-replicate, could be a promising strategy for treating deep lung infections where effective antibiotic concentrations are difficult to attain. Phage doses delivered by clinically relevant droplet fractions (<5 µm) were bactericidal against 24-hour P. aeruginosa biofilms, while antibiotic doses were ineffective. On-site replication may have contributed to the superior performance of lower nominal dose fractions of phage aerosol droplets. These results indicate nebulized phage treatment could be a feasible strategy to target lower airway infections where effective antibiotic concentrations are challenging to deliver. The work also provides data on the effective doses and delivery methods for inhaled antibiotics and phage therapy, which can inform strategies for treating lower respiratory tract infections.

Future directions – Future work can explore aerosolization delivery, safety, and efficacy of bactericidal agents in animal models of *P. aeruginosa* airway infection and the design of delivery vehicles (liposomes and polymeric particles) to co-deliver phage and antibiotics to elicit synergistic effects against *P. aeruginosa* biofilms.

7.4. REFERENCES

1. ASTM F2101. Standard Test Method for Evaluating the Bacterial Filtration Efficiency (BFE) of Medical Face Mask Materials , Using a Biological Aerosol of Staphylococcus aureus. *American Society for Testing and Materials* **i**, (2019).
2. Rengasamy, S., Shaffer, R., Williams, B. & Smit, S. A comparison of facemask and respirator filtration test methods. *J Occup Environ Hyg* **14**, (2017).
3. Poydenot, F. *et al.* Risk assessment for long- and short-range airborne transmission of SARS-CoV-2, indoors and outdoors. *PNAS Nexus* **1**, 1–10 (2022).
4. Sun, K. *et al.* Transmission heterogeneities, kinetics, and controllability of SARS-CoV-2. *Science (1979)* **371**, (2021).
5. Moriyama, M., Hugentobler, W. J. & Iwasaki, A. Seasonality of Respiratory Viral Infections. *Annu Rev Virol* **7**, 83–101 (2020).
6. Fiegel, J., Clarke, R. & Edwards, D. A. Airborne infectious disease and the suppression of pulmonary bioaerosols. *Drug Discovery Today* vol. 11 Preprint at https://doi.org/10.1016/S1359-6446(05)03687-1 (2006).
7. Edwards, D., Salzman, J., Devlin, T. & Langer, R. Nasal Calcium-Rich Salts for Cleaning Airborne Particles from the Airways of Essential Workers, Students, and a Family in Quarantine. *Mol Front J* **04**, 36–45 (2020).
8. Edwards, D. A. *et al.* Inhaling to mitigate exhaled bioaerosols. *Proc Natl Acad Sci U S A* **101**, (2004).
9. Cooney, D., Kazantseva, M. & Hickey, A. J. Development of a size-dependent aerosol deposition model utilising human airway epithelial cells for evaluating aerosol drug delivery. *ATLA Alternatives to Laboratory Animals* **32**, (2004).
10. Wong, C. Y. J. *et al.* Validation of a cell integrated next-generation impactor to assess in vitro drug transport of physiologically relevant aerosolised particles. *Int J Pharm* **624**, 122024 (2022).
11. Haghi, M., Traini, D. & Young, P. In vitro cell integrated impactor deposition methodology for the study of aerodynamically relevant size fractions from commercial pressurised metered dose inhalers. *Pharm Res* **31**, 1779–1787 (2014).